TECHNICAL APPENDIX D: EXPERT JUDGMENT ELICITATION

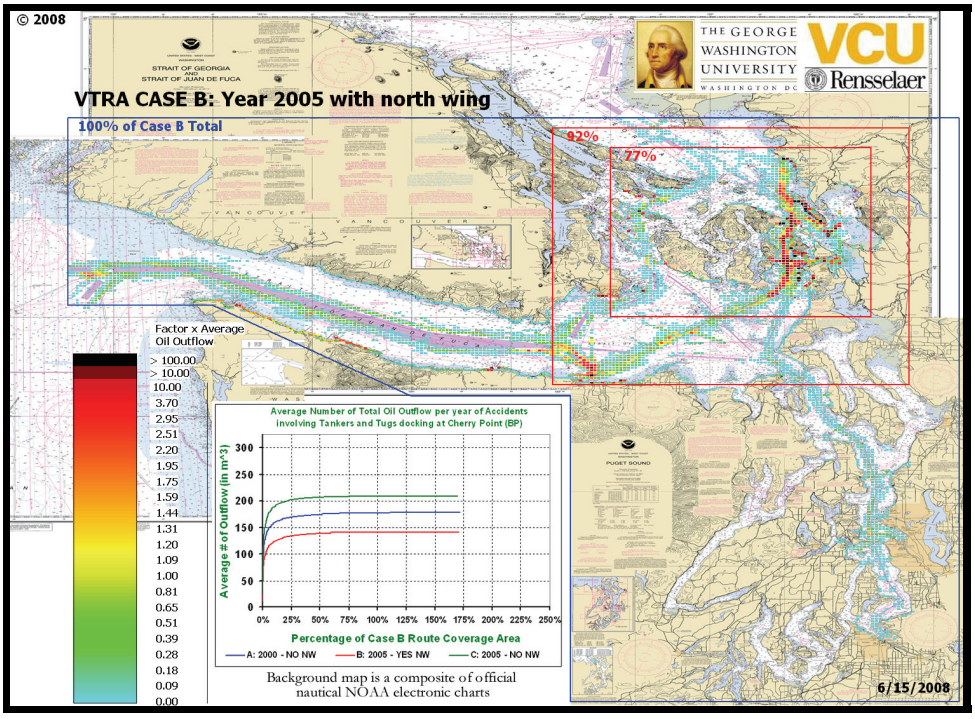

Assessment of Oil Spill Risk due to Potential Increased Vessel Traffic at Cherry Point, Washington

Submitted by VTRA TEAM:

Johan Rene van Dorp (GWU), John R. Harrald (GWU),

Jason R.. W. Merrick (VCU) and Martha Grabowski (RPI)

August 31, 2008

TABLE OF CONTENTS

Table of Figures D-3

Table of Tables D-6

D-1. Organizations that provided experts D-7
- D-1.1. Questionnaires Developed D-9

D-2. Overview of expert judgment techniques D-10
- D-2.1. Attribute scale development D-11
- D-2.2. Attribute Parameter Assessment D-22

D-3. Representative results of the expert judgment D-39

D-4. Turning expert judgment into annual accident frequencies D-42
- D-4.1. Simulation Counting D-43
- D-4.2. Incident Calibration D-49
- D-4.3. Accident Calibation D-50

References D-61

TABLE OF FIGURES

Figure D-1. Overview of a causal chain leading to an oil spill..... D-7
Figure D-2. Example introduction of a paired comparison questionnaire for..... D-15
accident attribute scale development
Figure D-3. Example explanation of a paired comparison question in a..... D-15
paired comparison questionnaire for accident attribute scale
development
Figure D-4. Example explanation of a paired comparison question in a paired..... D-16
comparison questionnaire for accident attribute scale development
Figure D-5. Attribute scale for traffic scenario using tanker and tug operator.....D-17
responses
Figure D-6. Attribute scale for Locations using tanker and tug operator responses..... D-18
Figure D-7. The Vessel Traffic Risk Assessment (VTRA) study area and the.....D-18
definition of its nine different locations for expert judgment purposes
Figure D-8. Attribute scale for tug barges using tug operator responses..... D-19
Figure D-9. Initial attribute scale for tug barges using tanker and tug operator.....D-21
responses.
Figure D-9. Initial attribute scale for tug barges using tanker and tug operator.....D-21
responses.
Figure D-10. Merged attribute scale for vessel types that follows from the scales..... D-21
presented in Figures D-9 and D-8.
Figure D-11. Example introduction of a paired comparison questionnaire of..... D-25
situations for accident attribute parameter assessment.
Figure D-12. Example question of a paired comparison questionnaire of situations..... D-25
for tanker collision accident attribute parameter assessment given
a propulsion failure.
Figure D-13. Example question of a paired comparison questionnaire of situations..... D-27
for tanker collision accident attribute parameter assessment given
all incidents.
Figure D-14. Matrix A_{22} in Equation (D-7).....D-28
Figure D-15. Matrix A_{21} in Equation (D-7).....D-28
Figure D-16. Apriori specification of tanker accident attribute parameters given..... D-31
a propulsion failure (prior to updating with the expert judgment
responses).

TABLE OF FIGURES (continued)

Figure D-17. Aposteriori tanker accident attribute parameters given a propulsion failure (after updating with the expert judgment responses). D-31
Figure D-18. Apriori setting (prior to updating with expert responses) of the relative likelihood of a collision given a propulsion failure on the tanker. D-40
Figure D-19. Expert responses to a pair wise situation comparison to assess relative likelihood of a collision given a propulsion failure on the tanker. D-40
Figure D-20. Analysis of relative likelihood of a collision given a propulsion failure when more than three accident attributes change when going from Situation 1 to Situation 2. .....D-41
Figure D-21. Analysis of relative likelihood of a collision given a propulsion failure when more than eleven accident attributes change when going from Situation 1 to Situation 2. .....D-41
Figure D-22. Schematic of counting procedure for vessel interactions.....D-44
Figure D-23. A risk profile as a function of time when two vessels cross..... D-44
Figure D-24. Exposure Counts of Cherry Point Tankers, ATB's and ITB's in the calibration case: VTRA CASE B. D-45
Figure D-25. Exposure Counts of all vessels in the calibration case: VTRA CASE B.....D-45
Figure D-26. Examples of vessel interaction counting in the VTRA maritime simulation. D-46
Figure D-27. Shore line definition in the VTRA maritime simulation D-47
Figure D-28. Examples of drift shore line interaction counting in the VTRA maritime simulation. D-48
Figure D-29. Examples of power shore line interaction counting in the VTRA maritime simulation. D-48
Figure D-30. Examples of allision interaction counting in the VTRA maritime simulation. D-48
Figure D-31. Encoding of interactions by the VTRA maritime simulation.....D-51
Figure D-32. Vessel interaction counts of Cherry Point Tankers, ATB's and ITB's in the calibration case: VTRA CASE B. D-53
Figure D-33. Annual collision frequencies of Cherry Point Tankers, ATB's and ITB's in the calibration case: VTRA CASE B. D-53
Figure D-34. Drift interaction counts of Cherry Point Tankers, ATB's and ITB's in the calibration case: VTRA CASE B D-55

TABLE OF FIGURES (continued)

Figure D-35. Annual drift grounding frequency of Cherry Point Tankers, ATB's and ITB's in the calibration case: VTRA CASE B. D-55

Figure D-36. Power interaction counts of Cherry Point Tankers, ATB's and ITB's in the calibration case: VTRA CASE B. D-57

Figure D-37. Powered grounding frequency of Cherry Point Tankers, ATB's and ITB's in the calibration case: VTRA CASE B. D-57

Figure D-38. Allision interaction counts of Cherry Point Tankers, ATB's and ITB's in the calibration case: VTRA CASE B. D-59

Figure D-39. Allision frequency of Cherry Point Tankers, ATB's and ITB's in the calibration case: VTRA CASE B. D-59

TABLE OF TABLES

Table D-1. Overview of questionnaires developed for and expert experience during the VTRA expert judgment elicitations. D-9
Table D-2. Accident attributes for tanker accident probability models D-12
Table D-3. Levels of accident attributes for tanker accident probability models D-12
Table D-4. Accident attributes for tug accident probability models D-13
Table D-5. Levels of Accident attributes for tug accident probability models D-13
Table D-6. Vessel type classifications of initial vessel type scale questionnaire D-20
Table D-7. Vessel type classifications to allow for a further refinement of the vessel type scale. D-20
Table D-8. The vector $\underline{b}$ summarizing expert responses (see Equation (11) in Szwed et. al (2006)) for the tanker collision accident probability questionnaire given a propulsion failure. D-30
Table D-9. The scalars c summarizing expert responses (see Equation (11) in Szwed et. al (2006)) for the tanker collision accident probability questionnaire given a propulsion failure. D-30
Table D-10. Attribute accident parameters for tanker accident probability models D-32
Table D-11. Attribute accident parameters for tug accident probability models D-32
Table D-12. Calibrations values for P_0 for the tanker and tug collision accident probability models D-33
Table D-13. Probabilities of grounding given an incident failure in the least risk state ($\underline{X} = 0$) and a time to shore of 5 hours. These follow from (D-18) and the tanker and tug accident accident probability parameters specified in Tables D-9 and D-10. ..... D-38
Table D-14. Probabilities of grounding given an incident failure in the most risk state ($\underline{X} = 1$) and a time to shore of 5 hours. These follow from (D-18) and the tanker and tug accident accident probability parameters specified in Tables D-9 and D-10. ..... D-38
Table D-15. Incident rates per route interaction for CHPT Tankers, ATB and ITB's D-50

D-1. Organizations that provided experts

Our model represents the chain of events that could potentially lead to an oil spill (see Figure D-1). This model and approach has been used in the Prince William Sound Risk Assessment, the Washington State Ferries Risk Assessment, and the Exposure Assessment of the San Francisco Bay ferries.

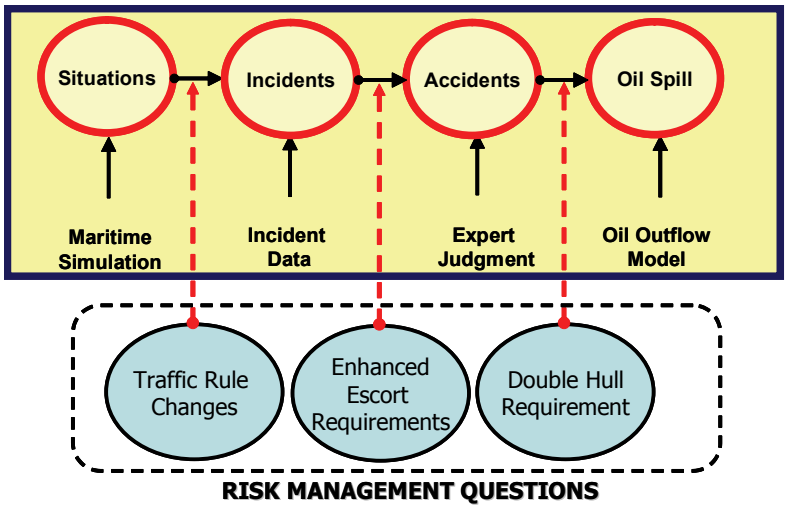

Figure D-1. Overview of a causal chain leading to an oil spill

It is based on the methodology developed for the dynamic risk simulation of tanker operations in Prince William Sound, Alaska (1995-96), for the Washington State Ferries (WSF) Risk Assessment (1998-1999) and for the San Francisco Bay Exposure Assessment (2002). The overall methodology is described in the following journal papers:

- J.R.W. Merrick, J.R. van Dorp, J.P. Blackford, G.L. Shaw, T.A. Mazzuchi and J.R. Harrald (2003). "A Traffic Density Analysis of Proposed Ferry Service Expansion in San Francisco Bay Using a Maritime Simulation Model", *Reliability Engineering and System Safety*, Vol. 81 (2): pp. 119-132.
- J.R.W. Merrick, J. R. van Dorp, T. Mazzuchi, J. Harrald, J. Spahn and M. Grabowski (2002). "The Prince William Sound Risk Assessment". *Interfaces*, Vol. 32 (6): pp.25-40.
- J.R. van Dorp J.R.W. Merrick , J.R. Harrald, T.A. Mazzuchi, and M. Grabowski (2001). "A Risk Management procedure for the Washington State Ferries", *Journal of Risk Analysis*, Vol. 21 (1): pp. 127-142
- **P. Szwed, J. R. van Dorp, J.R.W.Merrick, T.A. Mazzuchi and A. Singh (2006). "A Bayesian Paired Comparison Approach for Relative Accident Probability Assessment with Covariate Information", *European Journal of Operations Research*, Vol. 169 (1), pp. 157-177.**

The accident types included in this study are collisions between two vessels, groundings (both powered and drift), and allisions. However, as our maritime simulation counts the situations in which accidents could occur, it also records attributes that could affect the chance that the accident will occur; these include e.g. the proximity of other vessels, the types of the vessels, the location of the situation, and environmental variables, such as wind, current and visibility. The construction of this maritime simulation is described in Appendix C. We know how often accidents do occur from our analysis of incident and accident data. The accident and incident data collected for this particular project and its process is described in Appendix A. However, there is not enough data to say how each of these attributes affects the chances of an accident; accidents are rare! To determine this, we must turn to the experts (see the third event in Figure D-1) in maritime operations. Specifically, we must turn to experts who are primarily familiar with the sailing of tugs and tankers in the study area and preferably have long term sailing experience with either one or both of these vessel types. Experts were invited to and referred to the VTRA team through the United States Coast Guard and the Puget Sound Harbor Safety committee. The organizations that provided experts to construct our accident probability models are:

1. Puget Sound Pilots
2. ATC
3. US and Canadian Tug Companies operating in the VTRA study area:
   US-Based: Foss, Crowley, Olympic Tug and Barge (US),
   K-Sea, Sea Coast, Sause Bros.
   Canadian Based: Seaspan, Island Tug and Barge
4. The Washington State Ferries
5. Seattle sector US Coast guard VTS.

Expert judgment elicitation sessions were scheduled predominantly at the US Coast Guard VTS, sector Seattle in December 2006, February 2007, June 2007, August 2007, September 2007 and December 2007. The elicitation session with the ATC tanker captains and master was scheduled during an ATC conference in February 2007 in Portland,Oregon.

D-1.1. Questionnaires Developed

Table D-1 below summarizes the elicitation process that was followed in the overall expert judgment elicitation procedure. A total of 9 questionnaires were developed that were distributed to 38 experts over 7 separate elicitation sessions (2 elicitation sessions were held during February 2007) dispersed over a 1 year period. The combined numbers of years

sailing experience of the experts who participated in the elicitation process of the VTRA study area exceeds 922 years. The number of years experience of the experts by questionnaire is further detailed in Table D-14. The last expert judgment elicitation session was held in December 2007 after which final results were analyzed and were prepared for integration into the maritime vessel traffic risk assessment simulation tool. The first expert judgment elicitation session was held in December 2006.

Table D-1. Overview of questionnaires developed for and expert experience during the VTRA expert judgment elicitations.

9 QUESTIONNAIRES	38 EXPERTS - Numbers indicate years sailing experience in VTRA Study area	CUMULATIVE EXPERIENCE (YRS)	7 SESSIONS
Bradley-Terry Pair Wise Comparison Location Questionnaire	7 PILOTS (42,34,32,25,16,16) 6 TUG OPERATORS (39, 30, 30, 30, 15, 12) 4 FERRY OPERATORS (31, 30, 25, 8) 2 PORT CAPTAINS (27, 25) 1 VTS WATCH (25)	186 156 94 52 25	Dec-06 Feb-07
Bradley-Terry Pair Wise Comparison Traffic Scenario Questionnaire	7 PILOTS (42,34,32,25,16,16) 6 TUG OPERATORS (39, 30, 30, 30, 15, 12) 4 FERRY OPERATORS (31, 30, 25, 8) 2 PORT CAPTAINS (27, 25) 1 VTS WATCH (25)	186 156 94 52 25	Dec-06 Feb-07
Bradley-Terry Pair Wise Comparison 1st Traffic Type Questionnaire	7 PILOTS (42,34,32,25,16,16) 6 TUG OPERATORS (39, 30, 30, 30, 15, 12) 4 FERRY OPERATORS (31, 30, 25, 8) 2 PORT CAPTAINS (27, 25) 1 VTS WATCH (25)	186 156 94 52 25	Dec-06 Feb-07
Bradley-Terry Pair Wise Comparison 2nd Traffic Type Questionnaire	6 PILOTS (35, 34, 24, 22, >20, >20) 5 TUG OPERATORS (53, 32, 38, 20, 18) 2 PORT CAPTAINS (32, 30)	> 155 151 62	Apr-07 Aug-07 Sep-07
Bradley-Terry Pair Wise Comparison Tug Barge Questionnaire	7 TUG OPERATORS (53, 21, 20, 32, 30, 28, 18) 2 PORT CAPTAINS (32, 30)	202 52	Aug-07 Sep-07 Dec-07
Tanker Pair Wise Situation Collision Accident Probability Questionnaires Given Propulsion Failure	6 PILOTS (35, 34, 24, 22, >20, >20) 5 TANKER OPERATORS (21, 20, 21, 18, 16)	> 155 96	Feb-07 Apr-07
Tanker Pair Wise Situation Collision Accident Probability Questionnaires Given Steering Failure, Given Navigational Aid Failure Given Human Error Given Near By Vessel Failure	6 PILOTS (35, 34, 24, 22, >20, >20) 5 TANKER OPERATORS (21, 20, 21, 18, 16)	> 155 96	Feb-07 Apr-07
Tug Pair Wise Situation Accident Probability Questionnaires Given Propulsion Failure	7 TUG OPERATORS (53, 21, 20, 32 30, 28, 18) 2 PORT CAPTAINS (32, 30)	202 52	Aug-07 Sep-07 Dec-07
Tug Pair Wise Situation Collision Accident Probability Questionnaires Given Steering Failure, Given Navigational Aid Failure Given Human Error Given Near By Vessel Failure	7 TUG OPERATORS (53, 21, 20, 32 30, 28, 18) 2 PORT CAPTAINS (32, 30)	202 52	Aug-07 Sep-07 Dec-07

We were extremely fortunate that in November 2006 the Puget Sound Harbor Safety committee agreed to provide us a platform to present interim results of the VTRA study and ask for feedback from the Puget Sound maritime community. This platform and the close

relationship between the Puget Sound maritime community were instrumental in obtaining access to experts and the expert participation that we received. We were able to hold our first expert judgment elicitation session one month after the introduction to the Puget Sound Harbor Safety committee. Invitations to the expert judgement elicitation sessions were sent out initially by the US Coast Guard and later on by the Puget Sound Harbor Safety committee. None of the experts personally benefited from participating in the expert judgment elicitation. They donated their time for the enhancement of the safety levels in their maritime domain and they should be commended for it. Each expert judgment elicitation session consisted of a morning and afternoon session.

D-2. Overview of expert judgment technique

Of the four papers listed in the introduction, the fourth one Szwed et. (2006) (indicated in bold above) describes in detail how we estimate the parameters in our accident probability models using the expert judgment. For convenience it is included as a sub-appendix to this appendix. Below, we shall provide an overview of the specific implementation of this technique in this particular project.

The aim of our expert judgment elicitation technique is to be able to estimate the conditional probability of an accident given that a particular incident has occurred in a particular scenario on the water. This incident can either be a propulsion failure, a steering failure, a navigational aid failure, a human error or an event of a vessel nearby. We refer to the later incident as a NBV failure (NBV=Near By Vessel). Scenario on the water are summarized by a set of attributes and these sets of attributes are stored in a database using the maritime simulation and may be described by a vector $\underline{X}$. We shall refer to the elements of the vector $\underline{X}$ as accident attributes in the sense that the value of such an attribute may adversely affect the accident probability given that a particular incident has occurred. At what level these attributes affect an accident probability may very well depend on the incident type as well. We capture this multitude of effects via our expert judgment approach. Below we shall discuss in more detail our expert inducement procedure for our accident probability models. Separate accident probability models are constructed for tankers and tugs.

Our tanker and tug collision probability models follow the set-up in Szwed et al. (2006):

$$Pr(Collision|Incident,\ \underline{X}) = P_0 exp\left\{\underline{\beta}^T \underline{X}\right\}. \qquad \text{(D-1)}$$

Whereas in the Prince William Sound Risk Assessment (see, e.g. Merrick et. al (2002)), we used a similar formulation as (D-1) for groundings and allision accident probability models, we have enhanced the accident probability models in this project for groundings and allisions to allow for explicit representation of "a time to shore" variable t that is now also recorded in our maritime simulation. In the Prince William Sound Risk Assessment this time component was only taken into account implicitly through the attribute "Location". This, however, would not allow for modeling of a difference in convergence of the waterway <u>within</u> a particular location. The expressions for our accident probability models for grounding and allision are as follows:

$$Pr(Grounding|Incident, \underline{X}, t) = P_0 exp\Big\{ -\alpha_0[1 + \underline{\gamma}^T(\underline{1} - \underline{X})] \times t \Big\} \quad \text{(D-2)}$$

$$Pr(Allision|Incident, \underline{X}, t) = P_0 exp\Big\{ -\delta_0[1 + \underline{\kappa}^T(\underline{1} - \underline{X})] \times t \Big\} \quad \text{(D-3)}$$

The parameter vectors $\underline{\beta}, \underline{\gamma}, \underline{\kappa}$ describe the effect that a particular element in the attribute vector $\underline{X}$ has on the accident probability. The parameters P_0, α_0 and δ_0 are used for calibrating our maritime simulation model to the accident data that has been collected for the VTRA study area. The data collection procedure and process is described in detailed in Appendix A. Before we can estimate these parameters, however, we need to establish a measurement of scale for the various accident attributes $\underline{X}$. In the next section we shall discuss the scale development for the both the tanker and tug accident attributes.

D-2.1. Attribute scale development

Table D-2 summarizes the accident attributes $\underline{X}$ for tankers. The discretization column in Table D-2 gives the number of levels that a particular attribute may have. For example we have considered nine different locations in the accident probability model. The designations for the specific locations are specified in Table D-3. Table D-3 describes all the different levels of the various accident attributes listed in Table D-2 and that we have accounted for in our accident probability models. Tables D-4 and D-5 provide similar information for the tug accident probability models.

From Table D-2 it immediately follows that in our model the maximum number of possible situations that a tanker could encounter equals 2,156,544 or over 2 million different situations. Likewise, from Table D-3 we have modeled potentially 5,031,936 or over 5 million different situations for tugs. Needless to say, it is impossible to estimate the accident probability for each situation individuality and hence we have to resort to theoretical

Table D-2. Accident attributes for tanker accident probability models

	TANKER DESCRIPTION	DISCRETIZATION
1	Location	9
2	Direction	2
3	Cargo	2
4	Escorts	3
5	Tethering	2
	INTERACTING VESSEL	**DISCRETIZATION**
6	Vessel Type	13
7	Traffic Scenario	4
8	Traffic Proximity	2
	WATERWAY CONDITIONS	**DISCRETIZATION**
9	Visibility	2
10	Wind Direction	2
11	Wind Speed	4
12	Current	2
13	Current Direction	3

Table D-3. Levels of accident attributes for tanker accident probability models

LOCATION	DIRECTION	CARGO	ESCORTS	TETHERED
Cherry Point Area	Inbound	Unladen	2 Escorts	tethered
Puget Sound South	Outbound	Laden	1 Escort	untethered
Strait of Juan de Fuca East			No Escorts	
Strait of Juan de Fuca West				
Puget Sound North				
Saddle Bag Area				
Rosario Strait				
Haro Strait\Boundary Pass				
Guemes Channel				

VESSEL TYPE	TRAFFIC PROXIMITY	TRAFFIC SCENARIO
Tug without Barge	1 to 5 miles	Crossing Astern
Tug ATB's or ITB's	Less than 1 mile	Meeting
Tug Pushing Ahead		Overtaking
Container		Crossing the Bow
Tanker		
Bulk carrier		
Freighter		
Passenger vessel		
Service vessel		
Public vessel		
Fishing Vessel		
Tug Towing Astern		
Recreational Vessel		

VISIBILITY	WD	WIND SPEED	CURRENT	CUR_DIR
More than 0.5 mile	Along Vessel	Less than 10 knots	Almost Slack	Along Vessel - Opposite
Less than 0.5 mile	Abeam Vessel	20 knots	Max Eb or Max Flood	Along Vessel - Same Dir.
		30 knots		Abeam Vessel
		More than 40 knots		

Table D-4. Accident attributes for tug accident probability models

	TUG DESCRIPTION	DISCRETIZATION
1	Location	9
2	Direction	2
3	Cargo	7
4	Hook-up	4
	INTERACTING VESSEL	**DISCRETIZATION**
5	Vessel Type	13
6	Traffic Scenario	4
7	Traffic Proximity	2
	WATERWAY CONDITIONS	**DISCRETIZATION**
8	Visibility	2
9	Wind Direction	2
10	Wind Speed	4
11	Current	2
12	Current Direction	3

Table D-5. Levels of Accident attributes for tug accident probability models

LOCATION	DIRECTION	CARGO	HOOKUP
Cherry Point Area	Inbound	No Barge	No Barge
Puget Sound South	Outbound	Unladen Barge	ATB or ITB
Strait of Juan de Fuca East		Laden Container Barge	Pushing Ahead
Strait of Juan de Fuca West		Laden Bulk Cargo Barge	Towing Astern
Puget Sound North		Laden Derrick/Crane Barge	
Saddle Bag Area		Laden Oil Barge	
Rosario Strait		Log Tow	
Haro Strait\Boundary Pass			
Guemes Channel			

VESSEL TYPE	TRAFFIC PROXIMITY	TRAFFIC SCENARIO
Tug without Barge	1 to 5 miles	Crossing Astern
Tug ATB's or ITB's	Less than 1 mile	Meeting
Tug Pushing Ahead		Overtaking
Container		Crossing the Bow
Tanker		
Bulk carrier		
Freighter		
Passenger vessel		
Service vessel		
Public vessel		
Fishing Vessel		
Tug Towing Astern		
Recreational Vessel		

VISIBILITY	WD	WIND SPEED	CURRENT	CUR_DIR
More than 0.5 mile	Along Vessel	Less than 10 knots	Almost Slack	Along Vessel - Opposite
Less than 0.5 mile	Abeam Vessel	20 knots	Max Eb or Max Flood	Along Vessel - Same Dir.
		30 knots		Abeam Vessel
		More than 40 knots		

probability models that capture the effect on an accident probability from attribute to attribute and the effect within an attribute from level to level. The expressions for these accident probability models are given by equations (D-1, D-2, D-3) above. The first element X_1 representing "Location", the second element X_2 representing "Direction", etc. (see Tables D-2 and D-4).

The first step in creating our quantitative accident probability is to develop a measurement scale for each individual accident attribute. For some this is relatively straightforward. For example, in case of tankers X_9 represents visibility and we assign a value of 1 to "Less than 0.5 mile" and a value 0 to "More than 0.5 mile". Hence, the scale is ordered in such a manner that worse levels in an accident attribute attain a higher value. Creating such a scale for other attributes is less straightforward. For example consider the vessel type attribute in Table D-3. First of all, we have 13 levels for the vessel type attribute and while we have ordered the vessel types from best to worst in both Tables D-4 and Tables D-5, it is not all obvious if going from a "container vessel" to a "tanker" in this scale is as bad as going from a "tug towing astern" to a "recreational vessel".

An important class of elicitation techniques are the so-called the psychological scaling models that use the concept of paired comparisons. Origins of this class can be traced back to Thurstone's (1927a,b) pioneering work where Weber's and Fechner's law were used to quantify the intensity of psychophysical stimuli using a discriminative process. An extension of this concept found application in the field of consumer research (see, Bradley (1953)). An examination of the Bradley- Terry model is provided by Cooke (1991), among other numerous sources. We used the Bradley- Terry paired comparison method to develop attribute level measurement scales for the following attributes: Location, Vessel Type, Traffic Scenario, Cargo (for Tugs) and Hookup.

Figure D-2 and D-3 provide an example explanation used in one of our paired comparison questionnaires to established a scale for the traffic scenario attribute. As part of our Institutional Review Board procedure regarding research involving human subjects it is a requirement that the expert remains anonymous. However, the experts were asked to provide their job title and number of years of sailing experience (see Figure D-1) in the VTRA area (although they were not forced to provide this information to participate in the survey). It was explained to the experts that every effort will be made to keep their provided information confidential. There were instructed that if any of the questions they were asked

as part of this study made them feel uncomfortable they could refuse to answer that question.

Explanation of an Example Question

Your responses to this questionnaire will be used to develop an accident probability model to be used in conjunction with a Maritime Simulation for the Vessel Traffic Risk Assessment (VTRA) Study. The results of this questionnaire will allow a preliminary ordering of different traffic scenarios from a collision perspective. You will be asked to compare traffic scenarios through pair wise comparison. Before you compare two traffic scenarios, you are asked to imagine a vessel type common to both these traffic scenarios under particular weather conditions. For the comparison, this should preferably be a worst case collision scenario.

The responses you provide will be anonymous but we ask you to indicate your experience level with the marine environment in the VTRA study area above by stating your affiliation and the number of years you have been exposed to the VTRA study area.

Job Title:
Number of Years Experience:

Figure D-2. Example introduction of a paired comparison questionnaire for accident attribute scale development

An example question is as follows. Let the two traffic scenarios you are comparing be: Overtaking and Meeting situations. Next, you are asked assuming **a common vessel type for both traffic scenarios** to indicate the traffic scenario for which you would be more concerned for a collision to occur and you are asked to indicate your answer in the following format.

Overtaking	<--	=	-->	Meeting	?

If you are **equally** concerned about an overtaking and meeting situation you answer:

Overtaking	<--	X	-->	Meeting	?

If you are **more** concerned about an overtaking than a meeting situation you answer:

Overtaking	X	=	-->	Meeting	?

If you are **less** concerned about an overtaking than a meeting situation you answer:

Overtaking	<--	=	X	Meeting	?

If you cannot answer this question, you answer:

Overtaking	<--	=	-->	Meeting	X

Figure D-3. Example explanation of a paired comparison question in a paired comparison questionnaire for accident attribute scale development

WHICH ONE CONCERNS YOU MORE?

Meeting	<--	=	-->	Crossing the Bow	?
Overtaking	<--	=	-->	Crossing the Bow	?
Overtaking	<--	=	-->	Crossing astern	?
Overtaking	<--	=	-->	Meeting	?
Crossing astern	<--	=	-->	Crossing the Bow	?
Crossing astern	<--	=	-->	Meeting	?

Figure D-4. Example explanation of a paired comparison question in a paired comparison questionnaire for accident attribute scale development

They were allowed to take a break at any time during the study. They could stop their participation in this study at any time. It was explained to the experts that they will not benefit directly from their participation in the study, but rather that the benefits that might result from this study are to science, humankind and a scientific and impartial assessment of oil spill risk due to potential increased vessel traffic at Cherry Point, WA. If results of this research study are reported in journals or at scientific meetings, the people who participated in this study will not be named or identified.

Figure D-3 provides the format of the explanation of a paired comparison question, whereas Figure D-4 list all the paired comparison questions for the traffic scenario questionnaire. Since we are comparing pair wise four traffic scenarios we have a total of $\binom{4}{2} = 6$ questions. The Bradley-Terry paired comparison technique allows for testing the consistency of an expert. An expert commits what is called "a circular triad" if the expert responds $A > B$, $B > C$, but $C > A$.

The more circular triads are present within his/her expert judgment the less consistent the expert. Of course, the question arises how many circular triads would be too many. This is

(naturally) also a function of the number of pairwise comparison question he/she is asked to answer. The Bradley Terry methods considers an expert consistent if his/her number of committed circular triads compares favorable to a hypothetical expert responding at random. This is conducted via a statistical hypothesis test. If an expert had less than a 5% chance of having the number of circular triads if the expert had responded at random, the expert was deemed consistent. Otherwise, his/her responses were not considered in the analysis. Besides allowing for testing the inconsistency within an individual's expert judgment, the Bradley Terry method allows for testing agreement amongst the expert judgments. This is achieved by measuring the association of the various rankings from the individual experts through what is called a "measure of concordance". Higher values of this measure indicate a higher level agreement. A statistical test is formulated that evaluates a threshold such that there would be less than a 5% chance of achieving this measurement of concordance assuming all the expert rankings were independently generated (and thus not exhibiting agreement).

Figure D-5 provides the resulting scales from the Bradley Terry analysis for the four different Traffic Scenarios resulting from the responses of 13 consistent experts (with agreement amongst these experts). From Figure D-5 it follows that in terms of level of concern a "crossing the bow" situation is about 6.6 times worse than a "meeting" situation and an "overtaking" situation is about twice worse. Moreover, a "crossing astern" situation is approximately 7.7 times better than a meeting situation (in level of concern) making it about 52 times better than a "crossing the bow" situation.

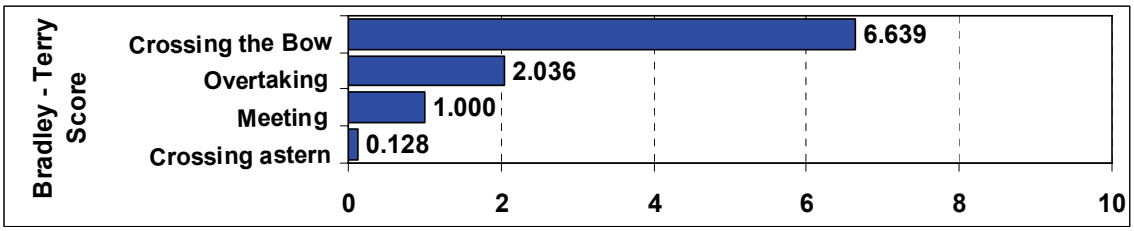

Figure D-5. Attribute scale for traffic scenario using tanker and tug operator responses

Figure D-6 provides the resulting scales from the Bradley Terry analysis for the nine different locations that we considered in the expert judgment elicitations. These scores followed from 8 consistent experts (with agreement amongst the experts). The definition of these nine different locations were provided to experts prior to the elicitation (see Figure D-

7). From Figure D-6 it follows that "Guemes Channel" is considered to be about 11 times worse in level of concern than the "Strait of Juan de Fuca East". Furthermore, it appears that "Haro-Strait\Boundary Pass" is similar in level of concern than "Rosario Strait" and the same applies to the grouping "Puget Sound North", "Stait of Juan de Fuca West", "Strait of Juan de Fuca East" and "Puget Sound South". The "Sadde Bag" area falls somewhere in between "Rosario Stait" and "Puget Sound North". Finally, the "Cherry Point Area" is about 2.7 times better in level of concern than the "Strait of Juan de Fuca East".

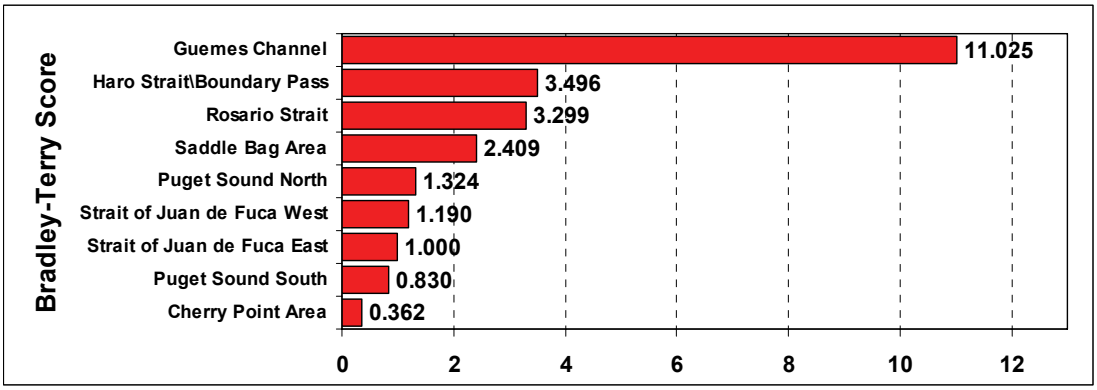

Figure D-6. Attribute scale for Locations using tanker and tug operator responses

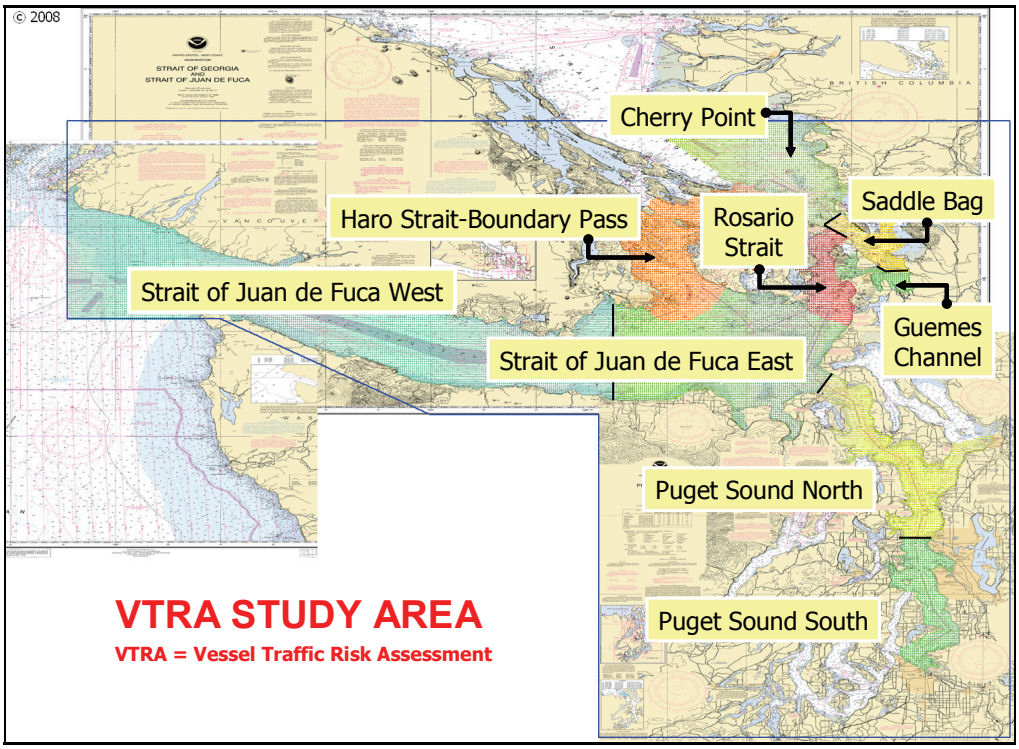

Figure D-7. The Vessel Traffic Risk Assessment (VTRA) study area and the definition of its nine different locations for expert judgment purposes

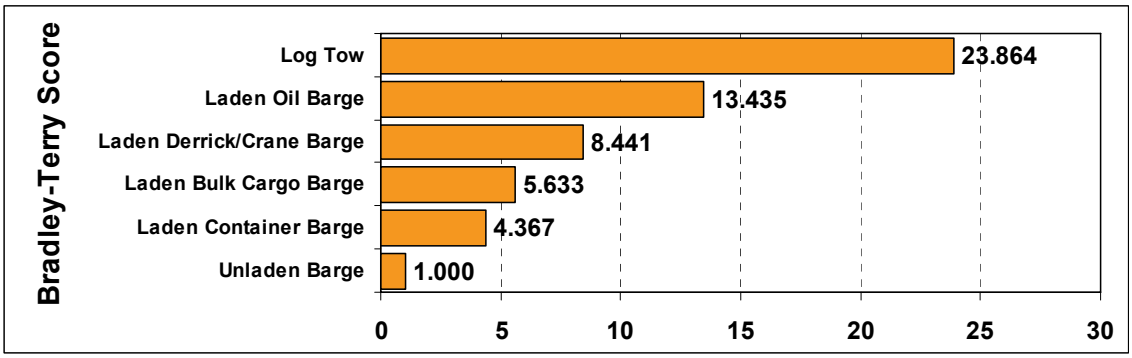

Figure D-8. Attribute scale for tug barges using tug operator responses.

Figure D-8 above provides the resulting scales from the Bradley Terry analysis for the six different barge configurations that we considered in the expert judgment elicitations. These scores followed from 8 consistent experts (with agreement amongst the experts). From Figure D-8 it follows that the "Log Tow" configuration obtains the highest level of concern (from a towing perspective) and the "unladen barge" the lowest level of concern. Laden "Bulk Cargo" and "Container" barges seem to obtain somewhat similar scores, where the "Laden Oil" barge obtain the second highest score in level of concern followed by the "Laden Derrick/Crane" barge.

The last attribute for which we constructed a scale using a Bradley Terry type analysis is the "Vessel Type" attributed listed in Tables D-2 and D-4. From Tables D-3 and D-5 it follows that we are considering 13 different vessel types in the various accident probability models. The full set of paired comparisons for that case would be $\binom{13}{2} = 78$ questions which could be considered too tasking resulting potentially in a proportionally larger number of triads and thus inconsistency in the expert judgment. In attempt to avoid such an adverse result, the development of the vessel type scale was developed using initially one questionnaire of 9 vessel types (involving 36 questions). The second questionnaire of 6 vessel types (involving 15 questions) was born from the observation amongst the Puget Sound Harbor Safety committee members that when encountering tugs that how the mariner views them depends on its tow configuration. Tables D-6 and D-7 list the classifications of vessel types provided to the experts for both questionnaires. Both questionnaires had the "tanker" and "passenger" vessel in common which allowed for the merging of the vessel scales that followed.

Table D-6. Vessel type classifications of initial vessel type scale questionnaire

	Vessel Type	Sub-Classification
1	Tanker	oil, chemical, product, LNG
2	Container	
3	Freighter	
4	Bulk carrier	
5	Tug/tow/barge/service vessel	
6	Passenger vessel	ferry, passenger ship, cruise lines, tour boat
7	Public vessel	USCG, USN, USNS, NOAA, etc.
8	Fishing Vessel	fish vessels and factories
9	Recreational Vessel	Yacht, Kayak, Jet Ski, etc.

Table D-7. Vessel type classifications to allow for a further refinement of the vessel type scale.

	Vessel Type	Sub-Classification
1	Tanker	Oil, Chemical, Product, LNG
2	Tug without Barge	
3	Tug Pushing Ahead	
4	Tug Towing Astern	
5	Tug ATB's or ITB's	
6	Passenger vessel	Ferry, Passenger Ship, Cruise Lines, Tour Boat

Figure D-8 provides the resulting scales from the Bradley Terry analysis for the initial nine different vessel types. These scores followed from nine consistent experts (with agreement amongst the experts). Figure D-9 provides the resulting scales from the Bradley Terry analysis for refinement of the vessel type scales to allow for a differentiation of tow configurations. These scores also followed from nine consistent experts (with agreement amongst the experts). Figure D-10 merges both scales from Figures D-8 and D-9. From Figure D-10 we may observes that a "recreational vessel" obtains the highest level of concern from an interaction perspective followed by a "tug towing astern". The other tug configurations "Tug Pushing ahead", "Tug ATB or ITB" and "Tug without a Barge" obtain the three smallest scores (with a much smaller score for the last one). Please note that we would not have achieved this distinction had we not further refined the vessel scale in Figure D-8. That is, the tug/tow/barge/service vessel score of 1.031 in Figure D-8 would have been the combined score for all these configurations. We can also observe from Figure D-10 that "service vessel, passenger vessel, freighter, bulk carrier, tanker and container" vessels classify in a similarity group from a vessel type perspective (when encountering them). The "Fishing Vessel" follows the "Tug Towing Astern", followed by the "Public Vessel".

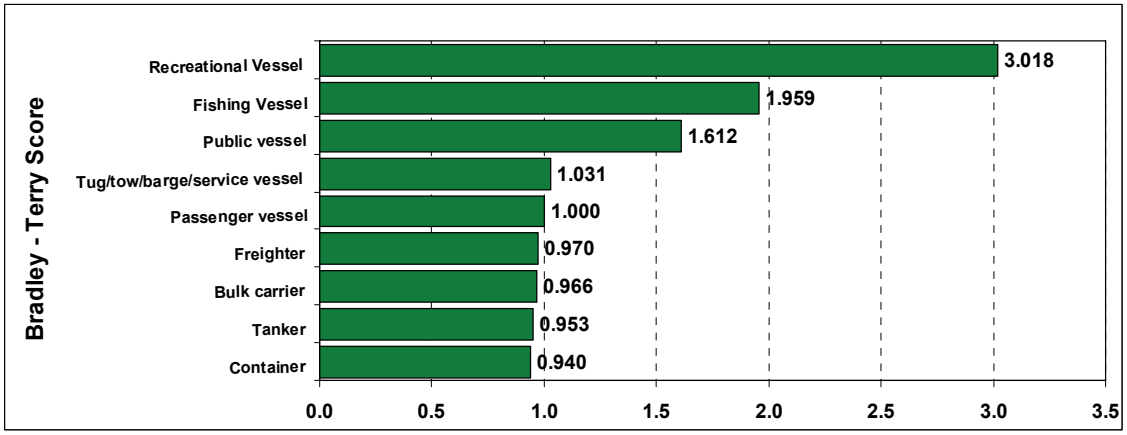

Figure D-8. Initial attribute scale for tug barges using tanker and tug operator responses.

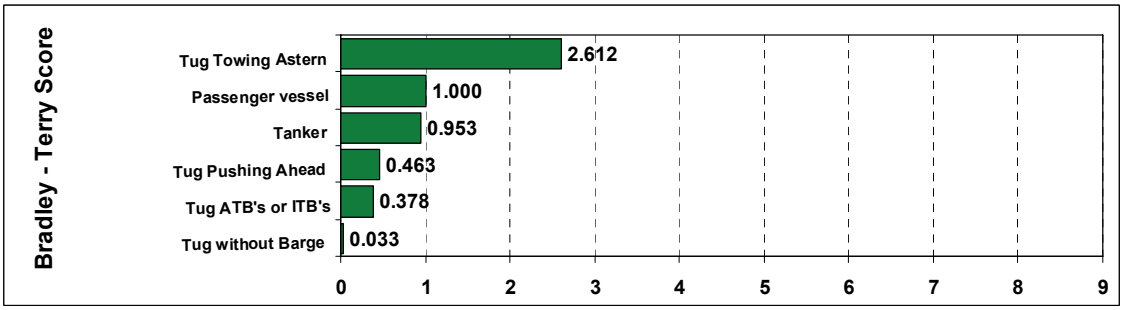

Figure D-9. Refined attribute scale for vessel types using tanker and tug operator responses.

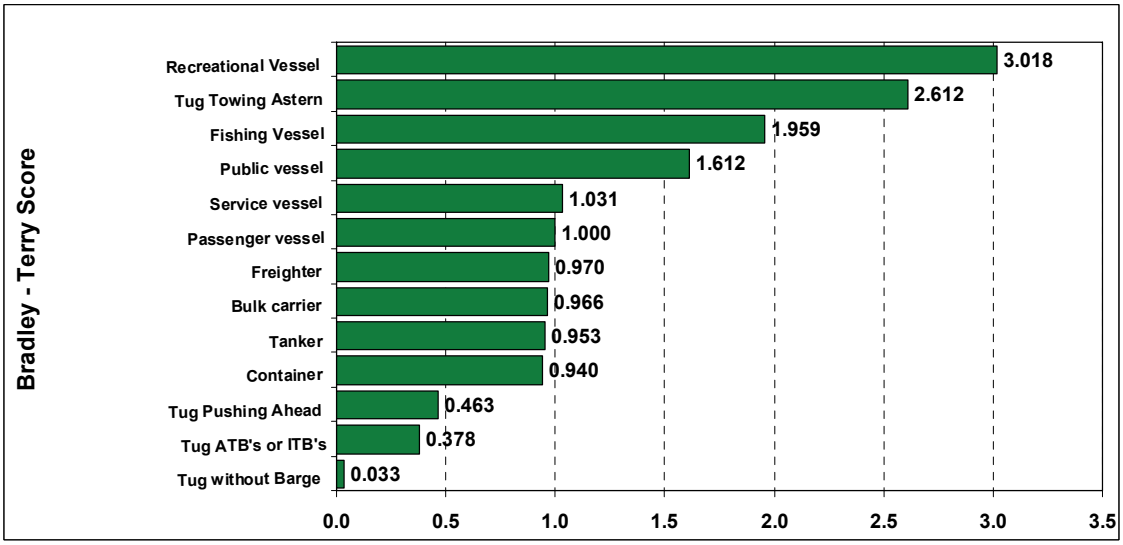

Figure D-10. Merged attribute scale for vessel types that follows from the scales presented in Figures D-9 and D-8.

Experts expressed that the US Navy vessels are of a higher concern within the "Public Vessel" classification in Table D-5, explaining possibly the relative high ranking of these vessels in the vessel type scale of Figure D-10.

While we did initially (in October 2008) arrive at individual consistency amongst 10 experts (5 pilots, 4 Ferry Masters and 1 Tug Master) in the vessel attribute scale, we unfortunately did not reach an agreement amongst these experts. When supplementing the expert judgment, however, with responses from three additional consistent tug operators (obtained in December 2008) while omitting the responses from the ferry masters, we did arrive at agreement amongst the tanker and tug operators. A possible reason for this phenomenon is that ferry masters evaluate waterway participants differently than tanker and tug operators. Following this outcome regarding vessel type scale development, it was decided for consistency to only use the tug and tank operators responses for the scale development of also the accident attributes "Location" and "Traffic Scenario" displayed in Figures D-5 and D-6. Scale developments for barges (Figure D-8) only involved tug operators from the start since only they have the appropriate experience level.

D-2.2. Attribute Parameter Assessment

Recall our collision accident probability model set-up specified by equation (D-1):

$$Pr(Collision|Incident,\ \underline{X}) = P_0 exp\left\{\underline{\beta}^T \underline{X}\right\}$$

In (D-1) an incident can either be a propulsion failure, steering failure, navigational aid failure, human error or, finally, a nearby vessel failure. The n-dimensional vector $\underline{X}$ describes particular situation on a waterway in terms of accident attributes. Attributes for the tanker and tug accident probability models are defined in Tables D-2 through D-5. The previous section discussed the development of quantitative measurement scales for the elements of the vector $\underline{X}$.

Prior to assessment of the parameter vector $\underline{\beta}$ all accident attributes $\underline{X}$ scales are pre-normalized on a $[0, 1]$ scale such that the vector $\underline{X} = \underline{0}$ describes the least "risky" situation and the vector $\underline{X} = \underline{1}$ describes the most "risky" situation. While some accident attributes have a natural ordering (such as bad visibility ($X = 1$) being worse than good visibility ($X = 0$) others required the use of expert judgment Bradley-Terry Paired comparison questionnaires to arrive at such an ordering (see Figures D-5, D-6, D-8 and D-10). From (1) we have:

$\underline{X} = \underline{0}$: $$Pr(Collision|Incident, \underline{X}) = P_0$$

$\underline{X} = \underline{1}$: $$Pr(Collision|Incident, \underline{X}) = P_0 exp\Big\{\sum_{i=1}^{n}\beta_i\Big\} > P_0 \Leftrightarrow \sum_{i=1}^{n}\beta_i > 0$$

Hence, the parameter P_0 may be interpreted as a base rate probability or the probability of a collision given the incident in the least "risky" situation. Each parameter β_i thus describes that going from best $(X_i = 0)$ to worst $(X_i = 1)$ in an accident attribute i, the base rate probability goes up by a multiplicative factor of $Exp(\beta_i) > 1$ if $\beta_i > 0$. Going from the least risky situation $\underline{X} = \underline{0}$ to the most risky situation $\underline{X} = \underline{1}$ then results in a multiplication factor of:

$$\prod_{i=1}^{n} Exp\{\beta_i\} = exp\Big\{\sum_{i=1}^{n}\beta_i\Big\} > 1 \;\Leftrightarrow\; \sum_{i=1}^{n}\beta_i > 0. \qquad \text{(D-4)}$$

The parameters β_i are estimated using expert judgment elicitation by fixing the incident type and asking a series of paired comparisons questions. In each question an experts is asked "how much more or less likely" a collision is to occur in Situation 1 ($\underline{X}_1$) compared to Situation 2 ($\underline{X}_2$) given the occurrence of an incident. His or her answer gives us, for this particular comparison of Situations 1 and 2, the value of:

$$\frac{Pr(Collision|Incident, \underline{X}_1)}{Pr(Collision|Incident, \underline{X}_2)} = \frac{P_0 exp\Big\{\underline{\beta}^T \underline{X}_1\Big\}}{P_0 exp\Big\{\underline{\beta}^T \underline{X}_2\Big\}} = exp\Big\{\underline{\beta}^T[\underline{X}_1 - \underline{X}_2]\Big\} \qquad \text{(D-5)}$$

Taking the natural logs on both sides of (D-5) results in:

$$\ln\left\{\frac{Pr(Collision|Incident, \underline{X}_1)}{Pr(Collision|Incident, \underline{X}_2)}\right\} = \underline{\beta}^T[\underline{X}_1 - \underline{X}_2]. \qquad \text{(D-6)}$$

From (D-6) it follows that the parameters β_i may now be estimated via a linear regression method on the log responses of the experts to a series of paired comparison questions. Details of our regression method are described in Szwed *et. al* (2006). The context for the example analysis in Szwed *et. al* (2006) was the Washington State Ferry Risk Assessment. In this study a total of 8 experts were used for the parameter assessment part of the collision probability model. In this VTRA study, 11 experts provided responses for the tanker collision accident probability model and 9 experts for the tug collision accident probability model.

Similar to the Bradley-Terry questionnaires the responses to the questionnaires are anonymous. Experts were told that the information they provide through the survey will be aggregated with that from other responders to link the occurrence of an incident (a failure that creates an unsafe situation) on the tanker or tug with the likelihood of a collision with another vessel. During a first questionnaire the incident in question was the propulsion failure (see Figure D-11).

Before starting the expert judgment elicitation session the graphical format (see Figure D-12) of an example question was explained to the experts. Figure D-7 was provided to explain the location attribute and Table D-6 was provided to explain the vessel type attribute in the example question of Figure D-12. It was explained that in the example question of Figure D-12 that in SITUATION 1 ON THE LEFT, an 'INBOUND' 'LADEN' tanker is en route in the 'STRAIT OF JUAN DE FUCA EAST'. It is being escorted by '1 ESCORT VESSEL' that is 'UNTETHERED'. A 'CROSSING THE BOW' situation is occurring with a 'SHALLOW DRAFT PASSENGER VESSEL' that is 'LESS THAN 1 MILE' away. The visibility is 'MORE THAN 0.5 MILE' and a wind of 'LESS THAN 10 KNOTS' is blowing with a direction 'ALONG' the tanker. The current is 'ALMOST SLACK' and the residual current is 'ALONG TANKER - OPPOSITE DIRECTION'. SITUATION 1 differs from SITUATION 2 in terms of visibility only, i.e. in SITUATION 1 the visibility is good and 'MORE THAN 0.5 MILE' vessel and in SITUATION 2 the visibility is bad and 'LESS THAN HALF MILE'.

It was explained to the experts that these situations in Figure D-12 describes the traffic scenario just before the occurrence of a COMPLETE PROPULSION LOSS on the TANKER. The expert were next asked, given the occurrence of the COMPLETE PROPULSION LOSS and the two traffic scenarios, to compare the two situations in terms of the likelihood of a collision with the interacting vessel. If they thought, given the COMPLETE PROPULSION LOSS on the TANKER, collision is equally likely in both situations they could circle 1 in the scale of Figure D-12. In Figure D-12, a six is circled towards Situation 1, which would mean that the expert would have assigned a six times higher likelihood of a collision in Situation 1 as compared to Situation 2.

Explanation of an Example Question

Your responses to this questionnaire will be used to develop an accident probability model to be used in conjunction with a Maritime Simulation for the Vessel Traffic Risk Assessment (VTRA) Study. The objective of this questionnaire is to link the occurrence of an INCIDENT (a failure that creates an unsafe situation) on the TANKER with the likelihood of a COLLISION with another vessel. The INCIDENT in this questionnaire is the occurrence of a COMPLETE PROPULSION LOSS on the TANKER while underway.

This questionnaire consists of a series of PAIRED SITUATION COMPARISONS. Each situational description consists of a set of important system characteristics. The paired situations in each question differ only in the value of one characteristic. For example, the two situations may be identical except for visibility. You are asked to compare each of the two situations described and answer the following questions:

1. Given that a COMPLETE PROPULSION has occurred on the TANKER and another vessel is close-by (this is described in more detail in the situations), in which situation would collision with this vessel be more likely?
2. How much more likely is the collision in the situation you selected in question 1, compared to the other situation.

Figure D-11. Example introduction of a paired comparison questionnaire of situations for accident attribute parameter assessment.

Q30		
Situation 1	**TANKER DESCRIPTION**	**Situation 2**
Strait of Juan de Fuca East	**Location**	-
Inbound	**Direction**	-
Laden	**Cargo**	-
1 Escort	**Escorts**	-
Untethered	**Tethering**	-
	INTERACTING VESSEL	
Shallow Draft Pass. Vessel	**Vessel Type**	-
Crossing the Bow	**Traffic Scenario**	-
Less than 1 mile	**Traffic Proximity**	-
	WATERWAY CONDITIONS	
More than 0.5 mile Visibility	**Visibility**	Less than 0.5 mile Visibility
Along Vessel	**Wind Direction**	-
Less than 10 knots	**Wind Speed**	-
Almost Slack	**Current**	-
Along Vessel - Opposite Direction	**Current Direction**	-
More? : ____	9 8 7 (6) 5 4 3 2 1 2 3 4 5 6 7 8 9	**____: More?**
Situation 1 is worse	<==========X==========>	**Situation 2 is worse**

Figure D-12. Example question of a paired comparison questionnaire of situations for tanker collision accident attribute parameter assessment given a propulsion failure.

Questionnaire 1 consisted for the estimation of the parameters of the tanker collision probability model of 44 pair wise comparison questions. The question were further subdivided in three parts. During Questions 1 through 18 the "Tanker Description" varied from Situation 1 to Situation 2 in a single attribute, whereas the description of the "Interacting Vessel" and the "Waterway Conditions" were held constant. During Questions 19 through 29 the "Interacting Vessel" varied from Situation 1 to Situation 2 in a single attribute, whereas the "Tanker Description" and the "Waterway Conditions" were held constant. Finally, during Questions 30 through 44 the "Waterway Conditions" varied from Situation 1 to Situation 2 in a single attribute, whereas the "Tanker Description" and the "Interacting Vessel" were held constant.

Questionnaire 1 consisted for the estimation of the parameters of the tug collision probability model of 47 pair wise comparison questions. The questions were further subdivided in three parts. During Questions 1 through 15 the "Tug Description" varied from Situation 1 to Situation 2 in a single attribute, whereas the description of the "Interacting Vessel" and the "Waterway Conditions" were held constant. During Questions 16 through 27 the "Interacting Vessel" varied from Situation 1 to Situation 2 in a single attribute, whereas the "Tug Description" and the "Waterway Conditions" were held constant. Finally, during Questions 28 through 47 the "Waterway Conditions" varied from Situation 1 to Situation 2 in a single attribute, whereas the "Tug Description" and the "Interacting Vessel" were held constant.

Figure D-13 shows the format of the same 44 pairwise comparison questions of a second questionnaire following Questionnaire 1. The purpose of the second questionnaire is to elicit the relative likelihood of a collision accident (of a tanker in case of Figure D-13) given the other incidents: steering failure, navigational aid failure, human error or a nearby vessel failure. Questionnaire 1 focused on the collision accident given a propulsion failure on the tanker. By separating the questionnaire in two parts the experts focus in Questionnaire 1 on the paired comparison of situations (given the propulsion failure). Before answering Questionnaire 2 experts were asked to first copy their answers from Questionnaire 1 in Questionnaire 2. Hence, this provided the benefit of having their answer of Questionnaire 1, prior to answering the paired comparison of situations for the other incident types. We believe this fosters consistency in the expert responses while experts were able to focus on the differences that the various incidents may have when answering a particular comparison of two situations.

Situation 1	TANKER DESCRIPTION	Situation 2
Strait of Juan de Fuca East	**Location**	-
Inbound	**Direction**	-
Laden	**Cargo**	-
1 Escort	**Escorts**	-
Untethered	**Tethering**	-
	INTERACTING VESSEL	
Shallow Draft Pass. Vessel	**Vessel Type**	-
Crossing the Bow	**Traffic Scenario**	-
Less than 1 mile	**Traffic Proximity**	-
	WATERWAY CONDITIONS	
More than 0.5 mile Visibility	**Visibility**	-
Along Vessel	**Wind Direction**	-
Less than 10 knots	**Wind Speed**	25 knots
Almost Slack	**Current**	-
Direction	**Current Direction**	-

Complete Propulsion Loss		
More? : ____	**9 8 7 6 5 4 3 2 1 2 3 4 5 6 7 8 9**	**____ : More?**
Situation 1 is worse	**<==========X==========>**	**Situation 2 is worse**

Complete Steering Loss at a Moderate Angle		
More? : ____	**9 8 7 6 5 4 3 2 1 2 3 4 5 6 7 8 9**	**____ : More?**
Situation 1 is worse	**<==========X==========>**	**Situation 2 is worse**

Complete Navigational Aid Loss		
More? : ____	**9 8 7 6 5 4 3 2 1 2 3 4 5 6 7 8 9**	**____ : More?**
Situation 1 is worse	**<==========X==========>**	**Situation 2 is worse**

Human Error		
More? : ____	**9 8 7 6 5 4 3 2 1 2 3 4 5 6 7 8 9**	**____ : More?**
Situation 1 is worse	**<==========X==========>**	**Situation 2 is worse**

Nearby Vessel Incident (but you do not know the specifics)		
More? : ____	**9 8 7 6 5 4 3 2 1 2 3 4 5 6 7 8 9**	**____ : More?**
Situation 1 is worse	**<==========X==========>**	**Situation 2 is worse**

Figure D-13. Example question of a paired comparison questionnaire of situations for tanker collision accident attribute parameter assessment given all incidents.

With all the responses recorded and having the attribute scales from the previous section we assess the values of the parameters $\underline{\beta}$ following our technique detailed in Szwed et. al (2006). Besides accounting for the direct effect of the attributes in Tables D-2 through D-5, we also allowed for the potential of some interaction effects. Interaction effects modeled involved "Location", "Cargo", "Escort" and "Tethered" as a group in case of tankers, and also "Fog", "Current" and "Current Directions" as a second group. Interaction effects modeled involved "Location", "Cargo", "Hookup" as a group in case of tugs and also "Fog", "Current", and "Current Directions" as a second group.

The tanker collision accident probability questionnaire given a propulsion failure consisted of 44 questions similar to the one displayed in Figure D-12. The questions were distributed evenly over the 13 accident attributes in Table 2 (i.e. 3 to 4 questions per changing attribute). The 22×22 design matrix A of the questionnaire (see Equation (11) in Szwed et. al (2006)) is of the following form

$$A = \begin{bmatrix} A_{11} & A_{12} \\ A_{21} & A_{22} \end{bmatrix} \tag{D-7}$$

where A_{11} is a 13×13 diagonal matrix with diagonal elements

$$(0.186, 4.0, 4.0, 6, 1.5, 3.0, 0.4716, 2.268, 3.0, 3.0,\ 4.0, 0.281, 3.0, 3.0) \tag{D-8}$$

and associated with the main attributes factors $X_1, \ldots, X_{13}$. (The matrix A_{11} in (D-7) is a diagonal matrix since the paired comparison scenarios $\underline{X}_1$ and $\underline{X}_2$ only differed in accident attributes (see Figure D-12)). The matrix A_{22} in (D-7) is a symmetric 9×9 matrix with elements displayed in Figure D-14 and is associated with the interaction effects $X_{14}, \ldots, X_{22}$. Finally, the matrix $A_{21} = A_{12}^T$ is a sparse 9×13 matrix with only positive elements associated with the contributing factors X_1, X_3, X_4, X_5, X_9, X_{12}, X_{13} that are included in the interaction effects $X_{14}, \ldots, X_{22}$. The matrix A_{21} is displayed in Figure D-15.

	LOC*BAL	LOC*ESC	LOC*TETH	BAL*ESC	BAL*TETH	ESC*TETH	FOG*CUR	FOG*CD	CUR*CD
LOC*BAL	.3707	.0232	.0465	.2755	.551	.	.	.	.
LOC*ESC	.0232	.1539	.0465	.3593	.	.2755	.	.	.
LOC*TETH	.0465	.0465	.2484	.	.6109	.1377	.	.	.
BAL*ESC	.2755	.3593	.	2.5	1.	1.	.	.	.
BAL*TETH	.551	.	.6109	1.	5.	.5	.	.	.
ESC*TETH	.	.2755	.1377	1.	.5	1.25	.	.	.
FOG*CUR	.	.	.	.	.	.	2.	.	.
FOG*CUR_DIR	.	.	.	.	.	.	.	2.	.
CUR*CUR_DIR	.	.	.	.	.	.	.	.	2.

Figure D-14. Matrix A_{22} in Equation (D-7).

	LOC	DIR	BAL	ESC	TETH	TT_1	TS_1	TP_1	FOG	WD	WS	CUR	CD
LOC*BAL	.1395	.	.8863	.	.	.	.	.	.	.	.	.	.
LOC*ESC	.0697	.	.	.3593	.	.	.	.	.	.	.	.	.
LOC*TETH	.093	.	.	.	.6109	.	.	.	.	.	.	.	.
BAL*ESC	.	.	1.	1.5	.	.	.	.	.	.	.	.	.
BAL*TETH	.	.	2.	.	3.	.	.	.	.	.	.	.	.
ESC*TETH	.	.	.	1.	.5	.	.	.	.	.	.	.	.
FOG*CUR	.	.	.	.	.	.	.	.	1.	.	.	1.	.
FOG*CD	.	.	.	.	.	.	.	.	1.	.	.	.	1.
CUR*CD	.	.	.	.	.	.	.	.	.	.	.	1.	1.

Figure D-15. Matrix A_{21} in Equation (D-7).

The questionnaire was designed in a manner such that the resulting questionnaire design matrix A is positive definite (and thus invertible), but equally important, involved meaningful

paired comparisons consistent with realistic scenarios in the VTRA study area. The latter required maritime knowledge about the VTRA maritime transportation system acquired by the team over the course of this project.

Table D-8 below summarizes the vector $\underline{b}$ (see Equation (11) in Szwed et. al (2006)) for each of the eleven expert responses to the 44 questions in terms of

$$\sum_{j=1}^{44} q_{ij} z_j$$

for each of the accident attributes $X_i, i = 1, \ldots, 13$ and interaction effects X_i, $i = 14, \ldots, 22$. From Table D-8 we may assess the consistency in the expert judgment with respect to the ordering of the attribute scale of the elements $X_i, i = 1, \ldots, 16$ developed in the previous section. A positive (negative) value indicates agreement with the ordering of that particular scale. For example, the row in Table D-8 associated with the contributing factor TP_1 (Traffic Proximity of interacting vessel) shows that all experts responded (not surprisingly) that vessels further away pose less (immediate) collision risk. The largest discrepancy with the ordering of an attributes scale amongst the 11 experts is observed in the TT_1 (Traffic Type of interacting vessels). Four out of the 11 experts exhibit a negative response coefficient for this particular accident attribute. The elements

$$c = \sum_{j=1}^{60} z_j^2$$

(see Equation (11) in Szwed et. al (2006)) for each individual expert are provided in Table D-9.

With the matrix A, vectors $\underline{b}$, scalars c, we can update apriori attribute parameters settings of the parameter vector $\underline{\beta}$ (see equation D-1) specified in Figure D-16 using a Bayesian analysis. The resulting aposteriori parameters settings are provided schematically in Figure D-17. The parameter ranges of ≈ 80 specified in Figure D-16 are the 80% a prior credibility intervals for the parameters $\underline{\beta}$ (i.e. the lower bound represents the 10% quantile and the upper bound the 90% quantile). Please note that apriori a zero average effect is assessed for each element in the parameter vectors $\underline{\beta}$. The posterior 80% credibility interval have a much smaller range with a maximum range of approximately 1.5. This demonstrates convergence of the expert judgment. The parameter vectors $\underline{\beta}$ for the tanker collision accident probability model (given a propulsion failure) will be set equal to the midpoints of these aposteriori 80% credibility

intervals. The values of these parameter settings are summarized in the first column of Table D-10.

Table D-8. The vector $\underline{b}$ summarizing expert responses (see Equation (11) in Szwed et. al (2006)) for the tanker collision accident probability questionnaire given a propulsion failure.

	EXP 1	EXP 2	EXP 3	EXP 4	EXP 5	EXP 6	EXP 7	EXP 8	EXP 9	EXP 10	EXP 11
LOC	0.000	1.929	1.308	0.922	1.340	0.685	0.860	0.897	0.598	1.010	1.046
DIR	0.000	0.000	0.000	0.000	0.000	0.000	0.000	0.000	0.000	0.000	0.000
BAL	5.011	0.000	4.159	6.174	6.215	3.178	5.704	2.890	4.394	3.178	6.215
ESC	1.946	4.494	2.079	2.485	0.000	1.792	1.733	1.445	1.040	1.956	2.890
TETH	2.890	0.000	3.466	4.159	3.296	2.485	2.890	2.079	2.079	2.079	3.178
TT_1	1.802	-1.743	-0.309	-0.164	0.659	0.347	0.233	0.651	-0.169	0.325	0.313
TS_1	-2.536	1.091	2.773	2.808	2.306	-0.047	2.349	2.022	3.735	2.022	1.395
TP_1	5.951	4.159	4.564	5.257	7.313	2.890	2.197	2.485	1.792	2.773	5.375
FOG	5.347	6.908	4.159	4.787	3.584	3.466	3.584	2.708	3.296	2.079	5.375
WD	5.886	3.892	0.000	0.000	0.693	4.605	1.099	1.099	1.386	-1.792	1.386
WS	0.318	1.084	1.192	0.672	0.260	0.780	0.520	0.824	0.520	0.000	0.520
CUR	-1.099	0.000	5.455	3.401	1.792	2.773	2.079	1.386	0.000	1.386	4.159
CD	3.584	0.000	1.386	3.401	0.000	1.099	1.386	0.693	0.693	0.693	1.386
LOC*BAL	1.144	1.345	1.918	2.025	2.454	1.262	2.045	1.157	1.422	1.437	2.160
LOC*ESC	0.536	1.897	1.034	0.983	0.472	0.687	0.745	0.772	0.511	0.956	1.126
LOC*TETH	0.559	1.032	1.429	1.383	1.317	0.747	1.033	1.021	0.722	0.959	1.174
BAL*ESC	3.555	4.494	3.466	4.277	1.609	2.890	3.342	1.445	2.138	3.055	4.500
BAL*TETH	6.109	0.000	5.545	7.560	6.515	4.277	6.109	2.773	4.277	3.871	6.397
ESC*TETH	2.495	2.996	1.733	2.079	0.549	1.445	1.936	1.445	1.040	1.956	2.485
FOG*CUR	0.000	2.303	3.258	2.890	2.485	2.079	1.792	1.609	1.099	1.386	3.178
FOG*CD	2.890	2.303	1.386	2.708	1.099	0.000	2.079	0.000	1.099	0.693	1.792
CUR*CD	2.996	0.000	3.178	3.219	0.693	2.485	1.386	1.386	0.693	0.693	2.773

Table D-9. The scalars c summarizing expert responses (see Equation (11) in Szwed et. al (2006)) for the tanker collision accident probability questionnaire given a propulsion failure.

EXP 1	EXP 2	EXP 3	EXP 4	EXP 5	EXP 6	EXP 7	EXP 8	EXP 9	EXP 10	EXP 11
81.113	91.757	59.527	61.779	70.927	36.457	36.245	28.921	28.885	26.179	60.289

The parameter settings for the tanker collision accident probability model given the remaining incidents are solved for in a similar manner. While the paired comparison questions remained the same (and thus also the questionnaire design matrix A), a separate set of response vectors $\underline{b}$, and scalars c follow for each remaining incident type: steering failure, navigational aid failure, human error and nearby vessel failure. The parameter settings of the vectors $\underline{\beta}$ for the collision tanker accident probability model are summarized in Table D-10. Table D-11 summarizes the parameters setting for the tug collision accident probability model for each incident type.

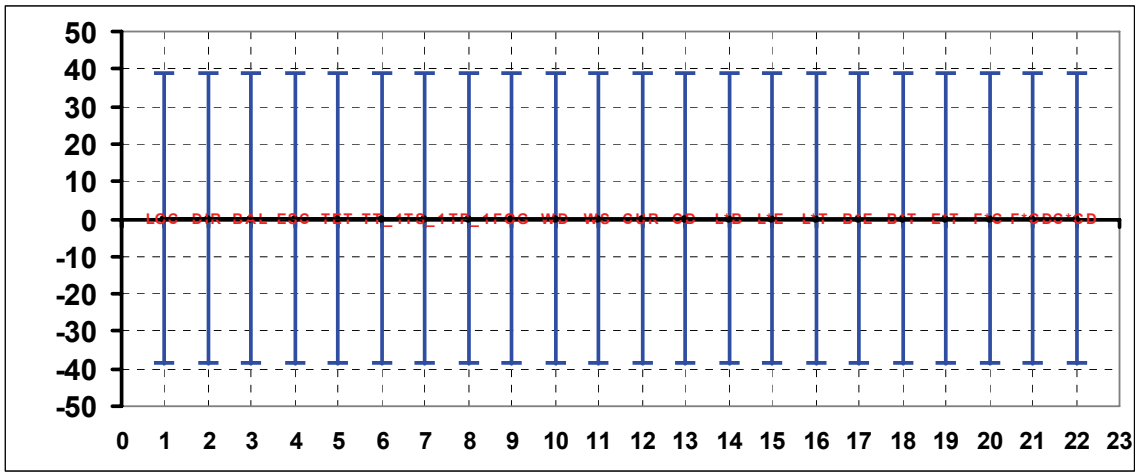

Figure D-16. Apriori specification of tanker accident attribute parameters given a propulsion failure (prior to updating with the expert judgment responses).

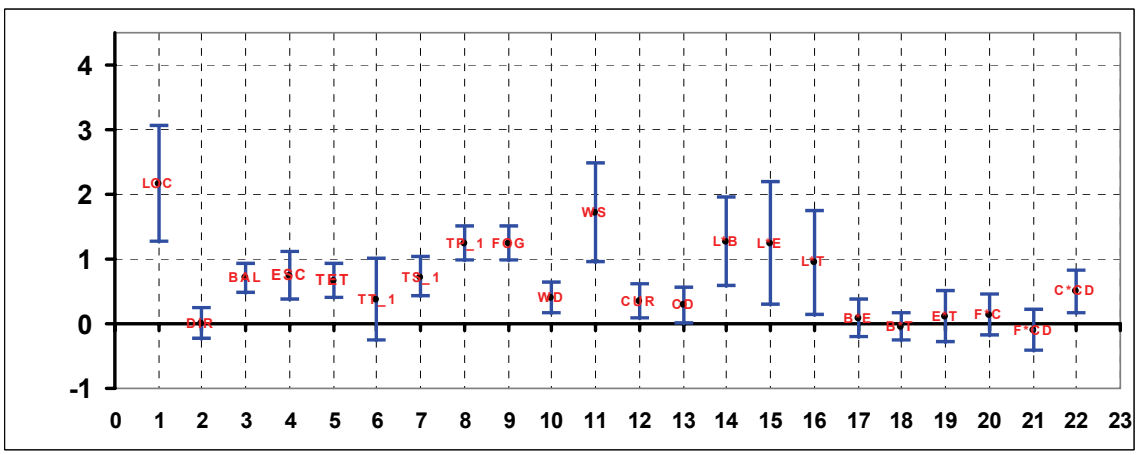

Figure D-17. Aposteriori tanker accident attribute parameters given a propulsion failure (after updating with the expert judgment responses).

The parameter P_0 in expression (D-1) does not follow from the expert judgment elicitation. Instead we solve for this parameter through a calibration step after the relative collision accident probability models for tugs and tankers have been integrated in a maritime simulation of the waterway. This maritime simulation records waterway situations as described by the attribute vectors $\underline{X}$ in Tables D-1 through D-4 in a database. Since these situations share the common base rate probability P_0 we may solve for P_0 by setting the expected number of collisions during a simulation run over a period equal to the empirical average annual number of collisions in that same period. Table D-12 provides the values for

P_0 given the different incident types for the tanker and tug collision accident probability model.

Table D-10. Attribute accident parameters for tanker accident probability models

ID	NAME	Propulsion Failure	Steering Failure	Nav. Aid Failure	Human Error	NBV Failure
1	LOC	2.164	3.038	1.642	2.969	1.785
2	DIR	0.000	-0.040	-0.015	-0.036	-0.024
3	BAL	0.700	0.876	0.542	0.937	0.691
4	ESCORTS	0.745	0.876	0.394	0.626	0.356
5	TETHERED	0.652	1.058	0.408	0.885	0.462
6	TT_1	0.369	0.185	-0.095	-0.063	0.183
7	TS_1	0.715	0.979	0.486	0.943	0.887
8	TP_1	1.231	1.607	0.847	1.387	1.138
9	FOG	1.247	1.413	1.442	1.446	1.310
10	WD	0.399	0.588	0.203	0.458	0.333
11	WS	1.708	1.631	1.037	1.440	1.429
12	CURRENT	0.345	0.831	0.565	0.814	0.599
13	CUR_DIR	0.278	0.475	0.477	0.436	0.426
14	LOC*BAL	1.271	1.746	0.879	1.631	1.020
15	LOC*ESC	1.229	1.424	0.673	1.265	0.768
16	LOC*TETH	0.940	1.554	0.803	1.242	0.743
17	BAL*ESC	0.084	0.392	0.119	0.260	0.117
18	BAL*TETH	-0.047	0.074	0.029	-0.001	0.000
19	ESC*TETH	0.104	0.104	-0.018	-0.076	-0.076
20	FOG*CUR	0.130	0.268	0.420	0.270	0.191
21	FOG*CUR_DIR	-0.109	0.024	0.261	0.171	0.130
22	CUR*CUR_DIR	0.490	0.237	0.107	0.146	0.051

Table D-11. Attribute accident parameters for tug accident probability models

ID	NAME	Propulsion Failure	Steering Failure	Nav. Aid Failure	Human Error	NBV Failure
1	LOC	0.760	0.822	0.737	1.270	0.846
2	DIR	0.028	0.194	0.032	0.184	0.067
3	Bal	1.909	1.630	1.168	1.611	1.337
4	HKP	1.336	1.482	0.865	0.981	0.876
5	TT_1	0.762	0.910	0.269	0.701	0.595
6	TS_1	0.661	0.654	0.663	0.820	0.825
7	TP_1	1.227	1.421	0.791	1.505	1.015
8	VIS	1.286	1.478	1.393	1.632	1.138
9	WD	1.145	1.024	0.558	0.862	0.701
10	WS	3.341	3.425	1.756	3.059	1.992
11	CUR	1.503	1.568	0.854	1.507	1.108
12	CUR_DIR	1.233	1.024	0.655	0.883	0.796
13	LOC*BAL	0.765	0.737	0.560	0.868	0.638
14	LOC*HKP	0.351	0.354	0.278	0.516	0.392
15	BAL*HKP	1.389	1.313	0.856	1.158	0.908
16	FOG*CUR	0.260	0.201	0.288	0.216	0.199
17	FOG*CUR_DIR	0.285	0.236	0.433	0.254	0.143
18	CUR*CUR_DIR	0.326	0.223	0.264	0.124	0.104

In our prior studies the grounding accident model had exactly the same form as (D-1), but separate grounding base rate probability P_0 were solved for by calibrating to an empirical average number of grounding accidents. Whereas the collision accident probability calibration used interaction counts with other vessel for calibration purposed, the grounding accident probability models only used the interaction counts of the tanker with the system and thus this was a purely time-based analysis. The grounding model in our prior studies was not able to directly take into account the congestion of a waterway and was only able to accommodate that indirectly through the location accident attribute. This analysis was next

followed by a separate drift grounding simulation to determine likely locations of groundings.

Table D-12. Calibrations values for P_0 for the tanker and tug collision accident probability models

	Po
Propulsion Failure	1.90743E-05
Steering Failure	1.90743E-05
Nav. Aid Failure	1.90743E-05
Human Error	2.15758E-05
NBV Failure	2.15758E-05

The grounding accident probability model (D-2) in this VTRA project is improved over the grounding model in the Prince William Sound Risk Assessment in the sense that it now explicitly accounts for the congestion of a waterway. We now record, within the maritime simulation, the time t to shore depending on the distance of a vessel from the shore and whether the vessel would be drifting to shore or would be under power. A powered grounding is interpreted as a grounding preceded by a human error, navigational aid failure or a nearby vessel failure. When the vessel is under power, a 5 hour straight track line is projected in the direction of the vessel to the closest shore point and we record the shore location and the amount of time to shore t in addition to the same accident attributes $\underline{X}$ as specified in Tables D-2 through D-5. Our motivation is here that those shore points that have a tanker or tug coming directly towards it more frequently, have a higher likelihood of power grounding keeping everything else the same. If a 5 hours track line does not intersect with the shore line, we assume that no interaction with the shore is occurring resulting effectively in a zero grounding probability for that case. Within the VTRA study area it would seem reasonable that it would be highly likely that a vessel traveling in a straight line for 5 hours would obtain a course correction as result of the external vigilance from the Canadian VTS or Seattle VTS. The counting procedure above is followed except in the case when a vessel has started docking procedures for a certain dock and is within one mile of its intended dock. In the latter case, we consider the interactions above to be allision interactions since the vessel intentionally tries to get close to shore in that case.

A drift grounding is interpreted as grounding preceded by a propulsion failure or a steering failure. When the vessel is drifting we project a drifting path taking into account wind direction and speed, current direction and speed, and the vessel slowing down through the

water as the result of a loss of propulsion. We evaluate the amount of time to shore t in addition to the same accident attributes $\underline{X}$ as in (D-1). We project here also a 5 hour time path. The same counting procedure as above applies to this 5 hour threshold as well. It would seem impossible given the established external vigilance within the VTRA study area that a vessel would be drifting for more than 5 hours without some form of intervention occurring in the mean time.

It is important to stress that when we evaluate the time to shore t and the location of the shore point interaction, that we make the assumption that the drift path or straight line path is not altered within this 5 hour time frame by some form of intervention. This too seems unlikely given the safeguards and vigilance already provided by the Puget Sound Pilots, the US Coast Guard, the Canadian Coast Guard and the other VTRA Study area users. However, how one would respond to an actual occurrence of an incident (as opposed to a simulated one in our simulation) involves making tactical decisions that takes the exact situation into account and not only the abstraction of reality that we have created in our maritime simulation. Indeed it would be impossible for us to model the complex human responses to such incidents occurring and evaluate the shore line interaction location accordingly. Hence, a disclaimer of our grounding analysis results is warranted in the sense that our analysis results should be used to make strategic (long term) decisions regarding waterway risk. Our geographic profile analysis results only display a tendency towards areas with higher and lower grounding accident rates keeping a broader risk management perspective in mind.

Returning to the development of and recalling the grounding accident probability model (D-2)

$$Pr(Grounding|Incident, \underline{X}, t) = P_0 exp\Big\{ -\alpha_0[1 + \underline{\gamma}^T(\underline{1} - \underline{X})] \times t\Big\}$$

$$= P_0 exp\Big\{ -\alpha_0 t - \alpha_0 \underline{\gamma}^T(\underline{1} - \underline{X})t\Big\} = P_0 exp\Big\{ -\alpha_0 t\Big\} exp\Big\{ -\alpha_0 \underline{\gamma}^T(\underline{1} - \underline{X})t\Big\}$$

we observe the probability of grounding decreasing when the time to shore t increases in the equation above. If the time to shore becomes very large (or goes to infinity) the grounding probability model goes to 0 under the conditions that

$$\alpha_0 > 0 \text{ and } \sum_{i=1}^{n} \gamma_i > 0.$$

Recalling that accident attributes $\underline{X}$ are all pre-normalized on a $[0,1]$ scale such that the vector $\underline{X} = \underline{0}$ describes the least "risky" situation and the vector $\underline{X} = \underline{1}$ describes the most "risky" situation, we have from (D-2):

$\underline{X} = \underline{0}$:

$$Pr(Grounding|Incident, \underline{X}, t) = P_0 exp\Big\{-\alpha_0 t\Big\} exp\Big\{-\alpha_0\Big[\sum_{i=1}^{n}\gamma_i\Big]t\Big\} \quad \text{(D-9)}$$

$\underline{X} = \underline{1}$:

$$Pr(Grounding|Incident, \underline{X}, t) = P_0 exp\Big\{-\alpha_0 \times t\Big\} \quad \text{(D-10)}$$

The parameter α_0 may thus be interpreted as the exponential rate of decrease in the probability of grounding as a function of time to shore in the most risky state $\underline{X} = \underline{1}$. Each parameter γ_i describes that by going from worst $(X_i = 1)$ to best $(X_i = 0)$ in an accident attribute this probability of grounding goes down by a multiplicative factor of $0 < exp\Big\{-\alpha_0\gamma_i t\Big\} < 1$. Going from the most risky situation $\underline{X} = \underline{1}$ to the least risky situation $\underline{X} = \underline{0}$, this probability of grounding goes down by a multiplicative factor of

$$0 < exp\Big\{-\alpha_0\Big[\sum_{i=1}^{n}\gamma_i\Big]t\Big\} < 1. \quad \text{(D-11)}$$

The parameters γ_i are envisioned to be estimated using expert judgment elicitation by fixing the incident type and by asking a series of paired comparisons questions. In each question an experts is asked "how much more or less likely" a grounding is to occur in Situation 1 ($\underline{X}_1$) compared to Situation 2 ($\underline{X}_2$) given the occurrence of an incident and still having t_q time to respond, where t_q is fixed for the entire questionnaire. The expert's answer would gives us, for a particular comparison of Situations 1 and 2, the value of:

$$\frac{Pr(Grounding|Incident, \underline{X}_1, t_q)}{Pr(Grounding|Incident, \underline{X}_2, t_q)} = \frac{exp\Big\{-\alpha_0[\underline{\gamma}^T(\underline{1} - \underline{X}_1) + 1]t_q\Big\}}{exp\Big\{-\alpha_0[\underline{\gamma}^T(\underline{1} - \underline{X}_2) + 1]t_q\Big\}} \Leftrightarrow$$

$$\ln\left[\frac{Pr(Grounding|Incident, \underline{X}_1, t_q)}{Pr(Grounding|Incident, \underline{X}_2, t_q)}\right] = -\alpha_0 t_q\Big\{[\underline{\gamma}^T(\underline{1} - \underline{X}_1) + 1] - [\underline{\gamma}^T(\underline{1} - \underline{X}_2) + 1]\Big\} \Leftrightarrow$$

$$\ln\left[\frac{Pr(Grounding|Incident, \underline{X}_1, t_q)}{Pr(Grounding|Incident, \underline{X}_2, t_q)}\right] = \{\alpha_0\, t_q \underline{\gamma}\}^T [\,\underline{X}_1 - \underline{X}_2] \qquad \text{(D-12)}$$

Now, substituting $\underline{\beta} = \{\alpha_0\, t_q \underline{\gamma}\}$ in (D-12) yields

$$\ln\left[\frac{Pr(Grounding|Incident, \underline{X}_1, t_q)}{Pr(Grounding|Incident, \underline{X}_2, t_q)}\right] = \underline{\beta}^T [\,\underline{X}_1 - \underline{X}_2] \qquad \text{(D-13)}$$

Please note that the right hand side of expression (D-13) is exactly the same as that of the right hand side of expression (D-6) when substituting

$$\underline{\beta} = \{\alpha_0\, t_q \underline{\gamma}\}^T \qquad \text{(D-14)}$$

Hence, similar to the accident probability models in the Prince William Sound Risk Assessment (see, Merrick et. al 2002) one could significantly reduce the expert judgment elicitation burden by reusing the parameter values β_i in Tables D-9 and D-10, provided we separately recalibrate the maritime risk simulation using grounding data and a separate counting routine to record powered and drift grounding interactions of a tanker or a tug with the shoreline (while recording the time to shore t). Further substitution of (D-14) into (D-2) yields,

$$Pr(Grounding|Incident, \underline{X}, t) = P_0 exp\Big\{-\alpha_0 t\Big\} exp\Big\{-\underline{\beta}^T(\underline{1} - \underline{X})\frac{t}{t_q}\Big\} \qquad \text{(D-15)}$$

and we may use t_q as a calibration constant similar to P_0 in the accident probability model.

Accessibility to experts during the Prince William Sound Risk Assessment (see, Merrick et al. 2002) was provided and guaranteed via a formal steering committee consisting of all stake holders. In the VTRA project expert judgment participation relied primarily on the willingness of experts (not directly affiliated with the project through their employer) to donate their time, without benefits to them other than that the results of the VTRA study could result in a "safer" waterway. We heavily relied on established relationships between the US Coast Guard and VTRA Waterway Participants and the Puget Sound Marine Exchange to arrange for elicitation session with tankers and tug boat operators. Despite this set-up we were able to muster the participation of 38 tanker and tug boat operators over seven separate elicitation session held over the course of one year. The participation of the experts to this study is greatly appreciated and these experts should be commended for their unselfish effort.

Unfortunately, however, the response rate to the organized elicitation sessions invitations at the US Coast Guard VTS decreased dramatically over time to the point that it became apparent that we had exhausted the available tanker and tug operator expert pool for this VTRA project. As soon as this became apparent over the course of the VTRA project, the use of expression (D-15) seems warranted. Moreover, when experts were asked informally the question (after the collision elicitation session) if their answers in the paired comparison scenario questionnaires would change if the accident scenario would have changed from a collision to a grounding, experts responded "no".

Further substitution of $\underline{X} = 1$ in (D-15) yields (see also (D-10)) :

$$Pr(Grounding|Incident, \underline{X} = 1, t) = P_0 exp\Big\{ - \alpha_0 t \Big\}. \qquad \text{(D-16)}$$

and from (D-16) we have;

$$\frac{Pr(Grounding|Incident, \underline{X} = 1, k)}{Pr(Grounding|Incident, \underline{X} = 1, (k-1))} = \frac{P_0 exp\Big\{ - \alpha_0 k \Big\}}{P_0 exp\Big\{ - \alpha_0 (k-1) \Big\}} = exp(- \alpha_0). \qquad \text{(D-17)}$$

Hence, we may interpret (D-17) such that in the worst state $(\underline{X} = 1)$, the probability of a grounding reduces by a factor of $exp(- \alpha_0)$. We propose to set $\alpha = ln(2)$. Indeed, in the absence of additional information, it would seem to be reasonable to assume that in a worst case scenario there is a $50 - 50\%$ chance that one would be able to perform a save on the vessel in distress in one additional available hour of time to respond. Over five hours this yields for the worst state $(\underline{X} = 1)$:

$$Pr(Grounding|Incident, \underline{X} = 1, 5) = P_0 (\frac{1}{2})^5 = \frac{P_0}{32} \qquad \text{(D-18)}$$

For the least risky state $(\underline{X} = 0)$ we obtain:

$$Pr(Grounding|Incident, \underline{X} = 0, 5) = P_0 (\frac{1}{2})^5 exp\Big\{ - \Big[\sum_{i=1}^{n} \beta_i\Big] \frac{5}{t_q} \Big\}. \qquad \text{(D-19)}$$

After calibration to 1 grounding accident per 11 years (this process will be discussed in more detail in the next section), we arrived at a value of $t_q = 0.834375$, a calibration value $P_0 = 0.52831297$
for the incident types "Human Error" and "Nearby Vessel Failure" and a calibration value $P_0 = 0.405335373$ given the incident types "Steering Failure", "Propulsion Failure" and "Navigational Aid Failure". Hence, with the parameters settings β_i for tankers and tugs in

Tables D-10 and D-11 we evaluate from (D-18) and (D-19) the values in Tables D-13 and D-14 for $Pr(Grounding|Incident, \underline{X}, 5)$ given least risk state ($\underline{X} = 0$) and the most risky state ($\underline{X} = 1$).

Table D-13. Probabilities of grounding given an incident failure in the least risk state ($\underline{X} = 0$) and a time to shore of 5 hours. These follow from (D-18) and the tanker and tug accident accident probability parameters specified in Tables D-9 and D-10.

	Tankers	Tugs
Propulsion Failure	9.729E-41	5.991E-51
Steering Failure	5.894E-53	2.756E-51
Nav. Aid Failure	8.714E-32	6.011E-35
Human Error	3.819E-47	9.576E-50
NBV Failure	4.367E-35	4.138E-38

Table D-14. Probabilities of grounding given an incident failure in the most risk state ($\underline{X} = 1$) and a time to shore of 5 hours. These follow from (D-18) and the tanker and tug accident accident probability parameters specified in Tables D-9 and D-10.

	Tankers	Tugs
Propulsion Failure	0.0127	0.0127
Steering Failure	0.0127	0.0127
Nav. Aid Failure	0.0127	0.0127
Human Error	0.0165	0.0165
NBV Failure	0.0165	0.0165

Please observe the information in Tables D-13 and D-14 to be consistent with the modeling assumption in the maritime simulation not to count interactions of a vessel with the shore when its future drifting path or straight line projection under power does not have an intersection with the shore within a five hour time frame.

Our approach towards parameter assessment of the accident probability model for allisions (D-3) is the same as that for the grounding accident probability model. The difference being primarily in the counting procedure of allision interactions. When a vessel is within one mile of its intended dock, the projected shore interactions of a drift path and a straight line path are designated as allision interactions instead of grounding interactions. Indeed, within one mile of the intended dock, docking procedures of the tankers and tugs will have commenced, speeds are lowered, escort vessels are in place and from that point on the vessel intentionally

tries to get close to the shore with a specific heading towards the shore. After calibration to 2 allision accidents per 11 years (this process will be discussed in more detail in the next section), we arrived at a value of $t_q = 0.384277$, a calibration value $P_0 = 1.039155$ for the incident types "Human Error" and "Nearby Vessel Failure" and a calibration value $P_0 = 0.894719$ given the incident types "Steering Failure", "Propulsion Failure" and "Navigational Aid Failure".

D-3. Representative results of the expert judgment

An example question in the collision accident probability questionnaire given a propulsion failure on a tanker was presented in Figure D-12. This question is repeated in Figure D-18 with underneath it the prior setting of the relative likelihood of a collision in Situation 1 compared to Situation 2. We refer to this as a prior setting, since this figure presents the relative likelihood prior to updating with the acquired expert knowledge (i.e. the expert responses). Observe from Figure D-18 that apriori we assign a 50-50% chance that Situation 1 has a higher likelihood than Situation 2 (and vice versa). In Figure D-18 the changing attribute is visibility and even though it would be quite natural to assign a higher likelihood of collision in Situation 2 (bad visibility) as compared to Situation 1 (good visibility), we still apriori assign a median likelihood of 1 to this relative likelihood. A 75% a priori credibility interval (an interval with 75% chance of falling in this interval) for the relative likelihood here equals $[1/6974,\ 6974]$. Hence, with 75% we say that the relative likelihood of Situation 1 is 6974 times higher than that of Situation 2, or vice versa. Summarizing, our apriori setting does not sway in one direction or the other regardless of the changing attribute in a particular pair wise comparison question of two situations.

Next, we update this apriori relative likelihood using the expert responses and the method described in Szwed et. al (2006). Figure D-19 provides the 11 expert responses to this particular question and even though the experts do no agree, we do notice that they all assign a higher relative likelihood to Situation 2 (bad visibility) than Situation 1 (good visibility). Included in Figure D-19 is also the empirical average (slightly larger than 4) of the average responses for this particular question. The aposteriori average in for this particular question (also indicated in Figure D-19) is slightly less than 4. The reason why this aposteriori average is different from the empirical average is that in the calculation of the aposteriori average also the responses of the experts to all the other questions are taken into account. Recalling the 75% apriori credibility interval of $[1/6974,\ 6974]$, we obtain after updating with the expert responses a 90% aposteriori credibility interval for the relative likelihood of $[2.47,\ 4.90]$ and an average aposteriori relative likelihood of 3.60.

Q30

Situation 1	TANKER DESCRIPTION	Situation 2
Strait of Juan de Fuca East	Location	-
Inbound	Direction	-
Laden	Cargo	-
1 Escort	Escorts	-
Untethered	Tethering	-
	INTERACTING VESSEL	
Shallow Draft Pass. Vessel	Vessel Type	-
Crossing the Bow	Traffic Scenario	-
Less than 1 mile	Traffic Proximity	-
	WATERWAY CONDITIONS	
More than 0.5 mile Visibility	Visibility	Less than 0.5 mile Visibility
Along Vessel	Wind Direction	-
Less than 10 knots	Wind Speed	-
Almost Slack	Current	-
Along Vessel - Opposite Direction	Current Direction	-
More? : ____	9 8 7 6 5 4 3 2 1 2 3 4 5 6 7 8 9	____ : More?
Situation 1 is worse	<==========X==========>	Situation 2 is worse

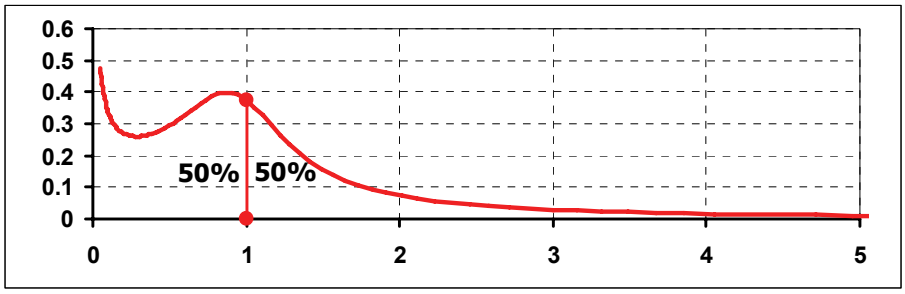

Figure D-18. Apriori setting (prior to updating with expert responses) of the relative likelihood of a collision given a propulsion failure on the tanker.

Q30

Situation 1	TANKER DESCRIPTION	Situation 2
Strait of Juan de Fuca East	Location	-
Inbound	Direction	-
Laden	Cargo	-
1 Escort	Escorts	-
Untethered	Tethering	-
	INTERACTING VESSEL	
Shallow Draft Pass. Vessel	Vessel Type	-
Crossing the Bow	Traffic Scenario	-
Less than 1 mile	Traffic Proximity	-
	WATERWAY CONDITIONS	
More than 0.5 mile Visibility	Visibility	Less than 0.5 mile Visibility
Along Vessel	Wind Direction	-
Less than 10 knots	Wind Speed	-
Almost Slack	Current	-
Along Vessel - Opposite Direction	Current Direction	-
More? : ____	9 8 7 6 5 4 3 2 1 2 3 4 5 6 7 8 9	10 : More?
Situation 1 is worse	<==========>	Situation 2 is worse

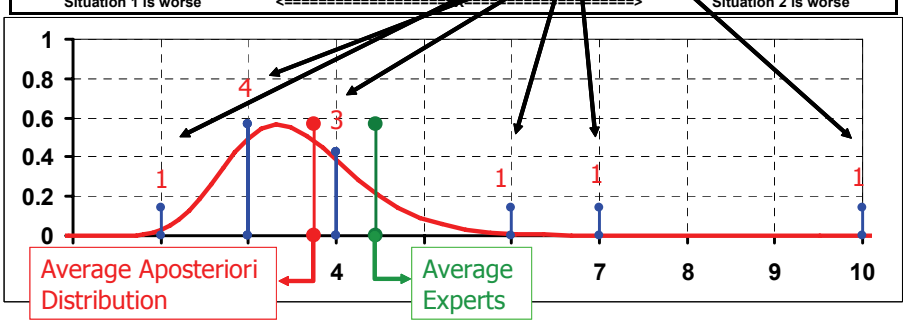

Figure D-19. Expert responses to a pair wise situation comparison to assess relative likelihood of a collision given a propulsion failure on the tanker.

Situation 1	TANKER DESCRIPTION	Situation 2
Rosario Strait	**Location**	Guemes Channel
Inbound	**Direction**	-
Laden	**Cargo**	-
1 Escort	**Escorts**	No Escorts
One Tethered	**Tethering**	Untethered
	INTERACTING VESSEL	
Shallow Draft Pass. Vessel	**Vessel Type**	-
Crossing the Bow	**Traffic Scenario**	-
Less than 1 mile	**Traffic Proximity**	-
	WATERWAY CONDITIONS	
More than 0.5 mile Visibility	**Visibility**	-
Along Vessel	**Wind Direction**	-
Less than 10 knots	**Wind Speed**	-
Almost Slack	**Current**	-
Along Vessel - Same Direction	**Current Direction**	-

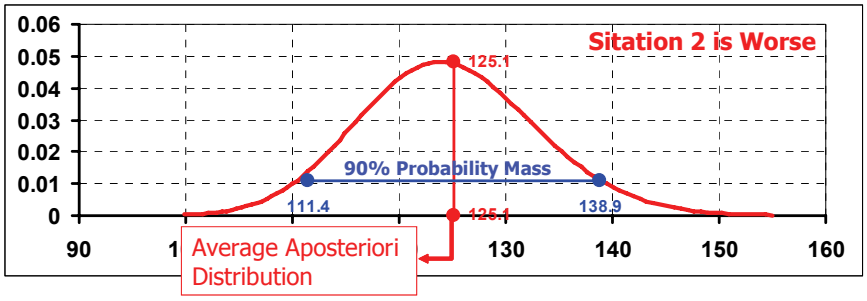

Figure D-20. Analysis of relative likelihood of a collision given a propulsion failure when three accident attributes change when going from Situation 1 to Situation 2.

Situation 1	TANKER DESCRIPTION	Situation 2
Strait of Juan de Fuca East	**Location**	Rosario Strait
Inbound	**Direction**	-
Laden	**Cargo**	Laden
2 Escorts	**Escorts**	No Escorts
One Tethered	**Tethering**	Untethered
	INTERACTING VESSEL	
Tug without Barge	**Vessel Type**	Recreational Vessel
Crossing Astern	**Traffic Scenario**	Crossing the Bow
1 to 5 miles	**Traffic Proximity**	Less than 1 mile
	WATERWAY CONDITIONS	
More than 0.5 mile Visibility	**Visibility**	Less than 0.5 mile Visibility
Along Vessel	**Wind Direction**	Abeam Vessel
Less than 10 knots	**Wind Speed**	-
Almost Slack	**Current**	Max Eb or Max Flood
Along Vessel - Same Direction	**Current Direction**	Abeam Vessel

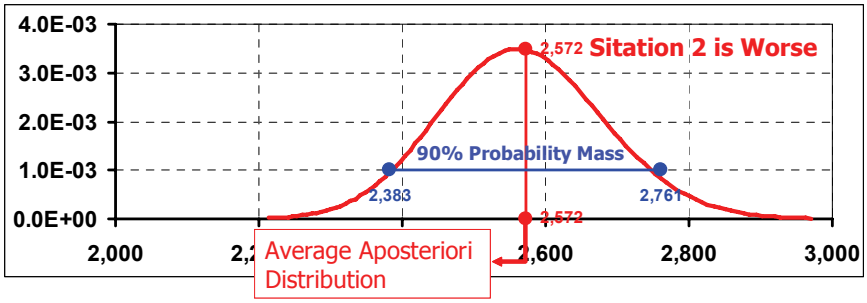

Figure D-21. Analysis of relative likelihood of a collision given a propulsion failure when eleven accident attributes change when going from Situation 1 to Situation 2.

Hence, the apriori 75% uncertainty range reduced dramatically when compared to the 90% aposteriori uncertainty range for this relative likelihood. When integrating the accident probability models with the VTRA expert judgment analysis we shall use the average aposteriori likelihoods.

After the expert judgment analysis and with the resulting parameter settings provided in Tables D-10 and D-11 our model has the ability to evaluate relative likelihoods of two situations when more than one accident attributed changes. In Figure D-20 we evaluate the relative likelihood of a collision with a shallow draft passenger vessel given a propulsion failure on the tanker when the tanker is not escorted in Guemes Channel (Situation 2) compared to the tanker being escorted and tethered in Rosario Strait. For Figure D-20 we evaluate that the collision is about 125 times more likely in Situation 2 as compared to Situation 1 (given also the settings of the remaining accident attributes in Figure D-20).

In Figure D-21 the change between Situation 2 and Situation 1 is even more dramatic. Situations 1 and 2 differ in Figure D-21 in eleven attributes. Situation 1 describes a tanker escorted by two escort vessels in the East Strait of Juan de Fuca interacting with Tug that is 1 to 5 miles away in good visibility. Situation 2 describes an unescorted laden tanker in Rosario strait with a passenger vessel crossing its bow within one mile distance in bad visibility. For Figure D-21 we evaluate that the collision is about 2572 times more likely in Situation 2 as compared to Situation 1 (given also the settings of the remaining accident attributes in Figure D-21).

With the ability of relative likelihood evaluations as in Figures D-20 and D-21, the accident probability models that evaluate accident probabilities per situation can be integrated with the VTRA simulation to evaluate annual accident frequencies. This process will be described in some detail in the next section.

D-4. Turning expert judgment into annual accident frequencies

Turning relative accident likelihoods per situation into annual accident frequencies require a calibration step and a VTRA simulation that records the values of the situation attributes needed for the accident probability models (as it simulates the maritime transportation system within the VTRA study area). In our causal chain accident probability model displayed in Figure D-1 an accident is preceded by an incident. The incidents that we have modeled are propulsion failures, steering failures, navigational aid failures, human error and a nearby vessel failure. The nearby vessel failure could either be a mechanical failure or a

human error on the nearby vessel. To calibrate at the incident level we need a counting routine that is time based. The accidents that we consider in the VTRA study are collisions, drift groundings, powered groundings and allisions. Collisions involve interactions with other vessels, drift groundings involve interactions of a vessel with the shore line while adrift, powered groundings involves interactions of a vessel with the shoreline while under power and allision interactions involve interactions of a vessels with its intended dock. The separate counting mechanisms within the VTRA simulation tool will be described in the next section. In the sections thereafter we shall discuss incident and accident calibration for our simulation for the year 2005 (i.e. VTRA Case B). For this year we are effectively replaying the movement of vessels rather than having to make use of additional probabilistic traffic arrival generators. Hence, VTRA CASE B is a natural calibration scenario.

D-4.1. Simulation Counting

Consider a hypothetical interaction of a vessel with a tanker as depicted in Figure D-22. Observe that both vessels cross in Figure D-22. Informally, the level of risk could follow a profile over time as depicted in Figure D-23. That is, when the vessel are far way from another the risk is low and the closer they get it increases. At some point the risk of the vessel interaction will attain its maximum value after which it will continue to decrease and eventually return to zero when the vessels have well passed the crossing point. We attempt to capture the behavior of such a time profile in the VTRA maritime transportation simulation by discretizing the time in intervals of finite length. Whereas during the Prince William Sound Risk Assessment (see, Merrick et al. (2002)) computation efficiency only allowed us to take a snapshot of the simulation once every five minutes, we are able to take a snapshot of the VTRA simulation once every minute.

During such a snapshot the variety of interactions are evaluated and written to their "counting databases". The VTRA study area is indicated by the blue border area in Figure D-24. A counting grid is overlaid on top of this VTRA study area with grid cells that are 0.5 nautical miles by 0.5 nautical miles wide. There is a separate counting database for "route interactions" that count the amount of minutes that a vessel of interest appears in a certain grid cell. Figure D-24 displays the counting profile of route interactions when the vessel of interests are tankers, ATB's and ITB's that dock at the BP Cherry Point terminal (hereafter referred to as CHPT vessels). This counting or exposure geographic profile will be used to calibrate the probability of a propulsion failure, steering failure, navigational aid vessel or human error on a CHPT vessel during a route interaction.

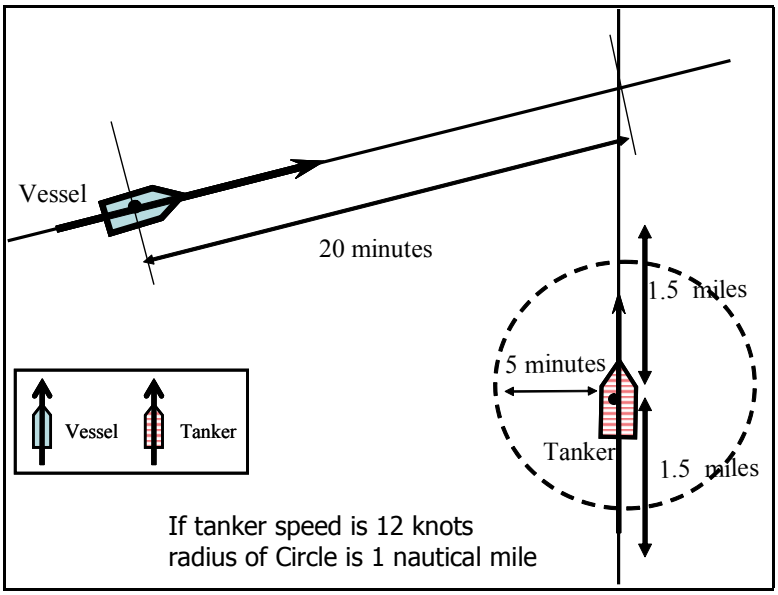

Figure D-22. Schematic of counting procedure for vessel interactions

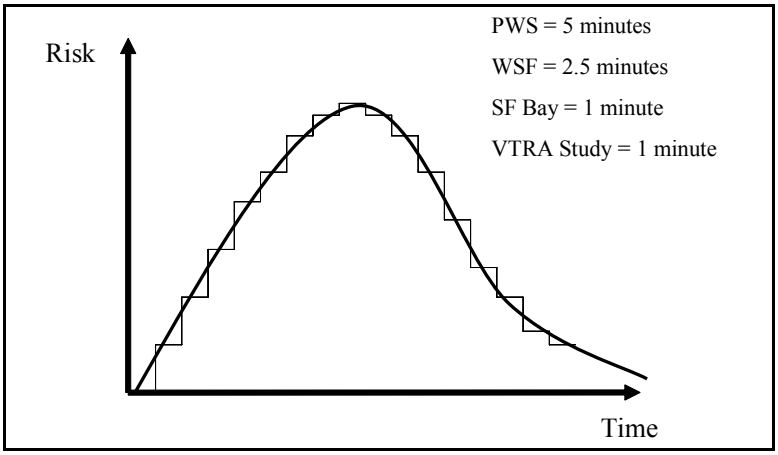

Figure D-23. A risk profile as a function of time when two vessels cross.

Figure D-25 displays the counting profile of route interactions when we count route interactions of all vessels. The counting profile in Figure D-25 is used to calibrate the probability of a nearby vessel failure during a route interaction. Please note that the color legends in Figures D-24 and D-25 are different, indicating a higher number of counts in a grid cells on both scales by a darker color.

Other "counting databases" capture vessel interactions, drift interactions, power interactions and allision interactions. A vessel interaction between a tanker and a vessel is always counted by the VTRA simulation when the interacting vessel is within a distance that

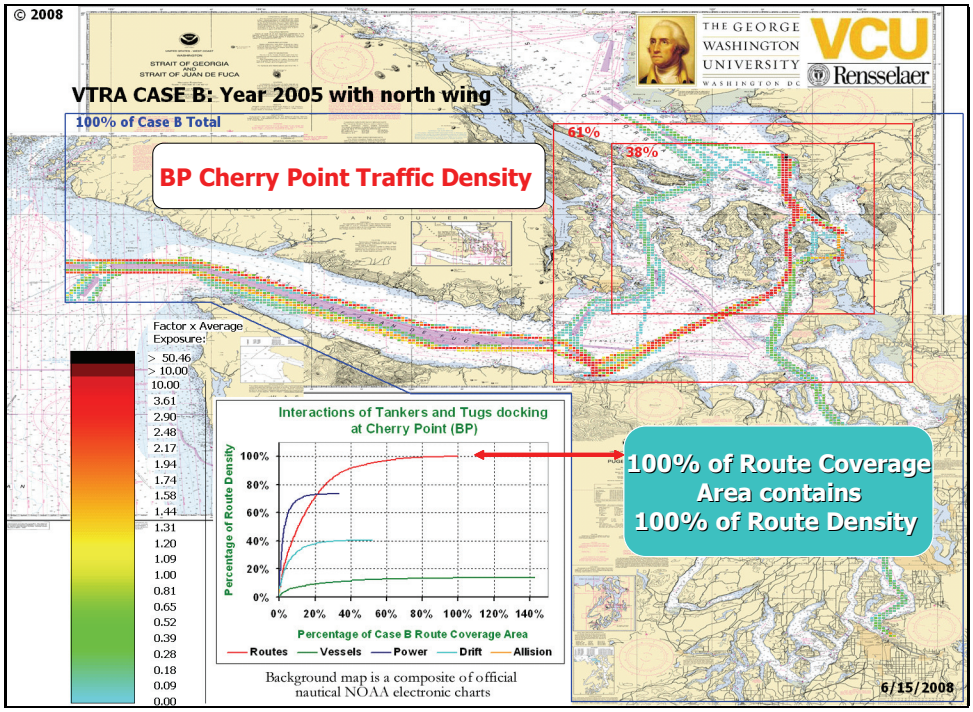

Figure D-24. Exposure Counts of Cherry Point Tankers, ATB's and ITB's in the calibration case: VTRA CASE B.

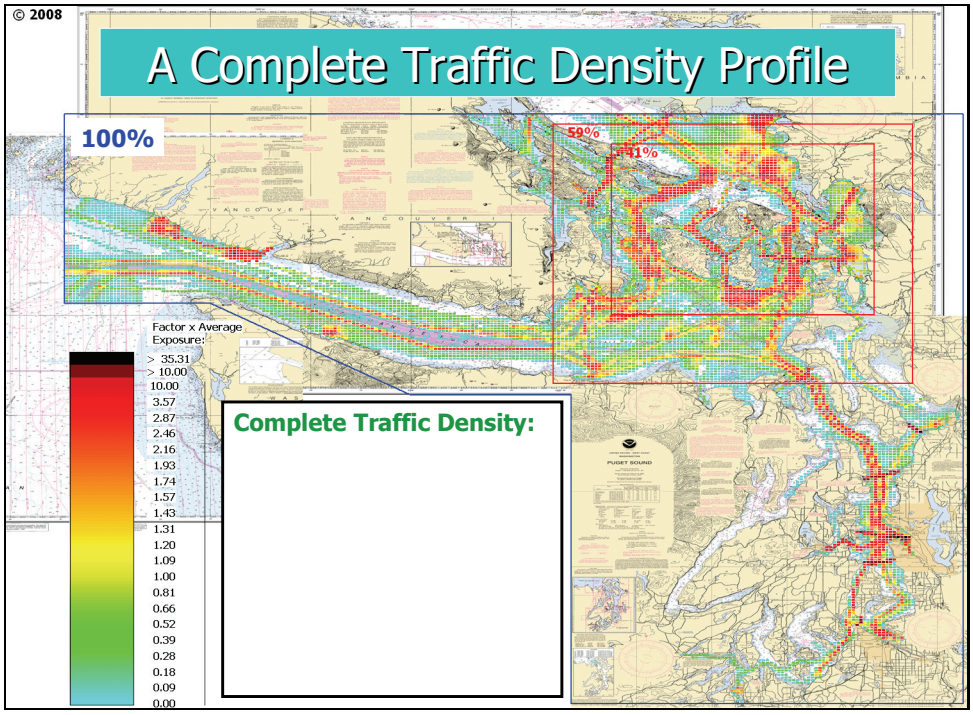

Figure D-25. Exposure Counts of all vessels in the calibration case: VTRA CASE B.

the tanker can travel within 5 minutes. Hence, when the speed of the tankers is 12 knots this distance would be one nautical mile (see Figure D-22). In previous studies this distance was fixed regardless of the speed of the vessel of interest. Our enhanced counting procedure enlarges or shrinks the vessel counting circle as function of the speed of the vessel of interest.

The left snapshot of the VTRA maritime simulation in Figure D-26 demonstrates an interacting vessel in the vessel of interest (134) "counting zone". The counting color scheme changes dynamically as the simulation counts while continuing to assign darker colors to those grid cells with a higher number of vessel interactions. The right snapshot of Figure D-26 demonstrates that it is also possible for an interaction to occur when a vessel is not within the immediate "counting zone" of the interacting vessel. This happens when the future crossing point of the interacting vessel is within 1.5 nautical miles from the front or the back of the vessel of interest and the crossing would occur within the next 20 minutes. This 1.5 nautical mile distance is set to capture the behavior of Figure D-23 when two vessels cross over time and depends on the grid cell size.

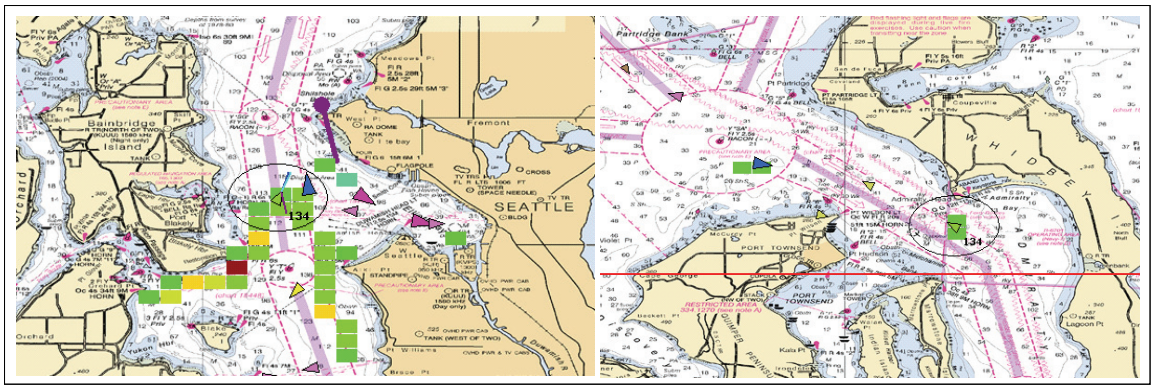

Figure D-26. Examples of vessel interaction counting in the VTRA maritime simulation.

To count drift or power interactions with the shore line when a vessel of interest is underway we first need to "define" the shore line. Figure D-27 provides this definition where each shoreline grid cell indicated in red is also 0.5 nautical miles by 0.5 nautical miles. To count drift interactions we predict the drifting path of tanker five hours out. This drifting path takes into account future wind speeds, currents and slows the tanker down over time as it drifts. The calculated future drift path follows the drift model of the NOAA (1997) publication. A drift interaction is recorded by the VTRA maritime simulation for the first

grid cell that falls on this drifting path and is part of the shore definition in Figure D-27. If a five hour project drift path does not intersect with the shoreline definition, no drift interaction is counted. Both snapshots of Figure D-28 below show a drifting path of a tanker as well as the grid cells of the shore definition. In both figure a drift interaction is recorded when this drifting path intersects the shore line definition for the first time. Similar to the vessel interaction counting, the color coding of the shore line grid cells that do have drift interactions are darker when it relatively encounters a higher number of drift interactions.

To count interactions with the shore line definition in Figure D-27 for powered groundings we project a straight line following the current direction of the vessel of interest. The assumption here is that those shoreline grid cells that have more frequently a vessel of interest coming directly towards them will also have a higher powered grounding risk. These straight line projections are drawn for a distance that the vessel of interest can travel in a five hour time frame (assuming its current speed over that time frame). The first grid cell of the shoreline definition that intersects this straight line projection will obtain a power interaction count. The two snapshots of the VTRA maritime simulation in Figure D-29 demonstrates the power interaction counting algorithm for two snapshots taking shortly after one another.

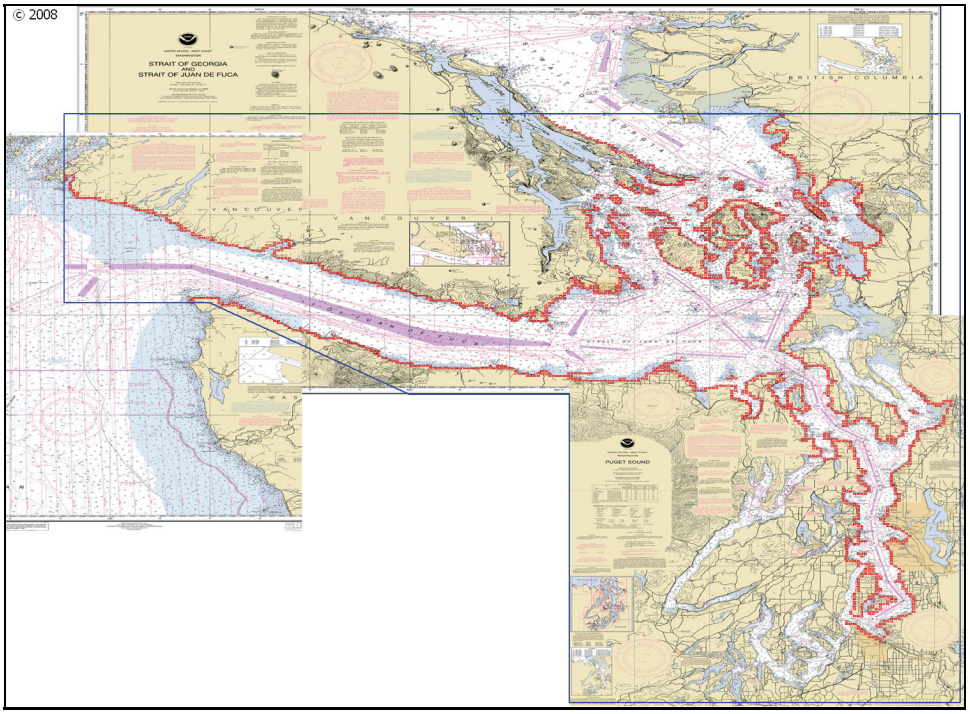

Figure D-27. Shore line definition in the VTRA maritime simulation.

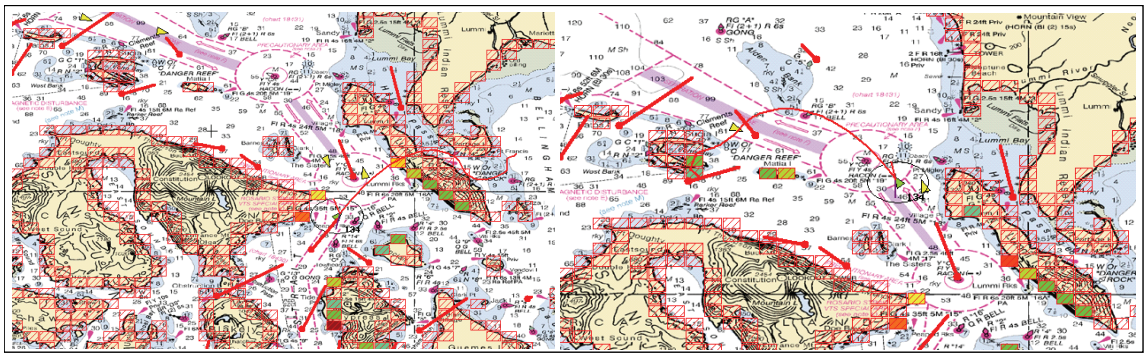

Figure D-28. Examples of drift shore line interaction counting in the VTRA maritime simulation.

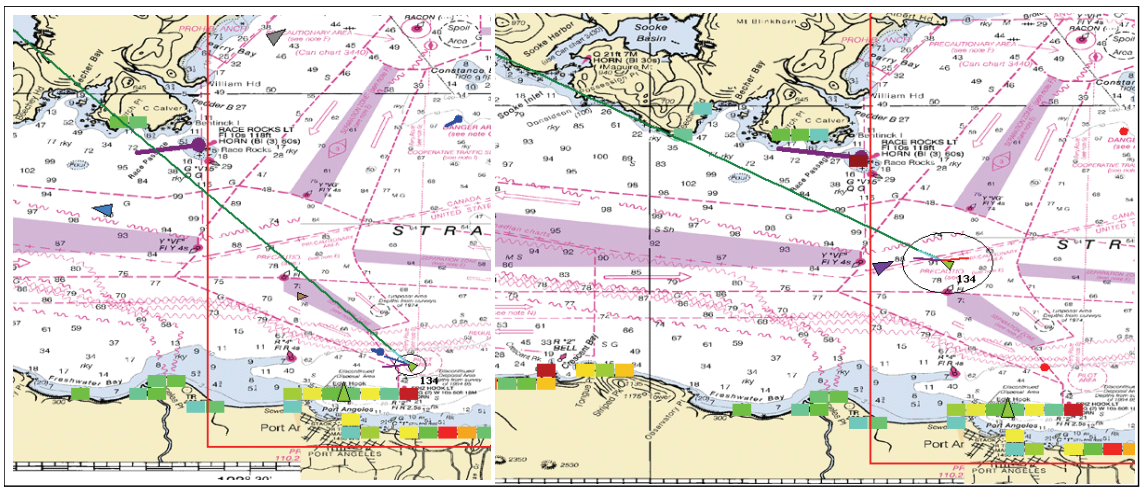

Figure D-29. Examples of power shore line interaction counting in the VTRA maritime simulation.

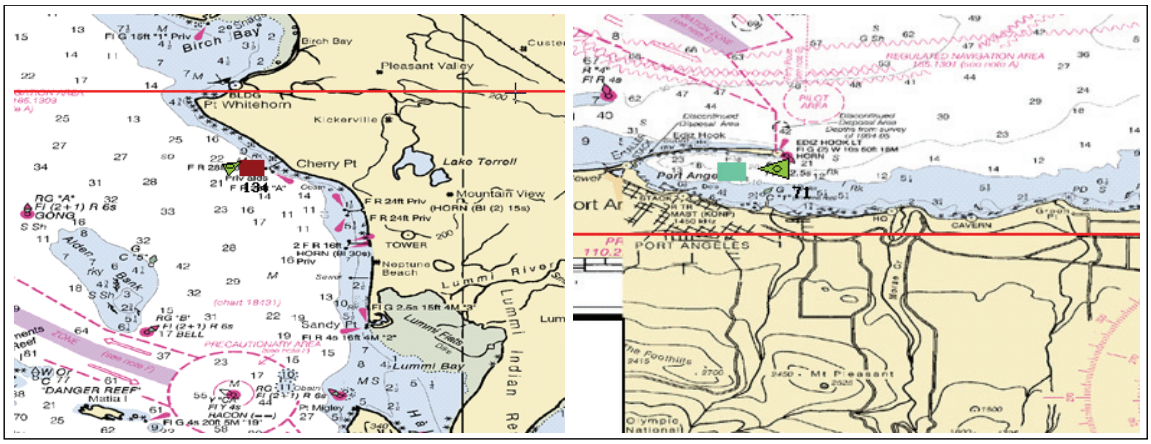

Figure D-30. Examples of allision interaction counting in the VTRA maritime simulation.

Finally, we have also implemented a counting algorithm for allision accidents. When a vessels is within one mile of its intended dock we use the straight line projection approach of the powered interactions to count allision interactions with the shore line definition in Figure D-27. From that point on neither drift or powered grounding interactions are counted anymore. Indeed, within one mile of the intended dock, docking procedures of the tankers and tugs will have commenced, speeds are lowered, escort vessels are in place and from that point on the vessel intentionally tries to get close to the shore with a specific heading towards its intended dock. Figure D-30 above shows two snapshots of the allision interaction algorithm implemented in the VTRA maritime simulation for the BP Cherry Point dock and a dock at Port Angeles.

D-4.2. Incident Calibration

From the analysis of accident and incident data it followed (See Appendix A) that over an 11 year period (1995-2005) the VTRA study area experienced 31 steering, 11 propulsion and 10 navigational aid failures on CHPT tankers totaling 52 mechanical failures. Over a 7.5 year period (the first ITB sailed about mid 1998) the VTRA study experienced 3 propulsion, 2 steering and 2 navigational aid failures on CHPT ATB's and ITB's totaling 7 mechanical failures. The data collection process in Appendix A demonstrated that human error incidents are rarely reported.

On the other hand over the data collection period (1995-2005) 4 accidents occurred, three of which were preceded by a human error. Hence, since human error incidents were rarely reported we also applied a three to one ratio (experienced at the accident level) at the incident level. Hence, with this assumption we obtain 156 human error for CHPT tankers over an 11 year period and 21 human errors for CHPT ATB's and ITB's over a 7.5 year period. These counts can next be converted to average yearly incident rates. For example, we arrive at an average annual total number of mechanical failures (i.e. propulsion, steering and navigational aid) of 5.661 and an average annual total of human errors for CHPT vessels of 22.642.

Dividing average yearly incident rates by the total number of interactions for CHPT tankers and separately by the total number of interactions for CHPT ATB's and ITB's over one year, yields the incident rates per interaction. The total number of interactions for CHPT tankers for the calibration year VTRA CASE B was 271526 and for ATB's and ITB's 172087. These counts combined resulted in the route interaction count distribution of Figure D-23. Table

D-15 present the incident rate analysis by incident type per interaction for CHPT Tankers and CHPT ATB's and ITB's to arrive at these annual totals.

Table D-15. Incident rates per route interaction for CHPT Tankers, ATB and ITB's.

	CHPT Tankers	CHPT ATB's and ITB's
Propulsion (per Year)	2.818	0.400
Steering (per Year)	1.000	0.267
Nav. Aid (per Year)	0.909	0.267
Human Error (per Year)	14.182	2.800
Annual Interactions	271526	172087
Propulsion (per Interaction)	1.038E-05	2.324E-06
Steering (per Interaction)	3.683E-06	1.550E-06
Nav. Aid (per Interaction)	3.348E-06	1.550E-06
Human Error (per Interaction)	5.223E-05	1.627E-05

Similarly, the accident incident analysis in Appendix A over the period from (1995-2005) showed a record of 1100 mechanical failure incidents and a worst case ratio of 78 to 1369 accidents that were preceded respectively by a mechanical failure or a human error. Hence, applying this worst case ratio of 17.6, we arrive at an annualized number of incidents for all vessels in the VTRA simulation of about 1855. Given a total number of interactions of all the vessels modeled in the VTRA simulation of 34519581 we arrive at an overall nearby vessel incident incident rate of 5.374E-05 per interaction. This results in a total number of nearby vessel failures for the vessels modeled in the VTRA simulation during the time that a CHPT vessel is underway of 23.84.

D-4.3. Accident Calibration

After the calibration of the VTRA simulation at the incident level, we can start the calibration process at the accident level. To calibrate VTRA simulation for a particular accident type to a given annual average number of accidents, we first need to evaluate for each recorded interaction the probability that an incident occurs and next evaluate per interaction the probability of an accident given an incident using the probability models (D-1), (D-2), (D-3). Evaluating the product of these two probabilities and summing them over all simulated interactions over one year of simulation time, yields the average annual number of accidents of that type generated by the VTRA maritime simulation. To be able to evaluate the accident probabilities given an incident using the models (D-1), (D-2), (D-3) the simulation records the accident attributes of these models. Figure D-31 displays a screen

shot of this recording process for the transit of the vessel of interest 134 identified in Figure D-31. The colored cells indicate the vessel interactions that have occurred thus far during its transit, while the database on the lower left corner shows the recording of the specific accident attributes during these vessel interactions. These interactions are recorded separately for route interactions, vessel interactions, drift interactions, power interactions and allision interactions as per the counting algorithms discussed in the previous sections.

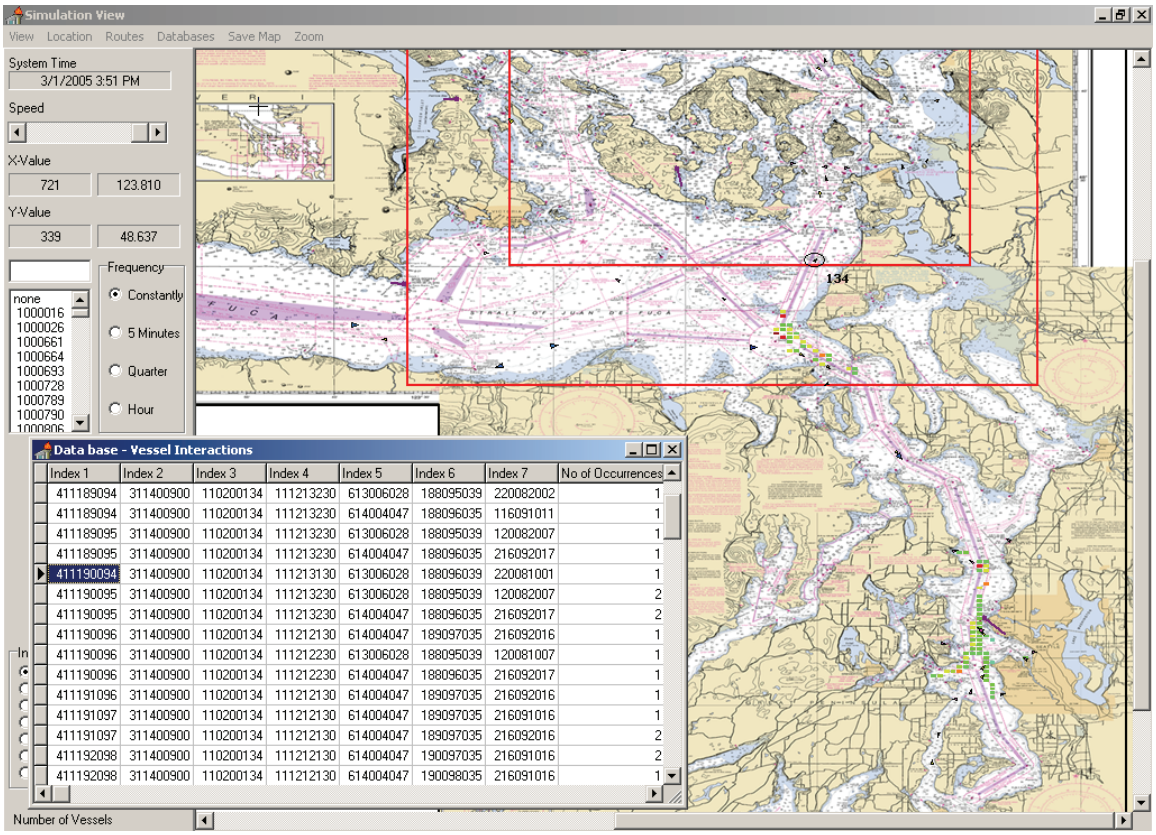

Figure D-31. Encoding of interactions by the VTRA maritime simulation.

Our accident collection process for the time period from (1995-2005) recorded 4 accidents for CHPT vessels (1 collision, 1 grounding and 2 allisions) and 3 of these accidents were preceded by a human error and 1 by a mechanical failure. During the calibrations process of our various accident type we shall maintain this ratio of 3 to 1 of average annual frequency caused by a human error or mechanical failure, for all accident types. To calibrate collisions we first ensure a ratio of 1 to 3 of frequency of collisions caused by mechanical failure compared to human errors. Next, we calibrate the collision model given a nearby vessel failure by ensuring that the average frequency of collisions caused by an incident on the CHPT vessels is the same as the average frequency of collisions caused by an incident on the

near by vessel (NBV), when restricting the nearby vessel to the CHPT vessels. By a symmetry argument these average annual frequencies have to be the same. Finally, we calibrate the VTRA simulation such that on average the number of collisions per year equals $1/11$. The respective calibration values for P_0 for the collision accident probability models given an incident are provided in Table D-12.

Figures D-32 and D-33 summarize the result of the calibration step for collisions. First note that the graph in Figure D-33 shows an average return time of collisions of 11 years (equivalent to an average annual frequency of collision of about 0.09 or 1 collision in 11 years). We may also observe from this graph that approximately 42% ($\approx$ 60%/140%) of all the grid cells that have vessel interactions, account for almost all of the total average frequency of collisions per year. The 140% in the previous calculation implies that the area of the grid cell coverage of vessel interactions is about 1.4 times the area of the grid cells through which CHPT vessel travel as displayed in Figure D-24. This follows since we do not only record the location of the CHPT vessel in these collision geographic profiles but also the location of the interacting vessel. Also observe from Figures D-32 and D-33 that the smallest red-square in Figure D-33 captures 63% of the collision frequency, whereas in Figure D-32 this red-square only captures 57% of the total vessel interactions. This difference is a direct results of overlaying the calibrated collision accident probability model (D-1) on top of the vessel interaction exposure profile of Figure D-32. When studying the color changes when going from Figure D-32 to D-33 we observe a darkening effect at the entrance from Rosario Strait to Guemes Channel, in Guemes Channel and Rosario Strait. Moreover, we observe a lightening effect at Port Angelas, East Strait of Juan de Fuca, from Rosario Strait onwards to the Cherry Point dock and possibly also a minor lightening effect in the Puget Sound area.

To calibrate to 1 grounding accident over an 11 year period of collected accident data, we first need to join the power and drift interaction database. Drift groundings in our model are those groundings that are preceded by a propulsion failure or a steering failure. The operating assumption for steering failures here is that when a steering failure occurs on a tanker, that one shuts down the propulsion and thus the vessel effectively starts drifting. Powered groundings in our models are those groundings that are preceded by a human error, navigational aid failure or a nearby vessel failure. Hence, the later incident accounts for those grounding scenarios where a vessel has to avert the nearby vessel.

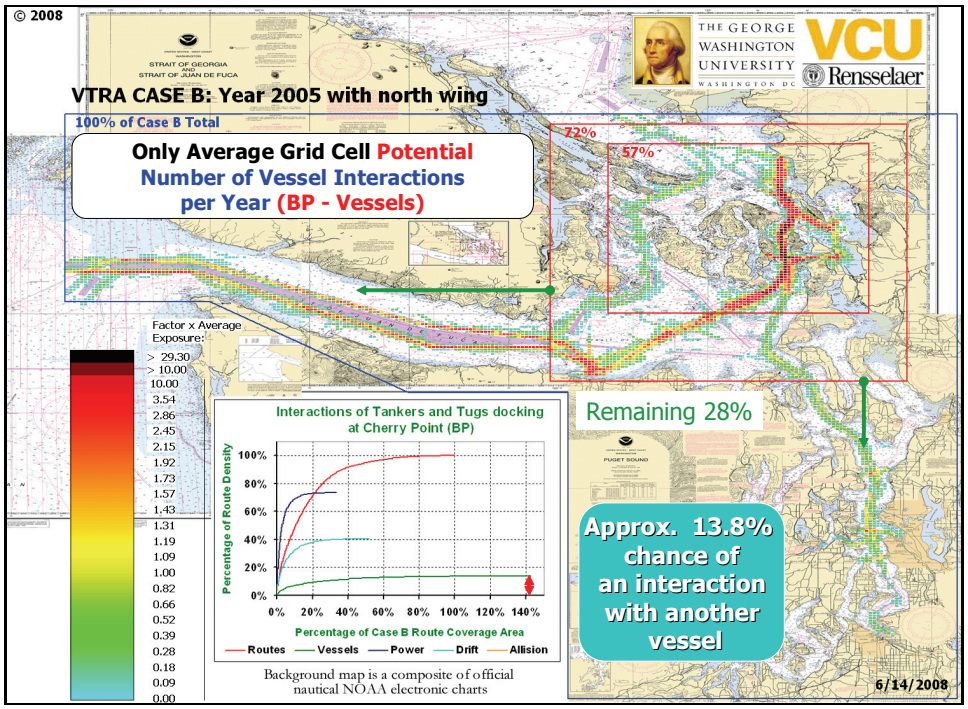

Figure D-32. Vessel interaction counts of Cherry Point Tankers, ATB's and ITB's in the calibration case: VTRA CASE B.

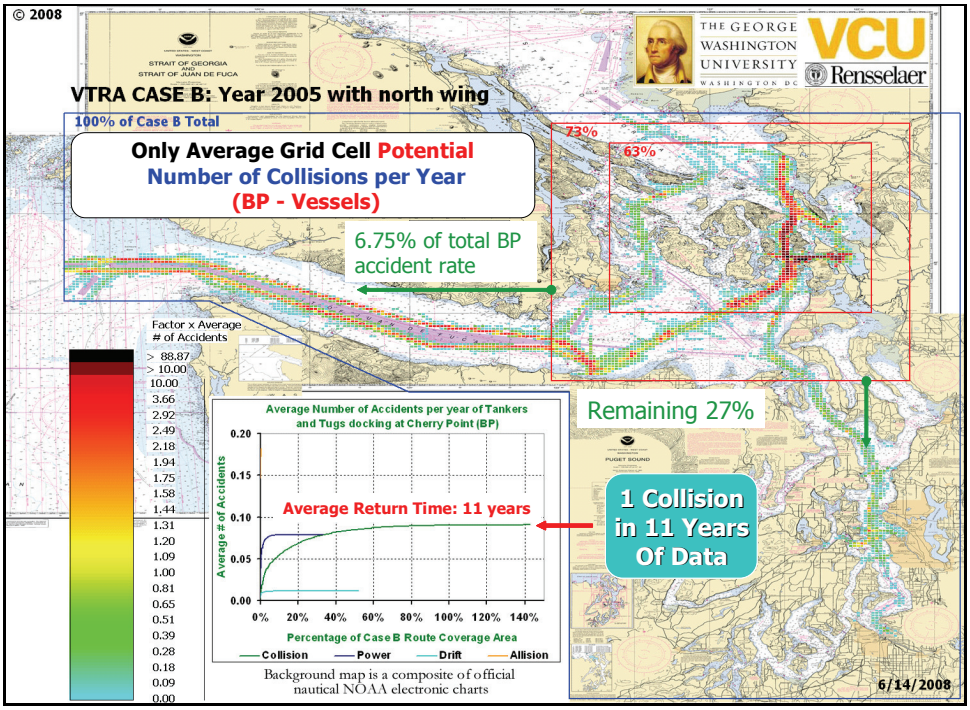

Figure D-33. Annual collision frequencies of Cherry Point Tankers, ATB's and ITB's in the calibration case: VTRA CASE B.

The calibration process of the grounding model (D-15) is considerably more complicated than the collision model as a result of the additional time-to-shore variable. Whereas in the collision model calibration involves solving a linear equation in a closed form, calibration the grounding model involves solving a non-linear equation using a bisection routine. Each iteration of this routine involves a complete run through all grounding interactions and hence this step is quite computationally intensive. We first solve for the calibration constant t_q in (D-15) by setting the annual frequency of groundings equal to $1/11$ (we observed 1 grounding in 11 years of data) using this bisection method. This results in a value $t_q = 0.834375$. However, after this step the ratio of groundings preceded by human error as compared to mechanical failures turns out to be 2.26 in stead of the desired ratio of 3. To correct this we solve for the remaining calibration constants P_0 by incident type in a similar manner as the collision model calibration. This step results in a calibration value $P_0 = 0.52831297$ for the incident types "Human Error" and "Nearby Vessel Failure" and a calibration value $P_0 = 0.405335373$ given the incident types "Steering Failure", "Propulsion Failure" and "Navigational Aid Failure".

Figures D-34 and D-35 summarize the result of the calibration step for drift groundings. Figures D-36 and D-37 summarize the result of the calibration step for powered groundings. While we have an overall annual frequency of groundings of ≈ 0.09 (average return time of 11 years), we obtain for average annual frequencies of drift grounding and powered grounding for VTRA Case B:

Drift Grounding: ≈ 0.012 (average return time of $\approx$ 85 years)
Powered Grounding: ≈ 0.079 (average return time of $\approx$ 13 years)

This coincides with a ratio of 6.8 of powered groundings to drift groundings. Hence, our model evaluates a much higher frequency of powered groundings as compared to drift groundings. This is explained primarily by the ratio of combined incident rates of human error, navigation aid failure and nearby vessel failure to combined incident rates of propulsion failure and steering failure, which is about 4.7 to 1. This takes into account that when a CHPT vessel is underway it has approximately a 13% chance of interacting with another vessel. The remain difference between the ratio of 4.7 to 1 compared to 6.8 to 1 is primarily explained by the time to shore variable in the grounding model. Indeed, given a steering failure or a propulsion failure the time to shore on average is higher than when the vessel remains under power given a human error, navigational aid failure or a near by vessel failure. Thus, the time to shore variable for the drift grounding is higher on average than for

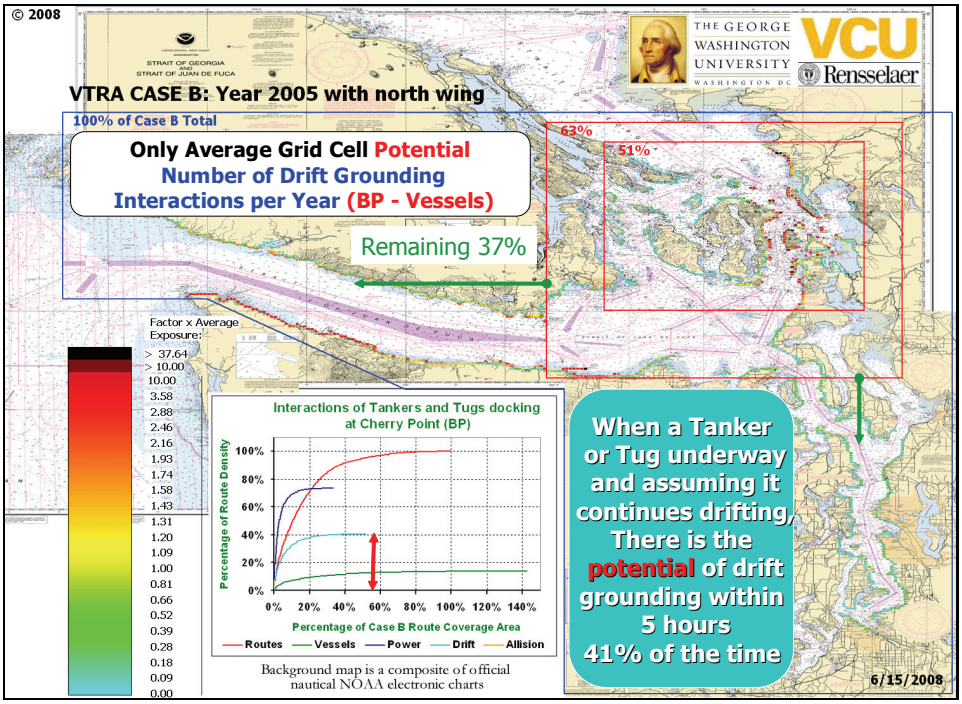

Figure D-34. Drift interaction counts of Cherry Point Tankers, ATB's and ITB's in the calibration case: VTRA CASE B.

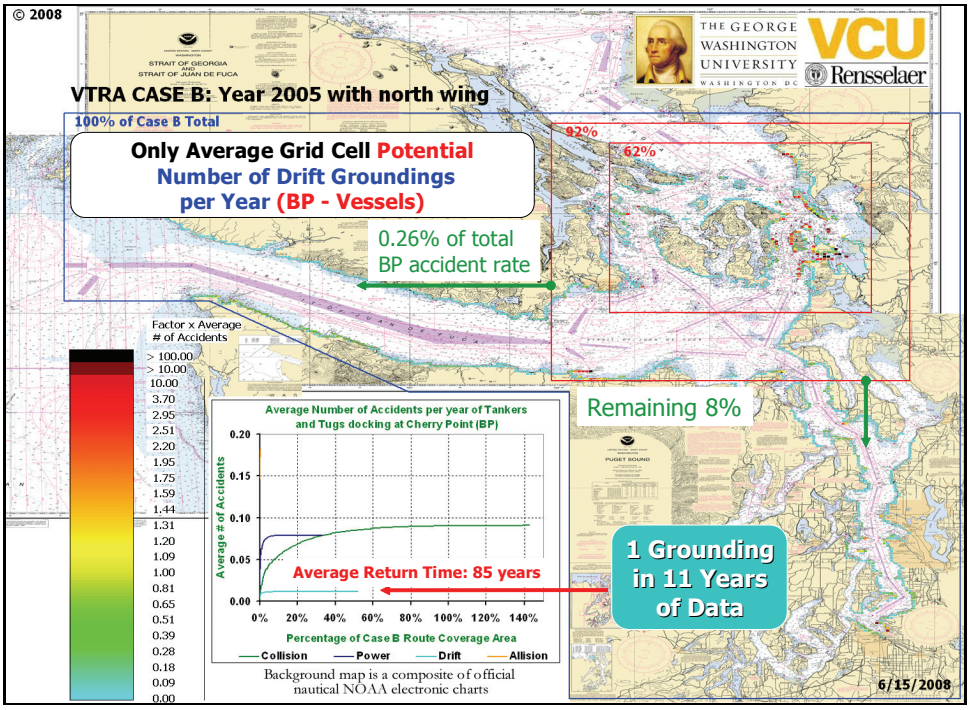

Figure D-35. Annual drift grounding frequency of Cherry Point Tankers, ATB's and ITB's in the calibration case: VTRA CASE B.

powered groundings resulting on average in a lower drift grounding accident rate per drift interaction than a powered grounding accident rate per power interaction. Observe from Figure D-34 that within our model about 41% of the time there is the potential that a CHPT vessel will run aground within a five hour time frame while adrift, whereas this percentage is 73% when the CHPT vessel is under power (see Figure D-36).

A further effect of the time to shore variable can be observed by comparing Figures D-34 and D-35. Note that while we observe 37% of the drift interactions outside the largest red square, we only observe an 8% of the overall drift grounding accident frequency outside this red square. This follows from larger time-to-shore drifting times overall in the areas outside this red square (especially in the West Strait of Juan de Fuca) compared the area within this red square (especially, the Guemes Channel and Rosario Strait areas and entrances). Indeed, of the total CHPT vessel annual accident frequency of $4/11 \approx 4/11$ (combining collisions, groundings and allisions), we evaluate that only 0.26% is represented on the average by drift groundings outside the largest red square!

The powered grounding analysis displays a similar behavior (see Figures D-36 and D-37). Note that while we observe 33% of the power interactions outside the largest red square, we only observe a 7% of the overall powered grounding accident frequency outside this red square. This too follows from larger time-to-shore times overall in the areas outside this red square (especially in the West Strait of Juan de Fuca) compared the area within this red square (especially, the Guemes Channel and Rosario Strait areas and entrances). Here, of the total CHPT Vessel annual accident frequency of $4/11 \approx 4/11$ (combining collisions, groundings and allisions), we evaluate that only 1.53% is represented on the average by powered groundings outside the largest red square.

Summarizing, the 92% percentage of annual frequency of drift groundings within the largest red square in Figure D-35 and the 93% of annual frequency of powered groundings in this red square in Figure D-37, demonstrates that comparatively within the VTRA study area the grounding risk is confined to this red square (although the remaining 8% and 7% outside should not be considered negligible).

The calibration process for allision is the same as that of groundings. The primary difference between these two accident probability models is the interaction counting as

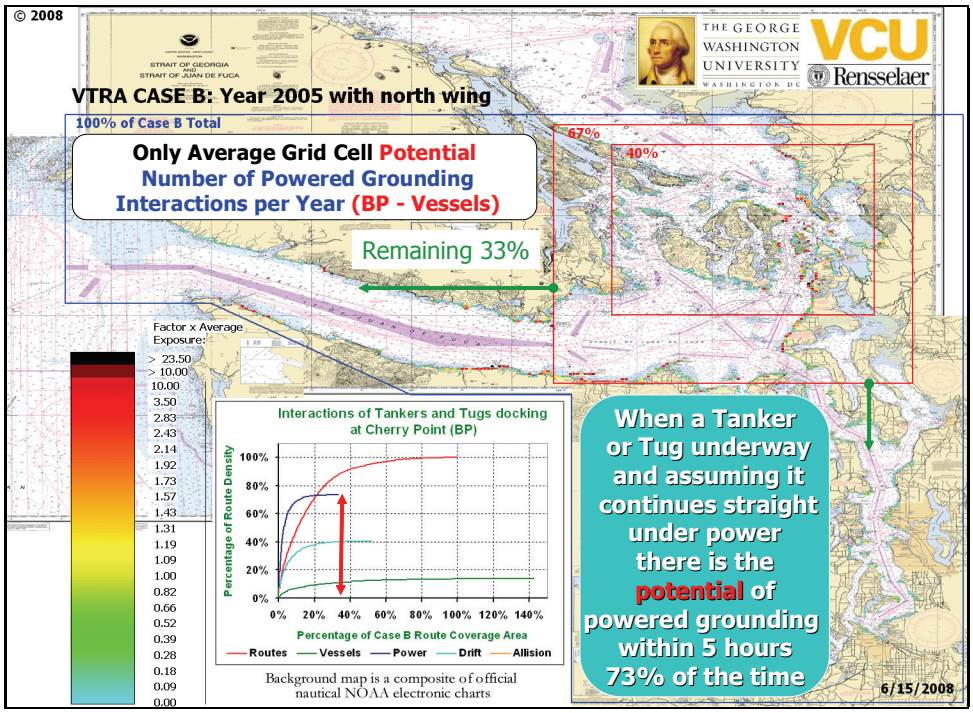

Figure D-36. Power interaction counts of Cherry Point Tankers, ATB's and ITB's in the calibration case: VTRA CASE B.

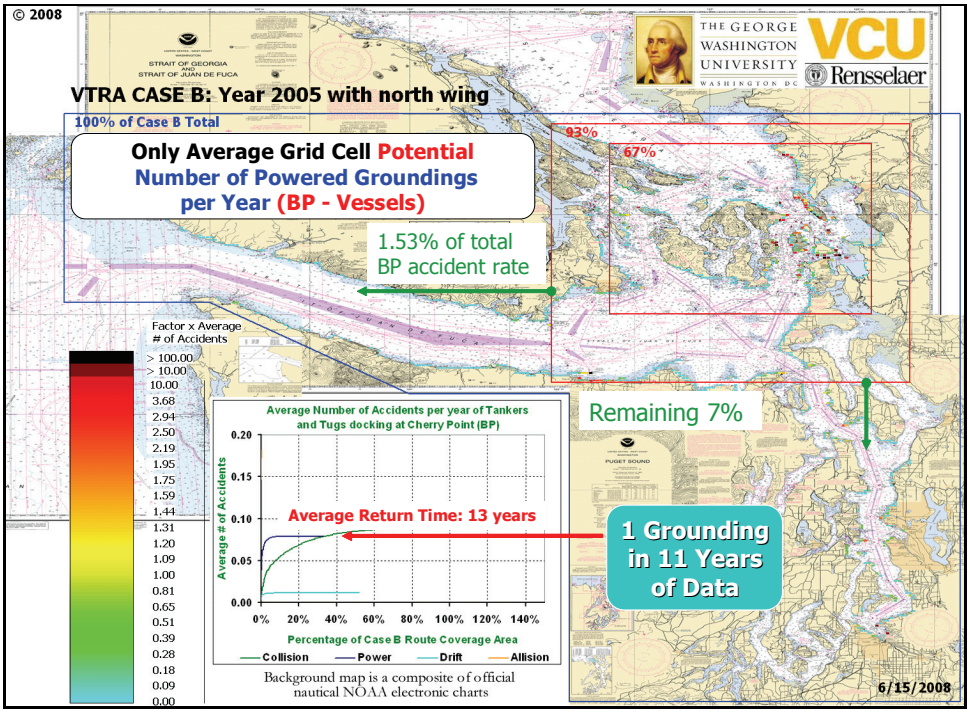

Figure D-37. Powered grounding frequency of Cherry Point Tankers, ATB's and ITB's in the calibration case: VTRA CASE B.

explained in the previous section. When a vessel is within one mile of its intended dock, the projected shore interactions of a straight line path are designated as allision interactions instead of power interactions. Indeed, within one mile of the intended dock, docking procedures of the tankers and tugs will have commenced, speeds are lowered, escort vessels are in place and from that point on the vessel intentionally tries to get close to the shore with a specific heading towards the shore. After calibrating to 2 allision accidents per 11 years, we arrived at a value of $t_q = 0.384277$, a calibration value $P_0 = 1.039155$ for the incident types "Human Error" and "Nearby Vessel Failure" and a calibration value $P_0 = 0.894719$ given the incident types "Steering Failure", "Propulsion Failure" and "Navigational Aid Failure". The interaction count geographic profile for allisions is presented in Figure D-38 and the allision accident frequency profile is presented in Figure D-39.

With the VTRA Case B calibrated for CHPT vessels, the VTRA Case B simulation generates on average the same frequencies of incidents and accidents as observed in the accident-incident database analysis described in detail in Appendix A. Modifications can now be made to this VTRA Case B simulation to represent various alternatives and scenarios. For example, VTRA Case B represents the 2005 year with the BP Cherry Point North wing dock in operation. We can simulate the behavior of the CHPT vessel traffic as if this North wing dock was not there. This case is labeled VTRA Case C. Next, we can compare the aggregate analysis results of VTRA Case C to those of VTRA Case B and draw overall conclusions regarding the aggregate effect of potentially removing the North wing in our model.

The geographic profiles allow us to further zoom-in on these aggregate effects by compare those of VTRA Case B (see Figures D-32 to D-39) to those of VTRA Case C (provided in Appendix G). By zooming in one obtains a better general understanding about where this aggregate change in level (and possibly migration) of accident frequency from one case to another comes from. Visual comparison of these geographic profiles allows one to draw conclusions regarding general tendencies about the changing "risk" behavior from case to case or alternative to alternative.

It should be noted, however, that the maritime transportation modeled within the VTRA simulation is highly dynamic (as demonstrated by a running simulation) and relatively sparse. Even though we evaluate a total of 61427 vessel interactions for VTRA Case B distributed over a total of 3454 grid cells, this results on average annually in about 18 interactions per grid cell. Hence, when making changes to the VTRA Case B simulation this may results in high relative differences from grid cell to grid cell (especially in those with an even smaller

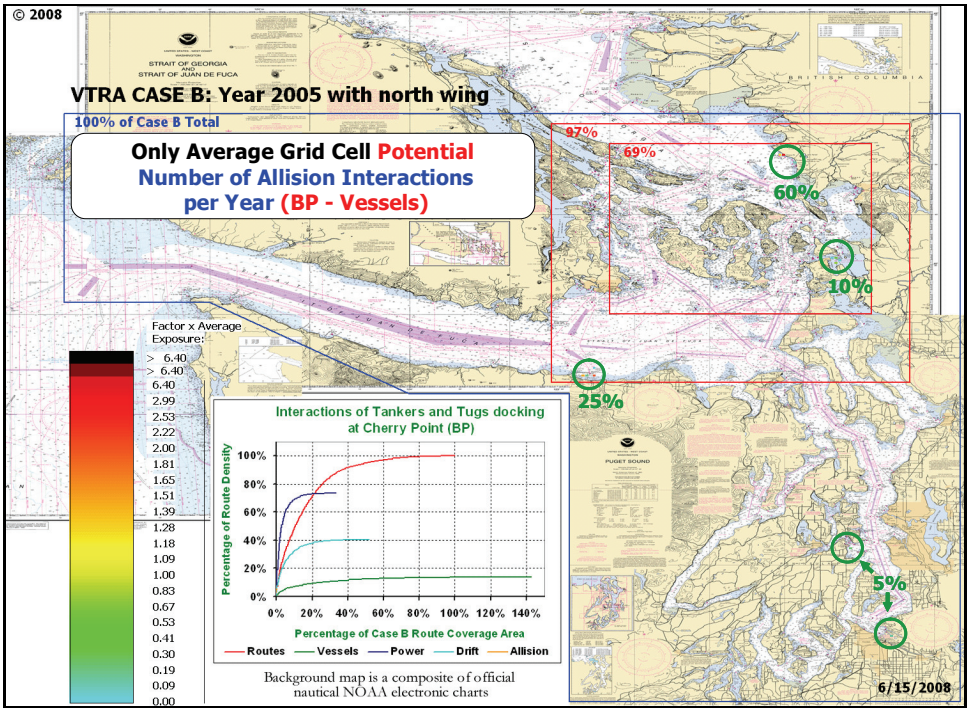

Figure D-38. Allision interaction counts of Cherry Point Tankers, ATB's and ITB's in the calibration case: VTRA CASE B.

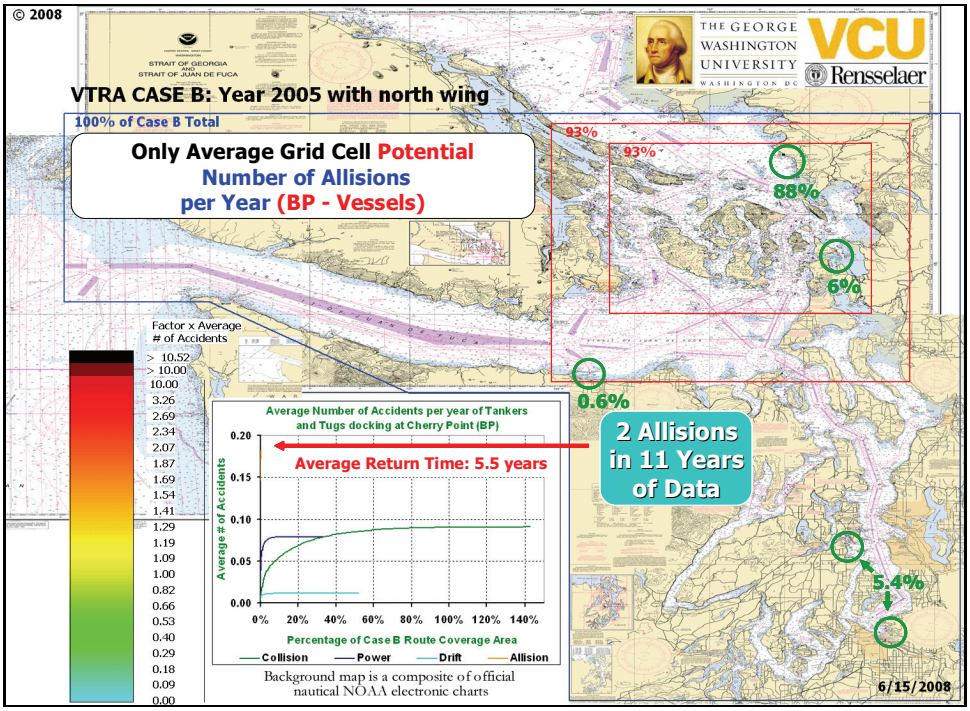

Figure D-39. Allision frequency of Cherry Point Tankers, ATB's and ITB's in the calibration case: VTRA CASE B.

number of interactions). In fact, from case to case one may experience an increase in one grid cell and a decrease in grid cells immediate adjacent to it. Hence, our general position is that these geographic profile analyses should not be used to perform grid cell by grid cell comparisons from case to case, but should only be used to observe general tendencies of change for larger areas.

References

R. Bradley (1953). "Some statistical methods in taste testing and quality evaluation", *Biometrics*, Vol. 9 (1): pp. 22-38.

R.M. Cooke (1991). *Experts in Uncertainty: Opinion and Subjective Probability in Science*, Oxford University Press, Oxford, U.K.

J.R.W. Merrick, J.R. van Dorp, J.P. Blackford, G.L. Shaw, T.A. Mazzuchi and J.R. Harrald (2003). "A Traffic Density Analysis of Proposed Ferry Service Expansion in San Francisco Bay Using a Maritime Simulation Model", *Reliability Engineering and System Safety*, Vol. 81 (2): pp. 119-132.

J.R.W. Merrick, J. R. van Dorp, T. Mazzuchi, J. Harrald, J. Spahn and M. Grabowski (2002). "The Prince William Sound Risk Assessment". *Interfaces*, Vol. 32 (6): pp.25-40.

National Oceanic and Athmospheric Administration (1997). *Ship Drift Analysis for the Northwest Peninsula and the Stait of Juan de FUca.* HAZMAT Report 97-3.

P. Szwed, J. R. van Dorp, J.R.W.Merrick, T.A. Mazzuchi and A. Singh (2006). "A Bayesian Paired Comparison Approach for Relative Accident Probability Assessment with Covariate Information", *European Journal of Operations Research*, Vol. 169 (1): pp. 157-177.

L.L. Thurstone, (1927a). "A law of comparative judgment", *Psychology Review*, Vol. 34: pp. 273-286.

L.L. Thurstone, (1927b). "Psychophysical Analysis", *American Journal of Psychology*, Vol. 38: pp. 368-389

J.R. van Dorp, J.R.W. Merrick , J.R. Harrald, T.A. Mazzuchi, and M. Grabowski (2001). "A Risk Management procedure for the Washington State Ferries", *Journal of Risk Analysis*, Vol. 21 (1): pp. 127-142

TECHNICAL APPENDIX E:
OIL OUTFLOW MODEL

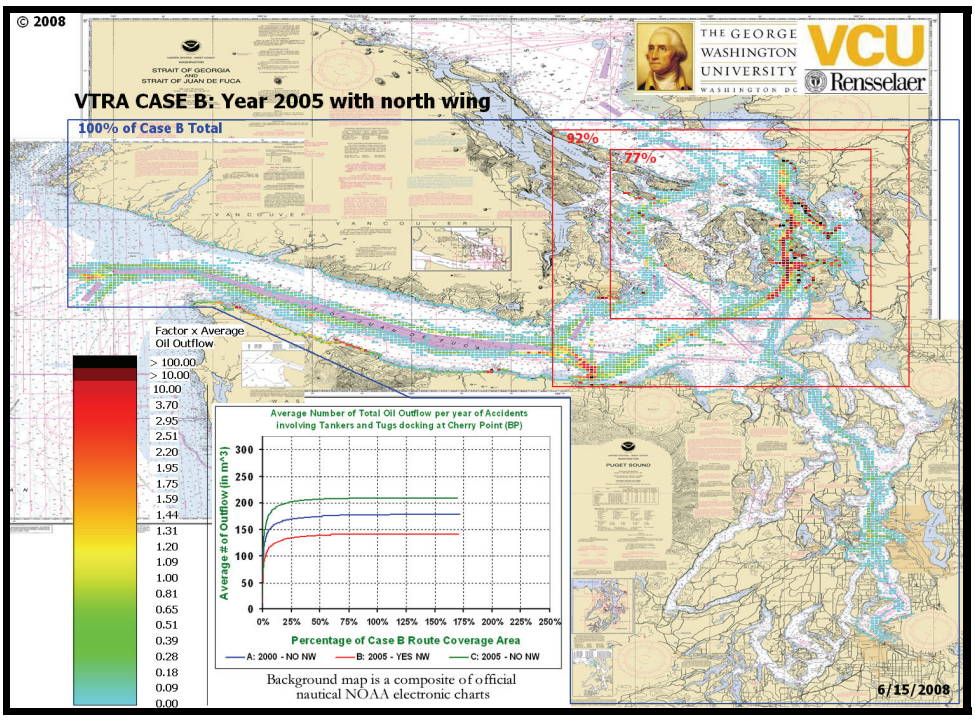

Assessment of Oil Spill Risk due to Potential Increased Vessel Traffic at Cherry Point, Washington

Submitted by VTRA TEAM:

Johan Rene van Dorp (GWU), John R. Harrald (GWU),

Jason R.. W. Merrick (VCU) and Martha Grabowski (RPI)

August 31, 2008

TABLE OF CONTENTS

Table of Figures.....E-3

Table of Tables.....E-5

E-1. The NRC oil outflow report.....E-6
E-3. Developing an oil outflow model.....E-7
E-2.1 Description of scenario data obtained from the NRC Oil outflow Report.....E-15
E-2.2. Striking and struck ship model.....E-17
E-2.3. Bunker fuel and diesel fuel regression models.....E-19
E-3. Representative results from the oil outflow model.....E-27

References.....E-37

Sub Appendix:.....E-38
G.F. van de Wiel (2008). "A Probabilistic Model for Oil Spill Volume in Tanker Collisions and Groundings", Master's Thesis: Applied Mathematics, Delft Univerisity of Technology, The Netherlands.

TABLE OF FIGURES

Figure E-1. Damage Extend PDFs, IMO Model (1995)..... E-6
Figure E-2. Cover of Special Report 259 publiseded by the Marine Board.....E-8
Transportation Reseach Board, The National Academies
Figure E-3. Tank configurations of 40kT tankers taken from the E-9
National Research Council Special Report 259.
Figure E-4. Tank configurations of 150kT tankers taken from the E-9
National Research Council Special Report 259.
Figure E-5. Worst case asssumption of oil outflow volume.....E-13
given a certain damage extent.
Figure E-6. Worst case assumption locations for bunker fuel tanks.....E-14
and diesel fuel tanks for Tankers.
Figure E-7. A schematic of a sticking ship-struck ship collision scenario.....E-16
Figure E-8. A schematic of a sticking ship-struck ship probability model.....E-18
Figure E-9. Deep draft vessel fuel data and least squares regression fits..... E-20
A: Scatter plot of bunker fuel volume by vessel length,
B: Scatter plots of diesel fuel by vessel length.
Figure E-10. Scatter plots of deep draft vessel bunker and diesel fuel data.....E-20
and least squares regression fits in a single plot.
Figure E-11. Scatter plot and least squares regression fit of diesel fuel E-21
data for tugs by vessel length.
Figure E-12. A 450 Series petroleum barge.....E-23
Figure E-13. Scatter plot and least squares regression fit of diesel fuel E-26
data for fishing vessels by vessel length.
Figure E-14. Scatter plot and least squares regression fit of diesel fuel E-26
data for motor yachts and service vessels by vessel length.
Figure E-15. Scatter plot and least squares regression fit of diesel fuel E-27
data for fsailing yachts by vessel length.
Figure E-16. Encoding of interactions by the VTRA maritime simulation..... E-28
Figure E-17. Annual average collision frequencies of Cherry Point Tankers,.....E-30
ATB's and ITB's in the calibration case: VTRA CASE B.
Figure E-18. Aggregate average oil outflow from collision with Cherry Point.....E-30
Tankers, ATB's and ITB's in the calibration case: VTRA CASE B.

TABLE OF FIGURES (Continued)

Figure E-19. Annual average drift grounding frequency of Cherry Point Tankers, ATB's and ITB's in the calibration case: VTRA CASE B. E-32
Figure E-20. Aggregate average oil outflow due to drift groundings of Cherry Point Tankers, ATB's and ITB's in the calibration case: VTRA CASE B. E-32
Figure E-21. Annual average powered grounding frequency of Cherry Point Tankers, ATB's and ITB's in the calibration case: VTRA CASE B. E-33
Figure E-22. Aggregate average oil outflow due to powered groundings of Cherry Point Tankers, ATB's and ITB's in the calibration case: VTRA CASE B. E-33
Figure E-23. Annual average allision frequency of BP Cherry Point Tankers, ATB's and ITB's in the calibration case: VTRA CASE B. E-35
Figure E-24. Aggregate average oil outflow due to allisions of BP Cherry Point Tankers, ATB's and ITB's in the calibration case: VTRA CASE B. E-35
Figure E-25. Aggregate average oil outflow from accident types involving Cherry Point Tankers, ATB's and ITB's in the calibration case: VTRA CASE B. E-36

TABLE OF TABLES

Table E-1. Example of modeled tank locations, dimensions and capacities.....E-15
for a 150kT double hull tanker.
Table E-2. Input variables and output results for the grounding oil outflow E-16
model in the VTRA maritime simulation.
Table E-3. Input variables and output results for the grounding oil outflow E-17
model in the VTRA maritime simulation.
Table E-4. Example of modeled tank locations, dimensions and capacities.....E-24
for a worst case oil barge.
Table E-5. Vessel dimensions of Washington State Ferries.....E-24
Table E-6. Approximate fuel tank locations and capacities for WSF's.....E-25
Table E-7. Example of modeled fuel tank locations of a Jumbo ferry.....E-25
Table E-8. Example of modeled fuel tank locations of an Issaquah ferry.....E-25
Table E-9. Average oil outflows per year by accident type.....E-29
for the calibration VTRA Case B (amounts are in cubic meters)
Table E-9. Percentages of average oil outflows per year by accident type..... E-29
for the calibration VTRA Case B (% of total average oil outflows)

E-1. The NRC oil outflow report

"The International Maritime Organization (IMO) is responsible for regulating the design of oil tankers to provide for ship safety and environmental protection. ... IMO's first attempt to apply a probabilistic methodology to tankers was in response to the US Oil Pollution Act of 1990 (OPA 90). In OPA 90 the US required that all oil tankers entering US waters must have double hulls. ... IMO responded to this unilateral action by requiring double hulls or their equivalent. Equivalency is determined based on probabilistic oil outflow calculations specified in IMO (1995)." (see, Brown (1995)). The purpose of the IMO model is to measure outflow performance of a particular tanker design. For this model, data was taken from approximately 100 historical collision and grounding scenarios from the period 1980-1990 to establish probability density functions (PDFs) for the location and extent of damage in a collision or grounding scenario (see Figure E-1). Based on these distributions, each unique combination of tanks or compartments in a given tanker design can be associated with a probability of being damaged.

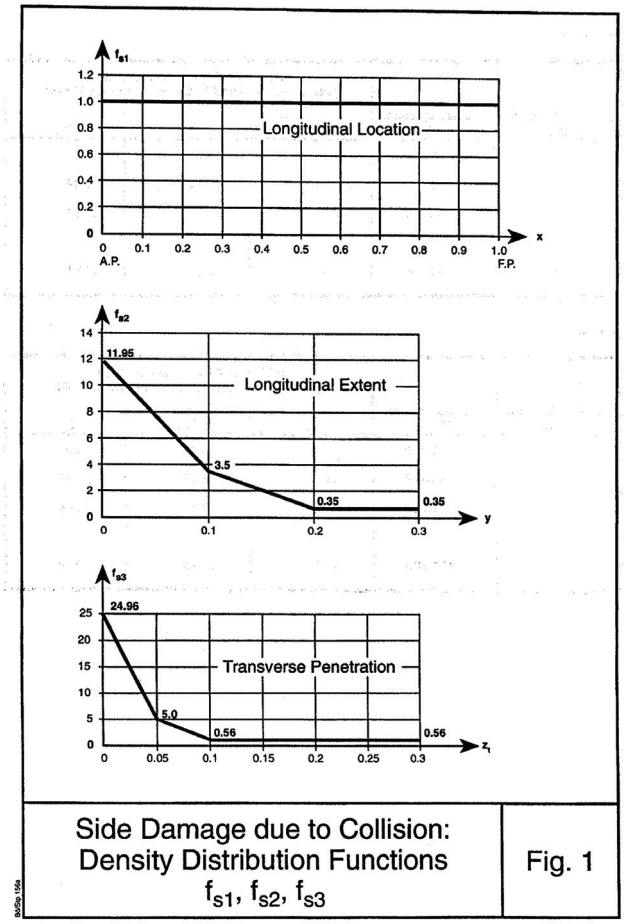

Figure E-1. Damage Extend PDFs, IMO Model (1995)

Unfortunately, the IMO model suffers from a number of fundamental limitations. Some of the objections raised by for example by Van der Laan(1997) and Brown (1998) (amongst others) are :

- The model uses a single set of damage extent PDFs from limited single hull data applied to all ships, independent of structural design; realistically, however, this data should only be used to model single hull accidents.
- Damage PDFs only consider damage that is significant enough to breach the outer hull. This penalizes structures able to resist rupture.
- Damage extents are treated as independent random variables when they are actually dependent variables, and should be described using a joint PDF.
- The IMO model does not have the ability to take the specifics of an accident scenario into account. Damage extents are sampled independently from the PDF's in Figue E-1.

In 2001, the Marine Board of the National Academy of Science published a report (see Figure E.2) assessing a methodology to compare double hull tanker designs to alternative designs NAS (2001). It too noted that the IMO (1995) model was insufficient for the goals outlined by the NAS (2001) report and that, consequently, further research was necessary: "Given the status of previous efforts to establish a methodology for comparing the environmental performance of alternative tanker designs, the committee concluded that the development of a new approach was warranted - NAS (2001)."

E-2. Developing an oil outflow model

The report NAS (2001) evaluates single hull and double tanker designs for both collisions and groundings. For their purpose they use physical simulations of accident damage inflicted on a tanker as developed by Brown (2001) and Tikka (2001) using the simulation programs SIMCOL resp. DAMAGE. For the Marine Board research, 10,000 collision and grounding scenarios were randomly generated and put through these simulation programs four times; each time using a different tanker design. This resulted in a data set of 40,000 collisions and 40,000 groundings, describing input (i.e. ship speed, displacement, collision angle) and output variables (i.e. damage length, outflow volume). The specific tanker designs that were evaluated by the NAS(2001) report are provided in Figures E-3 and Figures E-4. The goal of having these large data sets was for the NAS(2001) to compare typical outflow performance between single hull and double hull tankers.

While the physical simulation programs SIMCOL resp. DAMAGE by Brown (2001) and Tikka (2001), respectively, were used to develop the input and output data for 40,000 collision scenarios and 40,000 grounding scenarios of single hull and double hull tankers, an evaluation of a single scenario is quite computationally extensive on its own.

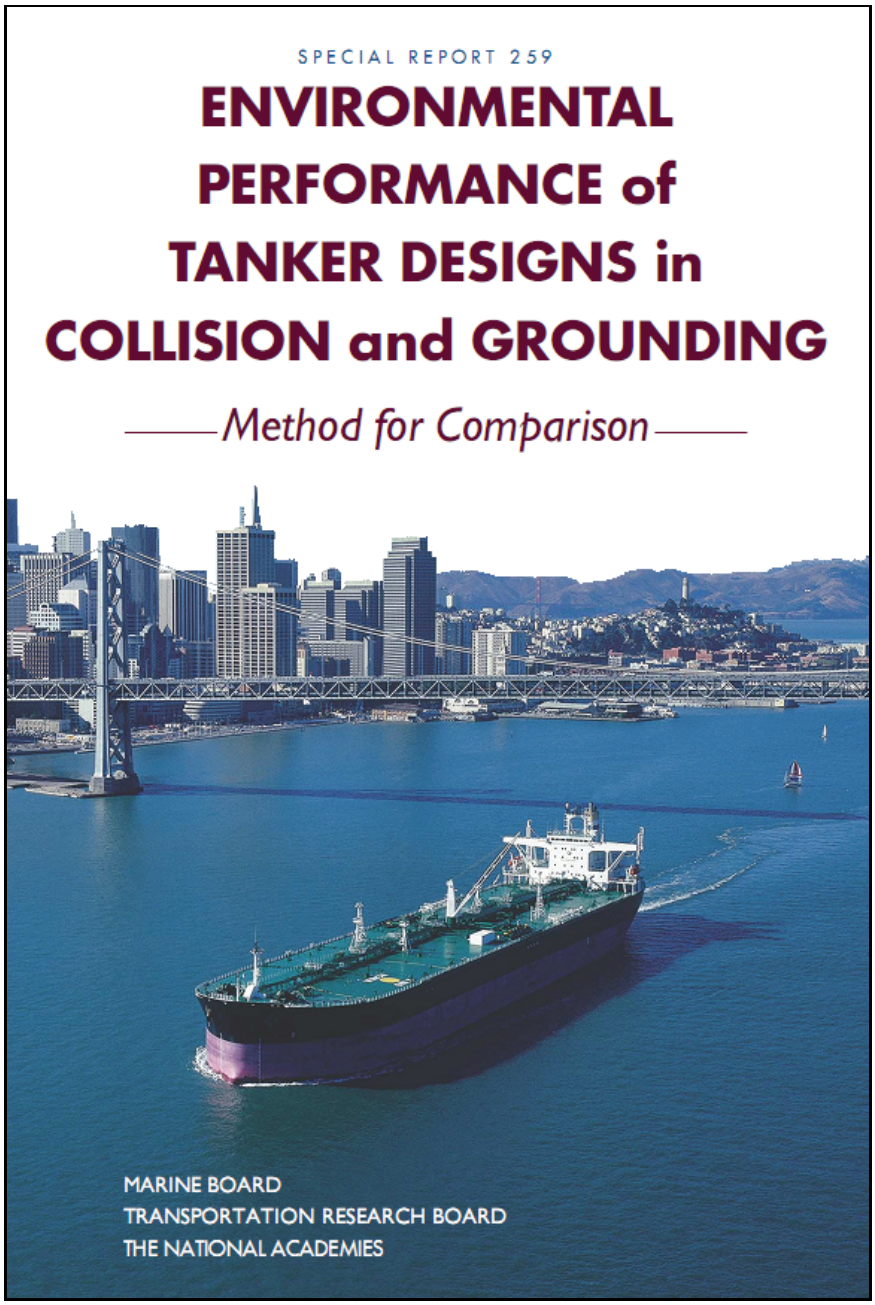

Figure E-2. Cover of Special Report 259 published by the Marine Board, Transportation Research Board, The National Academies.

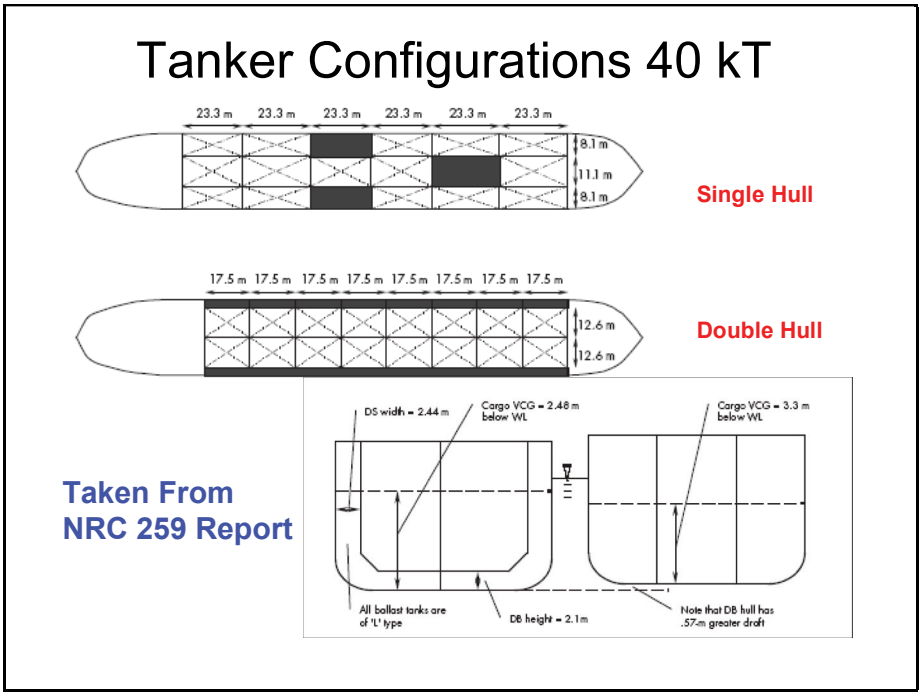

Figure E-3. Tank configurations of 40kT tankers taken from the National Research Council Special Report 259.

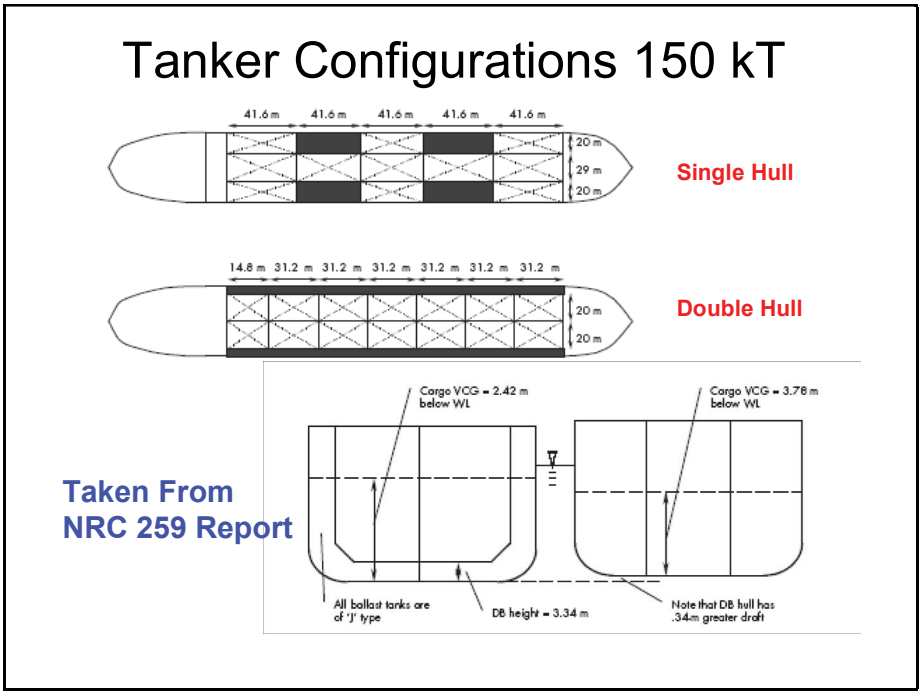

Figure E-4. Tank configurations of 150kT tankers taken from the National Research Council Special Report 259.

Therefore, these software programs at this time do not allow for a seamless integration with such tools as the Vessel Traffic Risk Assessment maritime simulation model that is computationally efficient as well. For example, the calibration scenario VTRA CASE B generates 61,427 vessel to vessel interactions and a future scenario VTRA CASE H has as many as 118,274 vessel to vessel interactions.

However, by carefully studying the relationships between input and output parameters of the large data sets made available through the NAS (2001) report one can "empirically" develop a probabilistic model that determines accident oil outflow based on statistical data analysis techniques rather can computationally intensive physical simulations; one that nevertheless needs to adhere to the same physical principles as the latter. An oil outflow model that explicitly describes the "albeit" statistical relationships between the input parameters and the output parameters can be integrated with the VTRA Maritime Simulation (provided that the simulation records available input data needed to evaluate the oil outflow of collision and grounding scenarios).

Such a model was developed by the Delft University of Technology over the course of this project in close coordination with the George Washington University to ensure a seamless connection between that oil outflow model and the VTRA Maritime Risk Simulation. Its construction is described in detail in the Sub Appendix to this appendix. Chapter 5 in this sub-appendix provides example oil outflow calculations for single hull and double hull tankers for collisions and groundings implemented for this VTRA project.
In this sub-appendix report, twelve accidental outflow models are presented: six collision models and six grounding models: a collision model for the single hull tanker and double hull tankers displayed in Figure E.3 (referred to in the Sub-Appendix as SH40 and DH40), a collision model and grounding model for the single hull and double hull tankers displayed in Figure E.4 (referred to in the Sub-Appendix as SH150 and DH150), a collision model and grounding model that was estimated using all single hull data (referred to as SHCOMB) and, finally, a collision and grounding model using all double hull data (referred to a DHCOMB). The SHCOMB and DHCOMB models allow for an interpolation between the different tankers sized displayed in Figures E-3 and E-4.

These models determine the amount of oil that flows from an oil tanker in case it is struck by another ship or runs aground on a rocky pinnacle. Based on specific scenario data, these models have the ability to evaluate the extent of collision or grounding damage, the probability of rupture and oil spill volume given a set of accident scenario variables. Chapter

5 in this sub-appendix provides example oil outflow calculations for single hull and double hull tankers for collisions and groundings implemented for this VTRA project. Each of these models can be quickly and straightforwardly be implemented in large scale system simulations of tanker movements because they involve formulas using only elementary functions and include an overseeable amount of parameters and coefficients. In short, they combine the power of the physical simulation software of SIMCOL resp. DAMAGE by Brown (2001) and Tikka (2001) with the simplicity of explicit functions. Moreover, these models improve significantly upon the previous IMO model since:

- They are based on a large data set obtained by physically meaningful simulations, rather than a model with simpler assumptions based on a small historic data set;
- They allow for ship size-dependent damage extent and probability of rupture assessments, whereas the old model gave damage and probability independently of ship size;
- Damage extent parameters are dependent on scenario input variables as opposed to independently distributed;
- Damage extent parameters take into account the physical characteristics of the ship designs and accident scenarios, such as speed, mass, collision angle, etc.

While on the outset of our project we set out to evaluate cargo losses from tank vessels that dock at BP Cherry point (referred to hereafter as BP CHPT vessels), we were requested over the course of the project to also consider the potential oil outflow from an interacting vessels when it potentially collides with a BP CHPT Vessel. Specifically, we were requested to separate the total expected oil outflow results by location and size from BP Cherry Point vessels and interacting vessels that potentially collide with them into the following four categories:

- Persistent Expected Oil Outflow results to include crude oil and bunker fuel from BP Cherry Point vessels.
- Persistent Expected Oil Outflow to include crude oil and bunker fuel from interacting vessels.
- Non-Persistent Expected Oil Outflow to include refined products and diesel fuel from BP Cherry Point vessels.
- Non-Persistent Expected Oil Outflow to include refined products and diesel fuel from interacting vessels.

Possibly the need for accounting fuel losses arose from the November 6, 2007 M/V Cosco Busan oil spill in San Francisco Bay. While the models in the sub-appendix were designed specifically for cargo losses from tank vessels, these models offer a flexibility to provide the outflow results above by making some reasonable assumptions.

Given an damage location *a* from mid ship, a damage length *b* and a damage penetration *b*, the model in the Sub-Appendix evaluates the compartments that have been "penetrated" by making two worst case assumptions as depicted in Figure E-5.

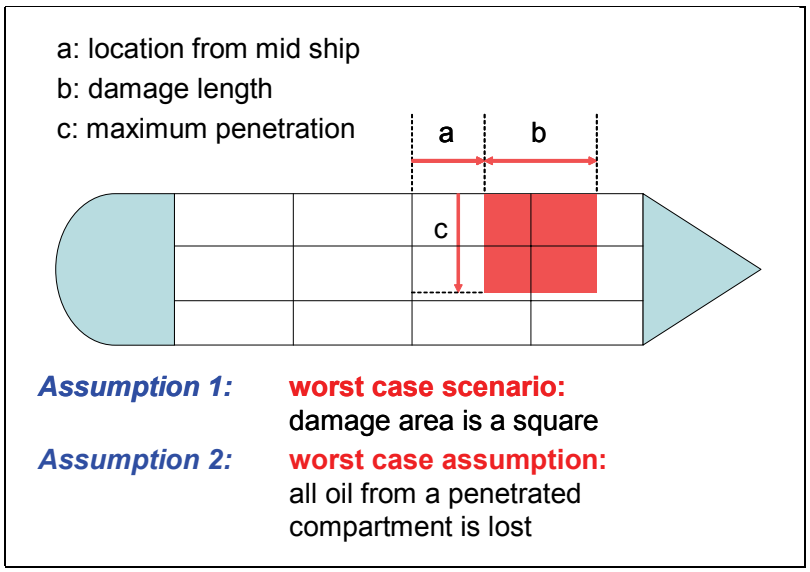

Figure E-5. Worst case assumption of oil outflow volume given a certain damage extent.

Hence, to be able to accomodate diesel fuel and bunker fuel oil outflow calculations for tankers one needs to augment the vessel compartmentalization of Figures E-3 and Figure E-4 with bunker fuel and diesel fuel compartments. While there certainly can be more than two tanks for bunker fuel and two tanks for diesel fuel on a given tanker one could assume (again from a worst case scenario perspective) the following locations for bunker fuel and diesel fuel for tankers as provided in Figure E-6. Note that it follows from Figure E-6 that we continue to provide the double hull tankers the benefit of the double hull for the diesel fuel and bunker fuel compartments. We located the bunker fuel compartments towards the stern (since this is where the main engine compartment is located) and the diesel compartments towards the bow. A reversal of these locations did not seem to make sense given that bunker volumes on deep draft vessels may differ in one order of magnitude (see Section E.2.2). Table E-1 provides the tanker dimensions and the location of the various compartment for

the DH150 tankers design that we used in the VTRA maritime simulation. Similar tables were developed for the SH40, DH40 and SH150 designs.

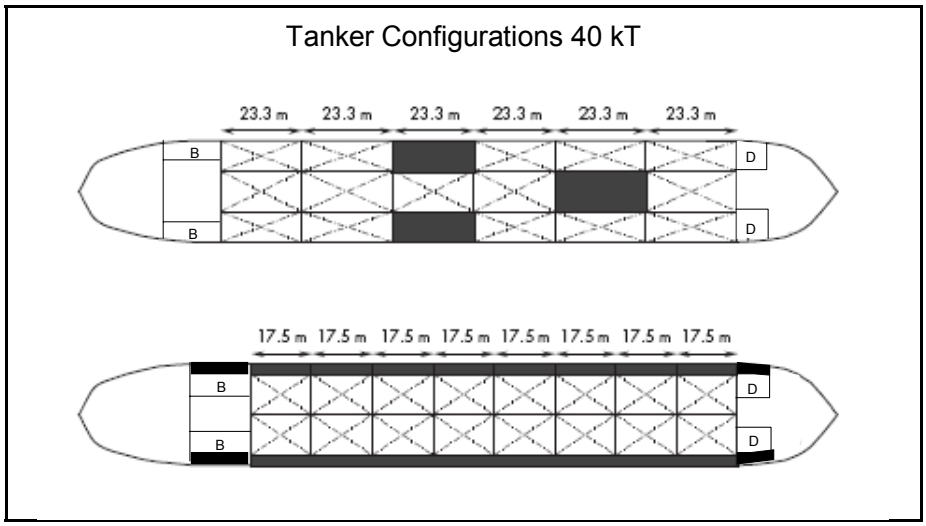

Figure E-6. Worst case assumption locations for bunker fuel tanks and diesel fuel tanks for Tankers.

The capacities provided in Table E-1 are full load capacities for each compartment. The VTRA simulation actually passes to the oil outflow model calculations, whether the tank vessel is carrying product or crude and also the cargo DWT of crude or product that it is carrying. This total capacity is next evenly distributed across the cargo tanks and the tanker is ballasted making the assumption that a tanker is 100% ballasted when the cargo tanks are empty and 0% ballasted when the cargo tanks are complete full (and following a linear relationship in between). Next, using the lightship weight information (also passed by the VTRA maritime simulation) we recalculate the displacement of a partially loaded tanker. The ship's mass (displacement) is one of the required input variables for oil outflow calculations as described in the sub-appendix. Before the above "re balancing" above, the size of a tanker design from the NAS (2001) report and its compartments are rescaled in a linear manner using the ship length and beam also passed to the oil outflow calculation model by the VTRA maritime simulation (but keeping the same format of the compartmentalization of the SH40, DH40, SH150 and DH150 tanker designs). A tank vessel's length is used to evaluate its bunker fuel load and diesel fuel load using a regression model for deep draft vessels (see Section E.2.2).

When restricting oil outflow calculations to those from BP CHPT vessels one could have made a worst case assumption that the BP CHPT vessel was always the stuck vessel in a

vessel interaction. However, with the requirement of evaluating oil outflow from interacting vessels when potentially colliding with a BP CHPT vessel, such an assumption is not reasonable since not both vessels can be "the stuck vessel" in a single vessel interaction scenario at the same time. In the sections below we shall discuss some additional detail regarding the oil outflow model described in the Sub-Appendix, describe a striking-struck ship model and regression models to relate a vessels lengths to its fuel carrying capacity.

Table E-1. Example of modeled tank locations, dimensions and capacities for a 150kT double hull tanker

	X	Y	Z	Length	Width	Capacity (m3)	Content
1	0.00	0.00	3.34	12.30	3.34	710.91	Empty
2	8.29	3.34	3.34	4.01	7.06	159.94	Diesel
3	8.29	39.60	3.34	4.01	7.06	159.94	Diesel
4	0.00	46.66	3.34	12.30	3.34	710.91	Empty
5	12.30	0.00	3.34	31.20	3.34	1803.28	Ballast
6	12.30	3.34	3.34	31.20	21.66	11694.30	Crude
7	12.30	25.00	3.34	31.20	21.66	11694.30	Crude
8	12.30	46.66	3.34	31.20	3.34	1803.28	Ballast
9	43.50	0.00	3.34	31.20	3.34	2262.78	Ballast
10	43.50	3.34	3.34	31.20	21.66	14674.20	Crude
11	43.50	25.00	3.34	31.20	21.66	14674.20	Crude
12	43.50	46.66	3.34	31.20	3.34	2262.78	Ballast
13	74.70	0.00	3.34	31.20	3.34	2259.11	Ballast
14	74.70	3.34	3.34	31.20	21.66	14650.40	Crude
15	74.70	25.00	3.34	31.20	21.66	14650.40	Crude
16	74.70	46.66	3.34	31.20	3.34	2259.11	Ballast
17	105.90	0.00	3.34	31.20	3.34	2259.23	Ballast
18	105.90	3.34	3.34	31.20	21.66	14651.20	Crude
19	105.90	25.00	3.34	31.20	21.66	14651.20	Crude
20	105.90	46.66	3.34	31.20	3.34	2259.23	Ballast
21	137.10	0.00	3.34	31.20	3.34	2259.17	Ballast
22	137.10	3.34	3.34	31.20	21.66	14650.80	Crude
23	137.10	25.00	3.34	31.20	21.66	14650.80	Crude
24	137.10	46.66	3.34	31.20	3.34	2259.17	Ballast
25	168.3	0	3.34	31.2	3.34	2137.522899	Ballast
26	168.30	3.34	3.34	31.20	21.66	13861.90	Crude
27	168.30	25.00	3.34	31.20	21.66	13861.90	Crude
28	168.30	46.66	3.34	31.20	3.34	2137.52	Ballast
29	199.50	0.00	3.34	14.80	3.34	850.37	Ballast
30	199.50	3.34	3.34	14.80	21.66	5514.70	Crude
31	199.50	25.00	3.34	14.80	21.66	5514.70	Crude
32	199.50	46.66	3.34	14.80	3.34	850.37	Ballast
33	214.30	0.00	3.34	52.00	3.34	2987.80	Empty
34	214.30	3.34	3.34	26.79	11.16	2649.93	Heavy Fuel
35	214.30	35.50	3.34	26.79	11.16	2649.93	Heavy Fuel
36	214.30	46.66	3.34	52.00	3.34	2987.80	Ballast

E-2.1. Description of scenario data obtained from the NRC Oil outflow Report

A complete description of the scenario data is provided in the Sub-Appendix, Chapter 2. Tables E-2 and E-3 provide an informal description of those input variables and output

variables from the NAS(2001) report that we were able to link directly within the VTRA maritime simulation. Figure E-5 depicts the input scenario information from Table E-2 graphically for a particular example collision scenario. With the exception of the damage location input variables listed in Tables E-2 and E-3, these input variables are recorded directly into the recording databases from the VTRA simulation. Such a recording was also necessary for the accident attributes of the accident probability models for collisions and groundings described in Appendix D.

Table E-2. Input variables and output results for the collision oil outflow model in the VTRA maritime simulation.

Input Variables	Output Variables
Striking ship velocity	Damage length
Struck ship velocity	Maximum penetration
Collision angle	Oil outflow volume
Displacement of Striking Vessel	
Displacement of Struck Vessel	
Collision location, relative from stern	
Striking ship type	

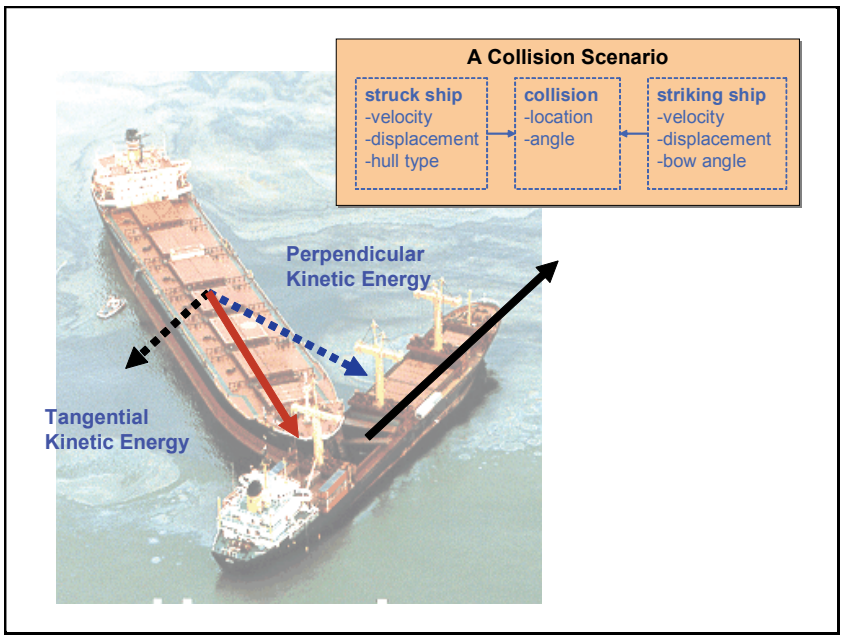

Figure E-7. A schematic of a sticking ship-struck ship collision scenario

Table E-3. Input variables and output results for the grounding oil outflow model in the VTRA maritime simulation.

Input Variables	Output Variables
Ship velocity	Begin Damage length
Displacement of Vessel	End Damage Length
Damage Location from Mid-Ship	Damage Width
	Damage Height
	Outflow Volume

Our VTRA Maritime simulation does not simulate the circumstances and movements of vessels immediately preceding accidents and as a result we cannot record the exact location of a collision or the location of the grounding relative to the dimensions of the vessel. Hence, instead we evaluate the oil outflow distributed over 100 discrete points across a vessel length for collisions and across a vessels half-width for groundings and we evaluate the average oil outflow per collision or per grounding across all these different locations.

The models constructed in the sub-appendix allow for an interpolation between the tanker sizes depicted in Figures E-3 and E-4. To that end, we converted the input variables in Tables E-2 and E-3 to ones that relate to a kinetic energy interpretation. For example, striking ship velocity, struck ship velocity, striking ship displacement and stuck ship displacement are converted into a tangential and perpendicular kinetic energies (see Figure E-7) which are then in turn related to damage length and damage penetration calculations.

As noted previously, in all scenarios in the NAS(2001) report the tanker is assumed to be the struck vessel (contrary to the example photo in Figure E-7.). The next section discusses the striking ship-struck ship model that we developed to account for the possibility that in fact the tank vessel is the striking vessel (as depicted in Figure E-7).

E-2-2. Striking and struck ship model

In the event of two identical ships crossing each others paths at a 90 degree angle traveling at exactly the same speeds, it would be reasonable to assume that their would be a 50-50 chance that either one would the struck or striking vessels. However, this assumption becomes less reasonable when their is a large speed differential or if their ship dimensions are much different. Take, for example, an interaction between a tanker and a recreational vessel. Simply from the point of size it would seem much easier to actually strike the tanker

than striking the recreational vessel. Who strikes and who is stuck has implications with respect to the oil outflow that one evaluates for such a collision scenario. We have developed a conditional probability model that evaluates a probability that either Vessel 1 or Vessel 2 is the struck vessel (given that a collision is about to occur between these two vessels). Needless to say, these two conditional probabilities need to sum up to 1 in that case by definition.

Figure E-6 provides a schematic and a geographic explanation of this striking-stuck ship model. Let L_1, w_1 and v_1 be the length, width and traveling speed of the first vessel. Let L_2, w_2 and v_2 be the length, width and traveling speed of the second vessel and let Φ be the angle of the crossing paths of these two vessels. From these parameters we first evaluate the distance that Vessel 1 is exposed to the potential of a collision which follows as

$$L_{1+}\frac{w_2}{\sin\phi}. \tag{E-1}$$

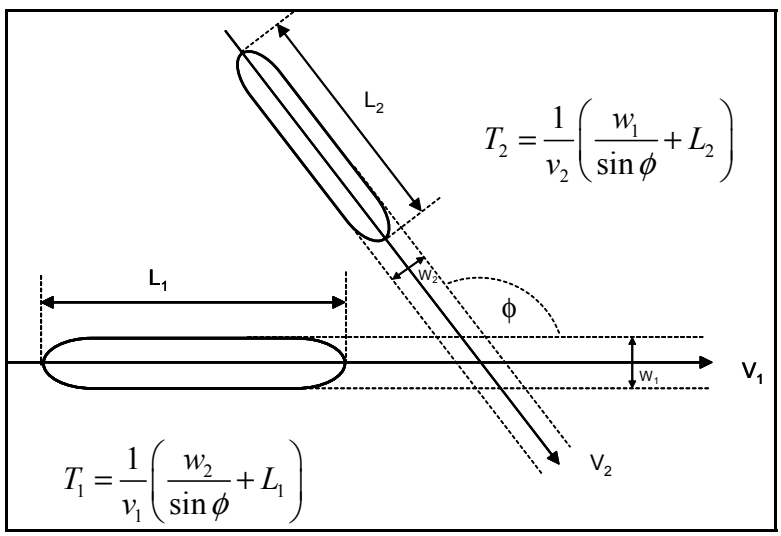

Figure E-8. A schematic of a sticking ship-struck ship probability model.

Dividing this distance by the Vessel 1 speed v_1 yields the length of time T_1 that Vessel 1 is exposed to the potential of a collision given the angle Φ of the tracks of Vessel 1 and Vessel 2 and the width of Vessel 2:

$$T_1 = \frac{1}{v_1}\left(L_{1+}\frac{w_2}{\sin\phi}\right). \tag{E-2}$$

Using a symmetry argument we evaluate for the length of time T_2 that Vessel 2 is exposed as:

$$T_2 = \frac{1}{v_2}\left(L_{2+}\frac{w_1}{\sin\phi}\right). \tag{E-3}$$

Next, we set:

$$Pr(\text{Vessel 1 is struck}) = \frac{T_1}{T_1 + T_2} \text{ and } Pr(\text{Vessel 2 is struck}) = \frac{T_2}{T_1 + T_2}. \tag{E-4}$$

From expression (E-4) we evaluate that two identical vessels traveling at the same speeds and crossing paths at a 90 degree angles indeed have a 50-50 chance of being the struck vessel. On the other hand we evaluate from (E-4), for example, that a DH150 tanker (with a length 266.3 meters and width of 50 meters) traveling at 8 knots crossing the path of a tug (with a length of 34 meters and a width of 12 meters) traveling at 12 knots at a ϕ=135 degree angle, has approximately an 80% probability of being struck. Hence, in that scenario the tug has approximately a 20% probability of being struck.

In the VTRA maritime simulation, the loss of oil from a struck vessel is weighted by the probability of the vessel being struck evaluated using expression (E-4). It is further assumed that no vessel fuel or oil cargo products is lost from the striking vessel. In the case of a traffic scenario that a small vessel is the struck vessel (in the sense that the length of the smaller vessel is less than or equal the width of the larger vessel) all diesel fuel on board of the smaller vessel is assumed lost. Otherwise the oil outflow models in the sub-appendix are used to evaluate damage length and penetration to determine those cargo or fuel tanks that are penetrated. For non-tankers the single hull parameters settings are used from the sub-appendix to evaluate these damage extents.

E-2.3. Bunker fuel and diesel fuel regression models

The vessels considered in the VTRA range in size and utility between Cherry Point oriented tankers and sailing regattas. The fuel or fuel oil capacities of these vessels are as diverse as the vessels themselves. In order to include diesel fuel and bunker fuel in the outflow models of VTRA maritime simulation multiple sources have been queried in order to develop model fuel oil capacities as a function of size and utility of the vessel being considered. This section outlines the sources of the data queried and the regression models that have been fitted to estimate a vessel's fuel capacity as a function of a vessel's length.

The fuel oil capacities for Cherry Point tankers are source in Vessels Particular Questionnaires (VP's) for each tanker that has made calls at the Cherry Point Facility. The

VP for each vessel offered the fuel oil type and volume capacity of each fuel oil tank. Bunker and diesel fuel vessel for other deep draft vessels in the VTRA maritime simulation were compiled from various regional and global vessel brokerage firm's web-sites (e.g. http://www.ship-technology.com) as well as from the publication Taggart (1980). The data from these data sources were combined to generate the scatter plots in Figure E-9.

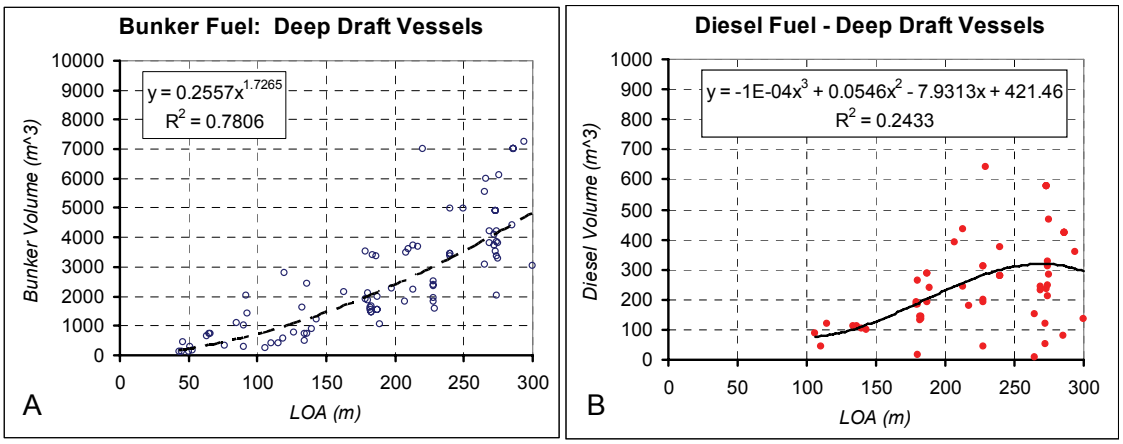

Figure E-9. Deep draft vessel fuel data and least squares regression fits, A: Scatter plot of bunker fuel volume by vessel length, B: Scatter plots of diesel fuel by vessel length.

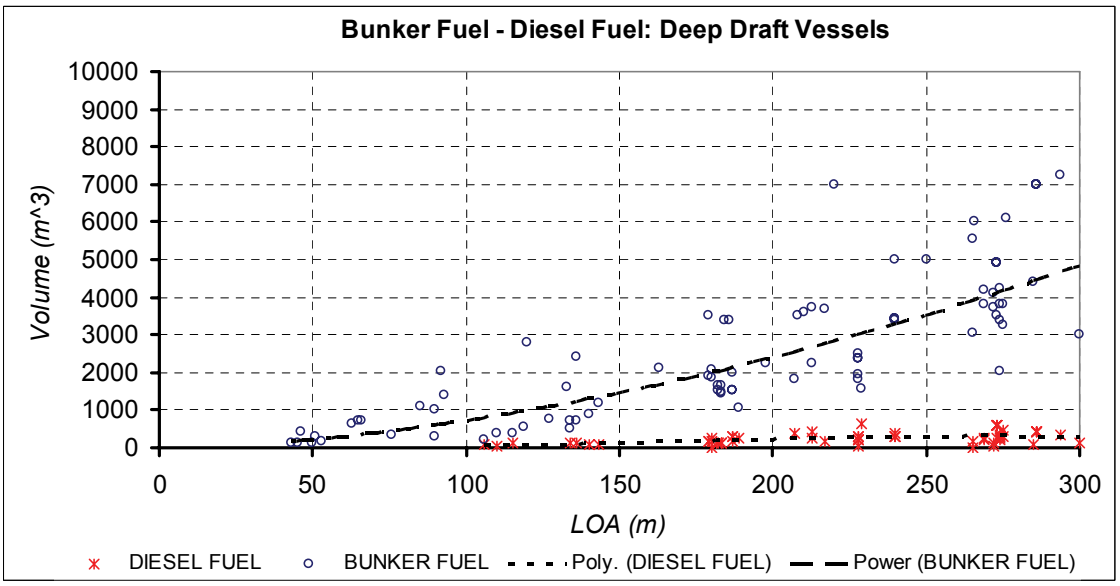

Figure E-10. Scatter plots of deep draft vessel bunker and diesel fuel data and least squares regression fits in a single plot.

Figure E-9A provides a scatter plot of the accumulated bunker fuel data and Figure E-9B provides a scatter plot of the accumulated diesel fuel data for deep draft vessels. Please note that the scale of the y-axis in Figure E-9A is one order of magnitude higher than that of Figure 9B. This becomes more apparent when combining both scatter plots in a single plot in Figure E-10. Figures 9A and 9B contains the equations of the regressions fits linking bunker and diesel fuel to a vessel's length, respectively. Note that the R^2 of 78% value for the bunker fuel is quite respectable, whereas the R^2 value of the diesel fuel is quite low. From Figure E-10 it follows that this lack-of-fit will be masked by the amount of bunker fuel on a tank vessel of a particular length.

The same locations for the bunker fuel tanks and the diesel fuel tanks given in Figure E-6 were assumed for other deep draft vessels than tankers. The parameters of the single hull damage models in the Sub-appendix were used to evaluate damage length and damage penetration for these deep draft vessels after which the analysis exemplified by Figure E-5 was used to determine if these fuel tanks were penetrated. If penetrated, all bunker fuel or diesel fuel in a penetrated tanks was assumed lost.

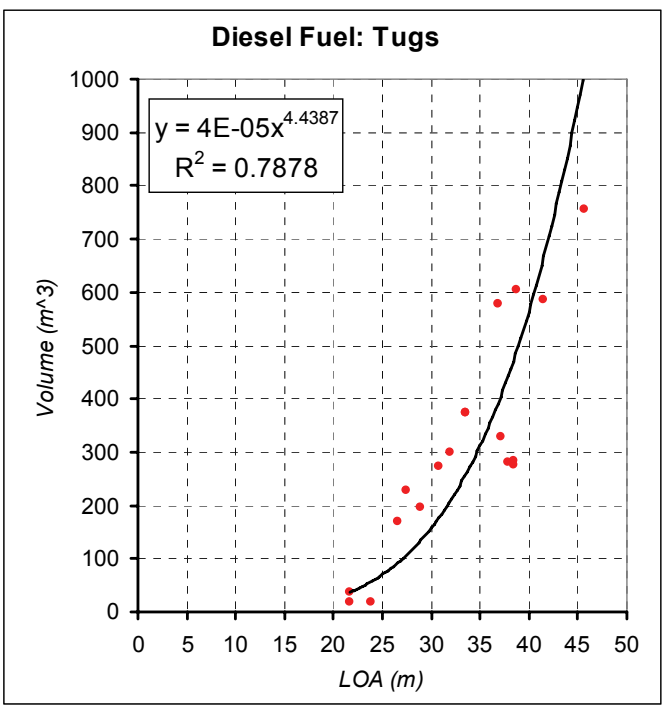

Figure E-11. Scatter plot and least squares regression fit of diesel fuel data for tugs by vessel length.

The fuel oil capacities for Cherry Point oriented ITB's and ATB's are sourced in the VPQ's as well. This information was combined with tug diesel capacity data from more general vessel design sources, specifically, specific vessel schematics made available through the web sites of various vessel brokerage firms, Tug operating companies in the Puget Sound region and Taggert (1980). The resulting scatter plot and regression fit (with an R^2 of about 79%) linking the length of tugs with their diesel carrying capacity are displayed in Figure E-11 above.

Scaled SH40 and DH40 tanker compartmentalizations were also assumed to model the oil outflow from ATB's and ITB's with the exception that the bunker fuel at the stern was replaced with diesel fuel with a carrying capacity determined by the length of the tug and the regression equation in Figure E-11. In the event of a light tug (i.e. a tug traveling by itself without a barge and given that the length of tug is typically smaller than the width of a BP CHPT tank vessel) all diesel fuel from a tug was assumed lost in the event it is the struck vessel. Indeed, DH150 tankers have a width of 50 meters (see Table E-1) whereas the upper bound of the scatter plot E-11 is 50 meters.

In the case that a vessel interaction occurred between a BP CHPT vessel and an oil barge being towed, we accounted for the potential oil loss from the oil barge. There are many different sizes of oil barges that are used within the Puget Sound area. We made a worst case assumption and used the configuration of one of the larger oil product barges depicted in Figure E-12 combined with the single hull oil outflow parameters from the sub-appendix. We modeled the tank locations of the oil barge as per Table E-4. Hence, we evaluated damage lengths and penetration following the oil outflow model in the sub-appendix and used the analysis exemplified in Figure E-5 to evaluate the tanks that were penetrated. All petroleum products from penetrated tanks were assumed lost.

One of the larger participants of the VTRA study area are the Washington State Ferries. Over the course of this project we have requested vessel rides on the Washington States Ferries given their unique distribution of their routes across the VTRA Study area and regular schedule. On every occasion we found the Washington State Ferry system to particularly accommodating and we are obliged for their assistance. When requesting the dimensions of the various WSF's in the system, their diesel fuel carrying capacity and the approximate locations of the fuel tanks we once again found the Washington State Ferries management to very responsive and our data request was honored in a matter of two weeks. We would like to thank the Washington State Ferry system for their participation as they too

(similar to the experts that participated in the expert judgment elicitation described in Appendix B) had no benefit to participating in this study other than that it possibly could enhance the safety of the waterway within the VTRA study area.

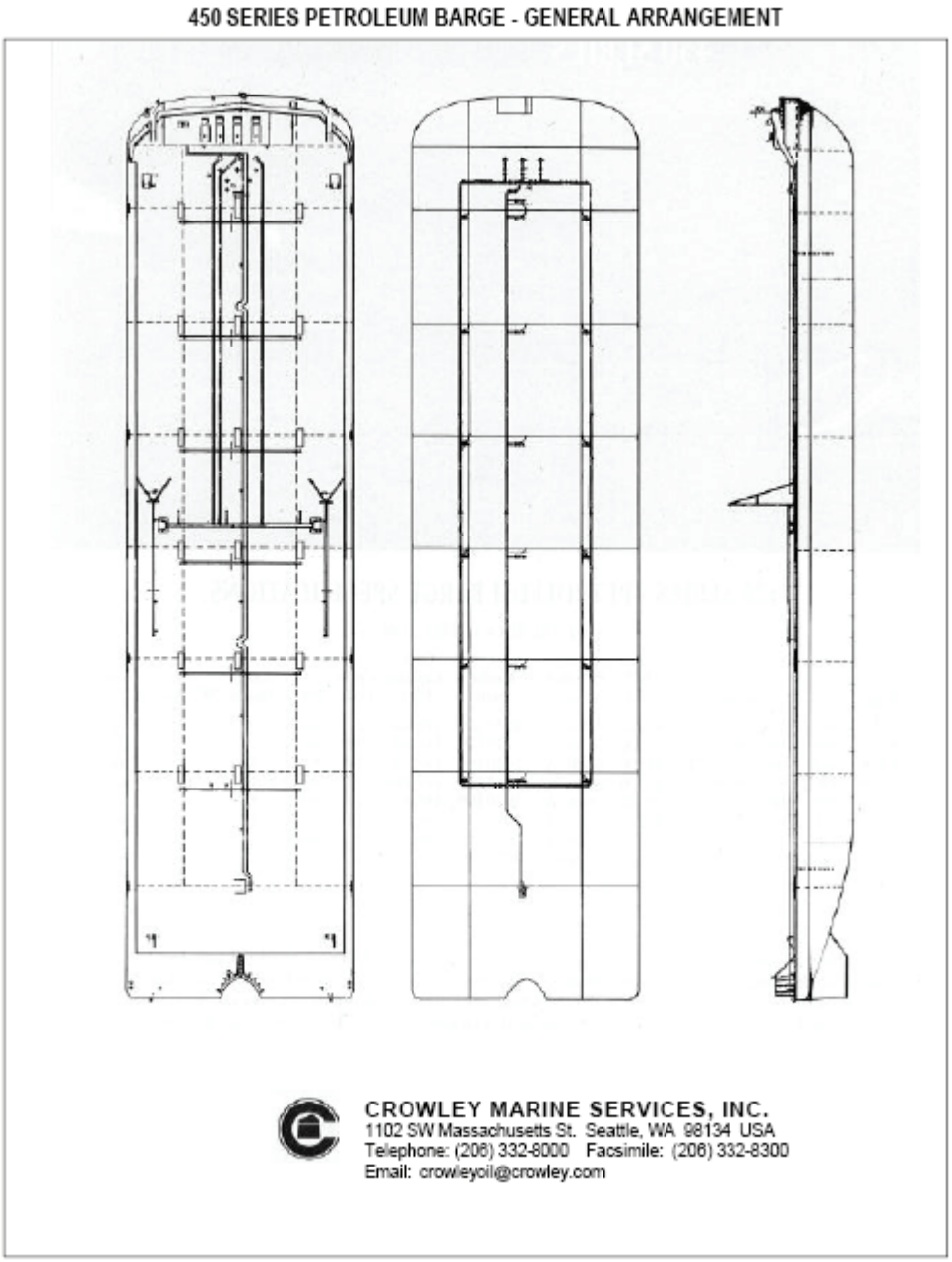

Figure E-12. A 450 Series petroleum barge.

The information that we received from the Washington Ferries System regarding the dimensions of their vessels and the approximate location of the fuel tanks in their vessels are

Table E-4. Example of modeled tank locations, dimensions and capacities for a worst case oil barge.

	X	Y	Z	Length	Width	Capacity (m3)	Content
1	0.00	0.00	0.00	7.62	30.30	0.00	Empty
2	7.62	0.00	0.00	7.62	7.58	473.82	Product
3	15.24	0.00	0.00	15.24	7.58	947.64	Product
4	30.48	0.00	0.00	15.24	7.58	947.64	Product
5	45.72	0.00	0.00	15.24	7.58	947.64	Product
6	60.96	0.00	0.00	15.24	7.58	947.64	Product
7	76.20	0.00	0.00	15.24	7.58	947.64	Product
8	91.44	0.00	0.00	15.24	7.58	947.64	Product
9	7.62	12.93	0.00	4.44	4.44	87.32	Diesel
10	15.24	7.58	0.00	15.24	15.15	1895.28	Product
11	30.48	7.58	0.00	15.24	15.15	1895.28	Product
12	45.72	7.58	0.00	15.24	15.15	1895.28	Product
13	60.96	7.58	0.00	15.24	15.15	1895.28	Product
14	76.20	7.58	0.00	15.24	15.15	1895.28	Product
15	91.44	7.58	0.00	15.24	15.15	1895.28	Product
16	7.62	22.73	0.00	7.62	15.15	473.82	Product
17	15.24	22.73	0.00	15.24	7.58	947.64	Product
18	30.48	7.58	0.00	15.24	7.58	947.64	Product
19	45.72	0.00	0.00	15.24	7.58	947.64	Product
20	60.96	0.00	0.00	15.24	7.58	947.64	Product
21	76.20	0.00	0.00	15.24	7.58	947.64	Product
22	91.44	0.00	0.00	15.24	7.58	947.64	Product
23	106.68	0.00	0.00	15.24	30.30	0.00	Empty

Table E-5. Vessel dimension of Washington State Ferries.

WSF Ferry	Class	Length	Beam	Draft	Speed	Displacement (Mtons)
Puyallup	Jumbo Mark II	460'2"	90'	17'3"	18	10690
Tacome	Jumbo Mark II	460'2"	90'	17'3"	18	10690
Wenatchee	Jumbo Mark II	460'2"	90'	17'3"	18	10690
Spokane	Jumbo	440"	87"	16'	18	9913
Walla Walla	Jumbo	440"	87"	16'	18	9913
Elwha	Super	382'2"	73'2"	18'9"	20	8005
Hyak	Super	382'2"	73'2"	18'9"	17	8005
Kaleetan	Super	382'2"	73'2"	18'9"	17	8005
Yakima	Super	382'2"	73'2"	18'9"	17	8005
Cathlamet	Issaquah 130	328'	78'8"	16'6"	16	6234
Chelan	Issaquah 130	328'	78'8"	16'6"	16	6234
Issaquah	Issaquah 130	328'	78'8"	16'6"	16	6234
Kitsap	Issaquah 130	328'	78'8"	16'6"	16	6234
Kittitas	Issaquah 130	328'	78'8"	16'6"	16	6234
Sealth	Issaquah 100	328'	78'8"	15'6"	16	6234
Evergreen State	Evergreen	310'	73'2"	15'10"	13	5466
Klahowya	Evergreen	310'	73'2"	15'10"	13	5466
Tillikum	Evergreen	310'	73'2"	15'10"	13	5466
Illahee	Steel Electric	256'2"	73'10"	12'9"	12	3550
Klickitat	Steel Electric	256'2"	73'10"	12'9"	12	3550
Nisqually	Steel Electric	256'2"	73'10"	12'9"	12	3550
Quinault	Steel Electric	256'2"	73'10"	12'9"	12	3550
Rhodondendron	Rhodondendron	227'6"	62'	10'	11	2423
Hiyu	Hiyu	162'	63'1"	11'3"	10	2043
Kalama	POV	112'	25"	8'	25	508
Skagit	POV	112'	25"	8'	25	508

Table E-6. Approximate fuel tank locations and capacities for WSF's.

WSF Ferry	Class	Total Fuel Capacity (in Gallons)	Number of Fuel Tanks	Location Fuel Tank (Mid-Ship, Starboard, Port)	Approximate length Fuel Tank	Approximate width Fuel Tank
Puyallup	Jumbo Mark II	110385	2	#1 Centerline #2 Centerline	37	30
Tacome	Jumbo Mark II	110385	2	#1 Centerline #2 Centerline	37	30
Wenatchee	Jumbo Mark II	110385	2	#1 Centerline #2 Centerline	37	30
Spokane	Jumbo	125000	2	#1 Centerline #2 Centerline	40	35
Walla Walla	Jumbo	125000	2	#1 Centerline #2 Centerline	40	35
Elwha	Super	62372	3	Port Center STB (MID)	27	24
Hyak	Super	77683	3	Port Center STB (MID)	27	24
Kaleetan	Super	77683	3	Port Center STB (MID)	27	24
Yakima	Super	77683	3	Port Center STB (MID)	27	24
Cathlamet	Issaquah 130	115400	4	Wing Port, Deep Port Deep STB Wing STB (MID)	1&4 -- 13'6" 2&3 -- 27'	#2&3 fuel oil tks. 22'-6"W, 1&4 fuel oil tks.14'-0"W
Chelan	Issaquah 130	115400	4	Wing Port, Deep Port Deep STB Wing STB (MID)	1&4 -- 13'6" 2&3 -- 27'	#2&3 fuel oil tks. 22'-6"W, 1&4 fuel oil tks.14'-0"W
Issaquah	Issaquah 130	115400	4	Wing Port, Deep Port Deep STB Wing STB (MID)	1&4 -- 13'6" 2&3 -- 27'	#2&3 fuel oil tks. 22'-6"W, 1&4 fuel oil tks.14'-0"W
Kitsap	Issaquah 130	115400	4	Wing Port, Deep Port Deep STB Wing STB (MID)	1&4 -- 13'6" 2&3 -- 27'	#2&3 fuel oil tks. 22'-6"W, 1&4 fuel oil tks.14'-0"W
Kittitas	Issaquah 130	115400	4	Wing Port, Deep Port Deep STB Wing STB (MID)	1&4 -- 13'6" 2&3 -- 27'	#2&3 fuel oil tks. 22'-6"W, 1&4 fuel oil tks.14'-0"W
Sealth	Issaquah 100	115400	4	Wing Port, Deep Port Deep STB Wing STB (MID)	1&4 -- 13'6" 2&3 -- 27'	#2&3 fuel oil tks. 22'-6"W, 1&4 fuel oil tks.14'-0"W
Evergreen State	Evergreen	30600	2	Port STB (MID)	13.5	14
Klahowya	Evergreen	30600	2	Port STB (MID)	13.5	14
Tillikum	Evergreen	30600	2	Port STB (MID)	13.5	14
Illahee	Steel Electric	9000	2	Port STB (MID)	12	6' Diameter
Klickitat	Steel Electric	9000	2	Port STB (MID)	12	6' Diameter
Nisqually	Steel Electric	9000	2	Port STB (MID)	12	6' Diameter
Quinault	Steel Electric	9000	2	Port STB (MID)	12	6' Diameter
Rhodondendron	Rhodondendron	11397	2	Center Line #1 end #2 end	20	12'
Hiyu	Hiyu	10000	2	Port STB #1 end	12'	NA
Kalama	POV	6714	2	Port STB (MID)	6	6
Skagit	POV	6714	2	Port STB (MID)	6	6

Table E-7. Example of modeled fuel tank locations of a Jumbo ferry.

	X	Y	Z	Length	Width	Capacity (m3)	Content
1	54.86	7.92	0.00	12.19	10.67	236.64	Diesel
2	67.06	7.92	0.00	12.19	10.67	236.64	Diesel

Table E-8. Example of modeled fuel tank locations of an Issaquah ferry.

	X	Y	Z	Length	Width	Capacity (m3)	Content
1	47.93	0.86	0.00	4.11	4.27	51.84	Diesel
2	45.87	5.13	0.00	8.23	6.86	166.63	Diesel
3	45.87	11.99	0.00	8.23	6.86	166.63	Diesel
4	47.93	18.85	0.00	4.11	4.27	51.84	Diesel

summarized in Tables E-5 and Tables E-6. This information was used to develop the the locations of the fuel tanks within a ferry for the purposes of oil outflow calculation as per the model described in the sub-appendix. Here too, we used the single hull parameters settings for the evaluation of oil outflow from WSF's. As examples, Tables E-7 and E-8 provide, respectively, our modeled locations of the two fuel tanks on a Jumbo Ferry (which has the larges fuel carrying capacity) and the four fuel tanks of Issaquah Ferry.

Figures E-13, E-14 and E-15 provides additional scatter plots of collected data and regressions fits linking vessel lengths to diesel fuel carrying capacity for, respectively, fishing

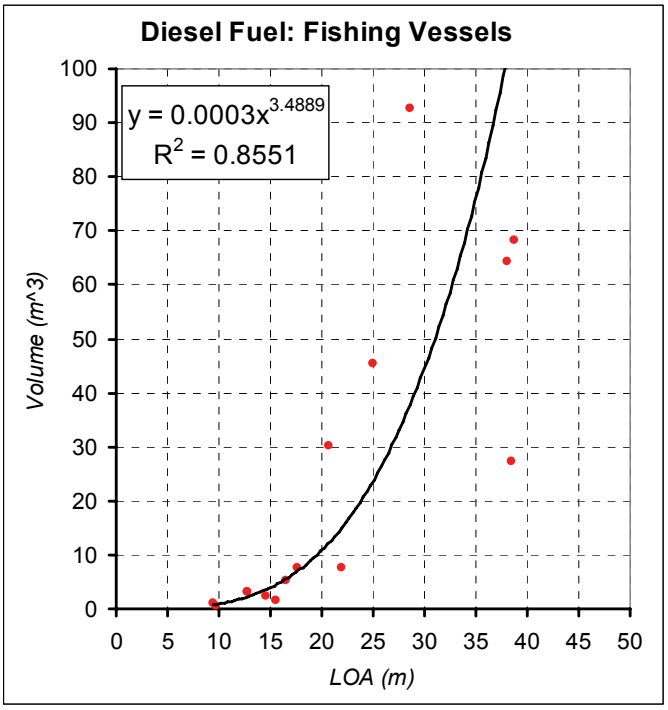

Figure E-13. Scatter plot and least squares regression fit of diesel fuel data for fishing vessels by vessel length.

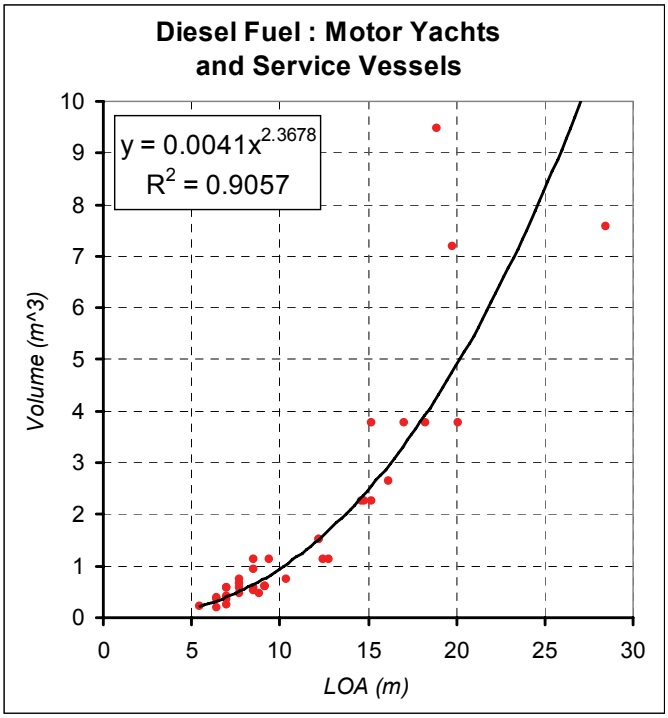

Figure E-14. Scatter plot and least squares regression fit of diesel fuel data for motor yachts and service vessels by vessel length.

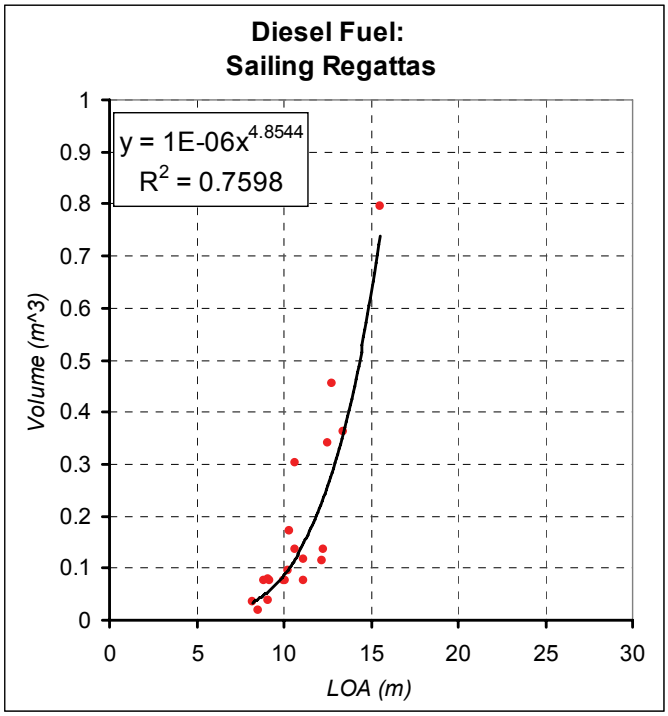

Figure E-15. Scatter plot and least squares regression fit of diesel fuel data for sailing yachts by vessel length.

vessels, motor yachts and service vessels and sailing regattas. The data for Figures E-13 through E-15 were compiled through the web sites of various regional vessel brokerage firms (see, e.g., http://www.yachts.com). The R^2 values for these regressions fits are in order 86%, 90% and 76%, which are all quite high. Please observe that in going from Figure E-13 to Figure E-15 the order of magnitudes of the y-axis goes down by 1 each time. The order of magnitude of the y-axis in Figure E-13 for fishing vessels is in turn one less than that of the y-axis in Figure E-12 for tugs. Finally, the order of magnitude of the y-axis in Figure E-13 for tugs vessels is one less than that of the y-axis in Figure E-11 for deep draft vessels. Moreover, whereas Figures E-12 through E-15 relate to diesel fuel, Figure E-11 relates to both bunker (heavy) fuel and diesel fuel.

E-3. Representative results from the oil outflow model

Similar to the recording of accident attributes for the accident probability models in Appendix D, the parameters for the oil outflow calculation are recorded by the VTRA maritime simulation program. Figure E-16 displays a screen shot of this recording process for the transit of the vessel of interest 134 identified in Figure E-16. The colored cells indicate the vessel interactions that have occurred thus far during its transit, while the

database on the lower left corner shows the recording of the specific accident attributes and input parameters for the oil outflow models during these vessel interactions. The oil outflow model in the sub-appendix together with its augmentations described in this appendix above are used to evaluate the oil outflow in terms of crude oil, petroleum products, heavy fuel and diesel fuel. Next, the crude oil and heavy-fuel outflows are combined into the category "persistent oil" and the petroleum (refined) products and diesel fuel are combined into the category "non-persistent oil". In addition, our analysis is able to separate these later two categories in terms of the originating sources BP CHPT vessels and interacting vessels that potentially collide with a BP CHPT vessels. Table E-9 and E-10 summarize the aggregate annual average oil outflow results that we have analyzed for calibration VTRA Case B.

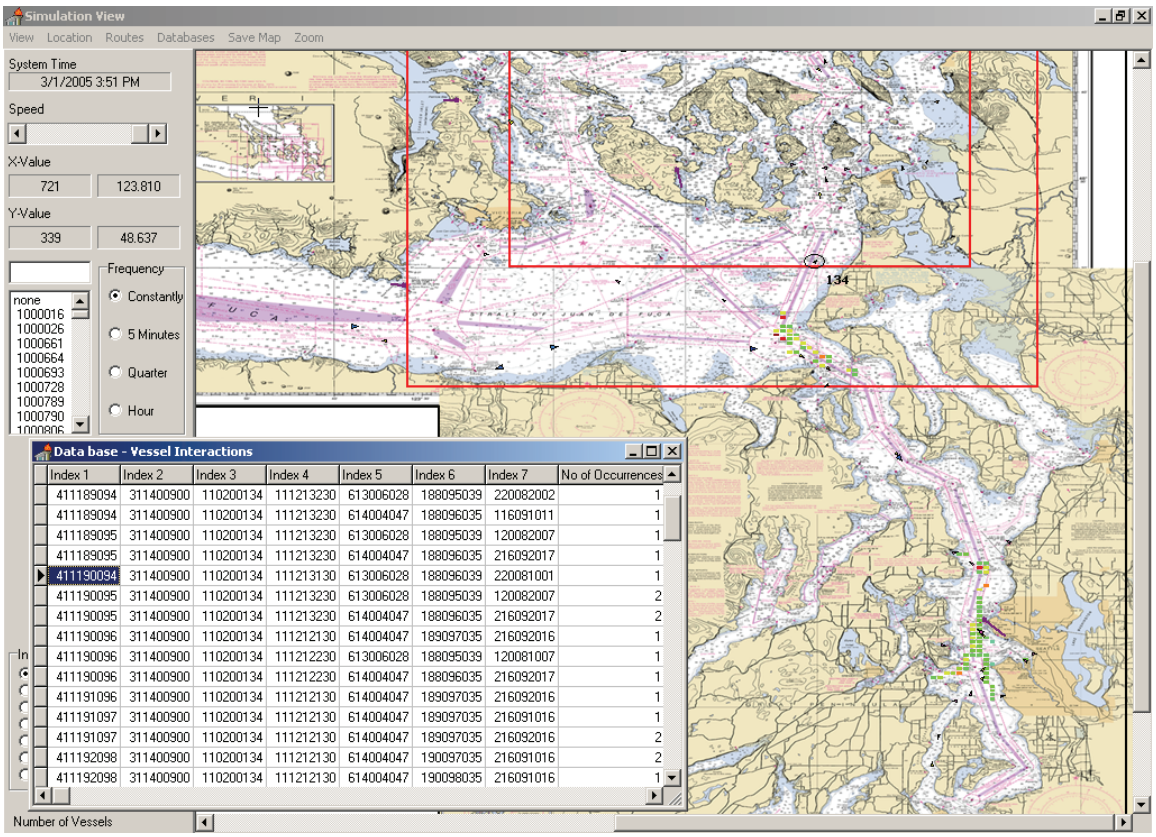

Figure E-16. Encoding of interactions by the VTRA maritime simulation.

From Table E-10 we observe that about 33% of the overall average yearly oil outflow for the calibration VTRA Case B can be attributed to collisions, 62% to powered groundings, 4% to drift grounding and 1% to allisions. Moreover, 97.5% can be attributed to the BP CHPT vessels and only 2.5% to the interacting vessels that potentially collide with BP CHPT Vessel. It is important to point out here that this study was only to consider the oil outflow

from BP Cherry Point vessels and those that potentially collide with them. Hence, of the total 33% attributed to collisions, 30.5% originated from the BP CHPT vessels, which perhaps should not be a surprise given that the interacting vessels are not necessarily tank vessels and hence carry much less oil. Finally, of the total annual average oil outflow we evaluate that 87.3% is persistent oil and 12.7% non-persistent. While these percentages are of interest by themselves, of at least an equal interest would be the comparison of theseoil outflow across the different VTRA Cases. This is not a topic of this appendix, but is described in the main report and Appendix G.

Table E-9. Average oil outflows per year by accident type for the calibration VTRA Case B (amounts are in cubic meters)

	Collisions	Powered Grounding	Drift Grounding	Allisions	Total Oil Outflow
BP CHPT Persistent	31.2	84.5	5.3	1.1	122.1
BP CHPT Non-Persistent	12.2	2.8	0.2	0.1	15.3
IV Persistent	1.0	N/A	N/A	N/A	1.0
IV Non - Persistent	2.6	N/A	N/A	N/A	2.6
Total Oil Outflow	47.0	87.3	5.5	1.2	141.0

Table E-10. Percentages of average oil outflows per year by accident type for the calibration VTRA Case B (% of total average oil outflows)

	Collisions	Powered Grounding	Drift Grounding	Allisions	Total Oil Outflow
BP CHPT Persistent	22.1%	59.9%	3.8%	0.8%	86.6%
BP CHPT Non-Persistent	8.6%	2.0%	0.2%	0.1%	10.9%
IV Persistent	0.7%	N/A	N/A	N/A	0.7%
IV Non - Persistent	1.8%	N/A	N/A	N/A	1.8%
Total Oil Outflow	33.4%	61.9%	3.9%	0.9%	100.0%

Aside from the aggregate results in Tables E-9 and E-10 we are able to develop geographic profiles of average oil outflow by grid cell similar to the geographic profiles of interactions and accident frequencies presented in Appendix D. Appendix G will provide the geographic profiles for each case for the different oil types: BP CHPT Persistent, BP CHPT Non-Persistent, Interacting Vessel (IV) persistent and Interacting Vessel Non-Persistent. In this appendix we shall suffice by showing the accident frequency geographic profile results by accident type (for the calibration VTRA Case B) followed by its aggregate geographic oil outflow profile. The comparison of these two profiles illustrates geographically the effect of the additional oil outflow analysis layer on top of the accident frequency layer.

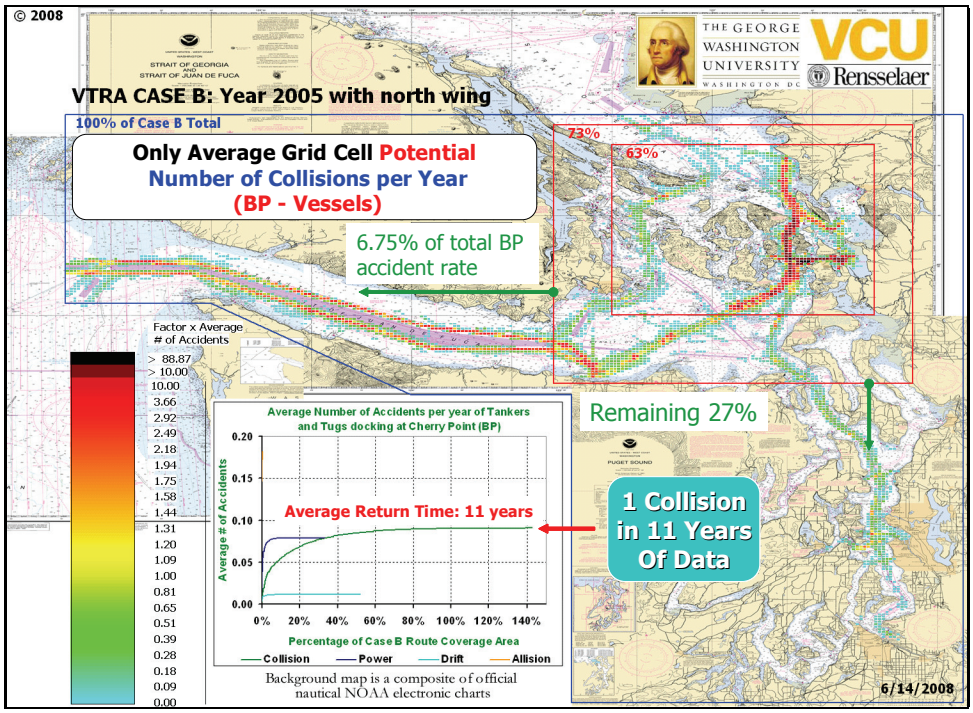

Figure E-17. Annual average collision frequencies of Cherry Point Tankers, ATB's and ITB's in the calibration case: VTRA CASE B.

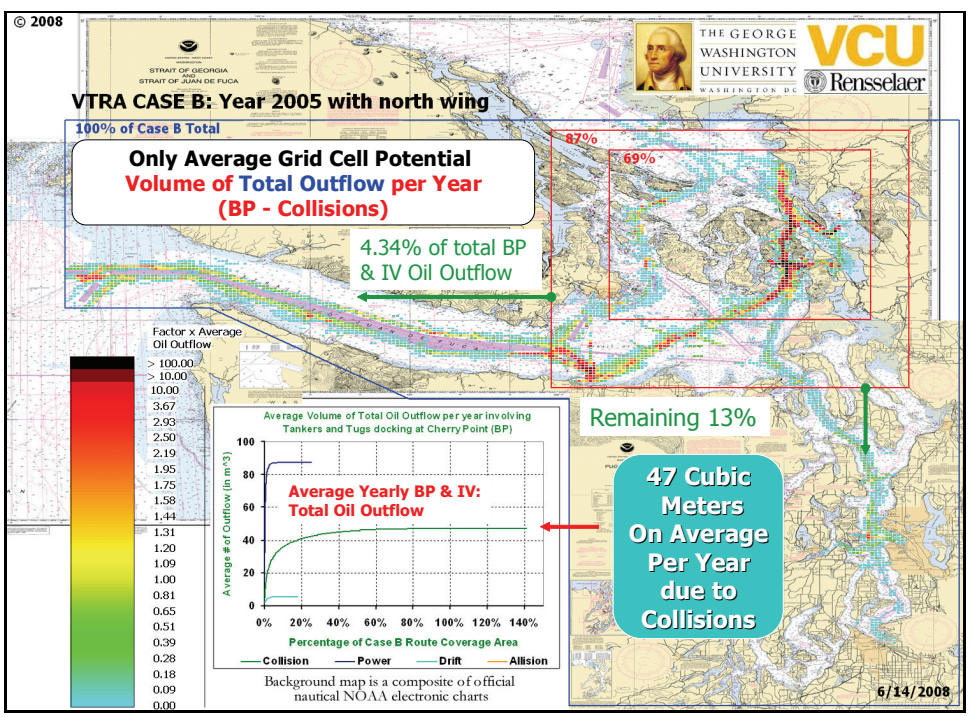

Figure E-18. Aggregate average oil outflow from collision with Cherry Point Tankers, ATB's and ITB's in the calibration case: VTRA CASE B.

Figures E-17 and E-18 respectively display the geographic profiles for collisions for the calibration VTRA Case B in terms of accident frequency and oil outflow. Firstly, we observe that the largest red square in Figure E-18 indicates 87% of the total oil outflow within this area whereas in terms of accident frequency this red square contains 73% of the accident frequency (a difference of 14%). Hence, we see a further concentration within this largest red-square when going from accident frequency to oil outflow. This is largely explained by the lightening of the colors in the West Strait of Juan de Fuca in case of the geographic oil outflow profile when compared to the geographic accident frequency profile. Finally, we observe only a difference of 6% in the percentage of accident frequency in the smallest red-square when going from oil outflow to accident frequency. This is exemplified by a darkening effect within the Rosario Strait area when going from accident frequency to oil outflow. While this too reflects a further concentration within this smaller red-square, the earlier difference of the 14% (when comparing the larger red-square) reflects a larger concentration effect outside the smallest red-square (but within the largest one). Indeed we do observe quite a darkening of color in front of the Port Angelas area when going from accident frequency geographic profile to oil outflow geographic profile.

Figures E-19 and E-20 respectively display the geographic profiles for drift groundings for the calibration VTRA Case B in terms of accident frequency and oil outflow. Figures E-21 and E-22 respectively display the geographic profiles for powered groundings for the calibration VTRA Case B in terms of accident frequency and oil outflow. While we have an overall annual frequency of groundings of ≈ 0.09 (average return time of 11 years), we obtain for average annual frequencies of drift grounding and powered grounding for VTRA Case B:

Drift Grounding: ≈ 0.012 (average return time of ≈ 85 years),
Powered Grounding: ≈ 0.079 (average return time of ≈ 13 years),

This coincides with a ratio of 6.8 of powered groundings to drift groundings. This ratio was explained in more detail in Appendix D. If we now evaluate the total average oil outflow for drift groundings and powered grounding we have (see Table E-9):

Drift Grounding: ≈ 5.5 (in cubic meters),
Powered Grounding: ≈ 87 (in cubic meters).

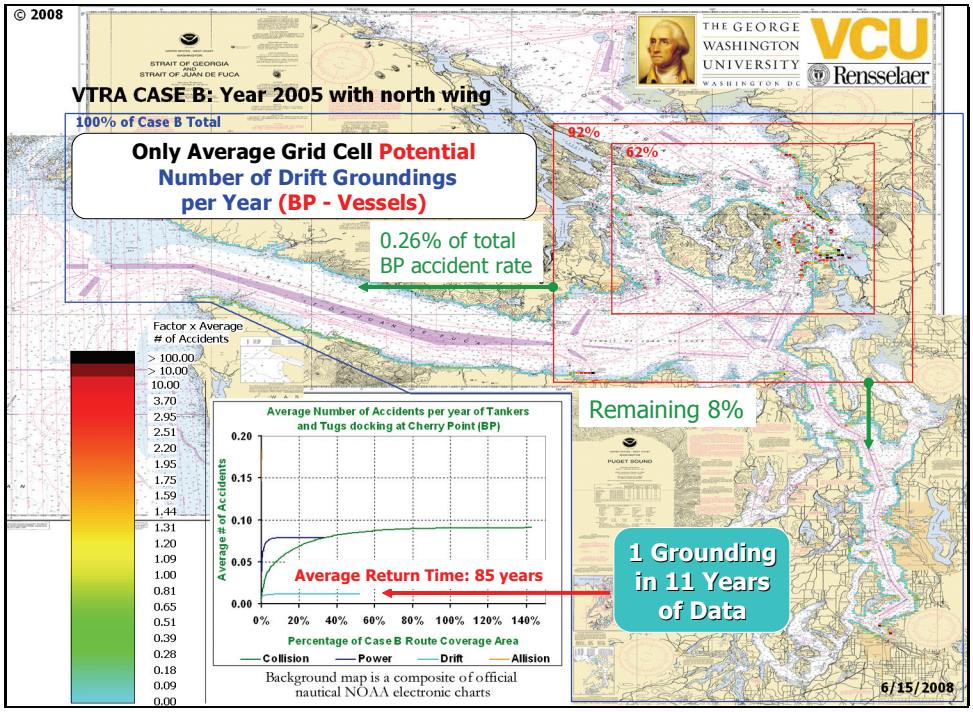

Figure E-19. Annual average drift grounding frequency of Cherry Point Tankers, ATB's and ITB's in the calibration case: VTRA CASE B.

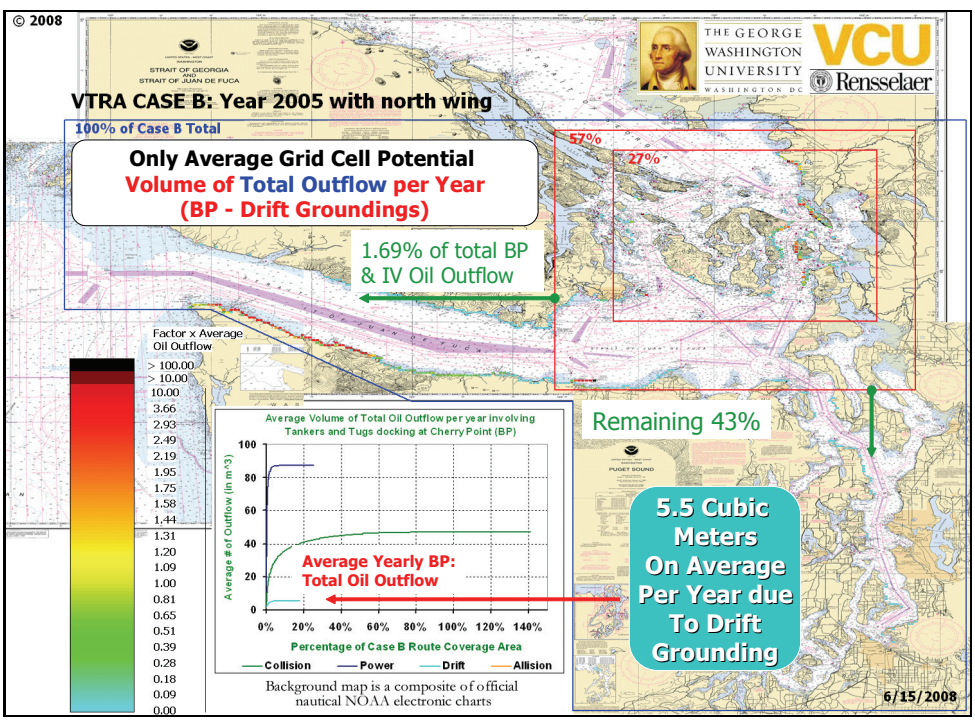

Figure E-20. Aggregate average oil outflow due to drift groundings of Cherry Point Tankers, ATB's and ITB's in the calibration case: VTRA CASE B.

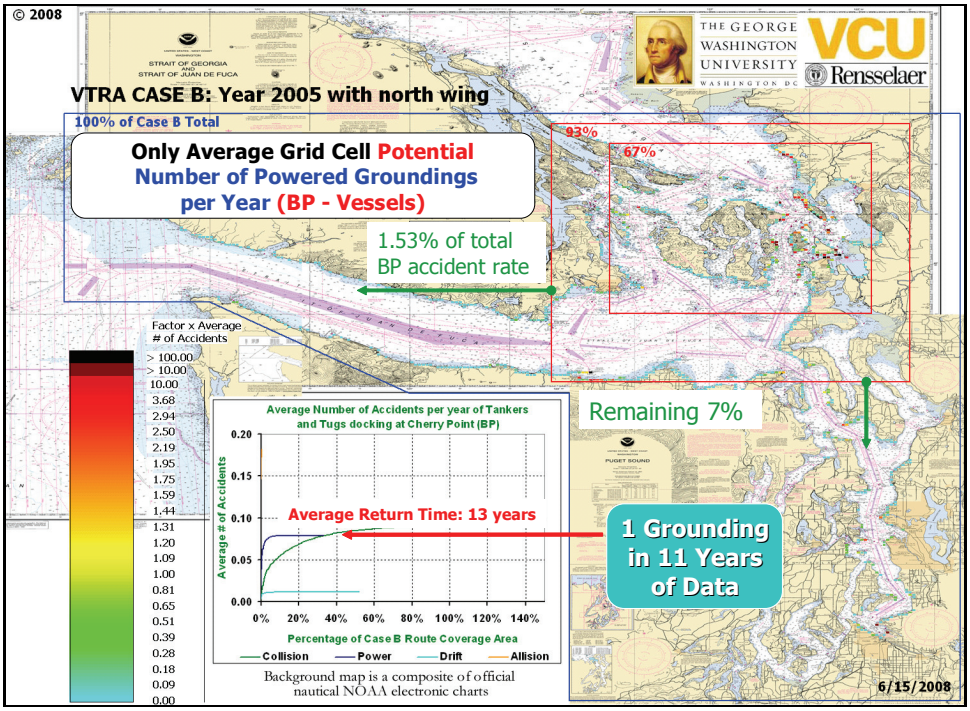

Figure E-21. Annual average powered grounding frequency of Cherry Point Tankers, ATB's and ITB's in the calibration case: VTRA CASE B.

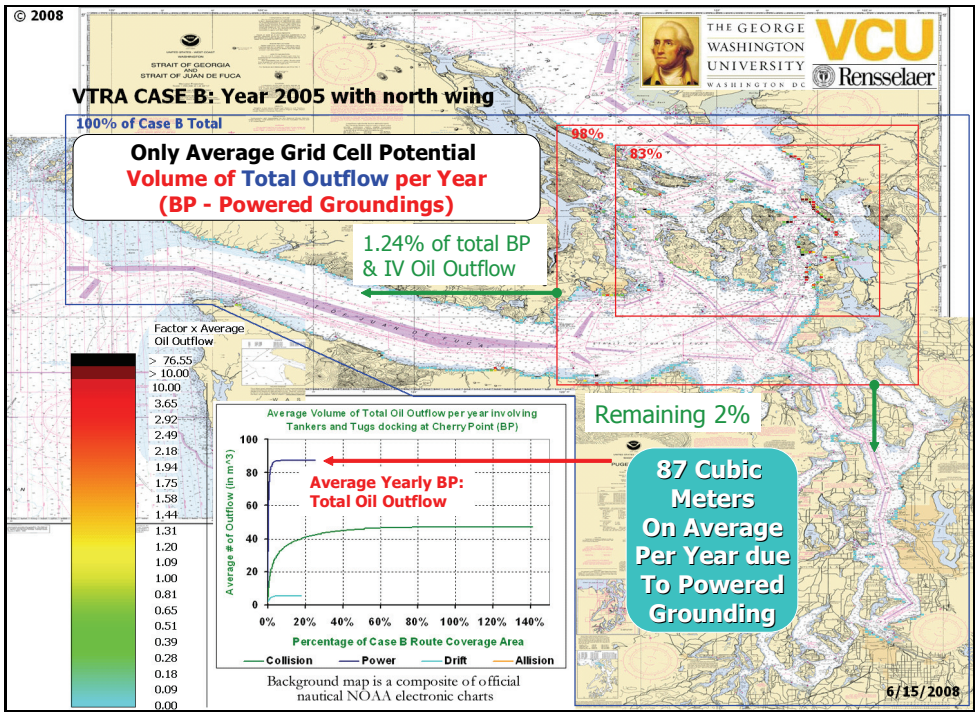

Figure E-22. Aggregate average oil outflow due to powered groundings of Cherry Point Tankers, ATB's and ITB's in the calibration case: VTRA CASE B.

This coincides with a ratio of 15.8 of powered groundings to drift groundings. The increase from the ratio 6.8 in terms of accident frequency is explained here by the higher speeds at the time of grounding when under power as compared to when drifting. This results in a higher kinetic energy at the time of impact, larger damage extents and thus higher oil outflows in the case of power groundings as compared to drift groundings.

Observe from Figures E-19 and E-20 that we go from 92% to 57% for drift groundings in the largest red square when going from accident frequency to oil outflow. Observe from Figures E-21 and E-22 that we go from 93% to 98% for powered groundings in the largest red square when going from accident frequency to oil outflow. Hence, we see a reversal in behavior with respect to this red square when we go from drift groundings to power groundings.

This is partially explained by the distribution of accidents in the West Strait of Juan de Fuca. While we see somewhat of an even distribution in case of powered groundings to the north and to the south in the West Strait of Juan de Fuca, one observes a higher propensity to the south of West Strait of Juan de Fuca in case of drift groundings. This is primarily explained by the drifting patterns as a results of prevailing winds and currents in this area. Combined with the fact that the inbound traffic in West Strait of Juan de Fuca contains the laden BP CHPT tankers, whereas the outbound tankers are part of the outbound traffic, we see an effect on the oil outflow redistribution relative to the largest red square as above. Perhaps a larger explanation of this redistribution is due to modeling assumption that we have applied to the speed of impact in case of a drift grounding when the tanker is tethered. We have applied an additional speed reduction at the time of impact of on average 0.44 knots per minute of the time-to-shore recorded variable along the drifting path when the tanker is tethered. We evaluated this average speed reduction per minute from the "Strait of Georgia Full-Scale Trials" report by Wingard and Gray (1997). Tethering is primarily practiced within the area of the largest read square.

However, if we combine with the information above the data from Table E-10 that in our analysis about 62% of the total average oil outflow arises from powered grounding and about 4% arises from drift grounding, we still arrive at the same conclusion towards the end of appendix D that the predominant oil outflows over the entire VTRA study area are confined to the largest red square. Indeed, when aggregating the average oil outflows from all accident types in a single plot we still arrive at a total percentage of 92% of average oil

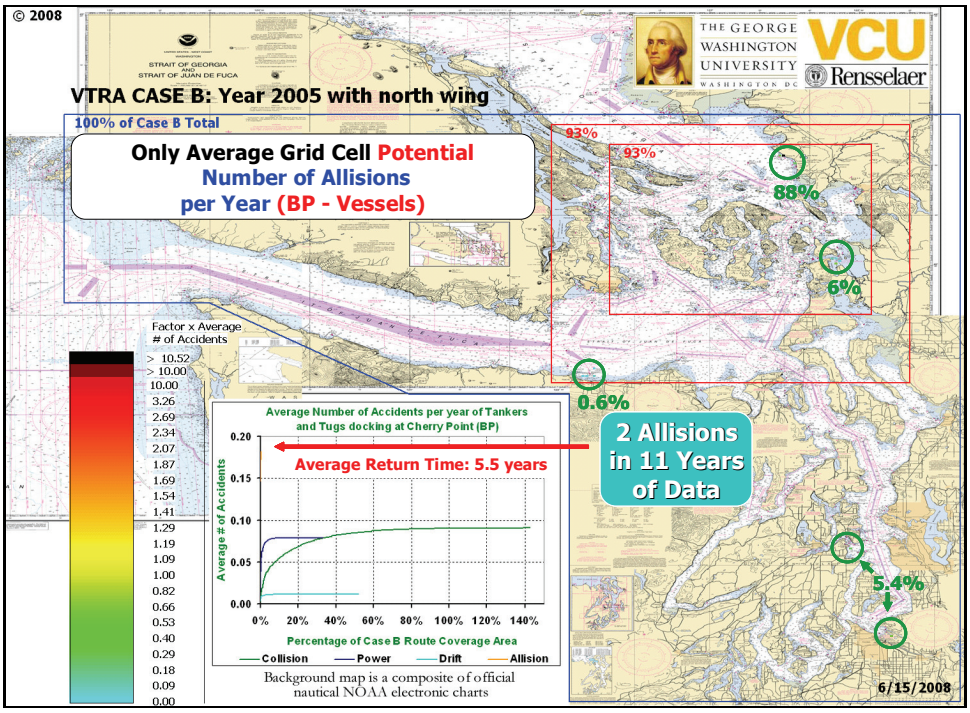

Figure E-23. Annual average allision frequency of BP Cherry Point Tankers, ATB's and ITB's in the calibration case: VTRA CASE B.

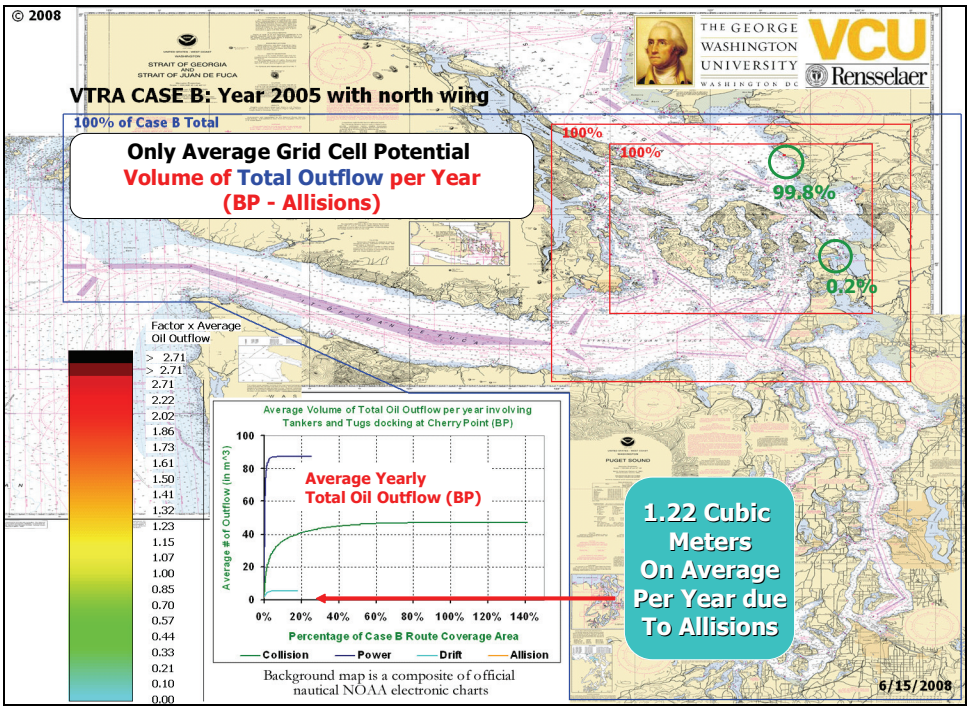

Figure E-24. Aggregate average oil outflow due to allisions of BP Cherry Point Tankers, ATB's and ITB's in the calibration case: VTRA CASE B.

outflow (see Figure E-24) within the largest red square (and thus 8% outside of it, which is not negligible).

Observe from Figures E-23 and E-24 that we go from 88% to 99.8% for allisions at the BP Cherry Point dock when going from accident frequency to oil outflow. This is primarily explained by the fact that when tankers dock at the BP Cherry Point dock they are fully laden whereas the other docks involve a mix of partially laden and even unladen tank vessels. While this change seems to be a dramatic one needs to bear in mind that of the total analyzed average annual oil outflow of about 141 cubic meters for the calibration VTRA Case B, only 1.22 cubic meters originates on average from allisions, which represents just about 1% of the total average oil outflow analyzed.

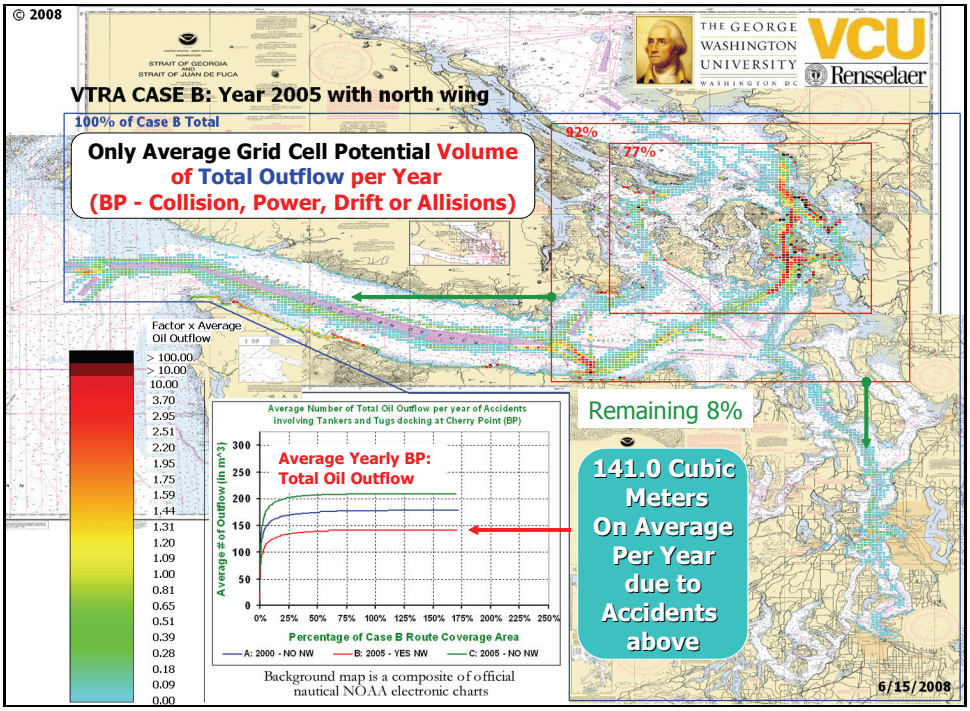

Figure E-25. Aggregate average oil outflow from accident types involving Cherry Point Tankers, ATB's and ITB's in the calibration case: VTRA CASE B.

With the VTRA Case B calibrated for CHPT vessels, the VTRA Case B simulation generates on average the same frequencies of incidents and accidents as observed in the accident-incident database analysis described in detail in Appendix A. Modifications can now be made to this VTRA Case B simulation to represent various alternatives and scenarios. For example, VTRA Case B represents the 2005 year with the BP Cherry Point North wing dock in operation. We can simulate the behavior of the CHPT vessel traffic as if this North wing

dock was not there. This case is labeled VTRA Case C. The case using a modification of the VTRA simulation to represent 2000 traffic levels is designated VTRA Case A. Next, we can compare the aggregate analysis results of VTRA Cases A and C to those of VTRA Case B and draw overall conclusions regarding the aggregate effect of potentially removing the North Wing in our model.

While the analysis above demonstrates that it is informative for the planning of potential future risk interventions where "average oil outflow risk is coming from" (both from an exposure, accident frequency and an oil outflow perspective), it also demonstrates that a comparison of different VTRA Cases ought to be based on average aggregate results for the entire VTRA study area. Such a comparison is provided also in the plot within Figure E-25. The red line indicates the aggregate oil outflow distribution over the grid cells that have oil outflow for VTRA Case B (2005 with North Wing) and the blue and green line respectively provide these results for VTRA Case A (2000 without North Wing) and VTRA Case C (2005 without North Wing). From this plot if follows that we analyzed the least annual aggregate average oil outflow over the entire VTRA Study area for the VTRA Case B (2005 with North Wing).

The geographic profiles allow us to further zoom-in on these aggregate effects by comparing those of VTRA Case B (see Figures E-17 to E-25) to those of VTRA Cases A and C (provided in Appendix G). By zooming in, one obtains a better general understanding about where this aggregate change in level (and possibly migration) of accident frequency or oil outflow from one case to another comes from. Visual comparison of these geographic profiles allows one to draw high level conclusions regarding general tendencies about the changing "risk" behavior from case to case or alternative to alternative.

It should be noted, however, that the maritime transportation modeled within the VTRA simulation is highly dynamic (as demonstrated by a running simulation) and relatively sparse. Even though we evaluate a total of 61427 vessel interactions for VTRA Case B distributed over a total of 3454 grid cells, this results on average annually in about 18 interactions per grid cell. Hence, when making changes to the VTRA Case B simulation this may results in high relative differences from grid cell to grid cell (especially in those with an even smaller number of interactions). In fact, from case to case one may experience an increase in one grid cell and a decrease in grid cells immediate adjacent to it. Hence, our general position is that these geographic profile analyses should not be used to perform grid cell by grid cell

comparisons from case to case, but should only be used to observe general tendencies of change for larger areas.

References

A. J. Brown (1995). "Oil Tanker Design Methodology Considering Probabilistic Accident Damage", *International Journal Of Advanced Manufacturing Systems*. Vol.4, Issue 1(2001) 25-34.

A. J. Brown (1998). Assessing the environmental performance of tankers in accidental grounding and collision", *SNAME Transactions,* Vol. 106: pp. 41-58.

A. J. Brown (2001). *Alternative Tanker Designs, Collision Analysis*. NRC Marine Board Committee on Evaluationg Double-Hull Tanker Design Alternatives.

International Marine Board (1995). "Interim Guidelines for Approval of Alternative Methods of Design and Construction of Oil Tankers under Regulation 13F(5) of Annex I of Marpol 73/78", Resolution MEPC.66 (37), Adopted September 14, 1995.

M. van der Laan (1997). *Environmental Tanker Design*. Delft University of Technology.

National Research Council (2001). "Environmental Performance of Tanker Designs in Collision and Grounding", Special Report 259, Marine Board, Transportation Research Board, The National Academies.

K. K. Tikka (2001). *Alternative Tanker Designs, Grounding Analysis*. NRC Marine Board Committee on Evaluationg Double-Hull Tanker Design Alternatives.

R. Taggart (1980). *Ship Design and Construction*, The Society of Naval Architects and Marine Engineers.

P.A. Wingard and D.L. Gray (1997). *Strait of Georgia Full-Scale Trials,* The Glosten Associates, Inc. File No. 97022.

SUB-APPENDIX:

G.F. van de Wiel (2008). "A Probabilistic Model for Oil Spill Volume in Tanker Collisions and Groundings", Master's Thesis: Applied Mathematics, Delft University of Technology, The Netherlands.

Delft University of Technology
Faculty of Electrical Engineering, Mathematics and Computer Science
Department of Risk Analysis

A Probabilistic Model for Oil Spill Volume in Tanker Collisions and Groundings

A thesis submitted to the
department of Risk Analysis
in partial fulfillment of the requirements

for the degree

MASTER OF SCIENCE
in
APPLIED MATHEMATICS

by

GIEL F. VAN DE WIEL

Delft, The Netherlands
June 2008

Copyright © 2008 by Giel F. van de Wiel. All rights reserved.

MSc THESIS APPLIED MATHEMATICS

"A Probabilistic Model for Oil Spill Volume in Tanker Collisions and Groundings"

GIEL F. VAN DE WIEL

Delft University of Technology

Daily supervisor

Dr. D. Kurowicka

Responsible professor

Prof. dr. R.M.Cooke

Other thesis committee members

Dr. ir. J.R. van Dorp

Dr. ir. P.H.A.J.M. van Gelder

June 2008

Delft, The Netherlands

Preface

This document presents the results from my thesis research at the George Washington University (GWU) in Washington, D.C., U.S.A. It was written for the purpose of completing the Master's Programme in Applied Mathematics at Delft University of Technology (DUT), The Netherlands. The research was supervised by Dr. Rene van Dorp at the GWU Department of Engineering Management and Systems Engineering and by Dorota Kurowicka at the DUT Department of Risk Analysis. Partial funding for this work was provided by The George Washington University.

Acknowledgements

Without the support of many people this report would not have been possible. First off I would like to thank Roger Cooke, Dorota Kurowicka, Rene van Dorp and Pieter van Gelder, for taking place in my thesis committee. In this regard, my thanks go out in particular to Roger Cooke and Thomas Mazzuchi for their support and advice throughout the thesis, both in practical as well as in academic terms; and a very special thanks to Rene van Dorp, who has given me the opportunity to take on this project and has supported me from its very start; whose knowledge, perseverance and enthusiasm I could not have found in any other supervisor.

Secondly, my gratitude goes out to all the friends I have come to know throughout my years of study and whose presence has played a big part in completing this thesis. I would like to thank the International Student House in Washington, D.C. and its residents for making my stay in the USA a truly memorable experience.

Lastly, I would like to thank my family: especially my parents, whose unconditional support helped me accomplish what I have today.

Contents

1 Introduction **1**
1.1 Background . . . 1
1.1.1 The Exxon Valdez Grounding . . . 2
1.1.2 Modelling Oil Spill Risk . . . 2
1.1.3 IMO Outflow Model . . . 3
1.1.4 Collision and Grounding Models . . . 6
1.2 Thesis Goal . . . 7
1.3 Thesis Outline . . . 7

2 Simulation Data **8**
2.1 Tanker Designs . . . 8
2.2 Collisions . . . 8
2.2.1 Input Data . . . 11
2.2.2 Output Data . . . 13
2.3 Groundings . . . 16
2.3.1 Input Data . . . 16
2.3.2 Output Data . . . 18

3 Collision Model **22**
3.1 Overview . . . 22
3.1.1 Model Structure . . . 22
3.1.2 Regression Analysis . . . 23
3.1.3 Statistical vs. Practical Significance . . . 23
3.2 Defining Predictor Variables . . . 25
3.3 Transformation of Predictor Variables to CDF . . . 29
3.3.1 CDFs of $E_{k,p}$, $E_{k,t}$ . . . 29
3.3.2 CDF of L' . . . 31
3.3.3 CDF of H . . . 31
3.4 Damage Extent . . . 35
3.4.1 Fitting Residual Distribution . . . 39
3.5 Probability of Rupture . . . 39
3.5.1 Binary Logistic Regression . . . 41
3.5.2 Validity of Binary Logistic Model . . . 43

3.6 Outflow Volume . . . 45
3.6.1 Determining Damaged Area . . . 45
3.7 Results . . . 50

4 Grounding Model 54
4.1 Defining Predictor Variables . . . 54
4.1.1 Transformation of Predictor Variables . . . 56
4.2 Damage Extent . . . 61
4.2.1 Fitting Residual Distribution . . . 62
4.3 Probability of Rupture . . . 64
4.4 Outflow Volume . . . 65
4.5 Results . . . 65
4.5.1 Damage Extent . . . 65
4.5.2 Probability of Rupture . . . 66

5 Calculation Examples 69
5.1 Struck Ship Configuration . . . 69
5.2 Collision Example . . . 70
5.2.1 Input Variables . . . 70
5.2.2 Transformations . . . 70
5.2.3 Step One: Damage Extent . . . 71
5.2.4 Step Two: Probability of Rupture . . . 72
5.2.5 Step Three: Outflow Volume . . . 72
5.3 Grounding Example . . . 73
5.3.1 Input Variables . . . 73
5.3.2 Transformations . . . 74
5.3.3 Step One: Damage Extent . . . 74
5.3.4 Step Two: Probability of Rupture . . . 75
5.3.5 Step Three: Outflow Volume . . . 75
5.4 Conclusions . . . 76

6 Conclusions and Recommendations 77
6.1 Collision Model Results . . . 78
6.2 Grounding Model Results . . . 78
6.3 General Remarks . . . 78
6.4 Recommendations for Further Research . . . 79

A Regression 82
A.1 Binary Logistic Regression . . . 82
A.1.1 Fitting the Logistic Regression Model . . . 82
A.2 Linear Regression . . . 84

B Probability Distributions **85**
B.1 Empirical Distribution Function 85
B.2 Typical Distributions 85
B.3 Generalized Power Distribution 86
B.4 Generalized Trapezoidal Distribution 86

C Tanker Data **88**

D Collision Model Results **92**

E Grounding Model Results **95**

List of Tables

2.1 Tanker specifications, collisions 11
2.2 Input variables, collisions 12
2.3 Striking ship type distribution 13
2.4 Striking ship displacement distribution, by type 13
2.5 Outflow volume distribution, collisions 14
2.6 Nonzero output values from collision simulations 16
2.7 Tanker specifications, groundings 16
2.8 Grounding input variables 17
2.9 Velocity distribution, groundings 18
2.10 Tidal variation distribution 18
2.11 Grounding output variables 19

3.1 Coefficients for Weibull fits, kinetic energy 31
3.2 Empirical CDF of H 33

4.1 Coefficients for GP distribution of O_a 59
4.2 Coefficients for GP distribution of O_r 59

5.1 Collision example variables 70
5.2 Grounding example variables 74

C.1 Tanker compartment volumes (m^3), SH40, collisions 88
C.2 Tanker compartment volumes (m^3), SH150, collisions 88
C.3 Tanker compartment volumes (m^3), DH40, collisions 89
C.4 Tanker compartment volumes (m^3), DH150, collisions 89
C.5 Tanker compartment volumes (gallons), SH40, groundings 89
C.6 Tanker compartment volumes (gallons), SH150, groundings 90
C.7 Tanker compartment volumes (gallons), DH40, groundings 90
C.8 Tanker compartment volumes (gallons), DH150, groundings 90
C.9 Bulkhead locations 91

D.1 Polynomial linear regression coefficients for $\ln y_l$, collisions 92
D.2 Parameters of GT distributions, R_l, collisions 93
D.3 Polynomial linear regression coefficients for $\ln y_t$, collisions 93

D.4 Parameters of GT distributions, R_t, collisions 94
D.5 Binary logistic regression coefficients, collisions 94
D.6 Binary logistic regression point-biserial correlation tests, collisions . 94
D.7 Damage location coefficients 94

E.1 Polynomial linear regression coefficients for $\ln y_l$, groundings 95
E.2 Polynomial linear regression coefficients for $\ln y_t$, groundings 96
E.3 Parameters of GT distributions, R_l, groundings 97
E.4 Parameters of GT distributions, R_t, groundings 97
E.5 Binary logistic regression coefficients, groundings 97
E.6 Binary logistic regression point-biserial correlation tests, groundings 97

List of Figures

1.1 Exxon Valdez 2
1.2 Damage extent PDFs 5

2.1 40,000 DWT tanker designs 9
2.2 150,000 DWT tanker designs 10
2.3 Two ships at the moment of collision 11
2.4 Collision damage 14
2.5 Maximum penetration histogram, collisions 15
2.6 Damage length histogram, collisions 15
2.7 Grounding simulation 17
2.8 Longitudinal damage extent histogram, groundings 19
2.9 Transversal damage extent histogram, groundings 20
2.10 Elevation histogram, groundings 20
2.11 Total outflow volume histogram, groundings 21
2.12 Scatterplot of obstruction depth vs. elevation, all ship types 21

3.1 Collision outflow model overview 24
3.2 Tangential velocity difference 27
3.3 Transformation of input variables to predictor variables 30
3.4 Probability plot & Weibull fit of empirical CDF, perpendicular kinetic energy, SH40 case 32
3.5 Probability plots of alternative parametric fits, perpendicular kinetic energy, SH40 case 33
3.6 Cumulative distribution function for L' 34
3.7 Empirical CDF of H 34
3.8 Matrix plot of y_t against $\mathbf{x}$, SH150 case 37
3.9 Matrix plot of $\ln y_t$ against $\mathbf{x}$, SH150 case 37
3.10 Residual plots for y_l resp. $\ln y_l$, SH150 case 40
3.11 Residual plots for y_t resp. $\ln y_t$, SH150 case 40
3.12 QQ-plot for the fit of residuals of $\ln y_t$, SH150 case 41
3.13 Scatterplot of z' against $\ln y_l$ and $\ln y_t$, SH40 case (left) and DH40 case (right) 42
3.14 QQ-plot of probability residuals, SH150 case, collisions 44

3.15 Bulkhead placement 45
3.16 Collision damage bounds 46
3.17 Determining position of damage location 47
3.18 Determining position of damage location with added parameter . . . 48
3.19 θ under different angles and relative tangential velocities 49
3.20 Effects of predictor variables on damage extent for a large ship using combined models 51
3.21 Expected probability of rupture as function of $\ln y_l$ and $\ln y_t$, SH150 vs. DH150 52

4.1 Grounding model schematic 55
4.2 QQ-plot, Empirical vs. Parametric CDF, O_a 58
4.3 QQ-plot, Empirical vs. Parametric CDF, O_r 58
4.4 QQ-plot, Empirical vs. Theoretical CDF, O_d 60
4.5 Obstruction depth distribution: fit vs. data 60
4.6 Transformation of input variables to predictor variables 61
4.7 Residual plots for $\ln y_l$, SH150 case 62
4.8 Residual plots for $\ln y_t$, SH150 case 63
4.9 QQ-plot of empirical vs. parametric CDFs of r_t, SH150 case 63
4.10 z' vs. $\ln y_v$, DH150 case 64
4.11 $E(Z')$ as function of $\ln y_v$ 67
4.12 Effects of predictor variables on damage extent for a large ship using combined models 68

List of Symbols

Collisions

Symbol	Description
$e_{k,p}$	Perpendicular kinetic energy
$e_{k,t}$	Tangential kinetic energy
m_1	Striking ship mass
m_2	Stuck ship mass
v_1	Striking ship velocity
v_2	Struck ship velocity
ϕ	Collision angle
l	Relative collision location
l'	Absolute collision location from center
t	Striking ship type
η	Striking ship bow half entrance angle
y_l	Damage length
y_t	Maximum penetration
z	Oil outflow volume
z'	Occurrence of oil outflow

Groundings

Symbol	Description
e_k	Kinetic energy
o_d	Obstruction depth
o_a	Obstruction apex angle
o_r	Obstruction tip radius
c	Obstruction eccentricity
y_l	Longitudinal damage extent
y_t	Transversal damage extent
y_v	Obstruction elevation
z	Oil outflow volume
z'	Occurrence of oil outflow

Chapter 1

Introduction

1.1 Background

Maritime transportation plays an unreplaceable and ever-growing role in the global economy, taking up 96% of the world's global freight in terms of weight [17]. In 2006, seaborne trade grew 5.5% to 30,686 billion ton-miles. Of goods loaded, crude oil and petroleum products represented 36% [22]. Of course, transportation of goods by sea carries the risk of marine accidents, i.e. an event where a ship adversely interacts with its environment, possibly causing damage to either the ship, the environment, or both. When oil tankers are involved in accidents, a typical consequence of resulting damage is the release of crude oil or petroleum products into the sea.

Seaborne oil spills from tanker ships have the potential to cause major environmental damage, interfering with marine and coastal biology and influencing human livelihoods for decades after a spill occurs. These spills are usually accidental in nature; from 1995 to 2004, over three quarters of spills greater than 7 tons were caused by collisions and groundings [8]. Although the trend in both frequency and volume of spills has gone down significantly over the decades, the environmental risk of a spill remains significant and severe because of both the immensity of worldwide maritime transportation, the large amounts of oil transported by a typical tanker, and the increased likelihood of vessels interacting with each other due to traffic growth in harbors and waterways.

The context of this study was a Vessel Traffic Risk Assessment in which The George Washington University was tasked to evaluate incremental oil transportation risk as a result of potential traffic increases due to a dock expansion of a refinery in Washington State. Oil transportation routes traverse through the San Juan Islands and the Straits of Juan de Fuca. The San Juan Islands area is considered an environmentally pristine area and serves as a habitat for an Orca Whale family. Moreover, The San Juan Islands and the Strait of Juan de Fuca are fishing grounds for both commercial and tribal salmon, crab and shrimp fisheries.

Figure 1.1: Left: the Exxon Valdez, grounded in Prince William Sound. Right: pooled oil stranded between rocks after the Exxon Valdez grounding. (Source: National Oceanic and Athmospheric Administration)

1.1.1 The Exxon Valdez Grounding

On March 24, 1989, the oil tanker *Exxon Valdez* ran aground shortly after leaving the Valdez oil terminal in Alaska, spilling 36,000 metric tons of crude oil into Prince William Sound and beyond, in total affecting 1,500 miles of coastline (see Figure 1.1). Although only the 28th largest historical spill by volume [12], this accident became world news as the spilled oil contaminated the Prince William Sound coastline, seriously affecting the health and abundance of local shoreline biology as well as compromising the economic and public value of Prince William Sound. In its aftermath, Exxon —the company owning the Exxon Valdez— payed about US$ 2 billion in cleanup costs and court settlements and was sentenced to pay US$ 2.5 billion in punitive damages. In response to the spill, the United States Congress passed the 1990 Oil Pollution Act to prevent further oil spills from occurring in the United States.

1.1.2 Modelling Oil Spill Risk

To improve prevention of future oil spills after Exxon Valdez, numerous models for analyzing oil spill risk were developed. In the Prince William Sound Risk Assessment [14], a system simulation of Prince William Sound that integrated shipping fleet, traffic rules and operating procedures was run to generate a dataset of accident types and locations over a timespan of 25 years. This assessment was based on Probabilistic Risk Analysis [1], which:

1. Identifies the series of events leading to an accident;
2. Estimates the probabilities of these events;

3. Evaluates the consequences of the accident.

Brown and Amrozowicz [4] propose a model that consecutively determines

1. Accident probability (grounding, collision, structural failure etc.);
2. Probability of zero outflow and mean outflow volume given a spill;
3. Immediate response to contain the spill;
4. Spill consequence.

A similar methodology is provided by the software package GRACAT [5], short for Grounding and Collision Analysis Toolbox, which has the following modelling capabilities:

1. Frequency: estimation of grounding or collision probability for a vessel operating on a specified route;
2. Damage: establishment of models for calculating the resulting grounding and collision damage;
3. Consequence: analysis of the conditions of the damaged vessel;
4. Mitigation: identification and evaluation of remedial measures for the considered consequences.

Looking at these methodologies, to model the risk of an individual tanker spill, one can argue that in general one has to:

1. Determine the probability of an accident *given* the state of the surrounding environment;
2. Determine the oil outflow volume *given* an accident;
3. Determine the spill consequence *given* the outflow volume.

This report focuses entirely on the 2nd item: the modelling of oil outflow volume from an oil tanker given that an accident involving the tanker has occurred.

1.1.3 IMO Outflow Model

A widely accepted model used in determining the oil outflow volume in tanker accidents was drafted by the International Maritime Organization [9]. The purpose of the model is to measure outflow performance of a particular tanker design against a reference double hull design.

For this model, data was taken from approximately 100 historical collision and grounding scenarios from the period 1980-1990 to establish probability density functions (PDFs) for the location and extent of damage in a collision or grounding scenario (see Figure 1.2). Based on these distributions, each unique combination of tanks or compartments in a given tanker design can be associated with a probability of being damaged.

In a collision, the assumption is made that all oil is lost from a damaged compartment. Hence the sum of cargo volumes of damaged compartments represent the total volume of spilled oil. In a grounding, a pressure balance calculation is carried out, where the water level surrounding the tanker determines the amount of oil that flows out.

After this calculation step, the probability of damage and outflow volume for each unique combination of compartments is known. Using these numbers, three parameters describe the environmental performance of the tanker design in question:

- Probability of no outflow P_O: the cumulative probability for all damage combinations for which there is no oil outflow.
- Mean outflow parameter O_M: the weighted average of outflow volumes of all combinations.
- Extreme outflow parameter O_E: the weighted average of outflow volumes of the damage combinations falling within the cumulative probability range between 0.9 and 1.0.

These parameters are then combined into a "pollution prevention index" E:

$$E = k_1 \frac{P_O}{P_{OR}} + k_2 \frac{0.01 + O_{MR}}{0.01 + O_M} + k_3 \frac{0.025 + O_{ER}}{0.025 + O_E} \tag{1.1}$$

where $k_1 = 0.4$, $k_2 = 0.5$ and $k_3 = 0.1$; and where P_{OR}, O_{MR} and O_{ER} are respectively the probability of no outflow, mean outflow parameter and extreme outflow parameter of the reference double hull design. If $E > 1$, then the design in question has "satisfactory characteristics". An analysis using this methodology was used by the Herbert Engineering Corporation [6] to evaluate 96 different tanker designs to propose a standard tanker design.

Unfortunately, the IMO model suffers from a number of fundamental limitations. The following objections are raised as such [16, 23]:

- The model uses a single set of damage extent PDFs from limited single hull data applied to all ships, independent of structural design; realistically, however, this data should only be used to model single hull accidents.

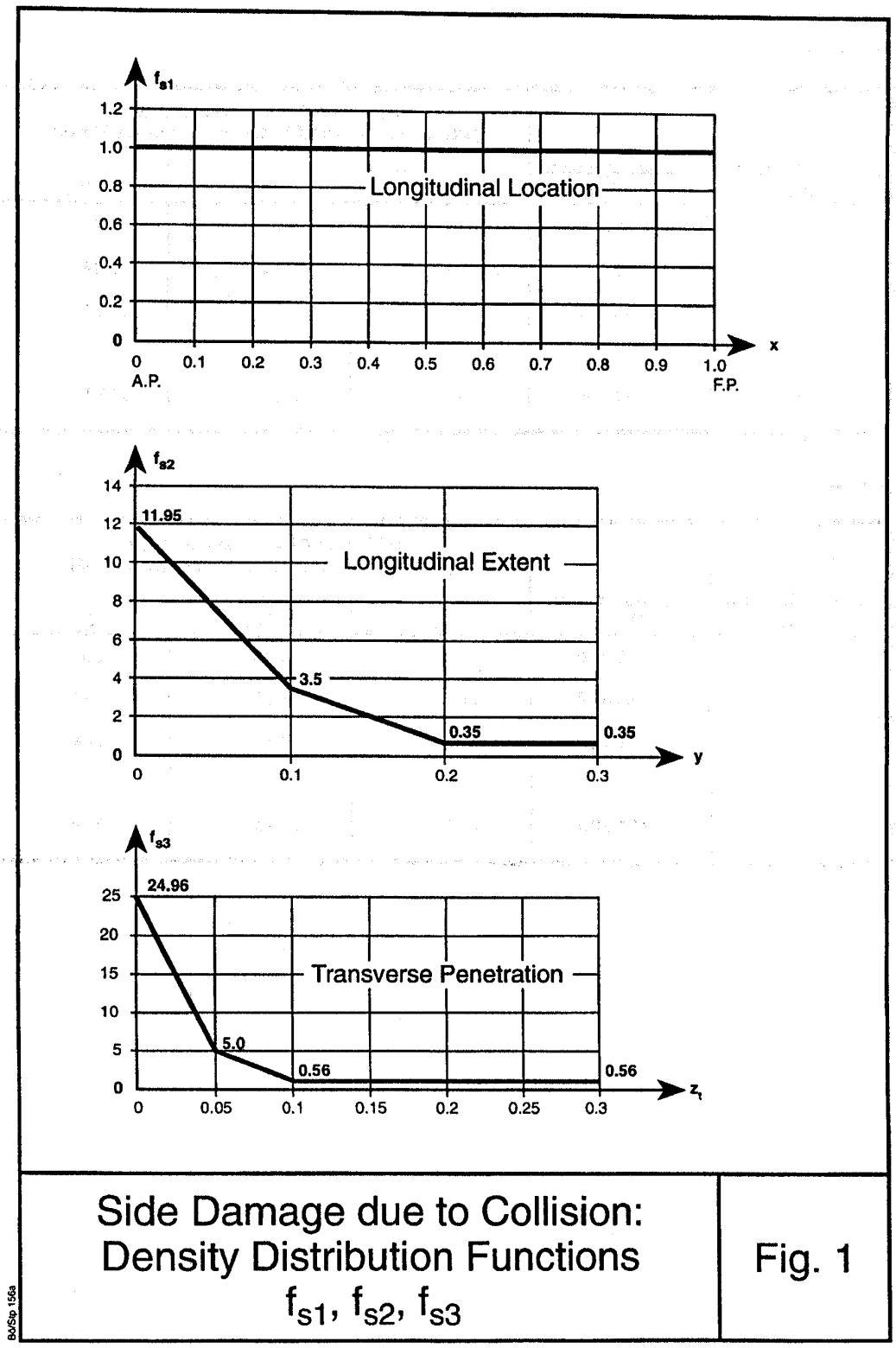

Figure 1.2: Damage extent PDFs, IMO model (source: IMO [9])

- Damage PDFs only consider damage that is significant enough to breach the outer hull. This penalizes structures able to resist rupture.
- Damage extents are treated as independent random variables when they are actually dependent variables, and ideally should be described using a joint PDF.
- Damage PDFs are normalized with respect to ship length, breadth and depth when damage may depend to a large extent on local structural features and scantlings. Most notably, Simonsen and Hansen [19] conclude that relative damage length in groundings is higher for larger ships than for smaller ones.

1.1.4 Collision and Grounding Models

In 2001, the Marine Board of the National Academy of Science published a report assessing a methodology to compare double hull tanker designs to alternative designs [20]. It noted that the IMO model was insufficient for the goals outlined by the report and that, consequently, further research was necessary. A risk-based methodology was therefore developed that included a model for generating probabilistic accident scenarios.

For both collisions and groundings this model is based on the physical simulation of accident damage inflicted on a tanker as developed by Brown [3] and Tikka [21] using the simulation programs SIMCOL resp. DAMAGE. For the Marine Board research, 10,000 collision and grounding scenarios were randomly generated and put through a simulation four times; each time using a different tanker design. This resulted in a dataset of 40,000 collisions and 40,000 groundings, describing input (i.e. ship speed, displacement, collision angle) and output variables (i.e. damage length, outflow volume).

The goal of having this large dataset was to compare outflow performance between single hull and double hull tankers; however, by carefully studying the relationships between input and output parameters of this large data set one can "empirically" develop a probabilistic model that determines accident oil outflow based on statistical data analysis techniques rather can computationally intensive physical simulations; one that nevertheless needs to adhere to the same physical principles as the latter.

The model is envisioned to be used in similar tools as the Prince William Sound Risk Assessment simulation [14]. These tools generate a large number of scenarios and hence the oil outflow volume evaluation needs to computationally efficient. Without oil outflow analysis, multiple year simulation runs take 8 hours or more, just to evaluate accident frequencies. Combining such a simulation tool with the physical damage simulations developed for the Marine Board is from a computational point of view impossible at this time. An explicit oil outflow model, however, that describes a statistical relationship between scenario input characteristics and oil outflow output

characteristics could very well be combined with such a simulation tool. These statistical relationships are estimated using the physical simulation data of the Marine Board report containing 80,000 collision and grounding scenarios.

1.2 Thesis Goal

The research goal of this thesis is to

- Develop a new method for modelling the oil spill volume of an oil tanker in a collision or grounding accident scenario, based on the simulation data as obtained from [3, 21];
- for both single hull and double hull tankers of specific designs;
- emphasizing on the practicality of implementation of the outflow model into large scale system simulations.

1.3 Thesis Outline

In the first chapter, the dataset generated by the collision and grounding simulations (as discussed above) are described. Next, the collision outflow model based on this data is explained and discussed extensively; following this, the grounding outflow model is treated. Because it adheres to the same principles as the collision model, only changes to the grounding methodology as opposed to collisions are mentioned. Third, a concise, practical example of the model is given to demonstrate its use in determining accidental oil outflow. Finally, the conclusions to the thesis goal and recommendations for further research are presented.

Chapter 2

Simulation Data

In the aforementioned research, 10,000 sets of input variables for both collisions and groundings were generated, and subsequently fed into a physical simulation model. These simulations were performed on four different tanker designs, resulting in a total of 80,000 sets of output variables; hence in total 80,000 pairs of input and output variables ('scenarios') are available. In this chapter, the ship designs, input variables, collision and grounding simulations, and resulting output variables are described and discussed in detail. It must be noted that there are differences between the ship designs used in the collision and grounding studies, which will be discussed when relevant.

2.1 Tanker Designs

An oil tanker is mainly characterized by its cargo area, which consists of one or more tanks or compartments. The cargo capacity is measured in deadweight tonnage (DWT) representing cargo mass. The displacement equals the water mass that the ship displaces. Among tankers, single-hull and double-hull designs are the most widespread used. As the name implies, in a single-hull design only one wall separates the cargo compartments from the surrounding water; in a double-hull design, these compartments are protected by ballast tanks. The four different tanker designs are designated by hull type and tonnage: SH40, SH150, DH40 and DH150. Their schematic designs can be found in Figures 2.1 and 2.2.

2.2 Collisions

In a collision, an oil tanker is struck by a striking ship (see Figure 2.3). The collision transforms translational motion mainly into rotational motion, elastic deformation and plastic deformation. It is assumed that the striking ship does not experience any damage. When a collision is severe enough, the hull of the oil tanker is penetrated and ruptured, resulting in a damaged area. If the damaged area overlaps with a compartment, all contents from this compartment are assumed spilled.

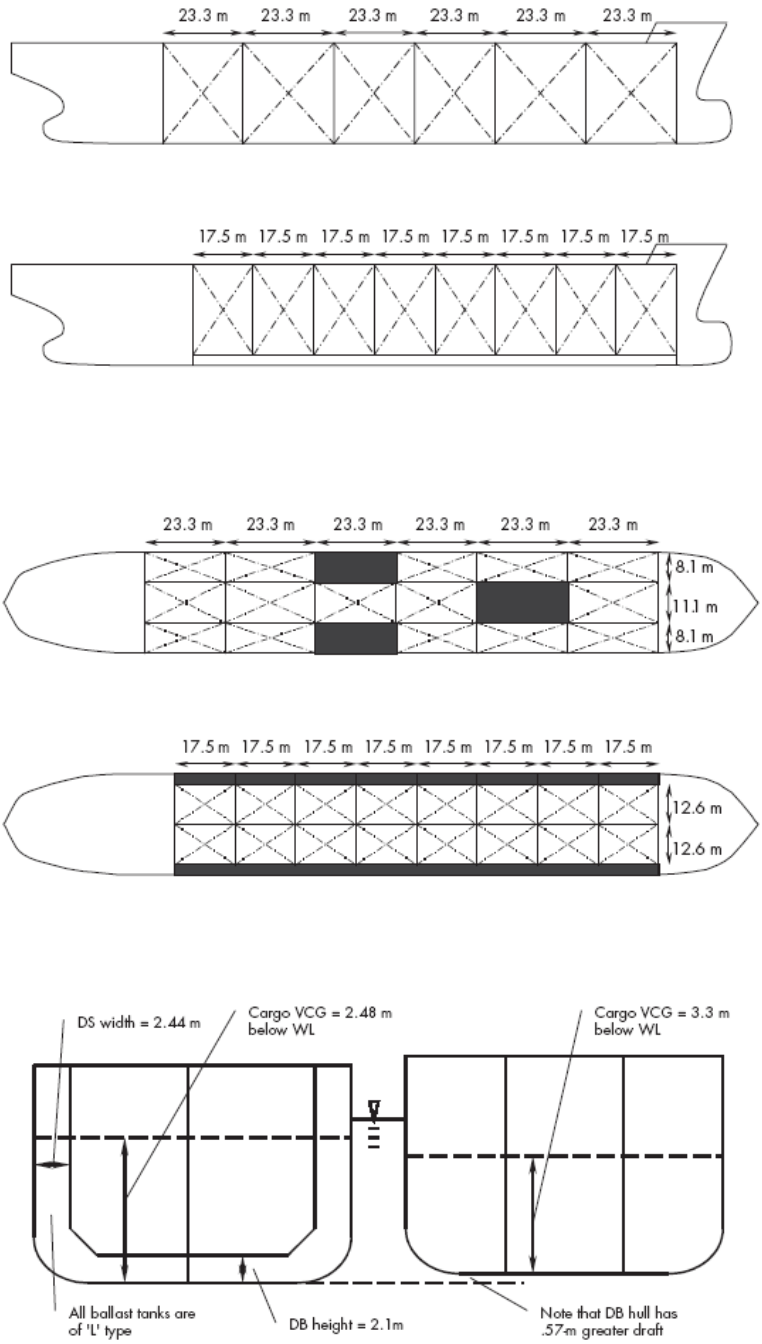

FIGURE 4-2 Profile, plan, and midship section for 40,000-DWT ships (VCG = vertical location of the center of gravity; WL = waterline).

Figure 2.1: 40,000 DWT tanker designs (source: National Academies Press [20])

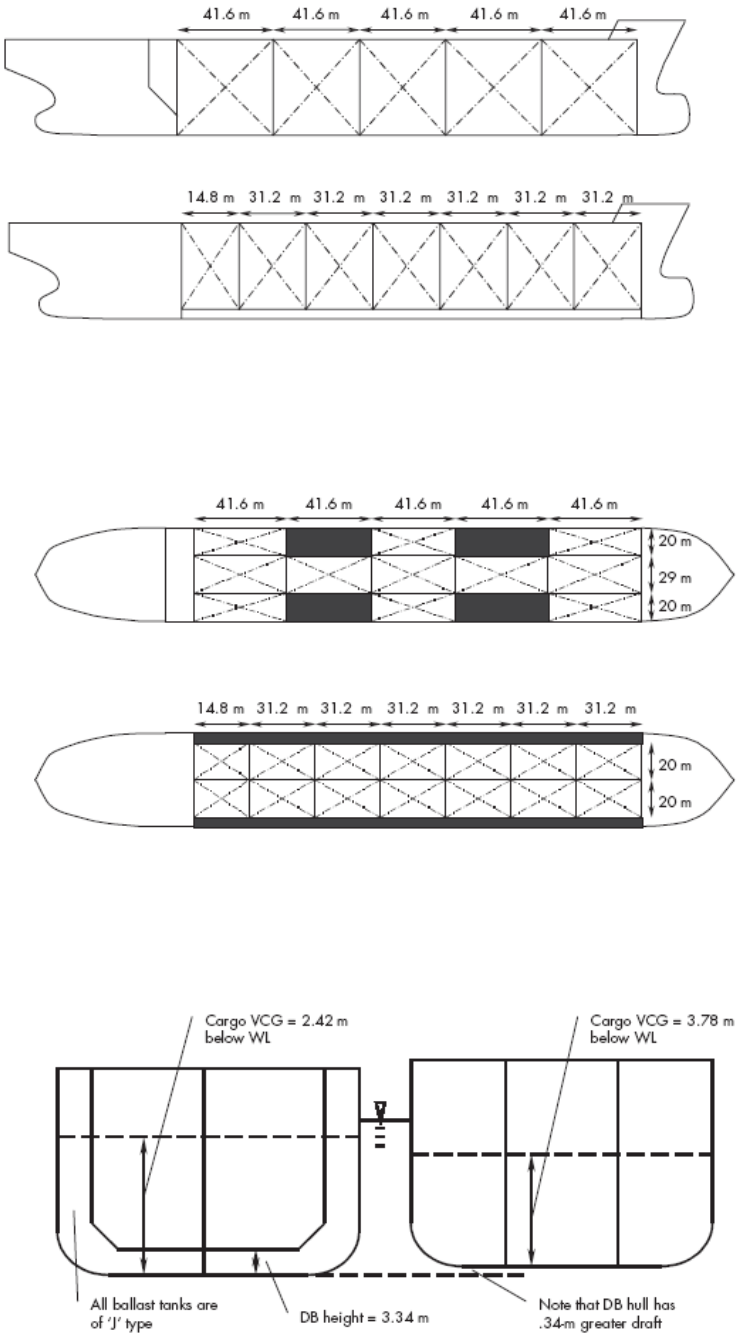

FIGURE 4-1 Profile, plan, and midship section for 150,000-DWT ships (VCG = vertical location of the center of gravity; WL = waterline).

Figure 2.2: 150,000 DWT tanker designs (source: National Academies Press [20])

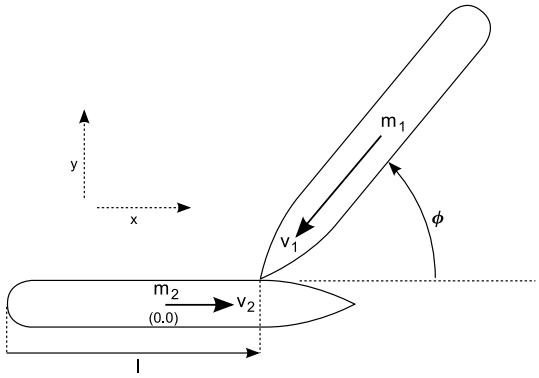

Figure 2.3: Two ships at the moment of collision

Name	Hull Type	Length (Meters)	Breadth (Meters)	Draft (Meters)	Deadweight Tonnage (Metric Tons)	Displacement (Metric Tons)
SH40	Single	201.168	27.432	10.603	40,000	47,547
SH150	Single	266.3	50.0	16.76	150,000	175,882
DH40	Double	190.5	29.26	10.58	40,000	47,448
DH150	Double	261.0	50.0	16.76	150,000	175,759

Table 2.1: Tanker specifications, collisions

2.2.1 Input Data

The specifications for the different tanker designs[1] that were used in the collision simulations are described in Table 2.1; an overview of compartment volumes for these ships is given in Table C.1 in the Appendix.nThe input variables in Table 2.2 are realizations of random variables with specific probability distributions. Together with other (fixed) parameters, like ship dimensions, plate thickness, compartment configurations etc. they define a collision scenario at the moment of impact. It is assumed that these variables are realizations of random variables which are defined by parametric distributions.[2]

- V_1 is characterized by a Weibull distribution with shape parameter $\alpha = 2.2$ and scale parameter $\beta = 6.5$;
- V_2 is given by an exponential distribution with parameter $\mu = 0.584$;
- Φ is the angle between port bows: if vessels travel in the same direction,

[1]Brown [3] is ambiguous as to whether the small designs (SH40 and DH40) have a deadweight tonnage (DWT) of 40,000 or 45,000; however, Tikka [21] gives a DWT of 40,000 for these designs. Therefore the decision was made to assume that the ships in the collision model also have a DWT of 40,000. Also, Brown mentions a length of 261.0m for the double hull in the report where the accompanying simulation file says 266.3m.

[2]By convention, random variables are denoted with capital letters; realizations of random variables are lowercase.

Input Variable	Symbol	Unit
Striking ship velocity	v_1	Knots
Struck ship velocity	v_2	Knots
Collision angle	ϕ	Degrees
Displacement of striking vessel	m_1	1000 metric tons
Collision location, relative from the stern	l	-
Striking ship type	t	-

Table 2.2: Input variables, collisions

$\Phi > 90°$; if not, $\Phi \leq 90°$. The distribution of Φ is approximated by a truncated Normal ($\mu = 90, \sigma = 28.97$) distribution; realizations are selected using Monte Carlo simulation on the interval $[0, 180]$. Although the use of Monte Carlo on a bounded support is only mentioned for Φ in the report, it is believed that this method is applied to other variables as well when a bounded support is imposed on distributions with infinite support.

- L gives the relative distance of the collision location from the Aft Perpendicular (AP) of the ship. $L = 0$ means the collision takes place at the AP, where $L = 1$ represents a collision at the FP[3]. It follows a $Beta(1.25, 1.45)$ distribution with support on $[0, 1]$ (see Appendix B for an explanation on distributions).

- T is one out of five types of striking ships: tanker, bulk cargo, freighter, passenger or container. Each type has its own characteristics; among the distinctions taken into account in the simulations is the bow half entrance angle η, which is the angle between bow and the longitudinal axis of the ship and is given for each type, and displacement M_1 which is a Weibull-distributed random variable. See Table 2.3 for the probability of occurrence of each striking ship type and Table 2.4 for the distribution of each type's displacement. Note that lower and upper bounds are given for displacement, whereas a Weibull distribution has support on $(0, \infty)$. Again, Monte Carlo simulation was probably used in selecting realizations of the Weibull distribution within the given bounds.

The aforementioned randomly generated variables are put into the collision simulation together with other parameters such as ship dimensions, struck ship displacement, compartment design, plate thickness, etcetera.

[3]The AP is the aftmost point of the bottom plane of the ship; the Forward Perpendicular (FP) is defined likewise.

Type t	Name	Probability of Occurrence	η (degrees)
1	Tanker	0.252	38
2	Bulk Carrier	0.176	20
3	Freighter	0.424	20
4	Passenger	0.014	17
5	Container	0.135	17

Table 2.3: Striking ship type distribution

		Weibull		Bounds (MT)	
Type t	Name	α	β	Lower	Upper
1	Tanker	0.84	11.2	699	273550
2	Bulk Carrier	1.20	21.0	1082	129325
3	Freighter	2.00	11.0	500	41600
4	Passenger	0.92	12.0	997	76049
5	Container	0.67	15.0	1137	58889

Table 2.4: Striking ship displacement distribution, by type

2.2.2 Output Data

When the simulation is over, three output variables are generated:

- Damage length y_l, meters
- Maximum penetration y_t, meters
- Oil outflow volume z, cubic meters

Damage length is the extent of the damaged area in the struck ship's longitudinal direction. Maximum penetration is the maximum extent of the damage in transversal direction. Oil outflow is the total sum of volumes of damaged compartments, i.e. compartments that coincide with the damaged area. See Figure 2.4 for a schematic view of an example of the damaged area. The distribution of the resulting output variables for all ship types are presented in Table 2.5 and Figures 2.5 and 2.6.

It must be noted that, when outflow occurs, y_l and y_t are nonzero; however, the reverse is not always the case. Therefore, there may be collision scenarios where there is damage but no outflow, for example in the case of plastic deformation without hull breach, or the rupture of ballast tanks (which contain no oil) but no oil compartments. This is especially likely in double hull tankers, where all oil compartments are seperated from the outer hull by ballast tanks. In Table 2.6, the number of nonzero values of y_l and y_t from the collision scenario are given as well as the number of cases of zero outflow for each ship type to show how many times this occurs.

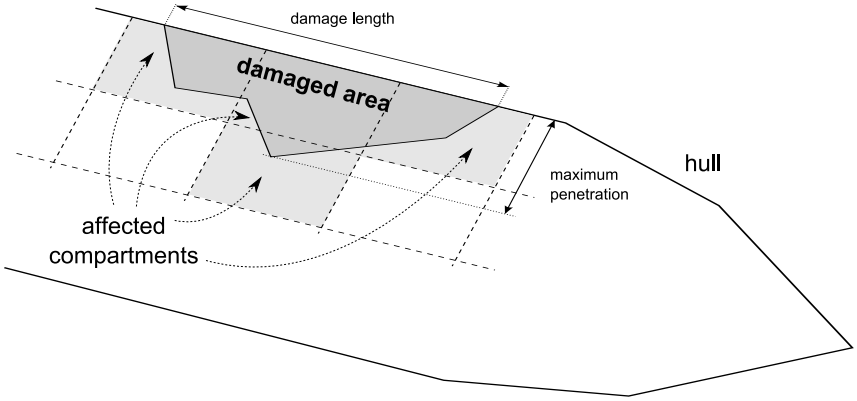

Figure 2.4: Collision damage

SH150		DH150		SH40		DH40	
Volume	Count	Volume	Count	Volume	Count	Volume	Count
0	6817	0	8974	0	5955	0	8596
3820	358	5515	84	1865	488	2270	97
8365	682	11694	86	2529	869	2277	133
12185	168	13862	129	2641	522	2670	189
13103	723	14650	119	2668	844	2825	84
15311	1150	14651	274	2674	797	2846	471
18864	7	14674	87	3644	20	5095	44
21567	13	19377	56	4506	116	5122	107
23479	5	26369	30	5197	156	5515	74
23676	1	28513	47	5314	131	5671	47
28023	2	29302	79	5507	10	5692	155
30882	8	29325	34	6171	21	7968	1
36875	11	43976	1	6312	12	10244	1
46888	13			6320	12	11383	1
51502	11			8147	6		
52449	8			8960	12		
55739	10			9956	13		
58441	12			9964	5		
70367	1			12483	8		
				12638	1		
				14275	1		
				16127	1		
Total	10,000	Total	10,000	Total	10,000	Total	10,000

Table 2.5: Outflow volume distribution, collisions

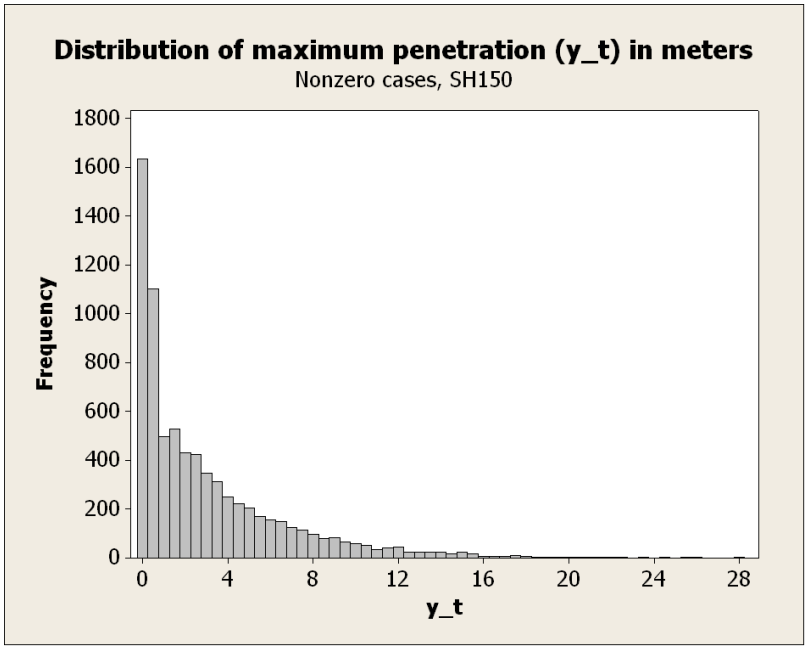

Figure 2.5: Maximum penetration histogram, collisions

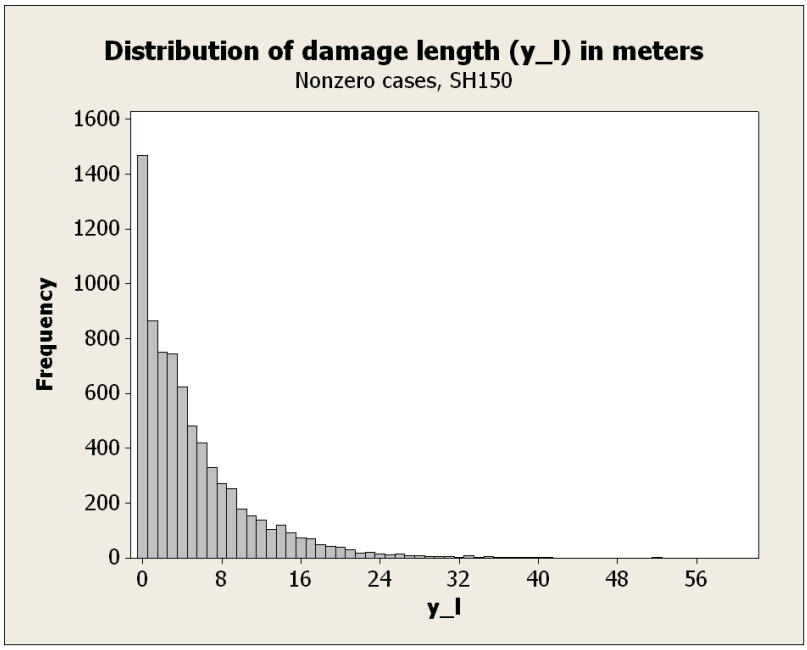

Figure 2.6: Damage length histogram, collisions

Type	SH40	SH150	DH40	DH150
number of nonzero z	4045	3183	1404	1026
number of nonzero y_l	7467	7473	7454	7466
number of nonzero y_t	7470	7478	7455	7467

Table 2.6: Nonzero output values from collision simulations

Name	Hull Type	Draft (Meters)	Deadweight Tonnage (Metric Tons)	Displacement (Metric Tons)
SH40	Single	10.58	40,000	47,448
SH150	Single	16.78	150,000	175,907
DH40	Double	11.17	40,000	49,410
DH150	Double	17.12	150,000	175,940

Table 2.7: Tanker specifications, groundings

2.3 Groundings

In a grounding, a tanker collides at the bottom with an obstacle, in this case a cone-shaped rocky pinnacle with a rounded tip (see Figure 2.7). The rock is assumed fixed and strong enough never to suffer any damage. Specifications for the struck ships in the grounding simulations differ slightly from those in collisions (see Table 2.7). An overview of compartment volumes for these ships is given in Tables C.5 through C.8 in the Appendix.

2.3.1 Input Data

The input variables in Table 2.8, along with fixed parameters such as ship dimensions, plate thickness etc. are put into the grounding simulation. They are realizations of random variables with specific probability distributions to form a specific grounding scenario at the moment of impact.

- V is distributed as in Table 2.9.
- In the report accompanying the grounding study [21], the distribution mentioned for O_d is different than the one found in the data. Therefore the latter distribution will be used later on to get a correct fit.
- O_a is distributed along a 'truncated' Normal distribution with support on the interval $[15, 50]$. Since the original report doesn't state the mean nor the variance of this normal distribution, it is assumed unknown and therefore a fit for this variable will also be determined later on.
- O_r is also characterized by a truncated Normal distribution on $[0, 10]$. Based on the data, it is assumed that the mean of the original distribution is 5, meaning

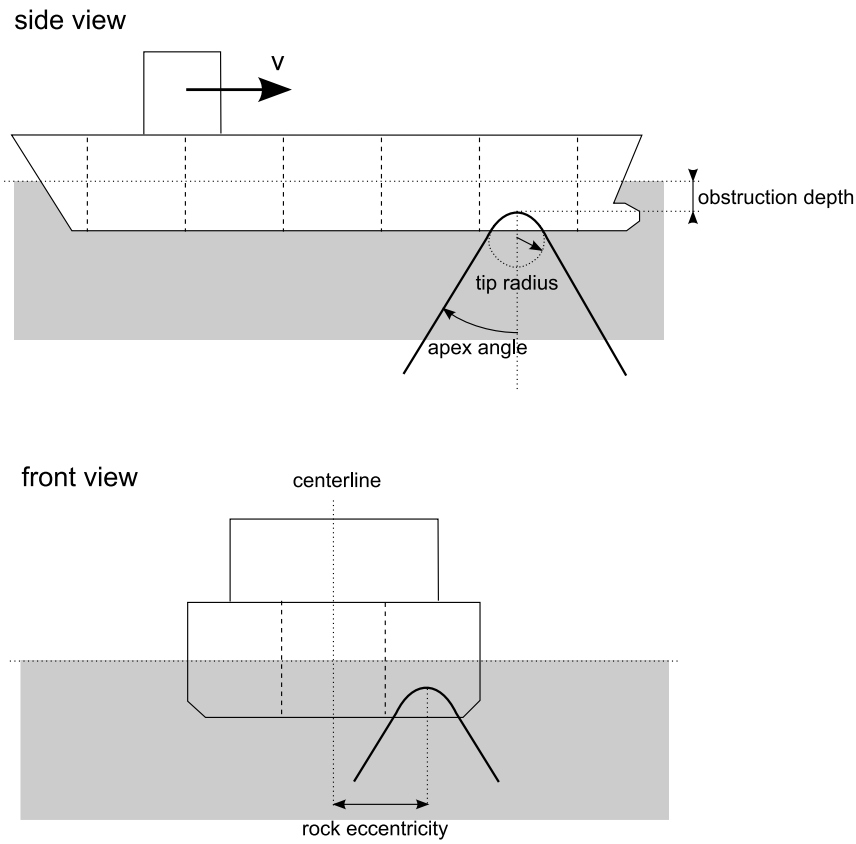

Figure 2.7: Grounding simulation

Input Variable	Symbol	Unit
Struck ship velocity	v	Knots
Obstruction depth from mean low water	o_d	Meters
Obstruction apex angle	o_a	Degrees
Obstruction tip radius	o_r	Meters
Rock eccentricity	c	-
Tidal variation from mean low water	τ	Meters
Inert tank pressure	p	mm water gauge
Capture in ballast tanks	b	% of tank volume
Minimum outflow	ν	% of ruptured tank volume

Table 2.8: Grounding input variables

Bin Bounds		
Lower	Upper	Probability
0	5	0.25
5	8	0.45
8	15	0.08
15	16	0.20
16	20	0.02

Table 2.9: Velocity distribution, groundings

Bin Bounds		
Lower	Upper	Probability
0	0.7	0.50
0.7	1.7	0.35
1.7	2.5	0.15

Table 2.10: Tidal variation distribution

$P(O_r \leq x) = 1 - P(O_r > 10 - x)$ for $x \in [0, 10]$. This variable will also be fitted later on.

- Rock eccentricity C is defined as the obstruction distance relative from the centerline, i.e. it is 0 if the obstacle hits the ship in the middle and 1 if it hits on either port or starboard side. C has a uniform $[0, 1]$ distribution.
- Tidal variation is distributed as in Table 2.10. Tank pressure, minimum outflow and ballast capture are uniformly distributed on intervals $[400, 1000]$, $[0.5, 1.5]$ and $[0, 50]$, respectively.

2.3.2 Output Data

Once a grounding simulation is complete, it generates the output variables described in Table 2.11. 'Elevation' is the height of the obstruction tip above the ship's bottom. If k is the number of cargo compartments, $z = \sum_{j=1}^{k} z_{c,j}$ is the total outflow volume (note that $z_{c,j} = 0$ if compartment j is not damaged). The histograms of the output variables y_{l1}, y_{l2}, y_t, y_v and z are displayed in Figures 2.8 through 2.11. Looking at the histogram of y_v (Figure 2.10), it seems that this variable is directly related to an input variable. Indeed, when plotted as a function of obstruction depth o_d (Figure 2.12), it becomes clear that

$$y_v = \max(0, s_d - o_d) \tag{2.1}$$

where s_d is the ship's depth. From the figure, it can be seen that this holds for all ship types.

Variable	Symbol	Unit
Begin of longitudinal damage extent	y_{l1}	Meters aft from midship
End of longitudinal damage extent	y_{l2}	Meters aft from midship
Transversal damage extent	y_t	Meters
Elevation	y_v	Meters from bottom hull
Outflow volume per cargo compartment j	$z_{c,j}$	Cubic meters
Volume captured in ballast tanks	z_b	Cubic meters

Table 2.11: Grounding output variables

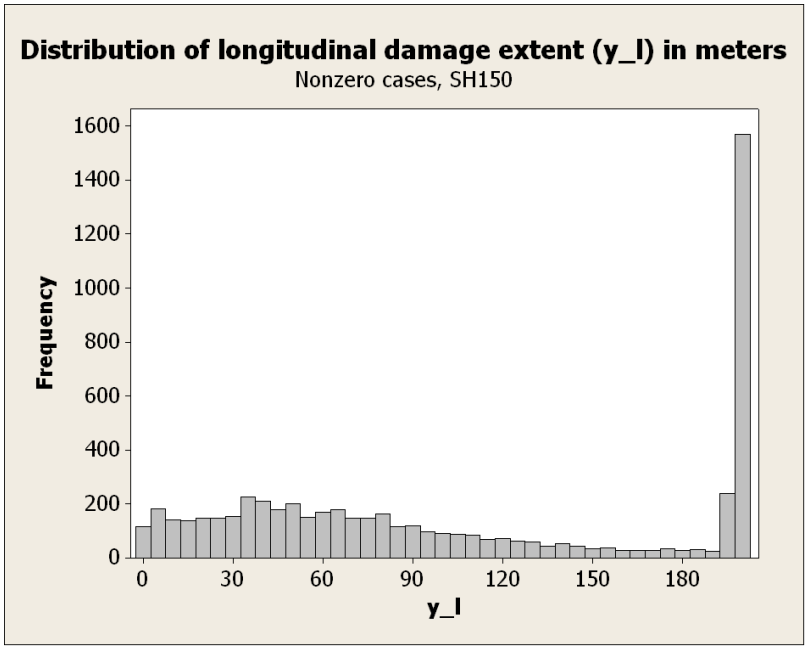

Figure 2.8: Longitudinal damage extent histogram, groundings

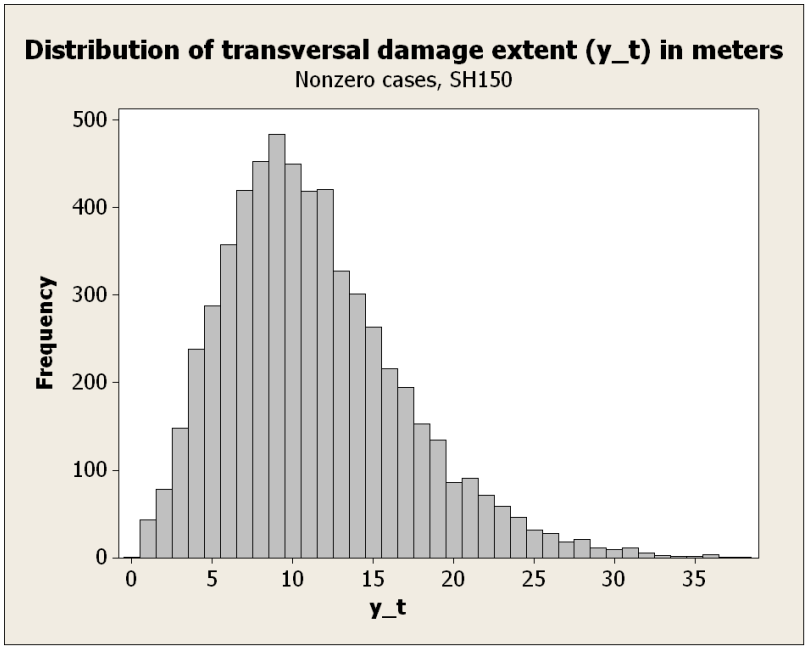

Figure 2.9: Transversal damage extent histogram, groundings

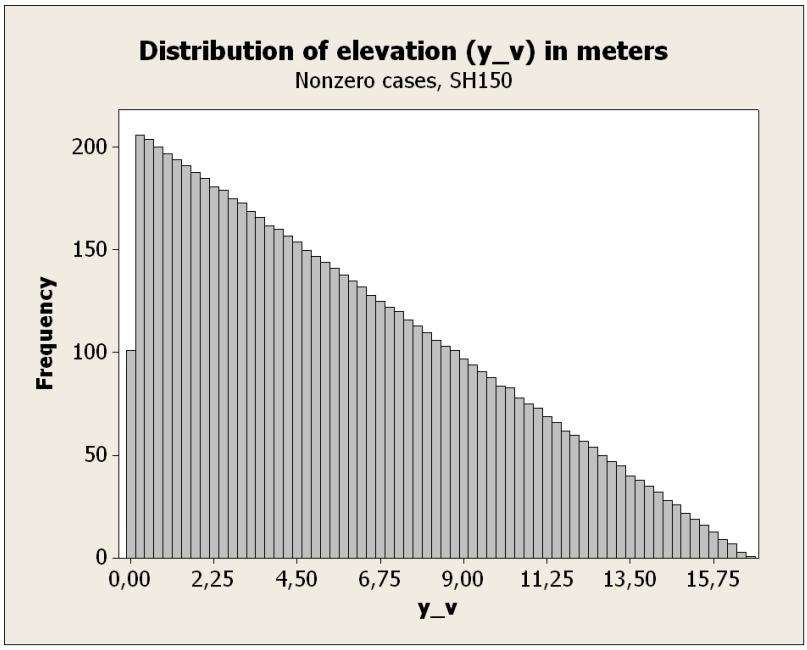

Figure 2.10: Elevation histogram, groundings

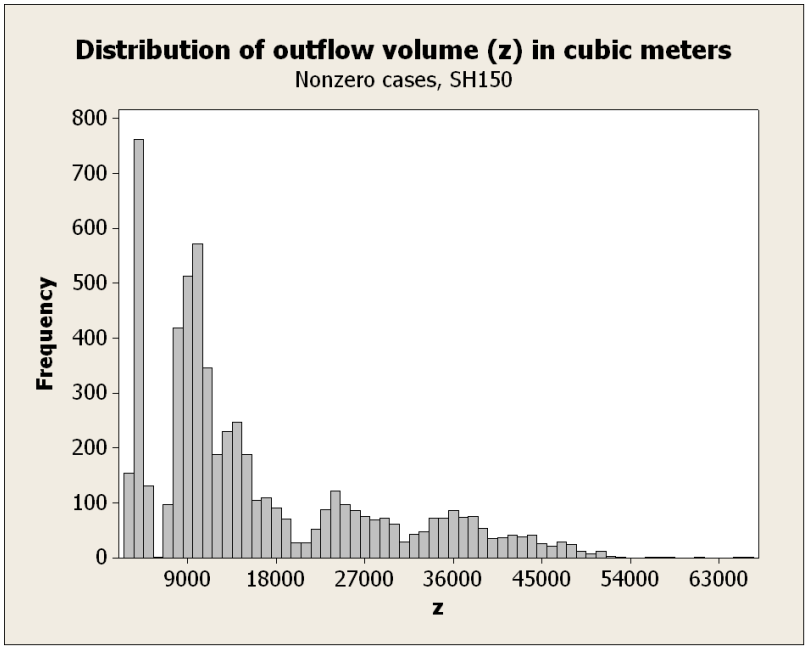

Figure 2.11: Total outflow volume histogram, groundings

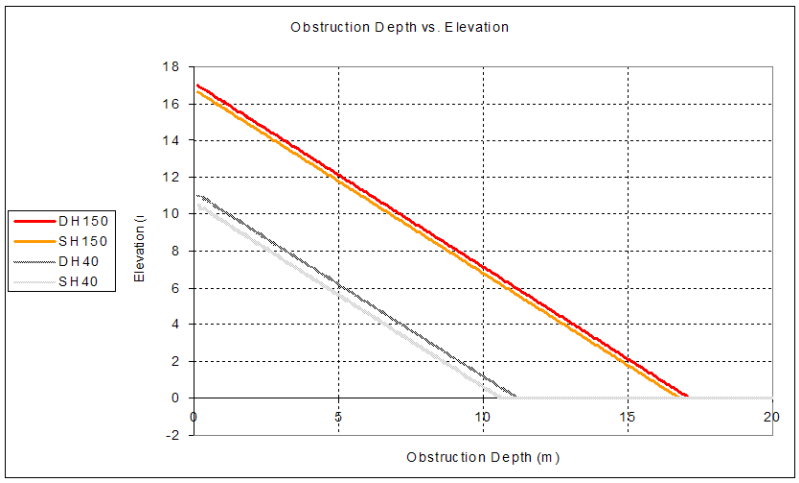

Figure 2.12: Scatterplot of obstruction depth vs. elevation, all ship types

Chapter 3

Collision Model

3.1 Overview

The simulated collision data discussed in Chapter 2 is used to construct a model that calculates outflow volume given a collision scenario. The essence of this model is to establish a relation between known input and output datapoints that are present in the given sample set, i.e. between velocity, collision angle etc. and oil outflow volume, so that outflow can be calculated for any given collsion scenario using these variables.

Just searching through a set of 40,000 datapoints is not practical; furthermore, if the specific scenario is not included in the 40,000 that were simulated, one would need to be able to interpolate between datapoints. A subsequent issue is that directly linking a set of input variables to outflow volume is not ideal. There are only a handful of different outflow values due to the assumption that all oil in a damaged compartment is lost; the limited number of compartments results in limited possible outflow outcomes. Also, in a high number of cases there is no outflow at all.

Since data on the size of the damaged area is available, as well as ship designs used in the simulations, it would be useful to include these aspects into the model.

3.1.1 Model Structure

The collision outflow model is ordered into sequential steps. Given the data obtained from collision simulations, the model should

1. calculate the damage extent to the struck ship given arbitrary scenario input variables;
2. determine the occurrence of rupture given damage extent;
3. calculate the oil spill volume given rupture.

Instead of a model that directly relates outflow volume to input variables, this one is not limited to the scenarios that were generated in the simulations. Also, it makes use of not only outflow data z but also damage data y_l and y_t. Furthermore, it makes use of the different types of data in a sequential fashion. Since data exists for four different ship types, four different collision models will be developed, each estimating the accidental outflow volume based on specific ship type -either single or double hull- and deadweight tonnage -either 40,000 or 150,000. Finally, combining simulation datasets results in generic models for single hull and double hull ships, i.e. models where the struck ship design is not fixed but defined by an additional variable. Thus in total, six models will be developed: four based on a particular design and two a combination of those.

In essence, this model allows interpolation between collision scenarios and between small and large ships of the same type (single hull or double hull).

Developing the outflow model requires several data analyses to be performed. Figure 3.1 gives a schematic overview of this model and the accompanying analysis in three sequential steps. It shows that the available simulation data is fed into different analytical methods in the analysis part (left); each of which is linked to a corresponding calculation method in the calculation part (right).

In the following sections discuss the choice of analytical methods and how they were performed.

3.1.2 Regression Analysis

The usual method of obtaining a relationship between sample sets is through regression analysis. The input variables are known as predictor- or independent variables; the output variable is called the response- or dependent variable. Analysis results in a regression model. Appendix A goes into more detail on various regression models.

3.1.3 Statistical vs. Practical Significance

Goodness-of-fit tests can be useful in determing whether it is suitable to fit a theoretical regression model to a dataset. However, these tests deal with statistical significance, while the practical significance of a model might be a more relevant issue:

> "The question is not whether the input model is absolutely correct; it is whether the input model is adequate for the analysis at hand. [...] The fallacy of the goodness-of-fit test is made obvious when a large real-world data set it fitted to many classical distributions and all are rejected; all are rejected because the large sample size yields large power and the error in the model is indeed statistically significant." [18]

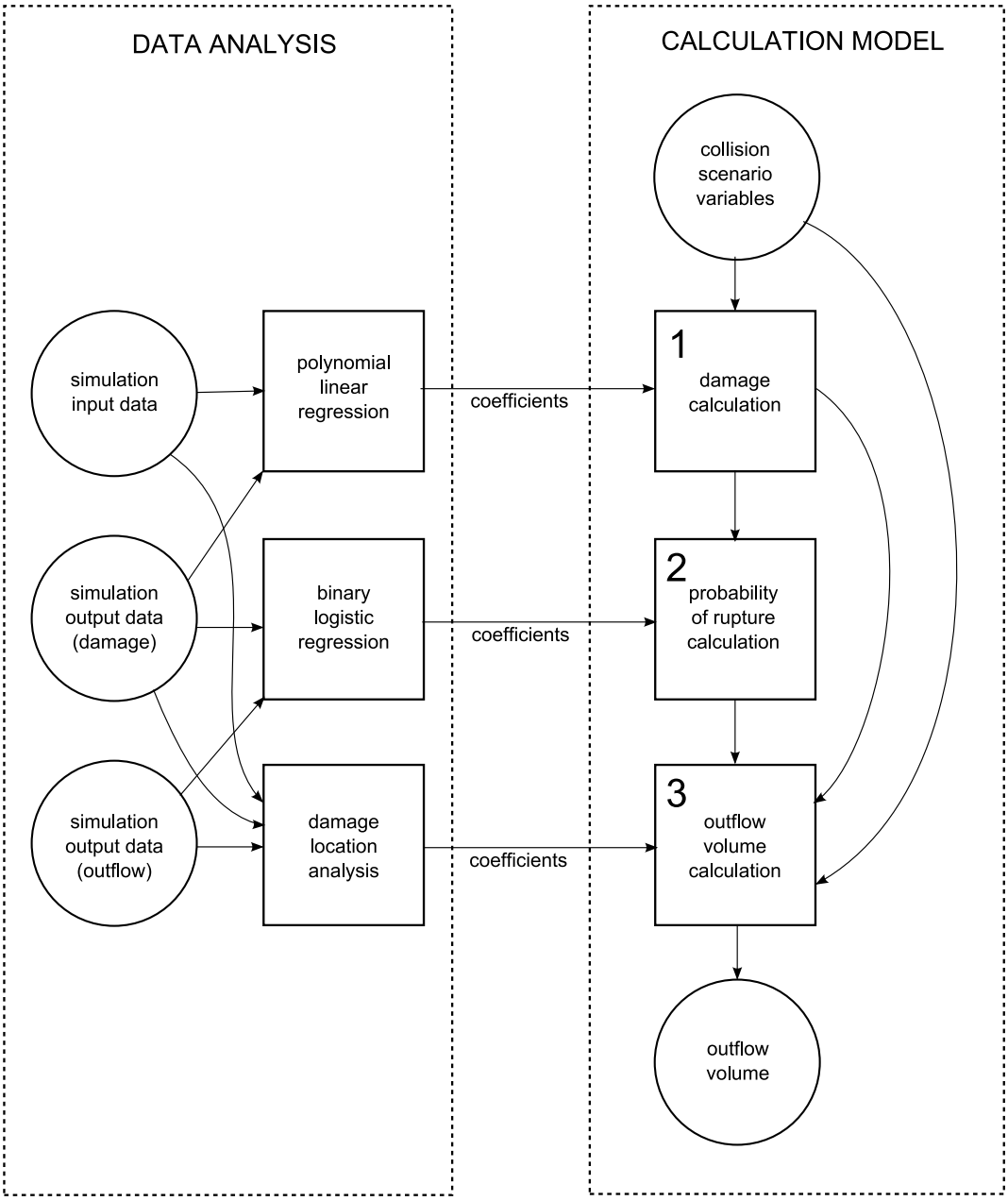

Figure 3.1: Collision outflow model overview

Because this report works with large datasets, validity of the models' significance is based on an "intuitive" judgment rather than statistical tests, although the latter will be taken into account.

3.2 Defining Predictor Variables

The input variables in the collision simulation sample (v_1, v_2, m_1, ϕ, l, t) could be directly used in regression; however, transforming them into other variables might result in a more natural, meaningful representation of a collision scenario. For example, a higher striking ship velocity (v_1) alone does not necessarily lead to a higher outflow probability or a larger damage area; this outcome also depends on the orientation of the striking ship against the struck ship (represented by collision angle ϕ). In this section, the predictor variables to be used in regression are obtained from the variables in the dataset.

Intuitively, when travelling at the same speeds, a heavy ship will release more kinetic energy in a collision than a light one; and and a fast-moving ship will release more kinetic energy than a slow-moving one with the same mass as the former. Therefore it is plausible that damage extent in a collision is related to kinetic energy. A relationship between dissipated energy in a collision and damage volume has been established empirically by Minorsky [15].

Important is the relative direction of motion. If two colliding ships travel in the same direction, less energy is released on collision than when going in the opposite direction. Also, since the striking ship collides under a certain angle, the inflicted damage varies depending on this angle. If it is very oblique, the striking ship will cause less damage than when it strikes perpendicular to the struck ship's longitudinal axis. Hence, it it critical that the energy variable(s) to be developed take into account relative velocities in the travelling direction of the struck ship and the collision angle to be effective in an analysis.

To accomodate this, a decomposition of kinetic energy into a tangential and perpendicular component is proposed.

Kinetic Energy

The kinetic energy of a body represents the amount of energy that is being released when this body is brought from a moving state to a full stop.

The total kinetic energy e_k of a system consisting of n separate masses $m_1, \ldots, m_n$ in a space is defined as

$$e_k = \sum_{j=1}^{n} \frac{1}{2} m_j v_j^2 \tag{3.1}$$

where v_j is the speed of m_j and $\vec{v}_j$ is the corresponding velocity vector with $v_j = \|\vec{v}_j\| = \sqrt{\langle \vec{v}_j, \vec{v}_j \rangle}$.

The coordinate system (x, y) used in the simulations is two-dimensional and defines the coordinate system's origin $(0, 0)$ as midship of the struck ship at the moment of collision. The struck ship, at that point, travels with speed v_2 in the positive x-direction; the striking ship moves towards the struck ship under an angle ϕ at speed v_1 (see also Figure 2.3). The corresponding velocity vectors are then:

$$\vec{v}_1 = (-v_1 \cos\phi, -v_1 \sin\phi) \tag{3.2}$$

$$\vec{v}_2 = (v_2, 0) \tag{3.3}$$

It is noteworthy that the y-components of the velocities are perpendicular to the struck ship's direction of motion, and that the x-components are tangential to it. Considering the ships as separate masses, total kinetic energy becomes

$$e_k = \frac{1}{2} m_1 v_1^2 + \frac{1}{2} m_2 v_2^2 \tag{3.4}$$

This term can be decomposed into perpendicular and tangential components, $e_{k,p}$ and $e_{k,t}$, respectively:

$$e_{k,p} = \frac{1}{2} m_1 (v_1 \sin\phi)^2 \tag{3.5}$$

$$e_{k,t} = \frac{1}{2} m_1 (v_1 \cos\phi)^2 + \frac{1}{2} m_2 v_2^2 \tag{3.6}$$

It follows that $e_k = e_{k,p} + e_{k,t}$. However, this decomposition does not discriminate in relative direction of motion. If two ships collide at certain speeds and $\phi = 0°$, $e_{k,t}$ will have the same value as when they travel at the same speeds and $\phi = 180°$. In Figure 3.2, it can be seen that in the left situation, a lot less damage will be inflicted as opposed to the right situation because of the difference in tangential velocity, although $e_{k,t}$ as defined in Equation 3.6 stays the same. Therefore, a modified definition of tangential kinetic energy could be introduced:

$$e_{k,t} = \frac{1}{2} m_1 \kappa(\phi) (v_1 \cos\phi)^2 + \frac{1}{2} m_2 v_2^2 \tag{3.7}$$

where

$$\kappa(\phi) = \begin{cases} 1, & 0 < \phi \leq \frac{\pi}{2} \\ -1, & \frac{\pi}{2} < \phi \leq \pi \end{cases} \tag{3.8}$$

However, in that case $e_{k,p}$ and $e_{k,t}$ do not sum up to e_k when $\kappa(\phi) = -1$ and is thus not consistent with the kinetic energy formulation of a set of seperate bodies. From this argument, the notion arises that the difference in perpendicular and tangential velocities has to be taken into account. Consider the following:

$$e_k = \frac{1}{2} m_1 v_r^2 + \frac{1}{2} m_2 v_2^2 \tag{3.9}$$

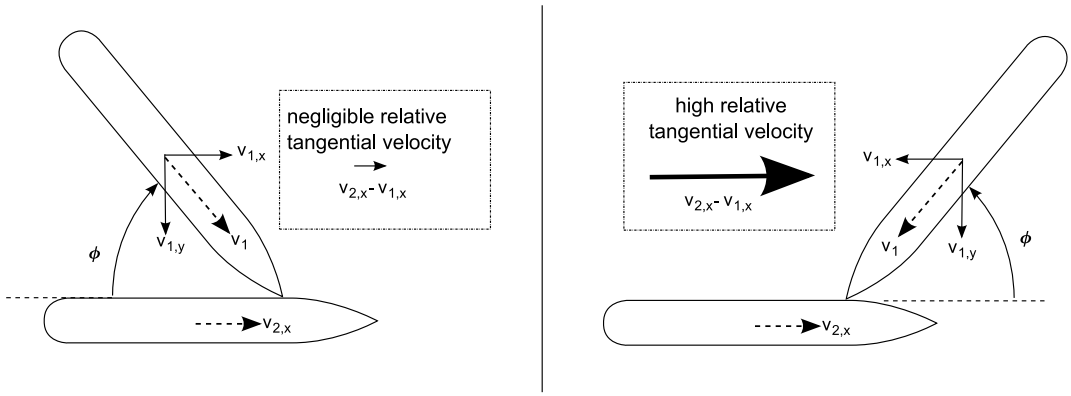

Figure 3.2: Tangential velocity difference

which might be decomposed into

$$e_{k,p} = \frac{1}{2}m_1 v_p^2 \tag{3.10}$$

$$e_{k,t} = \frac{1}{2}m_1 v_t^2 + \frac{1}{2}m_2 v_2^2, \tag{3.11}$$

where

$$\vec{v}_r = \vec{v}_2 - \vec{v}_1 = (v_2 + v_1 \cos\phi, v_1 \sin\phi) = (v_t, v_p)$$

is the velocity of the striking ship relative to the struck ship's velocity. However, consider again two ships travelling in the same direction with exactly the same speed. No collision damage will occur, but this decomposition will not accomodate that scenario.

Hence, it appears that interpreting the vessels as seperate bodies does not lead to a set of predictor variables with the desirable properties. To get a consistent decomposition of kinetic energy that holds up to the concepts mentioned at the beginning of this subsection, one should consider the two ships to represent a single mass at the exact moment of impact with a residual velocity that is the vector sum of the velocities of the individual vessels. Now imagine a measure of kinetic energy that represents the "collision kinetic energy", being the kinetic energy that can be released in a collision in perpendicular and tangential directions:

$$e_k = e_{k,p} + e_{k,t} = \frac{1}{2}m_{tot} v_r^2 \tag{3.12}$$

where

$$e_{k,p} = \frac{1}{2}m_{tot} v_p^2 \tag{3.13}$$

$$e_{k,t} = \frac{1}{2}m_{tot} v_t^2 \tag{3.14}$$

and $m_{tot} = m_1 + m_2$. It is important to mention that, using this kinetic energy model, two ships travelling in the same direction at the same speed will result in zero kinetic energy upon collision, regardless of their masses.

Location

The relative collision location l possibly has an influence on the ability to convert the perpendicular motion of the striking ship into rotational motion of the struck ship can be determined. If a collision occurs at the bow or stern, more kinetic energy is transformed into rotation of the struck ship around the vertical axis. When the collision instead occurs near midship, the struck ship is less able to transform perpendicular motion into rotation. A new variable l' is introduced that indicates how far a collision takes place from midship of the struck ship:

$$l' = \left| l - \frac{1}{2} \right| \tag{3.15}$$

Striking Ship Type

The striking ship type t determines the mass, dimensions and other parameters of the striking ship. t itself cannot be used as a predictor variable because it qualifies rather than quantifies a ship's characteristics ("type" cannot be measured whereas, for example, "mass" or "length" can). Since dimensions are directly related to mass [3], and since mass is already taken up in $e_{k,p}$ and $e_{k,t}$, the only variable that could further represent t is the bow half entrance angle η.

η affects the striking ship's ability to penetrate te struck ship. The sharper the angle, the higher the probability that the striking ship will penetrate the struck ship, and the further the striking ship will penetrate.

Combined Model Variable

In the combined collision models the single hull datasets (SH40, SH150) and double hull datasets (DH40, DH150) are combined into combined single hull and double hull datasets (SHCOM, DHCOM). These datasets are thus twice as long as the original ones and represent simulation data for a generic single hull or double hull ship. Because the variables in these sets do not present explicit information on the origin of the data -i.e., which dataset it belonged to originally- an additional variable will be added that improves the quality of the regression model. This variable, d, represents either the length or the width of the ship (depending on which dependent variable it is used on in regression, e.g. y_l or y_t). In a sense, it is an indicator variable, indicating ship type, but because it $d \in \mathbb{R}$ it can be used in regression among the other variables.

3.3 Transformation of Predictor Variables to CDF

Now there are four variables defining the input of a collision event for four types of tankers, and five variables for two combined tanker designs. Each set of predictor variables $(e^i_{k,p}, e^i_{k,t}, l'^i, \eta^i, d^i)$, for all $i \in \{1, \ldots, n\}$ can be seen as realizations of random variables $E_{k,p}, E_{k,t}, L', H$ and D. Their corresponding cumulative distribution functions (CDFs) are $F_{E_{k,p}}, F_{E_{k,t}}, F_{L'}, F_H$ and F_D. Instead of taking the predictor variables as they are, all realizations for each variable are transformed through their CDF values, resulting in the transformed predictor variables

$$\begin{aligned} x_{1,i} &= F_{E_{k,p}}(e^i_{k,p}), \\ x_{2,i} &= F_{E_{k,t}}(e^i_{k,t}), \\ x_{3,i} &= F_{L'}(l'^i), \\ x_{4,i} &= F_H(\eta^i), \\ x_{5,i} &= F_D(d^i), \\ & \quad \forall i \in \{1 \ldots, n\} \end{aligned} \tag{3.16}$$

The rationale behind this transformation step is as follows:

- The transformed variables are in the domain [0,1], increasing numerical stability in regression computations.
- The transformed variables are dimensionless, since a CDF typically represents the probability of an event. Any regression analysis performed on these variables will yield parameters that have the same dimension as the response variable.

Note that the CDFs for variables l' and η are the same in all collision models, even in the combined ones, but not $e_{k,p}$ and $e_{k,t}$ because the masses of the struck ships vary. Since d only plays a role in the combined models, it is not used in the other ones. Figure 3.3 gives an overview of the transformation steps converting the original variables to predictor variables to be used in the regression analysis.

3.3.1 CDFs of $E_{k,p}$, $E_{k,t}$

$E_{k,p}$ and $E_{k,t}$ are stochastic variables composed of other stochastic variables, as can be derived from Equations 3.13 and 3.14:

$$E_{k,p} = \frac{1}{2}(M_1 + m_2)V_1^2 \sin^2 \Phi \tag{3.17}$$

$$E_{k,t} = \frac{1}{2}(M_1 + m_2)(V_2 + V_1 \cos \Phi)^2 \tag{3.18}$$

Because of the complexity of these equations, it is difficult to find the exact distribution functions $F_{E_{k,p}}$ and $F_{E_{k,t}}$. An alternative would be to use the empirical CDFs

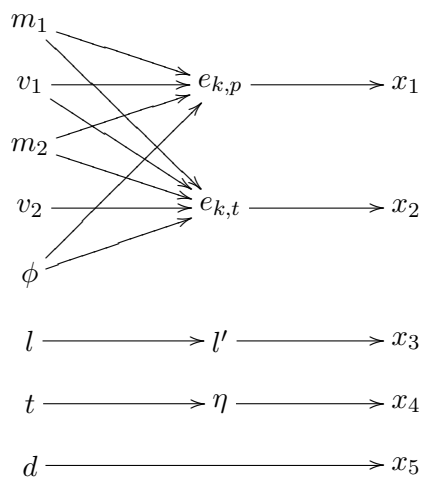

Figure 3.3: Transformation of input variables to predictor variables

of $E_{k,p}$ and $E_{k,t}$, which is found by looking at the distribution of the realizations of these random variables (see Appendix B). Since $n = 10,000$ and thus sufficiently large, the empirical CDFs for $E_{k,p}$ and $E_{k,t}$ would be excellent approximations for the real CDFs because of the strong limit properties of the empirical CDF.

Herein, however, also lies also a weak point: since there are $10,000$ realizations for $E_{k,p}$ and $E_{k,t}$, it would be cumbersome to implement their empirical CDF in the application of the outflow model: each time it is invoked, up to 10,000 values have to be looked up from a table containing the realizations, which will lengthen the run time of a application using the model significantly and makes the model higly unportable, i.e. these values have to be stored somewhere.

Therefore, it's better to find a parametric fit to the empirical CDF, which, in the case of a closed-form parametric fit, would require a calculation time that is magnitudes less than using empirical CDFs. A parametric CDF to fit a random variable X is denoted by $F_X(x|\alpha)$, where α is a set of parameters that define the function's characteristics. For $E_{k,p}$ and $E_{k,t}$, numerous options exist for a parametric distribution. The Weibull distribution (see Appendix B) does a good job, is only nonnegative, is closed-form and is shaped by two parameters instead of 10,000 realizations of random variables.

Fits for $F_{E_{k,p}}$ and $F_{E_{k,t}}$ were generated using Minitab: see Figure 3.4 for a comparison between the Weibull and empirical CDF of perpendicular kinetic energy in the SH40 case, and a probability plot that shows how well the data aligns with the fit. In Table 3.1 the coefficients for all Weibull fits are given.

The drawback to using the Weibull fit is that the p-value for the Anderson-Darling

		SH40	SH150	SHCOM	DH40	DH150	DHCOM
$E_{k,p}$	α	0.4699	0.4724	0.4515	0.4699	0.4724	0.4514
	β	320.3	1010	590.0	319.8	1010	589.4
$E_{k,t}$	α	0.4546	0.4567	0.4379	0.4546	0.4567	0.4378
	β	385.7	1217	709.9	385.1	1217	709.1

Table 3.1: Coefficients for Weibull fits, kinetic energy

test[1] is very low, which essentially means that the use of the parametric CDF as a fit for the empirical CDF has to be discarded. However, because the number of datapoints is so high, the margin of acceptance becomes extremely narrow and it is unlikely that any parametric fit would be accepted. For practical reasons, judging a fit by 'visual' goodness-of-fit trumps the statistical test (as discussed in Section 3.1.3). In that view, the Weibull distribution is accepted. Alternative parametric distributions, such as Gamma, Exponential (which is a special case of the Weibull family) and Logistic have significantly worse fits (see Figure 3.5).

3.3.2 CDF of L'

Given that $L \sim Beta(1.25, 1.45)$, Equation 3.19 returns the exact distribution of L' which was defined as $L' = |L - \frac{1}{2}|$. See figure 3.6 for a graph of $F_{L'}$.

$$\begin{aligned} F_{L'}(x) &= P(L' \leq x) \\ &= P(\left|L - \frac{1}{2}\right| \leq x) \\ &= P(-x \leq L - \frac{1}{2} \leq x) \\ &= P(\frac{1}{2} - x \leq L \leq \frac{1}{2} + x) \\ &= P(L \leq x + \frac{1}{2}) - P(L \leq -x + \frac{1}{2}) \\ &= F_L(x + \frac{1}{2}) - F_L(-x + \frac{1}{2}) \end{aligned} \tag{3.19}$$

3.3.3 CDF of H

Since H only takes on three possible values, namely 17, 20 and 38 degrees, the best transformation is the empirical CDF, which is given in Table 3.2 and Figure 3.3.3.

[1]The Anderson-Darling test puts up two hypotheses: one saying that the data follows the specified distribution (in this case Weibull), and one saying that it doesn't. A p-value below a certain level of signifcance, here 0.05, pleads for the latter hypothesis.

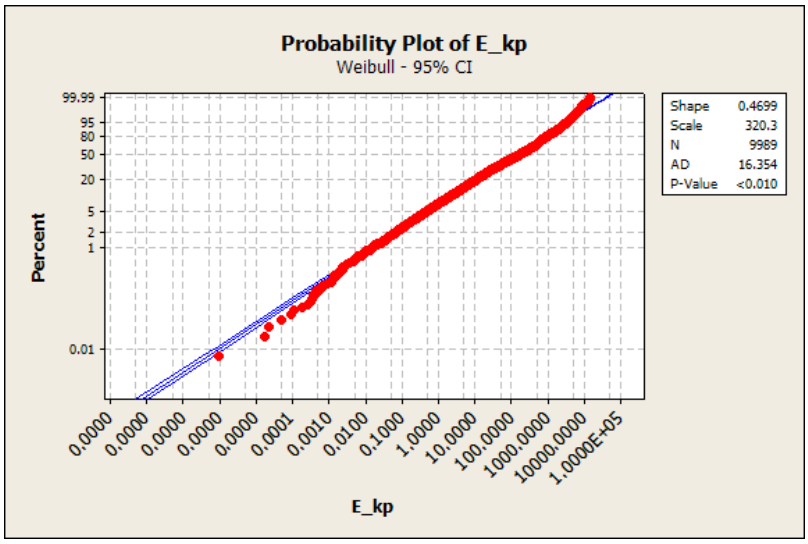

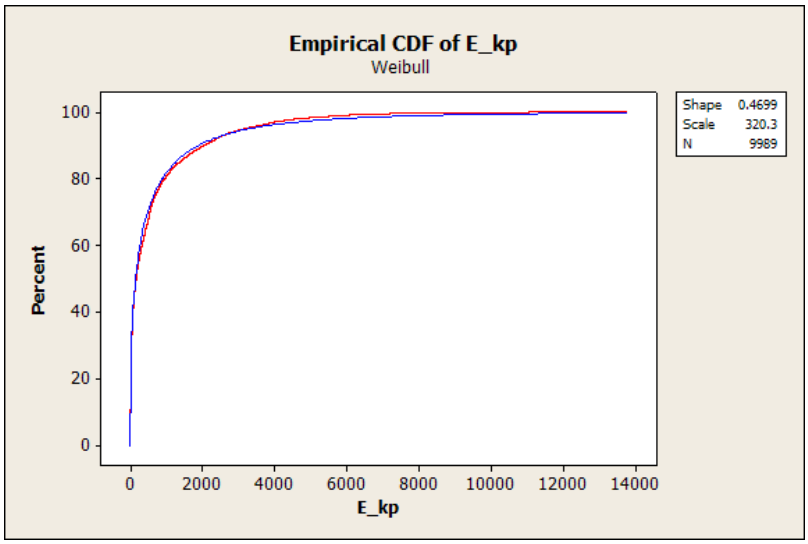

Figure 3.4: Probability plot & Weibull fit of empirical CDF, perpendicular kinetic energy, SH40 case

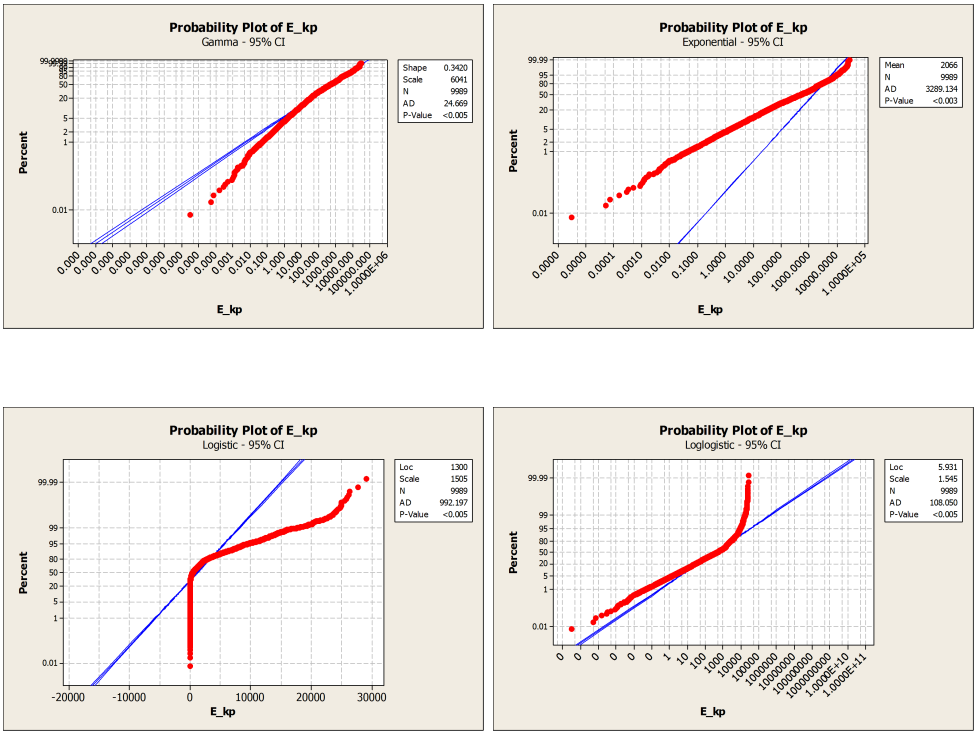

Figure 3.5: Probability plots of alternative parametric fits, perpendicular kinetic energy, SH40 case

η	Count	$F_H(\eta)$
17	2440	0.2440
20	5323	0.7763
38	2236	1.0000

Table 3.2: Empirical CDF of H

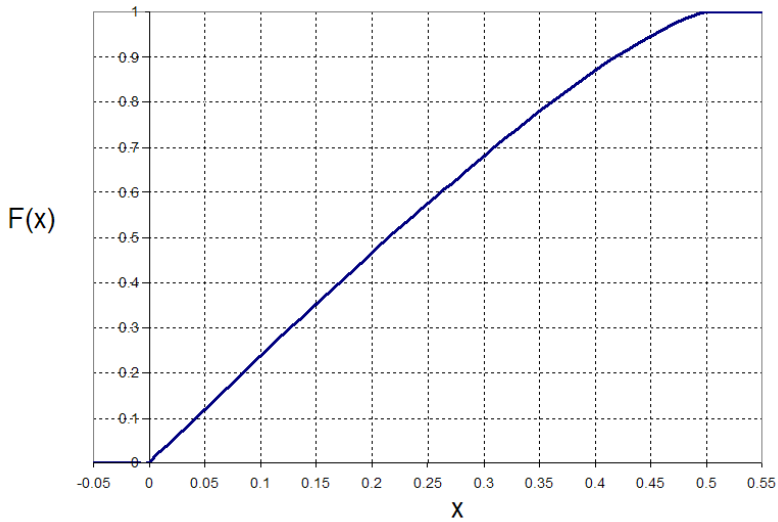

Figure 3.6: Cumulative distribution function for L'

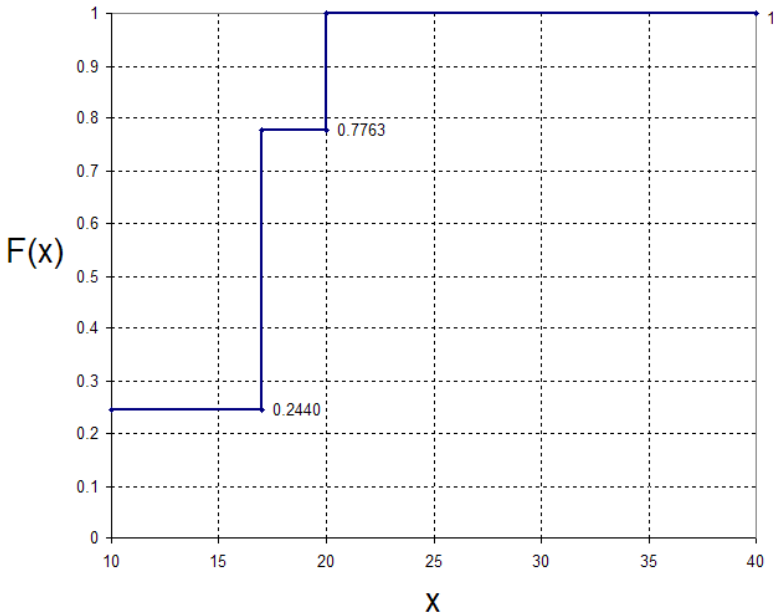

Figure 3.7: Empirical CDF of H

3.4 Damage Extent

Now that the predictor variables have been defined, it is time to look at the effect they have on damage extent. Damage extent is measured by two parameters: y_l and y_t, or damage length and maximum penetration (the damage is assumed to extend vertically along the entire depth of the ship). Assume that y_l^i and y_t^i are realizations of random variables Y_l and Y_t. Given a set of predictor variables $\mathbf{x}$, the goal is to give an estimate of Y_l and Y_t:

$$Y_l = h_l(\mathbf{x}) + R_l \tag{3.20}$$
$$Y_t = h_t(\mathbf{x}) + R_t, \tag{3.21}$$

where the functions h_l and h_t give a conditional expected value for Y_l and Y_t and R_l and R_t are random variables that give the variation in Y_l and Y_t that cannot be "explained" by $\mathbf{x}$. In linear regression, h_l and h_t are estimated by a set of coefficients $\beta = (\beta_0, \ldots, \beta_5)$:

$$E(Y_l|\mathbf{x}) = h_l(\mathbf{x}|\beta^l) = \beta_0^l + \beta_1^l x_1 + \ldots + \beta_5^l x_5 \tag{3.22}$$
$$E(Y_t|\mathbf{x}) = h_t(\mathbf{x}|\beta^t) = \beta_0^t + \beta_1^t x_1 + \ldots + \beta_5^t x_5 \tag{3.23}$$

Regression analysis on the datasets $\{(\mathbf{x}_1, y_l^1), \ldots, (\mathbf{x}_n, y_l^n)\}$ and $\{(\mathbf{x}_1, y_t^1), \ldots, (\mathbf{x}_n, y_t^n)\}$ yields the models

$$\hat{h}_l(\mathbf{x}) = h_l(\mathbf{x}|\hat{\beta}^l) \tag{3.24}$$
$$\hat{h}_t(\mathbf{x}) = h_l(\mathbf{x}|\hat{\beta}^t) \tag{3.25}$$

where $\hat{\beta}^l$ and $\hat{\beta}^t$ are found by minimizing the sum of squared residuals over β^l and β^t:

$$\min_{\beta^l} \sum_{i=1}^{n} (y_i^l - h_l(\mathbf{x}_i|\beta^l))^2$$
$$\min_{\beta^t} \sum_{i=1}^{n} (y_i^t - h_t(\mathbf{x}_i|\beta^t))^2$$

(See Appendix A for a concise discussion about linear regression.)

Linear regression for Y_l and Y_t might not be adequate, because this would assume the fitting of a flat slope through the data whereas the data shows a more curved behaviour. For example, take the SH150 case. From Figure 3.8, it can be seen that there is a strong nonlinear relationship between y_t and x_1 (the CDF of perpendicular kinetic energy): instead of a straight line, a nonlinear curve would describe this relation more accurately. Therefore linear regression is expanded to polynomial linear regression to accomodate for curve fitting: besides $x_1, \ldots, x_5$, their powers

(up to a certain order) are introduced as predictor variables, giving an extended set of variables

$$\mathbf{x} = \begin{array}{c} (x_1,\ldots,x_5, \\ x_1^2,\ldots,x_5^2, \\ \vdots \\ x_1^p,\ldots,x_5^p) \end{array} \tag{3.26}$$

Where p is the polynomial order. Note that polynomial linear regression is the same as linear regression: the solution is linear in the coefficients β^l and β^t of h_l and h_t, respectively. Polynomials were chosen because of their flexibility as a nonlinear function and because they are easy to integrate into linear regression.

What has to be noted is that the variation in y_t is small for low values of x_1 and large for high values of x_1, which is an undesirable effect. However, when transforming y_t by taking the natural logarithm, residual variation is much more constant: see Figure 3.9. Other transformations, such as taking the root, are possible as well. The natural logarithm is chosen typically to remove heteroscedasticity in residual performance which it achieved in this case; moreover, it gives reasonable regression fits.

Because $\ln(0)$ does not exist, all zero values of y_l and y_t are removed from the dataset. From now on in this section, the datasets $(\mathbf{x}_j, y_l^j)$ and $(\mathbf{x}_j, y_t^j)$ are used, with

$$j \in J \subset \{1,\ldots,n\}$$

such that $y_l^j > 0$ and $y_t^j > 0$ for all $j \in J$.

In Minitab, the linear regression for $\ln y_l$ and $\ln y_t$ is performed in three steps:

- First, a stepwise regression algorithm sequentially adds and deletes variables until a suitable set of predictor variables is obtained. The algorithm inserts variables based on a statistical significance test that requires an assumption of normality of the residuals. This technique is commonly applied even though the algorithm does not test for normality of residuals.

- After a set of candidate variables have been determined by the stepwise regression a best subset regression is performed on this set of variables. A best subset regression algorithm determines which superfluous variables can be removed from the previously obtained set without compromizing its quality, resulting in a best subset of variables. The removal of variables from subsets is heuristically determined by looking at each subset's Mallows' Cp-value, which indicates possible overfitting of a regression model. Mallow's Cp allows the residual distribution to be nonnormal for this method to work. (Alternatively, it would be possible to remove variables based on significance testing, but this

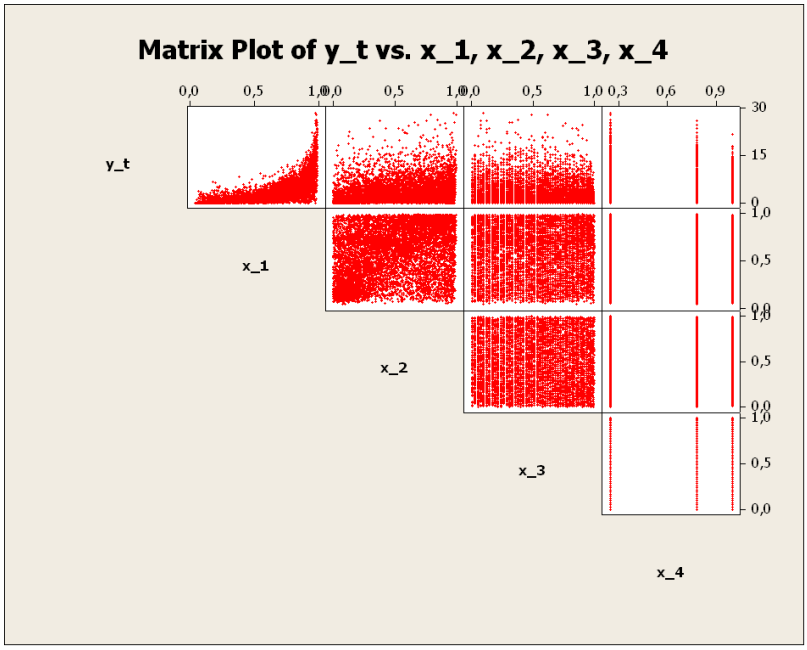

Figure 3.8: Matrix plot of y_t against $\mathbf{x}$, SH150 case

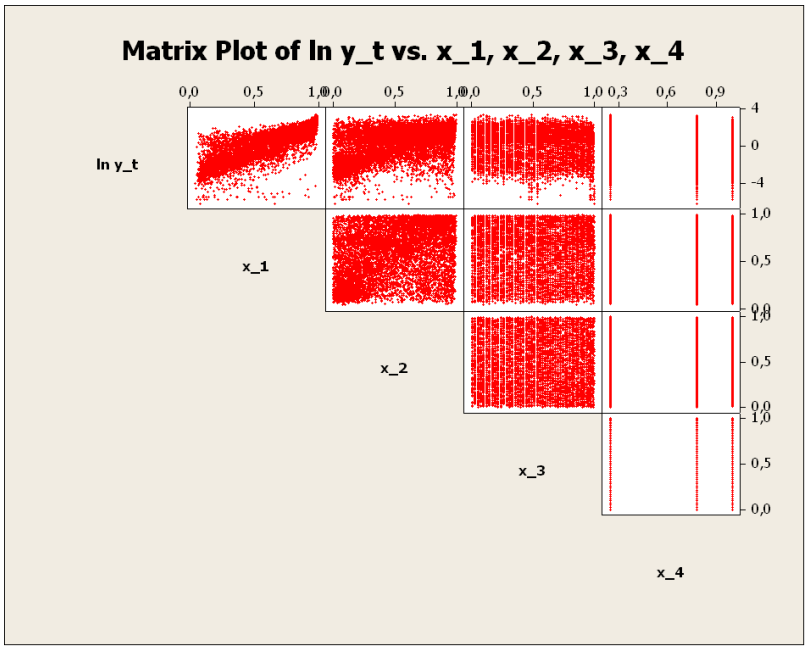

Figure 3.9: Matrix plot of $\ln y_t$ against $\mathbf{x}$, SH150 case

assumes normality of residuals.) A widely accepted approach is that subsets with N variables are suitable for regression when $N < Cp < 2N$, of which the subset with lowest number of variables is chosen [2].

- Third, linear regression analysis is done using this reduced best subset of variables, resulting in coefficients $\hat{\beta}$. Now, the multiple polynomial functions $\hat{h}_l$ and $\hat{h}_t$ express the expected value of $\ln Y_l$ and $\ln Y_t$ conditioned on the set of input variables $\mathbf{x}$:

$$\begin{aligned} h_l(\mathbf{x}|\hat{\beta}^l) &= \hat{\beta}^l_0 + \hat{\beta}^l_{1,1}x_1 + \ldots + \hat{\beta}^l_{1,5}x_5 + \\ &\quad \hat{\beta}^l_{2,1}x_1^2 + \ldots + \hat{\beta}^l_{2,5}x_5^2 + \\ &\quad \ldots + \\ &\quad \hat{\beta}^l_{p,1}x_1^p + \ldots + \hat{\beta}^l_{p,5}x_5^p \end{aligned} \tag{3.27}$$

In this study, $p = 5$ was chosen. The set of coefficients $\hat{\beta}^l$ and $\hat{\beta}^t$ for h_l and h_t, resulting from the regression analysis, can be found in Tables D.1 and D.3.

Correlation between Predictor Variables

When variables are correlated, some problems might appear that affect the overall robustness of a regression analysis. But even with very strong correlation (or multicollinearity) between predictor variables, the predictive value of the regression model may still be good as long as predictions are based on combinations of these variables [13]. The correlation matrix between $x_1, \ldots, x_4$ is as follows in the SH150-case:

	x_1	x_2	x_3
x_2	0.30		
x_3	0.01	−0.01	
x_4	0.02	−0.03	−0.02

There is only some positive correlation between x_1 and x_2 (as could be expected, since they are the CDFs of perpendicular and kinetic energy, which share some common variables such as speed and mass). Therefore, one should be cautious when using the coefficient estimates to explain the individual effects that their corresponding variables have on damage extent.

Since powers of the predictor variables have been used as variables in the polynomial linear regression, there is inevitable correlation between higher and lower powers. This is only problematic for x_5, which only takes 2 values: the CDF values of ship length (or width) distribution. x_5^2 is exactly collinear with x_5 and leads to a division by zero somewhere in the regression analysis. Minitab resolves these issues by means of notification during the regression process.

3.4.1 Fitting Residual Distribution

Now that the conditional expected value of $\ln Y_l$ and $\ln Y_t$ is known, the set of residuals can be used to model the randomness of the data. The residuals r_l and r_t are defined as

$$r_l^j = h_l(\mathbf{x}_j) - \ln y_l^j, \quad \forall j \in J \tag{3.28}$$

$$r_t^j = h_l(\mathbf{x}_j) - \ln y_t^j, \quad \forall j \in J \tag{3.29}$$

These sets can be seen as realizations of random variables R_l and R_t, respectively. These variables are typically assumed to have a Normal distribution with mean 0; this, however, is not a requirement of least squares estimation; in this case even, a Normal distribution would not fit as can be seen from the resisual plots and histograms in Figures 3.10 and 3.11. To this end, an alternative parametric distribution is introduced: the Generalized Trapezoidal distribution (see Appendix B.4). This distribution is fitted to the empirical CDFs of R_l and R_t by means of least squares. Because the distribution function is nonlinear in its coefficients, the least squares fit is approximated numerically. These coefficients are displayed in Table D.2 and D.4 in the Appendix.

The upper bound for the support of these distributions were found by determining the highest possible value of $\ln y_l$ and $\ln y_t$, which are restricted by respectively the length and width of the tanker types involved. Since $\ln y_l$ and $\ln y_t$ have no lower bound, the lower bounds for the GT distribution were determined by taking the difference between the highest and lowest residual value found and substracting this from the lowest residual value.

The quality of the fit can be measured by looking at the plot of the empirical CDF against the fitted CDF (see Figure 3.12). When this plot is close enough to the centerline (going from $(0, 0)$ to $(1, 1)$ in the graph) then the fit is a good representation of the actual CDF of the random variable.

As can be observed, this is a very close fit; all other plots are similarly close to the centerline.

3.5 Probability of Rupture

The next step is to relate this damage extent to the outflow volume, or rather the occurrence of outflow. It is assumed that zero outflow ($z = 0$) implies no rupture. Since occurrance of rupture this is a binary event (it either happens or it doesn't) the model should yield a measure of how likely rupture occurs, i.e. a probability of rupture. Binary regression analysis on the dataset $(y_l^i, y_t^i, z_i), i \in 1, \ldots, n$ will yield an expected probability of rupture conditioned on damage extent.

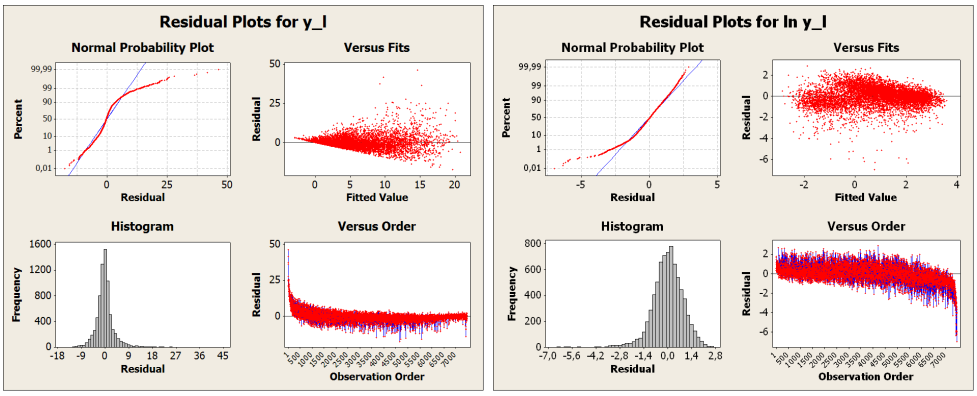

Figure 3.10: Residual plots for y_l resp. $\ln y_l$, SH150 case

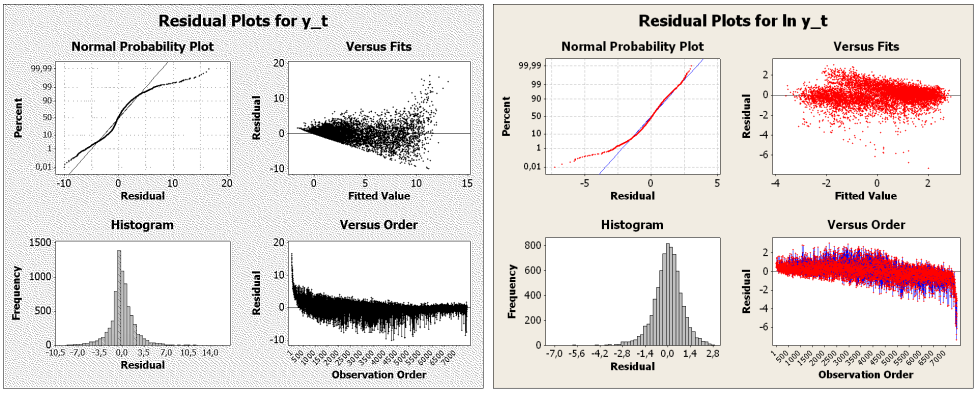

Figure 3.11: Residual plots for y_t resp. $\ln y_t$, SH150 case

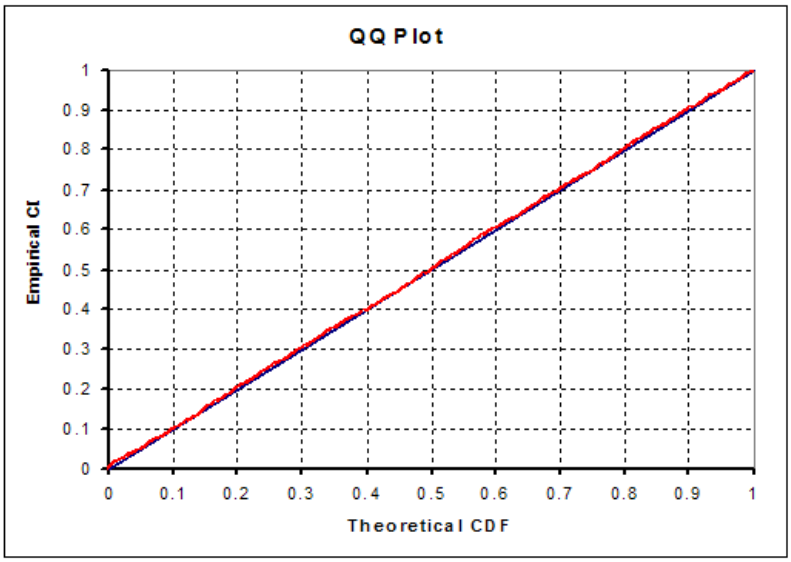

Figure 3.12: QQ-plot for the fit of residuals of $\ln y_t$, SH150 case

3.5.1 Binary Logistic Regression

Suppose the random variable Z expresses the outflow volume in a collision scenario. The following variable is introduced:

$$Z' = 1_{(0,\infty)}(Z) = \begin{cases} 1, & Z > 0 \\ 0, & Z = 0 \end{cases} \tag{3.30}$$

In other words, if outflow occurs, $Z' = 1$, otherwise $Z' = 0$. Again, by assumption, $Z' = 1$ means that rupture occurs. A binary logistic regression analysis (see Appendix Chapter A) can now be done on this variable against variables y_l and y_t. This analysis leads to coefficients that will be used in calculating the probability of rupture (which is the expected value of rupture occurrence $E(Z')$) in the outflow model.

However, since that calculation step comes after calculating damage extent (step 1), and since in the outflow model step 1 yields $\ln y_l$ and $\ln y_t$, the binary logistic regression will be done using the natural logarithms of damage length and maximum penetration.

Note that the logarithms of observed datapoints are used, not expected values calculated in Step 1 of the collision model. This results in a more accurate analysis in the sense that an estimation error in the first step (polynomial linear regression) does not propagate into the binary logistic regression.

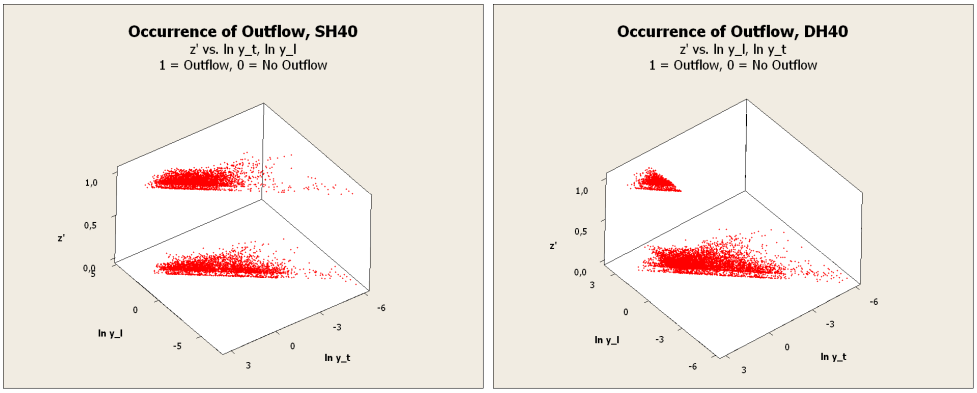

Figure 3.13: Scatterplot of z' against $\ln y_l$ and $\ln y_t$, SH40 case (left) and DH40 case (right)

The regression model is expressed as follows:

$$\begin{aligned} E[Z'|\ln y_l, \ln y_t] &= \pi(\ln y_l, \ln y_t|\beta) \\ &= \frac{\exp(\beta_0 + \beta_l \ln y_l + \beta_t \ln y_t)}{1 + \exp(\beta_0 + \beta_l \ln y_l + \beta_t \ln y_t)} \end{aligned} \tag{3.31}$$

It would have been possible to do binary logistic regression of Z' against predictor variables $x_1, \ldots, x_5$, i.e. the transformed variables used in determining $\ln y_l$ and $\ln y_t$ in the previous section. However, this would mean reusing the same data again and discard the information present in y_l^i and y_t^i.

In Figure 3.13, occurrence of outflow (z') is plotted against $\ln y_l$ and $\ln y_t$ for SH40 and DH40 tanker types, respectively. Note that in the single hull case, outflow occurs when damage extent is less severe than in the double hull case. From these figures it can be observed that $\ln y_l$ and $\ln y_t$ are interdependent. This means that any significance test on either one of these variables will be highly influenced by this interdependency, and thus no results from these tests may be used to discard either $\ln y_l$ or $\ln y_t$ from the binary logistic regression model.

The logistic function was chosen because it supports the behavior present in the data. Its range is between 0 and 1, which is essential because it represents a probability, and is monotonic (changing a predictor variable in a certain direction will either increase or decrease the logistic function), This fits the data as the number of outflow occurrences does not decrease when $\ln y_l$ or $\ln y_t$ go up.

3.5.2 Validity of Binary Logistic Model

QQ-plot

Is the binary logistic regression analysis worth the effort–does it provide enough information given the outflow data? Or would it be easier and simpler to determine the occurrence of outflow (0 or 1) by chance? In other words, it has to be determined if the resulting binary logistic model is different from a purely random model, i.e. a model where an alternative oil outflow variable Z'_{RND} is Bernouilli distributed with parameter p:

$$P(\{Z'_{RND} = 1\}) = p \tag{3.32}$$

$$P(\{Z'_{RND} = 0\}) = 1 - p, \tag{3.33}$$

where

$$p = \frac{\#\text{ outflow events}}{\#\text{ events}} \tag{3.34}$$

This hypothesis is tested by looking at the residuals of the expected probabilities with the outflow data versus the residuals of the expected probabilities with the randomly generated data. Two sets of residuals are determined from the binary logistic regression above, $\{r_{OUT,i}\}$ and $\{r_{RND,i}\}$:

$$r_{OUT,i} = z'_i - \hat{\pi}(\mathbf{x}_i), \quad i \in \{1, \ldots, n\} \tag{3.35}$$

$$r_{RND,i} = z'_{RND,i} - \hat{\pi}(\mathbf{x}_i), \quad i \in \{1, \ldots, n\} \tag{3.36}$$

Now, consider the empirical cumulative distribution functions of both residuals:

$$F_{OUT}(x) = \frac{1}{n}\sum_{i=1}^{n} 1_{(-\infty,x]}(r_{OUT,i}) \tag{3.37}$$

$$F_{RND}(x) = \frac{1}{n}\sum_{i=1}^{n} 1_{(-\infty,x]}(r_{RND,i}) \tag{3.38}$$

Both CDFs are set out against each other in a so-called QQ-plot (see Figure 3.14). If the plot does not diverge significantly from the centerline, one may conclude that the regression model concurs with both the available outflow data as with a randomly generated set of outflows. In other words, the BLR model then gives little information on whether the predictor variables, such as perpendicular kinetic energy, are significant in determining oil outflow. It would then be perfectly valid to determine the occurrence of outflow by chance. As can be seen from the figure, this is not the case.

It is quite possible that this methodology could be developed into a formal statistical hypothesis test, i.e. how close would the QQ-plot have to be to the centerline where one would say that the model doesn't distinguish between "real" data and randomly generated data?

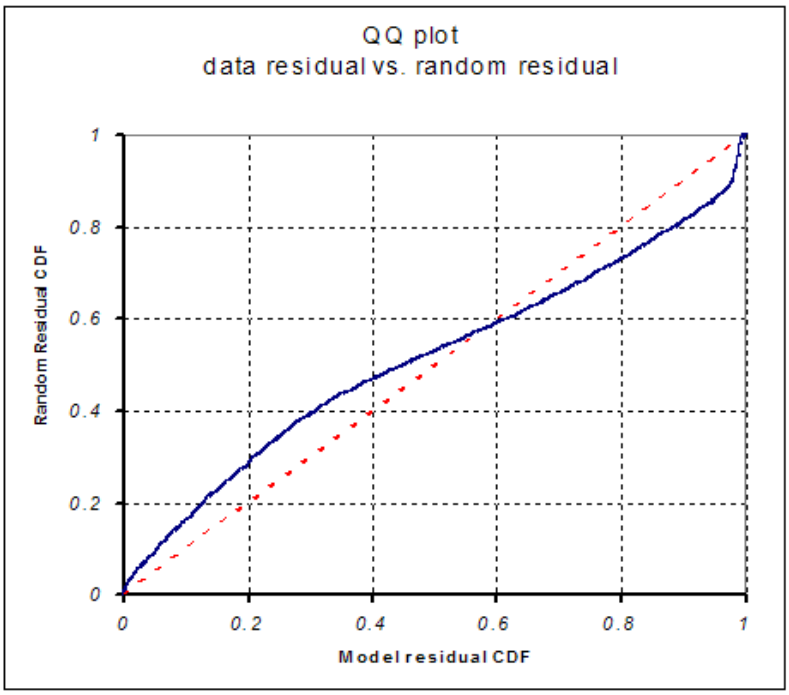

Figure 3.14: QQ-plot of probability residuals, SH150 case, collisions

Point-Biserial Correlation Coefficient

For now, the formal statistical model used to determine if the model should be rejected is the point biserial correlation coefficient r_{pb} using "real" occurence of outflow data and randomly generated data. r_{pb} determines correlation between a continuously measured variable (expectation of outflow Z', as calculated in the binary logistic regression) and a dichotomous variable (the actual occurence of outflow values z'):

$$r_{pb} = \frac{M_1 - M_0}{s_n}\sqrt{\frac{n_1 n_0}{n^2}}, \tag{3.39}$$

where

$$s_n = \sqrt{\frac{1}{n}\sum_{i=1}^{n}(z'_i - \bar{z}')^2}, \tag{3.40}$$

is the standard deviation of z', n_1 and n_0 are the number of occurrences of 1 and 0 in z', respectively, and M_1, M_0 are the mean values of Z' conditioned on the value of z' (either 1 or 0, respectively).

The statistic for assessing the significance of r_{pb} is

$$t = r_{pb}\sqrt{\frac{n_1 + n_0 - 2}{1 - r_{pb}^2}}.$$

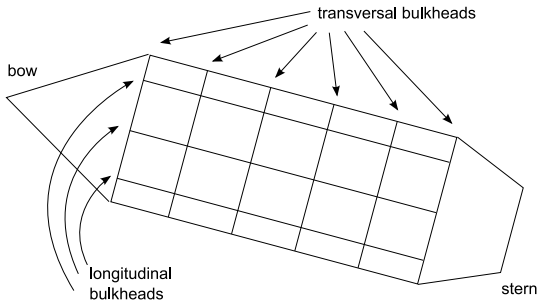

Figure 3.15: Bulkhead placement

If $P(T > t) < \alpha$, where T follows an unpaired Student's t-distribution with n_1+n_0-2 degrees of freedom, then the null hypothesis is rejected, i.e. the binary logistic model should be accepted.

The same thing can be done with random data: z' is then replaced by z'_{RND} which is generated in the same way as with the QQ-plot methodology.

The p-values for these tests (random an non-random) can be found in Table D.6.

3.6 Outflow Volume

Based on damage length, maximum penetration and collision location, the last section of the model involves calculating the oil outflow volume given that penetration has occurred and damage length and maximum penetration have been calculated.

3.6.1 Determining Damaged Area

As opposed to the original simulation, the model makes the assumption that the damaged area is a rectangular volume. Its longitudinal and transversal dimensions determined respectively by damage length (y_l) and maximum penetration (y_t). It is also assumed that damage occurs over the entire vertical extent of the ship, so this has no influence in the outflow volume. Furthermore, each compartment that coincides with the damaged area is assumed to lose all its oil. This differs from the original simulations, where the damaged area is not necessarily rectangular (see Figure 2.4).

For all four struck ship models, compartment configurations are available in the form of transverse and longitudinal bulkhead coordinates and compartment volumes. A schematic of one of these configurations is given below in Figure 3.15. Table C.9 in the Appendix gives the bulkhead coordinates.

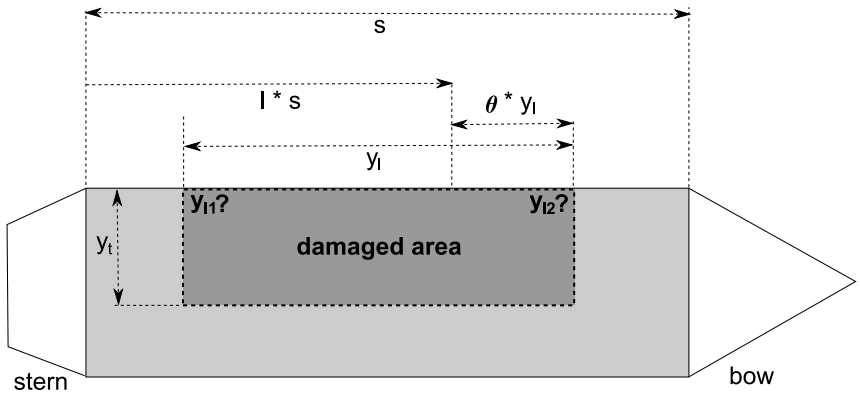

Figure 3.16: Collision location (l) and damage length (y_l) are known, start and end position (y_{l1}, y_{l2}) are unknown.

Determining Longitudinal Bounds

In each accident scenario, the longitudinal position of the damaged area is determined by the relative collision location l. However, neither a starting coordinate nor ending coordinate are present in the output data. Therefore these coordinates y_{l1}, y_{l2} have to be calculated by using ship length s, damage length y_l and a weight θ (see also Figure 3.16):

$$y_{l1} = (1-\theta)y_l + (1-l)s, \tag{3.41}$$

$$y_{l2} = -\theta y_l + (1-l)s, \tag{3.42}$$

$$\theta \in [0,1]$$

y_{l1} and y_{l2} are measured from the forward perpendicular because all bulkhead locations are given from this point as well. If $\theta = 0$, then all longitudinal damage is behind the collision location as measured from the forward point. If $\theta = \frac{1}{2}$, then the collision location is in the middle of the longitudinal damage. If $\theta = 0$, then all longitudinal damage is in front of the collision location.

By taking original datapoints (l_i, y_l^i, y_t^i), and calculating y_{l1} and y_{l2} for each i using a particular θ, one can also calculate which compartments have been breached and hence the total oil outflow $\tilde{z}_i$. If this outflow differs from the outflow value in the original data (z_i), then the model is incorrect. Since the assumption holds that no outflow implies no rupture, only cases where positive outflow occurs are taken into account.

Counting the fraction q of correct cases for all datapoints is a metric for assessing the quality of θ. Additionally, the average absolute error of outflow $\frac{1}{n}\sum|\tilde{z}_i - z_i|$ and conditional average absolute error of outflow can be assessed to this end.

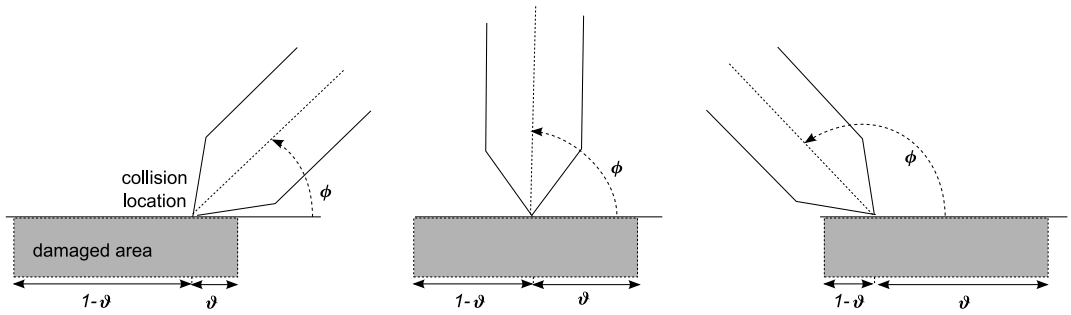

Figure 3.17: Determining position of damage location

The former measures the average error over all assessed cases, even if $|\tilde{z}_i - z_i| = 0$. The latter conditions on cases where $|\tilde{z}_i - z_i| > 0$. The goal is to find a suitable model for θ, and then optimize that model by maximizing q.

One can imagine a simple model:

$$\theta = \frac{1}{2} \tag{3.43}$$

i.e. in any situation, collision location will lengthwise always be in the middle of the longitudinal damage. However, when the collision angle is very oblique, the striking ship will probably cause the most longitudinal damage on one side of the collision location. Therefore the following model for is introduced as a function of collision angle ϕ (in degrees):

$$\theta = \frac{\phi}{180} \tag{3.44}$$

In short, if ϕ is near 0 degrees, longitudinal damage extends backwards of the collision location; if $\phi = 90$, the collision location is in the middle of longitudinal damage; if ϕ is near 180, then longitudinal damage extends forward of the collision location. In Figure 3.17 some examples are shown to clarify this model.

The proposed function is linear in ϕ, but an S-shape could be more appropriate as one would think that collision location stays close to one end of the longitudinal damage when $\phi < 90$ and close to the other end when $\phi \geq 90$. Therefore one might introduce an extra parameter n that describes this nonlinear behaviour:

$$\theta(\phi; n) = \begin{cases} 0, & \phi = 0 \\ \frac{1}{2}(\frac{\phi}{90})^n, & 0 < \phi < 90 \\ 1 - \frac{1}{2}(\frac{180-\phi}{90})^n, & 90 \leq \phi < 180 \\ 1, & \phi = 180 \end{cases} \tag{3.45}$$

Note that this model includes the previous models. If $n = 0$, then $\theta = \frac{1}{2}$. If $n = 1$, then $\theta = \frac{\phi}{180}$. For $n < 0$, θ will have a very unusual if not unrealistic profile, so this

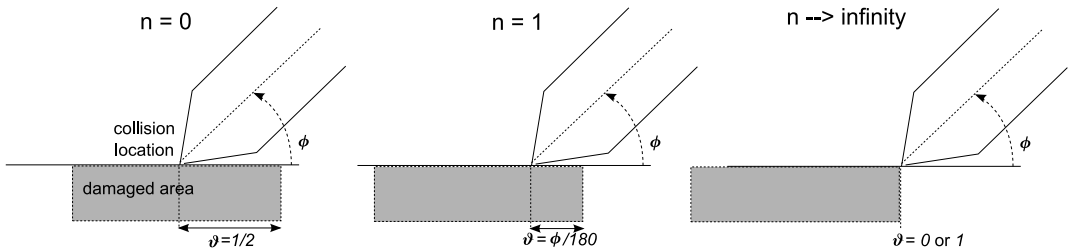

Figure 3.18: Determining position of damage location with added parameter

possibility is discarded. If $n \to \infty$, then

$$\lim_{n\to\infty} \theta(\phi; n) = \begin{cases} 0, & 0 \leq \phi < 90 \\ 1, & 90 \leq \phi \leq 180 \end{cases} \tag{3.46}$$

Some profiles of θ for different values of n are shown in Figure 3.18.

Finally, one could argue that relative tangential velocity v_t plays a role in determining where longitudinal damage occurs relative to the collision location. If $v_{1,x}$ and $v_{2,x}$ are the x-components of the striking and struck ships' velocities, respectively, then $v_t = v_{1,x} - v_{2,x}$. If the striking ships moves faster than the struck ship in the direction of the struck ship, then $v_t \geq 0$; if the striking ship moves slower in that direction, then $v_t \leq 0$. The direction of v_t should be a factor in the location of longitudinal damage. So, to integrate relative velocity into θ, the following model is proposed:

$$\theta(\phi, v_t; m, n) = \begin{cases} 0, & \phi = 0 \\ (\frac{1}{2}(\frac{\phi}{90})^n)^{\exp(mv_t)}, & 0 < \phi < 90 \\ (1 - \frac{1}{2}(\frac{180-\phi}{90})^n)^{\exp(mv_t)}, & 90 \leq \phi < 180 \\ 1, & \phi = 180 \end{cases} \tag{3.47}$$

m determines how much influence v_t has on θ. The use of the exponential allows for positive and negative values of v_t. Note that if $m = 0$ then θ is the same as in Equation 3.45. If $m \neq 0$, then v_t influences θ because this assumes that if the striking ship moves faster than the struck ship, longitudinal damage is oriented forward; otherwise it is oriented backwards. In Figure 3.19, the function $\theta(\phi, v_t; 1, 1)$ is plotted to give an impression of this model.

The idea is now to find optimal values $\hat{m}$ and $\hat{n}$ for each ship design, i.e. values that result in the highest fraction of correct outflow predictions q.

This maximization method is not easily solvable by general methods (the goal function invokes an algorithm to count the number of damaged compartments). Also, q is not continuous. Therefore a "brute force" approach was chosen to find a local maximum $\hat{m}, \hat{n}$ by taking a grid containing evenly spread values for m and n spread

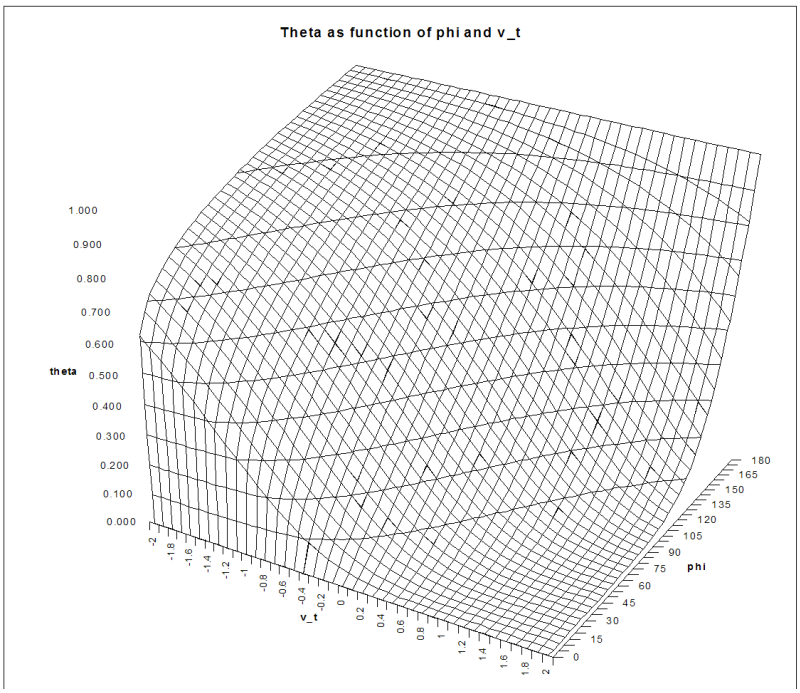

Figure 3.19: θ under different angles and relative tangential velocities

out over heuristically determined intervals and counting the corresponding value of q. After calulating these values, the values of m and n for which q was the highest were used as midpoints of a narrower grid. This was repeated down to 3 significant digits, beyond which it was deemed unlikely that any increase in significant digits would lead to a higher maximum of q. The maximum values of q are given in Table D.7.

3.7 Results

Damage Extent

Tables D.1 and D.3 show that the fits calculated for estimating the expected value of $\ln y_l$ and $\ln y_t$ have R^2-values between 68% and 75%. Interpreting these values as a qualitative metric to explain variation in the response variable, this result means that damage extent can be explained reasonably well by the input variables. The smaller vessels give slightly better R^2-values than the larger ones.

For $\ln y_l$, overall, x_1 and x_2 (representing kinetic energy) seem to account mostly for this explanation when looking at the coefficients (note that these variables are correlated). This fits with the idea that longitudinal damage extent is largely caused by the released amount of energy in the tangential direction. However, x_3 and x_4 also come into play depending on ship type. A few selected graphs are displayed in Figure 3.20 to show the difference between the effects of the variables on single hull and double hull damage (in the combined cases).

For $\ln y_t$, x_1 and x_2 are again dominant in causing transversal damage. x_3 (absolute collision location relative from the center) is also a major factor but only for the SH models. x_4 (bow angle) has little influence overall on the transversal damage extent. Again, this is a reasonably adequate argument for the notion that transversal damage is caused mostly by the energy release in the struck ship's perpendicular direction.

A switch in polarity and increase of magnitude of consecutive coefficients (for example $\beta_{3,1}, \beta_{3,2}, \ldots, \beta_{3,5}$ in Table D.1) can be observed.

Especially for the DHCOM model and, to a lesser extent for SHCOM, the added variable used to differentiate between the small ship dataset and the large ship's one seems not very significant for either $\ln y_l$ or $\ln y_t$.

Probability of Rupture

Table D.5 presents the coefficients that determine the probability of rupture $E(Z')$ given $\ln y_l$ an $\ln y_t$. Striking is the fact that the coefficient for transversal damage (β_t) is far bigger than β_l in the DH models, and the reverse is true for the SH models although to a far lesser extent; its coefficients are smaller (see also Figure 3.21).

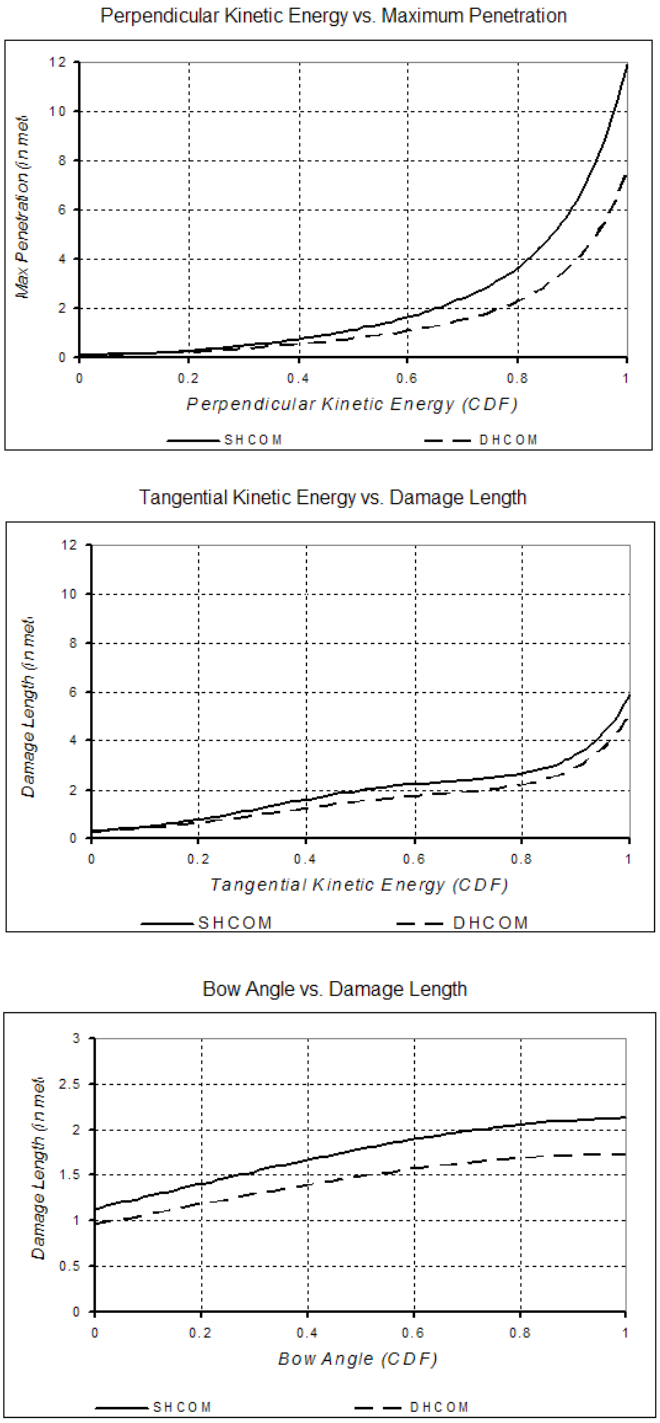

Figure 3.20: Effects of predictor variables on damage extent for a large ship using combined models

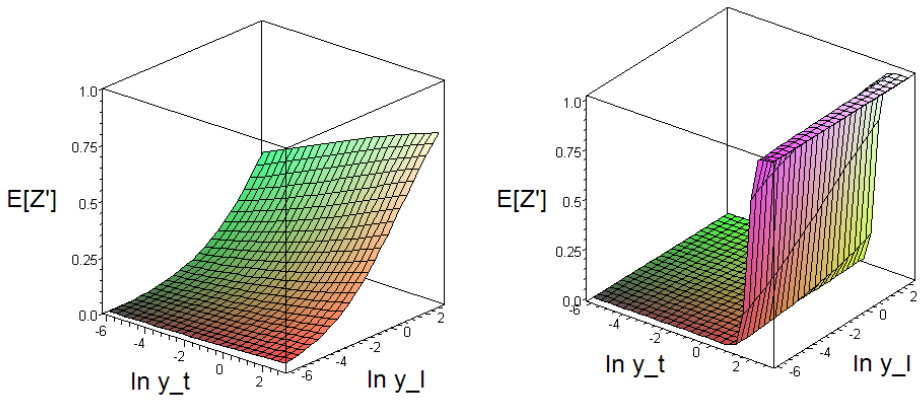

Figure 3.21: Expected probability of rupture as function of $\ln y_l$ and $\ln y_t$, SH150 vs. DH150

Also, in the latter, the intercept (β_0) is closer to 0.

These observations make clear that, in this model, probability of rupture in double hull ships is mainly due to transversal damage and that this probability does not start to become siginificantly large until a certain level of longitudinal damage is sustained; beyond this threshold, however, rupture becomes a near certainty. For single hull ships, probability of rupture increases more gradually and becomes quite large for modest damage extents.

The goodness-of-fit test values given in the table are mostly 0, meaning that —strictly speaking— their corresponding fits should be rejected based on the tests. As mentioned before, because of the large sample size, it is highly unlikely that any test would accept these fits. The QQ-plot (see Figure 3.14 of the data residual vs. random residual fits of the regression model show that the regression analysis matters in determining probability of rupture. The point biserial correlation coefficient, comparing the model with the data, gives significantly high values in all cases (between 0.5 and 0.8), thereby rejecting the null hypothesis. Moreover, testing with random data leads to a failed rejection of the null hypothesis.

Outflow Volume given Damage Extent and Rupture

By optimizing coefficients of a function that gives longitudinal damage location in relation to collision angle and relative tangential velocity, correct outflow volumes can be calculated with 95%—98% accuracy (see Table D.7). On average, this gives an outflow error between 88 and 417 m^3.

The calculation method of start- and endpoints for longitudinal damage might be improved upon by finding a more principled optimization algorithm. Also, for very low and very high values of ϕ the model might not be accurate.

Chapter 4

Grounding Model

Since the grounding model follows the same principles as the collision model, it is divided into three consecutive stages as well: based on the grounding input and output variables presented in Chapter 2, the model is supposed to

1. calculate the damage extent to the struck ship given the scenario input variables;
2. calculate the probability of rupture given damage extent;
3. calculate the oil spill volume given rupture.

This model is represented schematically in Figure 4.1.

The damaged area determines which compartments are ruptured. When the damage area overlaps a compartment it is assumed again that all its cargo is lost. Note that this methodology differs from the grounding simulation methodology [21] which this model is based on, because the latter invokes hydrostatic balance equations to determine final outflow volume. Another difference with the collision model is that no detailed analysis can be performed in determining damage locations, since the grounding simulation study does not provide bulkhead locations describing compartment locations.

In total, six different grounding models will be developed: four models based on individual tanker types and two combined models that are each based on simulation data from two tanker types.

4.1 Defining Predictor Variables

Kinetic Energy

Again, the grounding input variables can be transformed into predictor variables. Just as with collisions, kinetic energy is a desired variable to include in the grounding

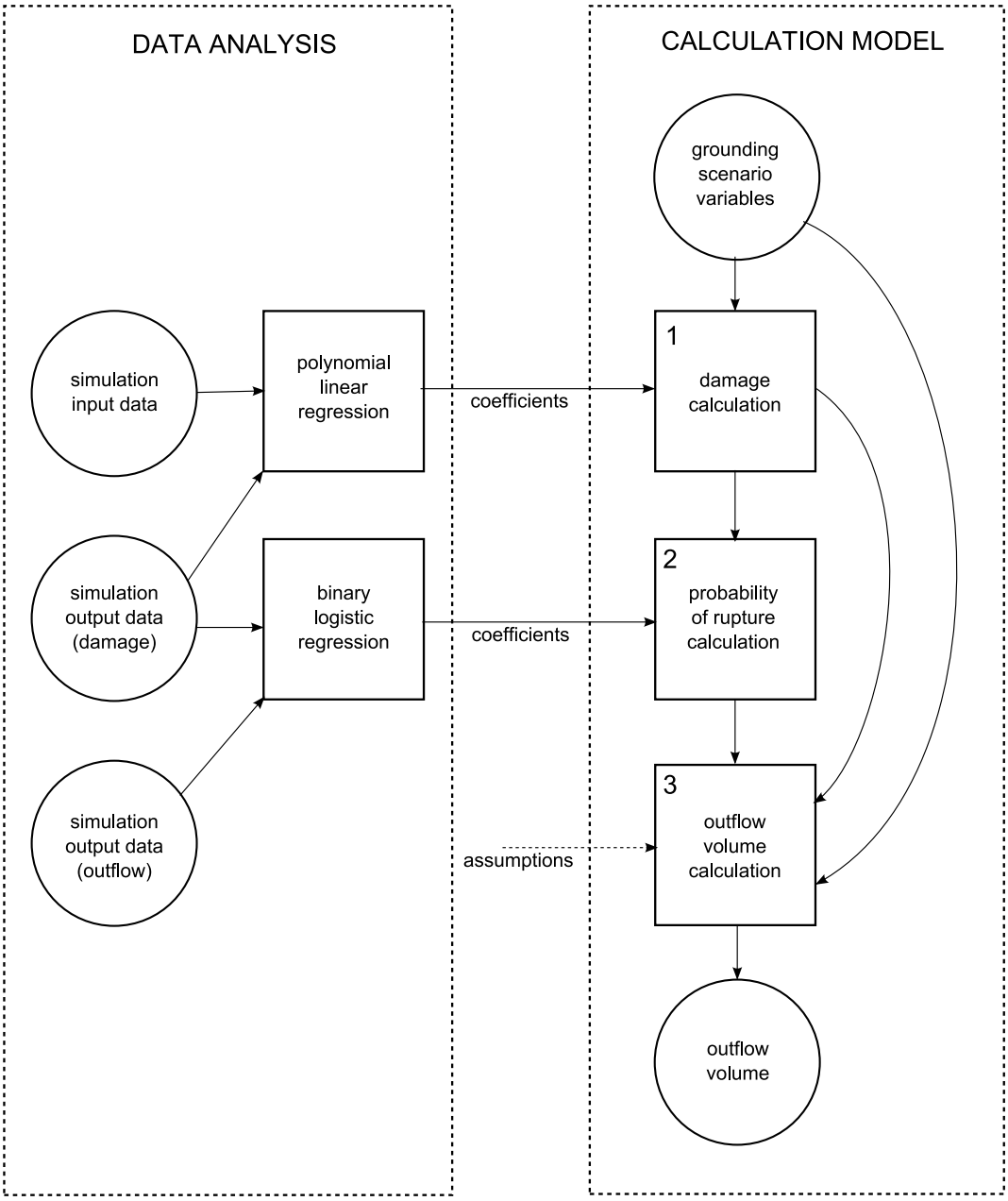

Figure 4.1: Grounding model schematic

model. Since groundings are head-on, and includes only one moving object, kinetic energy is defined as

$$e_k = \frac{1}{2}mv^2 \tag{4.1}$$

where m is the ship's mass and v its speed.

Obstruction Variables

Obstruction apex (o_a), obstruction depth (o_d), obstruction tip radius (o_r) and rock eccentricity (c) are straightforward variables and could have a strong influence on damage size. o_a, o_d and o_r describe the obstruction geometry and thus have a direct relationship with damage, whereas c describes how well a tanker can convert the tanker's longitudinal motion into other degrees of freedom. If $c = 0$, the rock tip is located at the centerline of the ship, making it difficult for the forward motion to change into a yawing or rolling motion. However, if $c = 1$ the rock tip is at either port or bow and leaves some leverage for the tanker to turn, thereby reducing forward speed and thus kinetic energy.

Other Variables

Since it is assumed that a breached compartment loses all its cargo, variables such as minimum outflow percentage ν and ballast tank capture b have no influence on the total amount of outflow. Furthermore, inert tank pressure p is unlikely to influence outflow since its maximum value (1000 mm water gauge) corresponds to approximately 0.1 atmosphere. This pressure refers to the inert gas that is added to the air in cargo compartments to prevent accidental combustion. Overpressure in the compartments might increase grounding damage and thus influence the probability of outflow or the size of the damage area, but since the tanks are assumed 98% full, the case can be made that the volume of air is too small to be of any influence; p should not make any difference to this argument. Finally, tidal variance τ is used in hydrostatic balance equations which is ignored in this study's grounding models. Hence, ν, b, p and τ will not be used as predictor variables in the model.

4.1.1 Transformation of Predictor Variables

As with the collision model, the predictor variables are transformed over their cumulative distribution functions. In some cases, these CDFs are known exactly: in other cases, a parametric distribution has to be fitted.

Kinetic Energy

Because the struck ship's mass m is a constant (four different masses are used for the four different ship types), kinetic energy is proportional to velocity squared:

$e_k = \frac{1}{2}mv^2$. The probability distribution of v is known from Table 2.9. From this, the probability distribution of the kinetic energy random variable E_k kan be derived:

$$
\begin{aligned}
P(E_k \leq x) &= P(\frac{1}{2}mV^2 \leq x) \\
&= P(V \leq \sqrt{\frac{2x}{m}}) \\
&= \begin{cases}
0, & \sqrt{\frac{2x}{m}} \leq 0 \\
\frac{1}{20}\sqrt{\frac{2x}{m}}, & 0 < \sqrt{\frac{2x}{m}} \leq 5 \\
\frac{1}{4} + \frac{3}{20}\ (\sqrt{\frac{2x}{m}} - 5), & 5 < \sqrt{\frac{2x}{m}} \leq 8 \\
\frac{7}{10} + \frac{2}{175}\ (\sqrt{\frac{2x}{m}} - 8), & 8 < \sqrt{\frac{2x}{m}} \leq 15 \\
\frac{39}{50} + \frac{1}{5}(\sqrt{\frac{2x}{m}} - 15), & 15 < \sqrt{\frac{2x}{m}} \leq 16 \\
\frac{49}{50} + \frac{1}{200}(\sqrt{\frac{2x}{m}} - 16), & 16 < \sqrt{\frac{2x}{m}} \leq 20 \\
1, & \sqrt{\frac{2x}{m}} > 20
\end{cases}
\end{aligned}
\tag{4.2}
$$

This distribution is used only for the SH40, SH150, DH40 and DH150 models. For the combined models (SHCOM and DHCOM), combining the kinetic energy dataset gives a different probability distribution:

$$
P(E_k \leq x) = \frac{1}{2}[P(E_{k_1} \leq x) + P(E_{k_2} \leq x)] \tag{4.3}
$$

Where E_{k_1} represents the kinetic energy of the smaller ship (SH40 or DH40) and E_{k_2} the one belonging to the larger ship (SH150 or DH150), both following a distribution as in Equation 4.2. The probabilities are weighted equally because the datasets are equally large.

Obstruction apex

A parametric distribution is fitted to the realizations of O_a because it is a truncated Normal distribution with unknown mean and variance. A generalized power distribution (see Appendix B.3) was chosen because it has a closed-form mathematical expression and is very flexible for a distribution that has bounded support. The coefficients of the fit are described in Table 4.1.

The fit is chosen by means of the least squares sum method, with n the same on each side to ensure the fitted probability distribution function is continuous. a and b were fixed, leaving α, m and n the coefficients to be determined. See Figure 4.2 for a QQ-plot that compares the fit with the cumulative CDF of O_a.

The parameters for the GP distribution of O_a are listed in Table 4.1.

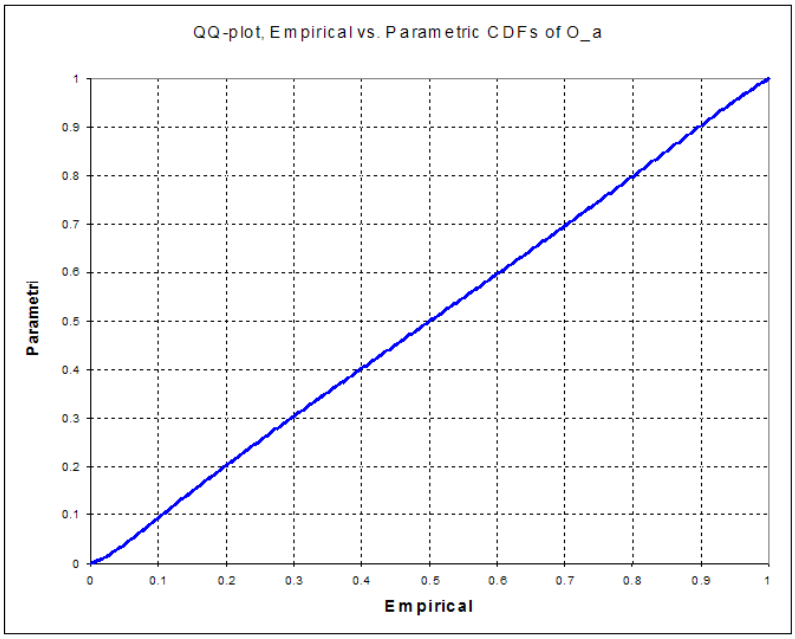

Figure 4.2: QQ-plot, Empirical vs. Parametric CDF, O_a

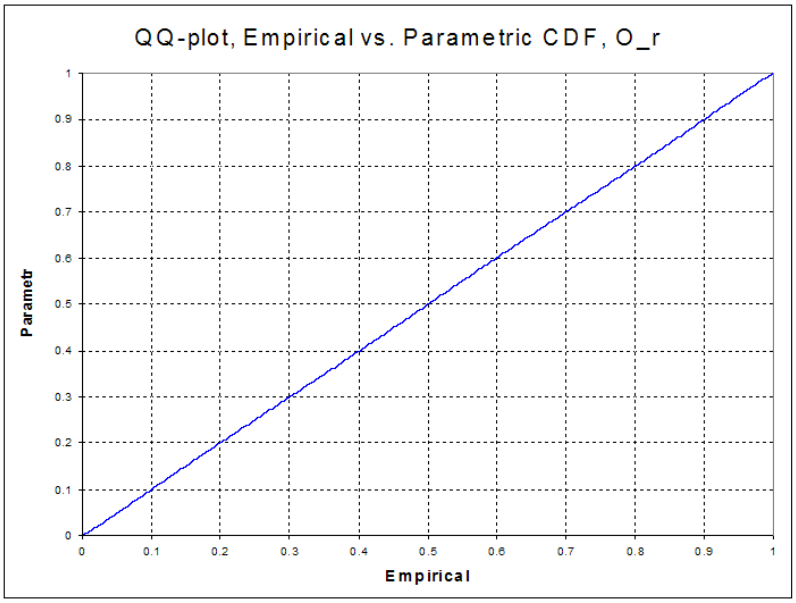

Figure 4.3: QQ-plot, Empirical vs. Parametric CDF, O_r

Coefficient	Value
a	15
m	19.557
b	50
α	1.186
n	4.018

Table 4.1: Coefficients for GP distribution of O_a

Coefficient	Value
a	0
m	5
b	10
α	1.507
n	2.379

Table 4.2: Coefficients for GP distribution of O_r

Obstruction Tip Radius

For O_r the generalized power distribution was selected for fitting since the original distribution is a truncated Normal as well. Since the probability distribution is symmetric around the mean 5, the fit is optimized by means of the least squares sum method with fixed mean and unknown variance. See Figure 4.3 for a QQ-plot that compares the fit with the cumulative CDF of O_r. The parameters for the GP distribution are listed in Table 4.2.

Obstruction Depth

By analyzing the grounding data, it is clear that obstruction depth O_d has CDF

$$P(O_d \leq x) \quad = \quad F_{O_d}(x) = \frac{1}{400}x^2, \quad x \in [0, 20] \tag{4.4}$$

(see Figure 4.5), which is validated by plotting this CDF against the empirical CDF obtained from the Data (Figure 4.4).

Rock Eccentricity

Rock eccentricity C is distributed uniformly on the interval $[0, 1]$.

So now each set of predictor variables $(e_k^i, o_d^i, o_a^i, o_r^i, c^i, d^i)$ for all $i \in \{1, \ldots, n\}$ can be seen as realizations of the aforementioned random variables E_k, O_d, O_a, O_r, C and D. Their corresponding CDFs are F_{E_k}, F_{O_d}, F_{O_a}, F_{O_r}, F_C and F_D which are given. The realizations are transformed through their corresponding CDF functions,

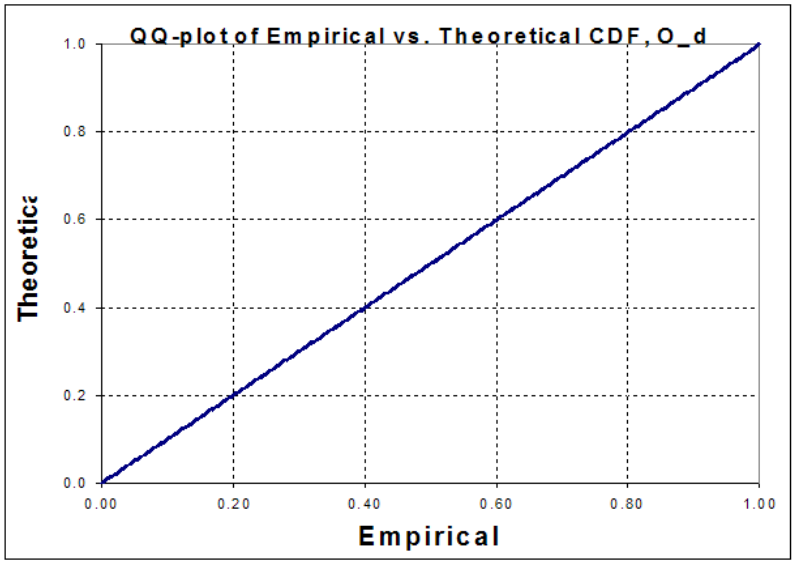

Figure 4.4: QQ-plot, Empirical vs. Theoretical CDF, O_d

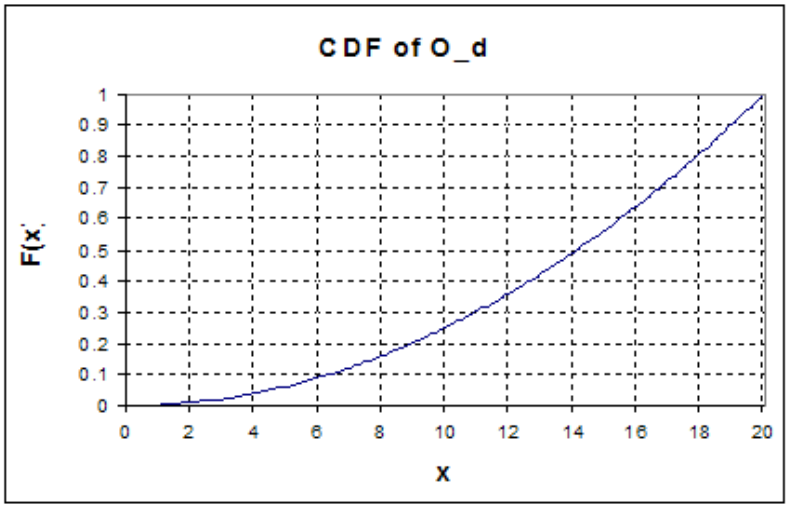

Figure 4.5: Obstruction depth distribution: fit vs. data

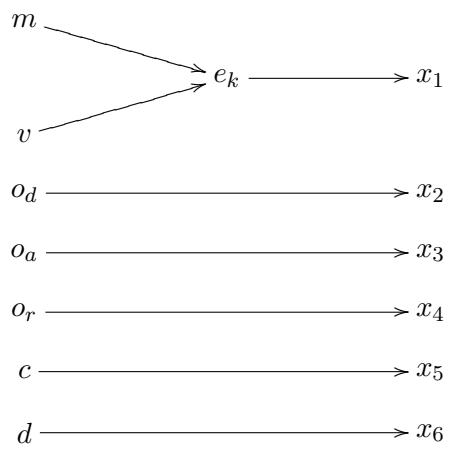

Figure 4.6: Transformation of input variables to predictor variables

resulting in the following transformed predictor variables:

$$\begin{aligned} x_{1,i} &= F_{E_k}(e_k^i) \\ x_{2,i} &= F_{O_d}(o_d^i) \\ x_{3,i} &= F_{O_a}(o_a^i) \\ x_{4,i} &= F_{O_r}(o_r^i) \\ x_{5,i} &= F_C(c^i) \\ x_{6,i} &= F_D(d^i) \\ & \quad \forall i \in \{1 \ldots, n\} \end{aligned} \tag{4.5}$$

An overview of the transformation steps from input variables to predictor variables is given in Figure 4.6.

4.2 Damage Extent

The damage extent given input variables is determined by polynomial linear regression on the available datasets, just the same as in the collision model. Assuming that y_l^i and y_t^i are realizations of random variables Y_l and Y_t, polynomial linear regression determines the expected values of these variables conditioned on input variables $\mathbf{x}_i = (x_{i,1}, \ldots, x_{i,6})$. Again, the logarithm of damage extent variables (y_l and y_t) is taken to ensure the correct application of linear regression. Since obstruction elevation y_v is directly related to obstruction depth o_d, there is no need to do linear regression on this variable.

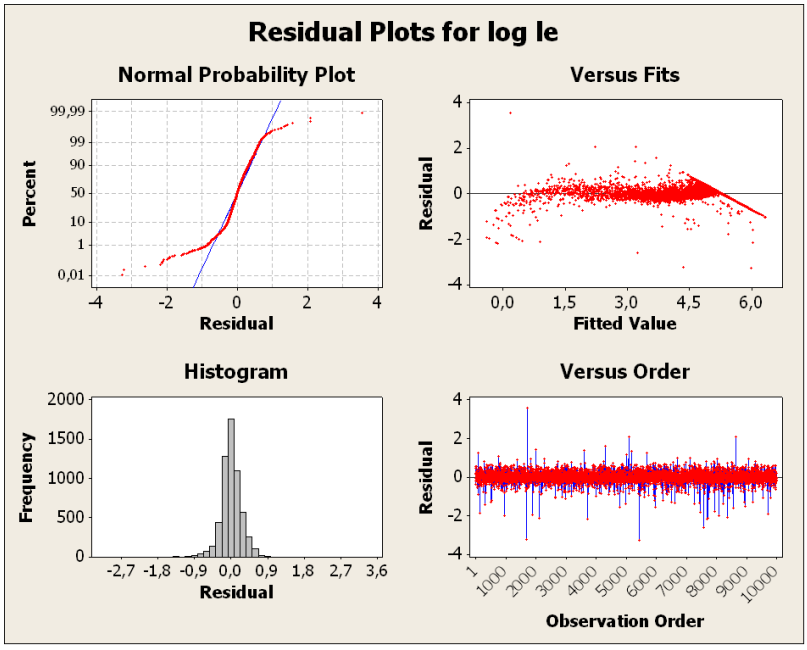

Figure 4.7: Residual plots for $\ln y_l$, SH150 case

$\ln Y_l$ is given as follows:

$$\begin{aligned} \ln Y_l &= h_l(\mathbf{x}|\beta^l) + R_l \\ &= \beta_0^l + \beta_{1,1}^l x_1 + \ldots + \beta_{1,6}^l x_6 \\ &= + \ldots \\ &= +\beta_{p,1}^l x_1^p + \ldots + \beta_{p,6}^l x_6^p \end{aligned} \tag{4.6}$$

($\ln Y_t$ is expressed analogously.) For this linear regression, $p = 5$ was chosen with the same procedure for selecting variables as in the collision model. The coefficients found by minimizing the sum of squares $\hat{\beta}^l$ and $\hat{\beta}^t$ can be found in Appendix E. Figures 4.7 and 4.8 show the residual plots.

4.2.1 Fitting Residual Distribution

This analysis is exactly the same as in the collision chapter. Residuals are treated as realizations of random variables R_l and R_t. The distributions of these variables are approached by the cumulative CDFs determined by the realizations, which in turn are fitted by a generalized trapezoidal distribution using a least squares method. The coefficients of this distribution are found in Tables E.3 and E.4 for $\ln y_l$ and $\ln y_t$, respectively. The QQ-plot of the empirical vs. the GT distributions of the residual R_t is plotted in 4.9.

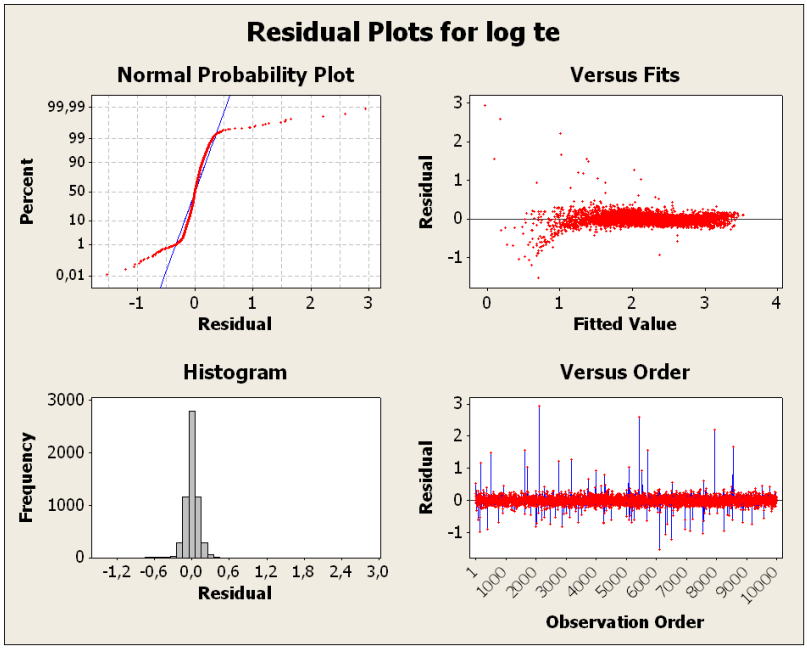

Figure 4.8: Residual plots for $\ln y_t$, SH150 case

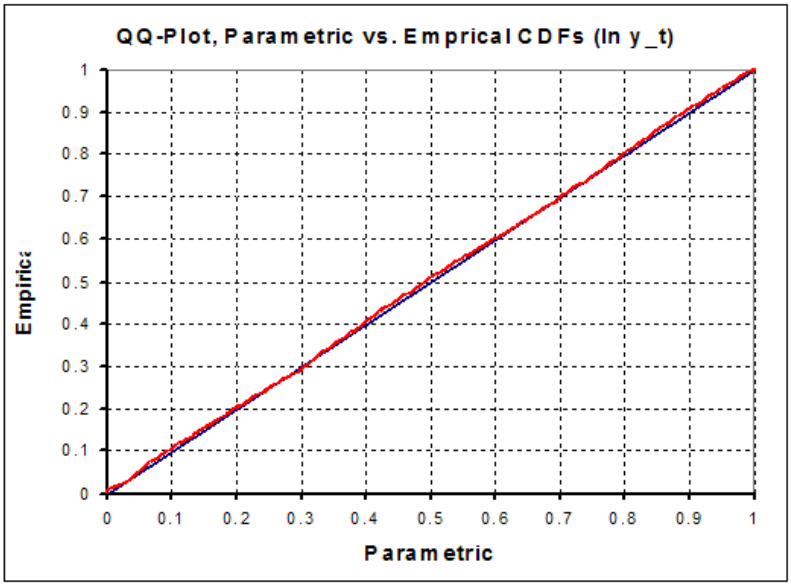

Figure 4.9: QQ-plot of empirical vs. parametric CDFs of r_t, SH150 case

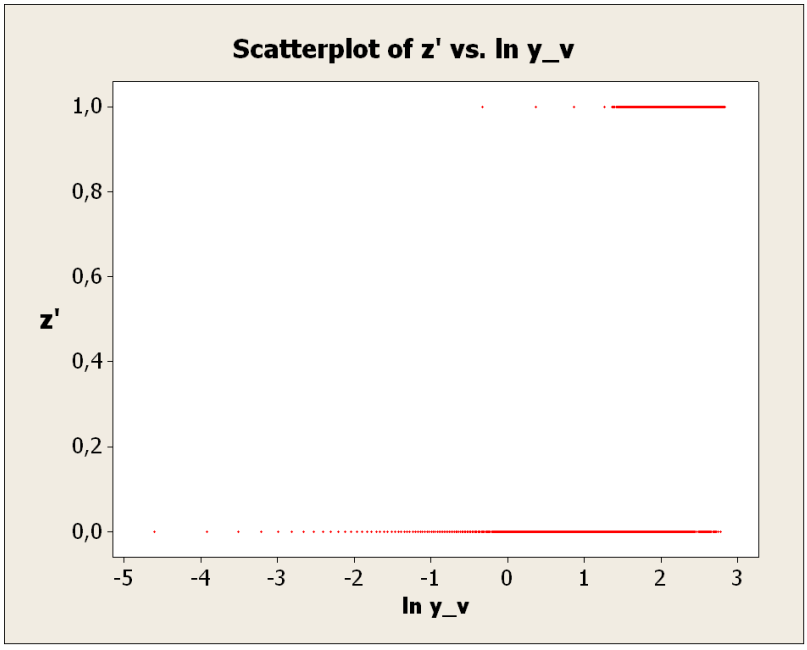

Figure 4.10: z' vs. $\ln y_v$, DH150 case

4.3 Probability of Rupture

The probability of rupture given grounding damage is determined by binary logistic regression of the occurrence of outflow, just the same as in the collision model. Again, the assumption goes that no outflow means no rupture. However, from the three variables that determine grounding damage - y_l, y_t and y_v - only y_v has positive values when $z' = 0$, i.e. when there is no outflow. This means that when transforming these variables by taking the natural logarithm, zero values of y_l, y_t cannot be used and leaves only those cases where outflow occurs. But binary logistic regression requires that all possible values of z' are present in the data, making regression on z' by y_l and y_t impossible. Therefore, binary logistic regression is carried out with only one predictor variable, $\ln y_v$, resulting in the following model:

$$E(Z'|\ln y_v) = \frac{\exp(\beta_0 + \beta_v y_v)}{1 + \exp(\beta_0 + \beta_v y_v)} \tag{4.7}$$

In Figure 4.10 the occurrence of outflow z' is plotted against $\ln y_v$. Results are given in Table E.5.

The significance of this model against a purely random model is measured again by looking at the departure of the residuals of this model with the current dataset against the residuals of this model with a Bernouilli generated dataset (which generates 1's with probability p and 0's with probability $1 - p$, p being the frequency of

outflow occurrence).

For formal significance testing, the point-biserial correlation coefficients are tested in the same way as in collisions, for the real data and randomly generated data. Results of these tests are in Table E.6.

4.4 Outflow Volume

Both start and end locations (y_{l1} and y_{l2}) appear in the original dataset for longitudinal damage extent. However, because $y_{l1} = 0$ in an overwhelming amount - above 98.5% and 94% in SH and DH cases, respectively - it is assumed in the modelling of oil outflow that $y_{l1} = 0$.

There is no data available on innermost and outermost edges of transversal damage extent y_{t1} and y_{t2} but it is assumed that these factors are determined as

$$y_{t1} = (\frac{1}{2} + c) \cdot s_b - \frac{1}{2} y_t \tag{4.8}$$

$$y_{t2} = (\frac{1}{2} + c) \cdot s_b + \frac{1}{2} y_t \tag{4.9}$$

Unlike in the collision model, there are no bulkhead locations given for the ship types in groundings so there is no way to validate these assumptions directly. When the grounding bulkhead locations are set to be the same as with collisions (as in Table C.9) there is a poor match with the real data w.r.t. which compartments are damaged.

Furthermore, setting the damaged area equal to a rectangular volume with dimensions y_l, y_t and y_v at the determined coordinates, all compartments coinciding with this volume will be assumed ruptured and all oil from these compartments is assumed lost.

4.5 Results

4.5.1 Damage Extent

By looking at the coefficients in Table E.1, $\ln y_l$ is by far the most dependent on kinetic energy (x_1) in the polynomial linear regression model. Obstruction depth (x_2) and tip radius (x_4) to a much lesser extent with some minor significance to rock eccentricity in the DH models. The R^2-values are high: around 93% for all SH models, and above 87% for the DH40 and DH150 models. Only the combined DH model performs less according to this metric, but is still reasonably good at 79%.

The regression results for $\ln y_t$ (see Table E.2) are even better in this view: all six models have R^2-values ranging between 90% and 94%. x_4 is the most influential variable, followed by x_2. A simple explanation for this is the fact that

- a bigger tip radius makes a bigger hole;
- because its shape is broader at the base, the rock will create more transversal damage if its tip is at lower depth;
- a higher apex angle means a broader cone base and thus creates a bigger hole.

Finally it should be noted that in the combined models for $\ln y_l$, the added variable (x_6) doesn't play a big role and shows a negative relationship. In $\ln y_t$, this variable is more substantial.

In Figure 4.12 some graphs are plotted between predictor variables and response variables y_l (longitudinal damage extent) and y_t (transversal damage extent) where, for each graph, all other variables are fixed at 0.5. It appears that damage extents are smaller for the SH40 case than for the SH150 case. It can be seen that

Tip radius has a negative influence on damage length; this is because the force exerted on the ship is greater when tip radius is larger. Note that longitudinal damage goes down when the kinetic energy CDF increases in the last few percentiles. This is not plausible and could be attributable to artifacting of the polynomial function.

4.5.2 Probability of Rupture

From Table E.5, it seems that the double hull ships are more resistant to rupture (the lower values for β_0 mean that the probability of rupture is near zero even for a relatively high $\ln y_v$). Probability of rupture goes up fast after a certain threshold has been reached (higher values for β_v). A plot of all logistic fits are given in 4.11. At least one of the goodness-of-fit tests for each binary logistic model give a p-value of 1 (see Table E.5), with the DH40 model scoring a p-value over 0.05 in all three tests. The point biserial correlation coefficient gives significantly high values in all cases (over 0.58), thereby rejecting the null hypothesis. Moreover, testing with random data leads to a failed rejection of the null hypothesis.

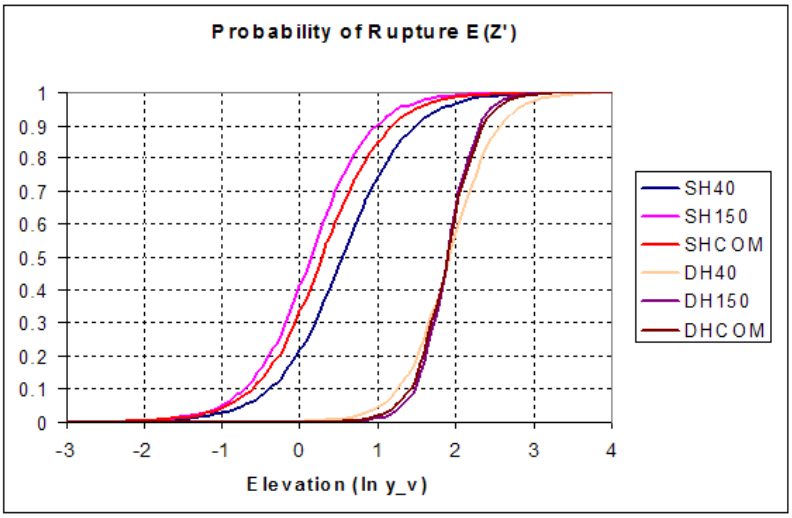

Figure 4.11: $E(Z')$ as function of $\ln y_v$

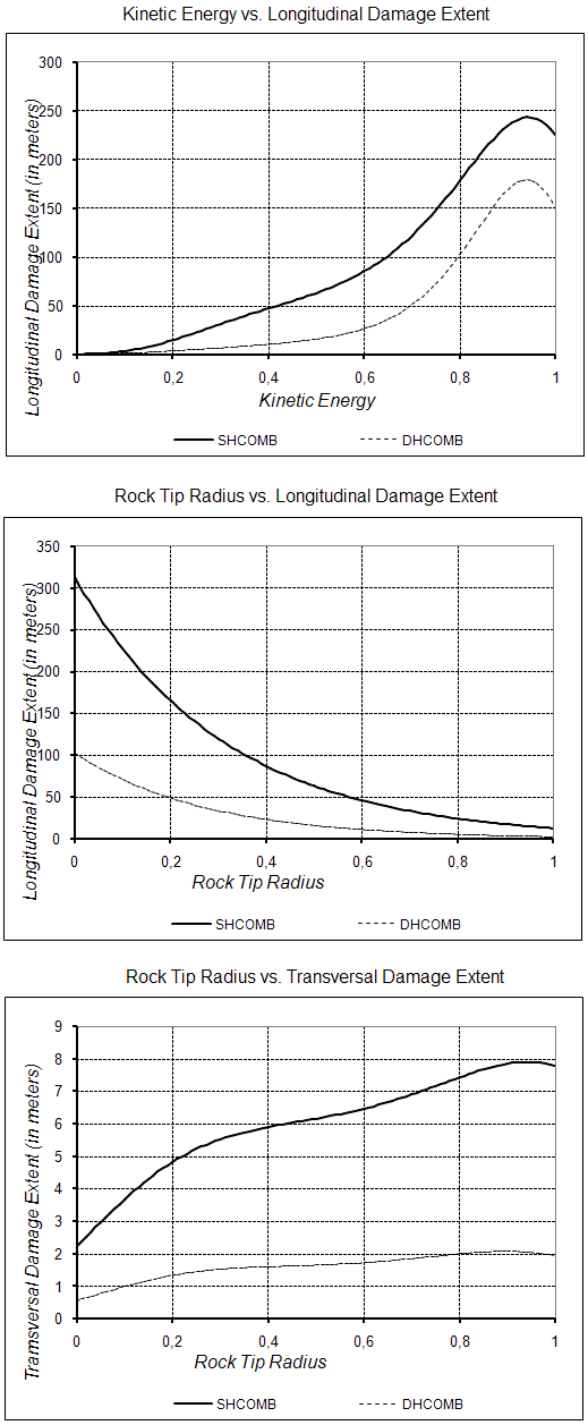

Figure 4.12: Effects of predictor variables on damage extent for a large ship using combined models

Chapter 5

Calculation Examples

Now that the outflow models have been discussed, a collision example and a grounding example are given to suggest how these models should be applied.

5.1 Struck Ship Configuration

To keep things simple, a single hull and double hull design are used in the examples in this chapter, each sharing the same input variables. The struck ship parameters that need to be configured are:

- Displacement
- Dimensions (length, breadth, depth)
- Bulkhead locations (longitudinal and transversal)
- Compartment volumes

For both collisions and groundings, a struck ship is chosen with 175,000 metric tonnes displacement.

- The dimensions, bulkhead locations and compartment volumes for the collision struck ships are determined according to the configurations of the SH150 and DH150 tankers as specified in the collision section of Chapter 2.
- For groundings, the dimensions and compartment volumes are the same as in the grounding section of Chapter 2; the bulkhead locations will be the same as the collision struck ships.

The outflow models of choice will be the combined single hull (SHCOM) and combined double hull (DHCOM). Because the struck ship dimensions are the same as the large ships specified in Chapter 2, the dimensional variable d is set to 1 in all models.

Variable	Value	Unit
v_1	12	knots
m_1	50	$\times$ 1000 metric tons
v_2	5	knots
ϕ	45	degrees
l	0.7	-
η	25	degrees

Table 5.1: Collision example variables

5.2 Collision Example

5.2.1 Input Variables

In a collision scenario, aside from the struck tanker's parameters, six input variables are needed to calculate expected damage size and expected probability of rupture. In Table 5.1, five arbitrary input variables are given. These fall within the bounds given by the probability distributions in Chapter 3.

Note that to obtain the collision models in Chapter 3, the variable t was involved in determining bow angle η. In this section η is arbitrarily chosen directly instead. This factually introduces a new striking ship type and shows the flexibility of the collision model.

5.2.2 Transformations

Now, calculate $e_{k,p}$ and $e_{k,t}$ as in Equation 3.13:

$$\begin{aligned} e_{k,p} &= \frac{1}{2}(m_1 + m_2)(v_1 \sin\phi)^2 \\ &= \frac{1}{2}(50 + 175)(12 \cdot \frac{1}{2}\sqrt{2})^2 \\ &= 8100 \qquad (5.1) \\ e_{k,t} &= \frac{1}{2}(m_1 + m_2)(v_2 + v_1 \cos\phi)^2] \\ &= \frac{1}{2}(50 + 175)(5 + 12 \cdot \frac{1}{2}\sqrt{2})^2 \\ &= 20458 \qquad (5.2) \end{aligned}$$

Calculate l':

$$l' = |l - \frac{1}{2}| = |0.7 - \frac{1}{2}| = 0.2 \qquad (5.3)$$

Transforming these through CDFs from Chapter 3 gives the set of input variables $\mathbf{x} = (x_1, x_2, x_3, x_4, x_5)$:

$$x_1 = F_{E_{k,p}}(e_{k,p}) = 1 - \exp(-\frac{e_{k,p}}{\beta})^\alpha \tag{5.4}$$

$$x_2 = F_{E_{k,t}}(e_{k,t}) = 1 - \exp(-\frac{e_{k,t}}{\beta})^\alpha \tag{5.5}$$

$$x_3 = F_{L'}(l') = Beta(l' + \frac{1}{2}|1.25, 1.45) - Beta(-l' + \frac{1}{2}|1.25, 1.45) \tag{5.6}$$

$$x_4 = F_H(\eta) = 1 \tag{5.7}$$

$$x_5 = F_D d = 1 \tag{5.8}$$

Because the transformation parameters for $e_{k,p}$ and $e_{k,t}$ are almost the same for single hull and double hull models, the transformations have (almost) the same values:

	Single Hull	Double Hull
x_1	0.962	0.962
x_2	0.987	0.987
x_3	0.465	0.465
x_4	1	1
x_5	1	1

5.2.3 Step One: Damage Extent

Given the input variables $\mathbf{x}$, one can now get the expected logarithm of damage length ($\ln y_l$), the expected logarithm of maximum penetration ($\ln y_t$) and their associated random error terms r_l and r_t:

$$\ln y_l = h_l(\mathbf{x}|\hat{\beta}^l) + r_l \tag{5.9}$$

$$\ln y_t = h_t(\mathbf{x}|\hat{\beta}^t) + r_t, \tag{5.10}$$

or, taking the exponential,

$$y_l = \exp(h_l(\mathbf{x}|\hat{\beta}^l) + r_l) \tag{5.11}$$

$$y_t = \exp(h_t(\mathbf{x}|\hat{\beta}^t) + r_t) \tag{5.12}$$

where h_l and h_t are functions given in Equation 3.27; r_l and r_t are the corresponding error terms and generated from random variables R_l and R_t. For simplicity, the random terms are ignored in this calculation. The coefficients $\hat{\beta}^l$ and $\hat{\beta}^t$ can be found in Tables D.1 and D.3. Calculating results in the following values:
Or:

	Single Hull	Double Hull
$\ln y_l$	3.376	3.084
$\ln y_t$	2.289	1.915

	Single Hull	Double Hull
y_l	29.249	21.854
y_t	9.863	6.789

5.2.4 Step Two: Probability of Rupture

Next, $\ln y_l and \ln y_t$ are put into the probability function $\pi(\ln y_l, \ln y_t|\hat{\beta})$, where coefficients $\hat{\beta}$ can be found in Table D.5.

$$\pi(\ln y_l, \ln y_t|\hat{\beta}) = \frac{\exp(\beta_0 + \beta_l \ln y_l + \beta_t \ln y_t)}{1 + \exp(\beta_0 + \beta_l \ln y_l + \beta_t \ln y_t)} \tag{5.13}$$

This is the probability of rupture. The results are:

	Single Hull	Double Hull
π	0.822	0.976

5.2.5 Step Three: Outflow Volume

With the probability of rupture $\pi = P(Z' = 1)$, the actual occurrence of rupture can be determined by "flipping a coin" (i.e. sampling a Bernouilli distributed random variable with parameter π). Suppose that the outcome is zero: then no rupture occurs and thus no outflow. In the other case, the longitudinal coordinates of the damaged area have to be determined.
Take m, n from D.7:

	Single Hull	Double Hull
m	0.112	0.091
m	5.91	5.62

Then $v_t = v_2 + v_1 \cos(\phi)$ and θ can be calculated (see Equation 3.47):

$$\theta(\phi, v_t; m, n) = (\frac{1}{2}(\frac{\phi}{90})^n)^{\exp(mv_t)} \tag{5.14}$$

This results in:

	Single Hull	Double Hull
θ	≈ 0	≈ 0

Determine damaged compartments from y_{l1}, y_{l2} and y_t using ship length s:

$$y_{l1} = (1-\theta)y_l + (1-l)s \tag{5.15}$$
$$y_{l2} = -\theta y_l + (1-l)s \tag{5.16}$$

Which leads to

	Single Hull	Double Hull
y_{l1}	79.89	78.30
y_{l2}	109.14	100.15

Now, for the single hull tanker, the bulkheads have to be looked up from the second column of Table C.9 that bound these locations: these are bulkheads 2 and 4 (which are 53.9 resp. 137.1 meters away from the FP). From this it can be seen that the longitudinal damage runs across the 3rd and 4th compartment as counted from the FP. (The first compartment is in between the FP and the first bulkhead.) Since $y_t = 9.863$ meters, the transversal damage extends only into the outermost compartments. Thus, the 3rd and 4rd outer compartments have been ruptured. Looking at Table C.2, the 3rd contains $15311m^3$ of oil; the other zero. Hence the total outflow volume z for the single hull tanker equals 15311 m^3.

In the double hull case, the bulkhead locations are looked up from the 4th column of Table C.9. This shows that the longitudinal damage is contained by bulkheads 3 and 4. Since $y_t = 6.789$, transversal damage reaches 2 compartments inward from the outer hull. Thus, one outer and one inner compartment in the the 4th row from the front are ruptured. Since the outer one is a ballast tank (compartment volume is 0) only the inner compartment spills oil, which amounts to 14651 m^3.

5.3 Grounding Example

5.3.1 Input Variables

In Table 5.2, some possible values of grounding input variables are given.

The only predictor variable that has to be calculated is e_k:

$$e_k = \frac{1}{2}mv^2 = \frac{1}{2} \cdot 175 \cdot 8.1^2 = 5741 \tag{5.17}$$

Variable	Value	Unit
v	8.1	knots
o_d	15	meters
o_a	42	degrees
o_r	6.7	meters
c	0.61	-

Table 5.2: Grounding example variables

5.3.2 Transformations

$\mathbf{x}$ is determined through transformating the input variables through their CDF values:

$$x_1 = F_{E_k}(e_k) = \frac{7}{10} + \frac{2}{175}(\sqrt{\frac{2e_k}{m}} - 8) = 0.7001 \tag{5.18}$$

$$x_2 = F_{O_d}(o_d) = \frac{1}{400}o_d^2 = \frac{1}{400}225 = \frac{9}{16} \tag{5.19}$$

$$x_3 = F_{O_a}(o_a) = 0.843 \tag{5.20}$$

$$x_4 = F_{O_r}(o_r) = 0.737 \tag{5.21}$$

$$x_5 = F_C(c) = c = 0.61 \tag{5.22}$$

5.3.3 Step One: Damage Extent

y_l and y_t are determined using the polynomial linear regression model, whose coefficients β^l and β^t can be found in Tables E.1 and E.2, respectively.

$$\ln y_l = h_l(\mathbf{x}|\hat{\beta}^l) + r_l \tag{5.23}$$

$$\ln y_t = h_t(\mathbf{x}|\hat{\beta}^t) + r_t \tag{5.24}$$

r_l and r_t are the corresponding error terms and generated from random variables R_l and R_t. Again, for simplicity the random terms are ignored. The coefficients $\hat{\beta}^l$ and $\hat{\beta}^t$ can be found in Tables D.1 and D.3, resulting in:

	Single Hull	Double Hull
$\ln y_l$	4.602	3.740
$\ln y_t$	2.462	1.755

Or:

	Single Hull	Double Hull
y_l	99.63	42.10
y_t	11.73	5.781

Using the ship depth $s_d = 16.76$ for both ships, one can calculate $y_v = \max(0, s_d - o_d) = 1.76$.

5.3.4 Step Two: Probability of Rupture

Next, put $\ln y_v$ into the binary logistic model $\pi(\ln y_v|\hat{\beta})$, where coefficients $\hat{\beta}$ can be found in Table E.5.

$$\pi(\ln y_v|\hat{\beta}) = \frac{\exp(\beta_0 + \beta_v \ln y_v)}{1 + \exp(\beta_0 + \beta_v \ln y_v)} \tag{5.25}$$

This results in the following probabilities

	Single Hull	Double Hull
π	0.665	0.002

5.3.5 Step Three: Outflow Volume

Given rupture, it is assumed that damage starts at the front of the ship. Also, rock eccentricity c is assumed to be in the middle of transversal damage extent. So,

$$y_{l1} = 0 \tag{5.26}$$
$$y_{l2} = y_l \tag{5.27}$$
$$y_{t1} = \frac{1}{2}(1+c) \cdot s_b - \frac{1}{2}y_t \tag{5.28}$$
$$y_{t2} = \frac{1}{2}(1+c) \cdot s_b + \frac{1}{2}y_t \tag{5.29}$$

This results in

	Single Hull	Double Hull
y_{l1}	0	0
y_{l2}	99.63	42.10
y_{t1}	34.38	37.36
y_{t2}	46.12	43.14

Where $s_b = 50.0$ is the ship's breadth in meters. Since y_{t2} is larger than the ship's breadth, it is reset at 50.

Using these coordinates, ruptured compartments can be determined using the bulkhead locations in Table C.9.

In the single hull case, longitudinally, the first four compartments as seen from the FP are damaged; transversally, the center and side compartments. The corresponding cargo volumes are presented in Table C.6, and thus the total outflow volume can be

calculated:

$$\begin{aligned} z &= 3,951,288 + 2,911,920 + 4,793,184 + 0 \\ &+ 4,792,392 + 3,402,960 + 4,192,584 + 0 \\ &= 24,044,328 \text{ gallons,} \end{aligned}$$

corresponding to $91,018\ m^3$.

In the double hull case, longitudinally, the first two compartments as seen from the FP are damaged; transversally, the center compartments. The corresponding cargo volumes are presented in Table C.8, and thus the total outflow volume can be calculated:

$$z = 2,593,272 + 3,254,064 = 5,847,336 \text{ gallons,}$$

corresponding to $22,135\ m^3$.

5.4 Conclusions

Comparing the example results, it should be noted that the double hull ships incur less damage extent given the same input variables: particularly in the grounding examples, the damaged area is more than four times smaller in the double hull case. This results an outflow volume four times smaller than in the single hull case. The difference in the collision examples is much less striking.

Chapter 6

Conclusions and Recommendations

In this report, twelve accidental outflow models have been presented: six collision models and six grounding models. These models determine the amount of oil that flows from an oil tanker in case it is struck by another ship or runs aground on a rocky pinnacle. Based on simulation data, these models have the ability to calculate fairly accurately the extent of collision or grounding damage, the probability of rupture and oil spill volume and the damage location given a set of accident variables. Uncertainties in outcomes of damage extent have been accurately modeled by fitting residuals to a parametric distribution.

Each of these models can be quickly and easily implemented in large scale system simulations of tanker movements because they involve formulas using only elementary functions and include an overseeable amount of parameters and coefficients. In short, they combine the power of physical simulations with the simplicity of explicit functions.

Moreover, these models improve significantly upon the previous IMO model since

- they are based on a large dataset obtained by physically meaningful simulations, rather than a model with simplistic assumptions based on a small historic dataset;
- they allow for size-dependent damage extent and probability of rupture assessments, whereas the old model gave damage and probability independently of ship size;
- damage extent parameters are dependent on scenario input variables as opposed to independently distributed;
- damage extent parameters take into account the physical characteristics of the ship designs and accident scenarios, such as speed, mass, collision angle etc.

6.1 Collision Model Results

- Kinetic energy is mostly responsible for damage extent;
- The regression model for damage extent fits reasonably well with data, giving R^2-values of 68%-75%;
- Single hull ships incur more damage overall than double hull designs;
- The regression model for probability of rupture shows higher rupture resistance for double hull tankers;
- Probability of rupture is strongly influenced by maximum penetration for double hull designs, whereas damage length is mostly responsible for rupture in single hull ones;
- Probability of rupture shows significant correlation with outflow occurrence in data;
- Damage location and outflow calculation model gives 95%-98% accuracy of outflow volume given rupture and damage extent.

6.2 Grounding Model Results

- Kinetic energy is mostly responsible for longitudinal damage;
- A large obstruction tip radius reduces longitudinal damage;
- Variables that describe rock geometry have the overhand in predicting transversal damage;
- The regression models for damage extent fits very well to the data, with 10 out of 12 giving R^2-values over 90%;
- The rupture probability model shows higher rupture resistance for double hull tankers, given obstruction elevation;
- Probability of rupture shows significant correlation with outflow occurrence in data.

6.3 General Remarks

A number of aspects should be considered in light of this research.

- The actual shape of the damaged area in collisions and groundings cannot be determined from the data: the models are only based on simplified measurements. They assume the damaged area to be a rectangular block, which holds the maximum damage volume possible.

- Given rupture, all compartments coinciding with the damaged area are assumed ruptured, whereas it might be possible that rupture takes place in a fraction of that area.
- All oil in a ruptured compartment is assumed lost, which is —in the case of grounding— a worst case simplification.
- The event that no outflow occurs is assumed to imply that there is no hull rupture, since no information is provided that would allow one to conclude otherwise.

6.4 Recommendations for Further Research

Below are some issues that may be considered topics of further research.

Using the large data set and great number of predictor variables available, reasonable to good fit performance was achieved for both polynomial linear and binary logistic regressions. As with any regression technique and especially due to the large number of predictor variables, other combinations of independent variables (taking advantage of e.g. interaction terms) could potentially lead to even better performance in terms of fit. A preliminary investigation of the use of interaction terms only showed a marginal improvement, while not reducing the number of variables.

The outflow models are based on statistical analysis, where output data is compared to input data. These factors mostly concern the 'outside' aspects of the struck tanker: no consideration is given to the influence of the ship's inner conditions, such as number of bulkheads etc. on damage size or probability of rupture—they only matter in determining the outflow volume. Improvements could be made in this, but it should be noted that the model in its current form is already both simple and effective; therefore any inclusion of mentioned internal aspects should only marginally increase the model's complexity. It then has to be tested how effective this inclusion is.

Bibliography

[1] Bedford, T., and Cooke, R. *Probabilistic Risk Analysis: Foundations and Methods.* Cambridge University Press, Cambridge, U.K., 2001.

[2] Bookrags. Mallows' cp summary. http://www.bookrags.com/wiki/Mallows

[3] Brown, A. *Alternative Tanker Designs, Collision Analysis.* NRC Marine Board Committee on Evaluating Double-Hull Tanker Design Alternatives, 2001.

[4] Brown, A., and Amrozowicz, M. Tanker environmental risk - putting the pieces together. *Joint SNAME/SNAJ Conference on Designs and Methodologies for Collision and Grounding Protection of Ships* (1996).

[5] Friis-Hansen, P., and Simonsen, B. Gracat: software for grounding and collision risk analysis. *Marine Structures 15* (2002), 383–401.

[6] Herbert Engineering Corp. Oil outflow analysis for a series of double hull tankers, 1998. Report No. 9749-1 Rev. A.

[7] Hosmer, D., and Lemeshow, S. *Applied Logistic Regression. Second Edition.* Wiley-Interscience, 2000.

[8] Huijer, K. Trends in oil spills from tanker ships, 1995-2004. London.

[9] International Maritime Organization. Interim guidelines for the approval of alternative methods of design and construction of oil tankers under regulation 13f(5) of annex i of marpol73/78, 1995.

[10] Jongbloed, G., and Groeneboom, P. *Voortgezette Statistiek.* Technische Universiteit Delft, 1999.

[11] Kotz, S., and van Dorp, J. *Beyond Beta. Other Continuous Families of Distributions with Bounded Support and Applications.* World Scientific Publishing, Singapore, 2004.

[12] Marine Board Commission on Engineering and Technical Systems. Tanker spills: Prevention by design, 1991.

[13] Meko, D. Applied time series analysis, lecture notes 11: Multiple linear regression, 2007. http://www.ltrr.arizona.edu/ dmeko/geos585a.html#cLesson11.

[14] Merrick, J., et al. The prince william sound risk assessment. *Interfaces 32*, 6 (2002), 25–40.

[15] Minorsky, V. An analysis of ship collisions with reference to protection of nuclear power plants. *Journal of Ship Research 3*, 1 (1959).

[16] Rawson, C., Crake, K., and Brown, A. Assessing the environmental performance of tankers in accidental grounding and collision. *SNAME Transactions 106* (1998), 41–58.

[17] Rodrigue, J.-P., Comtois, C., and Slack, B. *The Geography of Transport Systems.* Routledge, New York, 2006.

[18] Schmeiser, B. Advanced input modelling for simulation experimentation. *Proceedings of the 1999 Winter Simulation Conference* (1999).

[19] Simonsen, B., and Hansen, P. Theoretical and statistical analysis of ship grounding accidents. *Journal of Offshore Mechanics and Arctic Engineering 122* (2000), 200–207.

[20] The National Academies. *Special Report 259. Environmental Performance of Tanker Designs in Collision and Grounding.* The National Academies Press, 2001.

[21] Tikka, K. *Alternative Tanker Designs, Grounding Analysis.* NRC Marine Board Committee on Evaluating Double-Hull Tanker Design Alternatives, 2001.

[22] UNCTAD. Review of maritime transport 2007. New York / Geneva, 2007.

[23] van der Laan, M. *Environmental Tanker Design.* Delft University of Technology, 1997.

[24] van Dorp, J., and Kotz, S. Generalized trapezoidal distributions. *Metrika* (2003).

Appendix A

Regression

A.1 Binary Logistic Regression

This section discusses binary logistic regression as described by Hosmer and Lemeshow Chapters 1 and 2 [7]. Given is a binary random variable Y. In a regression analysis, the expected value of Y (the response variable) is related to a function of a set of predictor variables $\mathbf{x} = (x_1, \ldots, x_m)$, which in turn is based on a sample set $(\mathbf{x}_i, y_i), \quad i \in \{1, \ldots, n\}$.

In a binary logistic regression, this function is the logistic function π and represents the expected value of Y conditioned on $\mathbf{x}$. Notation:

$$E(Y|\mathbf{x}) \quad = \quad \pi(\mathbf{x}|\beta) \tag{A.1}$$

Where π is defined as

$$\pi(\mathbf{x}|\beta) \quad = \quad \frac{e^{g(\mathbf{x}|\beta)}}{1 + e^{g(\mathbf{x}|\beta)}}. \tag{A.2}$$

With

$$g(\mathbf{x}|\beta) \quad = \quad \beta_0 + \beta_1 x_1 + \ldots + \beta_m x_m \tag{A.3}$$

$\beta = (\beta_0, \ldots, \beta_m)$ is a set of coefficients that defines the shape of g and thus π. Binary linear regression determines an optimal set of coefficients $\hat{\beta}$, i.e. coefficients that result in the 'most accurate' fit of π against the variables.

A.1.1 Fitting the Logistic Regression Model

Given n realizations of independent, identically distributed sets of variables

$$(\mathbf{X}_i, Y_i), \quad i \in \{1, \ldots, n\} \tag{A.4}$$

Now, the coefficients β are fitted from the dataset of scenarios $\mathbf{x}_i$ by means of the maximum likelihood estimation. Consider the set $(\mathbf{x}_i, y_i)$ of observed data, where y_i

is the dependent variable corresponding to independent variables $\mathbf{x}_i$.

The maximum likelihood method yields values for the unknown coefficients β which maximize the probability of obtaining the observed set of data. This is done by constructing a likelihood function l, which expresses the probability of observed data as a function of β.

Since, by definition,

$$E(Y|\mathbf{x}) = 0 \cdot P(Y = 0|\mathbf{x}) + 1 \cdot P(Y = 1|\mathbf{x}) \tag{A.5}$$

$$= P(Y = 1|\mathbf{x}) \tag{A.6}$$

for any $\mathbf{x}$, it follows that $P(Y = 1|\mathbf{x}) = \pi(\mathbf{x}|\beta)$ and $P(Y = 0|\mathbf{x}) = 1 - P(Y = 1|\mathbf{x}) = 1 - \pi(\mathbf{x}|\beta)$. Then, one may express the contribution for the pair $(\mathbf{x}_i, y_i)$ to the likelihood function as

$$\pi(\mathbf{x}_i|\beta)^{y_i}\left[1 - \pi(\mathbf{x}_i|\beta)\right]^{1-y_i}. \tag{A.7}$$

As the observations are assumed independent, the likelihood function is obtained as the product of these contributions:

$$l(\beta) = \prod_{i=1}^{n} \pi(\mathbf{x}_i|\beta)^{y_i}[1 - \pi(\mathbf{x}_i|\beta)]^{1-y_i}. \tag{A.8}$$

Now, β is estimated as the value which maximizes the right hand side of A.8, also referred to as $\hat{\beta}$. The loglikelihood is defined as follows:

$$L(\beta) = \ln[l(\beta)] \tag{A.9}$$

$$= \sum_{i=1}^{n} y_i \ln[\pi(\mathbf{x}_i)] + (1 - y_i)\ln[1 - \pi(\mathbf{x}_i)] \tag{A.10}$$

Because l and L have a maximum at the same value(s) of β, It becomes relatively straightforward to find β by maximizing L (as opposed to l), which in turn is done by partially differentiating $L(\beta)$ to $\beta_0, \ldots, \beta_m$ and equating the resulting expressions to 0:

$$\frac{\partial L}{\partial \beta_0} = 0 \tag{A.11}$$

$$\frac{\partial L}{\partial \beta_j} = 0, \quad j \in \{1, \ldots, m\} \tag{A.12}$$

These are the likelihood equations; solving them for $\beta_0, \ldots, \beta_m$ will result in the *maximum likelihood estimate* $\hat{\beta}$. However, these equations are nonlinear and the workings of the required solving method go beyond the scope of this report. The statistical software package Minitab 15 is capable of performing this method and was used in this report.

The maximum likelihood estimate of $\pi(\mathbf{x}|\beta)$, which is $\pi(\mathbf{x}|\hat{\beta})$, is denoted as $\hat{\pi}(\mathbf{x})$ and represents a "best" estimate of the probability that outflow occurs, given a scenario $\mathbf{x} = (x_1, \ldots, x_m)$. Thus, $\hat{\pi}(\mathbf{x})$ is the *probability* of the event $Y = 1$ happening based on binary logistic regression.

A.2 Linear Regression

The method of linear regression as described here was based on Chapter 3 of [10]. Given a set of scenarios $\mathbf{x}_1, \mathbf{x}_2, \ldots, \mathbf{x}_n \in \mathbb{R}^p$ and outcomes $y_1, y_2, \ldots, y_n \in \mathbb{R}$ realizations of random variables $Y_1, Y_2, \ldots, Y_n$. Then a linear regression model expresses the relationship between Y_i and $\mathbf{x}_i$ as follows:

$$\begin{aligned} Y_i &= h(\mathbf{x}_i|\beta) + R_i && \text{(A.13)} \\ &= \beta_0 + \beta_1 x_{i,1} + \ldots \beta_p x_{i,p}, \quad \forall i \in \{1, \ldots, n\} && \text{(A.14)} \end{aligned}$$

Where $R_1, R_2, \ldots, R_n$ are assumed to be uncorrelated random variables with mean zero and finite variance. Y_i is the response variable and x_i is the vector containing predictor variables. h is the function that needs to be determined by changing the coefficients in vector $\beta = (\beta_0, \beta_1, \ldots, \beta_p) \in \mathbb{R}^{p+1}$.

Based on a sample $\{(\mathbf{x}_1, y_1), \ldots, (\mathbf{x}_n, y_n)\} \in \mathbb{R}^p \times \mathbb{R}$, an estimate of β can be found. A systematic method to do this is the least squares method, whereby a least squares estimate $\hat{\beta}$ is found by minimizing the sum of squares of the residuals over β:

$$\begin{aligned} S(\hat{\beta}) &= \min_{\beta} S(\beta) && \text{(A.15)} \\ &= \min_{\beta} \sum_{i=1}^{n} (y_i - h(\mathbf{x}_i|\beta))^2 && \text{(A.16)} \end{aligned}$$

Minima of S are found by determining the partial derivatives of S to β, equating these derivatives to 0 and solving these equations for β, resulting in the linear regression estimator $\hat{\beta}$. If S is convex, then $\hat{\beta}$ is a global minimum.

$$\begin{aligned} \frac{\partial S}{\partial \beta_j} &= 2 \sum_{i=1}^{n} \epsilon_i \frac{\partial \epsilon_i}{\partial \beta_j} && \text{(A.17)} \\ &= -2 \sum_{i=1}^{n} (y_i - f(\mathbf{x}_i, \beta)) \frac{\partial f(\mathbf{x}_i, \beta)}{\partial \beta_j}, \quad , \forall j \in \{0, \ldots, p\} && \text{(A.18)} \end{aligned}$$

Appendix B

Probability Distributions

B.1 Empirical Distribution Function

For a random variable X the cumulative distribution function F is defined as $F(x) = \mathbb{P}(\{X \leq x\})$. The empirical cumulative distribution function F_n of a sample of n i.i.d. random variables $X_1, \ldots, X_n \sim X$ is defined as

$$F_n(x) = \frac{1}{n} \sum_{i=1}^{n} 1_{(-\infty,x]}(X_i) \tag{B.1}$$

,
Where $1_{(-\infty,x]}(y) = 1$ if $y \leq x$, and $1_{(-\infty,x]}(y) = 0$ otherwise. The empirical CDF has the property that $F_n(x) \to F(x)$ almost surely for a fixed x by the strong law of large numbers.

B.2 Typical Distributions

Beta Distribution

The Beta probability distribution function is given as

$$f(x; \alpha, \beta) = \frac{\Gamma(\alpha + \beta)}{\Gamma(\alpha) + \Gamma(\beta)} x^{\alpha-1}(1-x)^{\beta-1} \tag{B.2}$$

Where Γ is the Gamma function and α, β are the function's parameters.

Normal Distribution

The Normal probability distribution function is given as

$$f(x; \mu, \sigma) = \frac{1}{\sigma\sqrt{2\pi}} \exp(-\frac{(x-\mu)^2}{2\sigma^2}) \tag{B.3}$$

Where μ and σ^2 are the mean and variance and determine location and scale of the distribution, respectively.

Weibull Distribtion

The Weibull distribution has the following cumulative distribution function:

$$F(x|\alpha,\beta) \quad = \quad 1 - e^{(-\frac{x}{\beta})^{\alpha}} \tag{B.4}$$

Where $\alpha \geq 0$ is the shape parameter and $\beta \geq 0$ is the scale parameter. Note that for $\alpha = 1$, the Weibull distribution is equivalent to the Exponential distribution with parameter β.

B.3 Generalized Power Distribution

For $0 < m < 1$ and $0 \leq x \leq 1$, the Generalized Power Distribution [11] is defined as follows:

$$f(x|\alpha,m,n) \quad = \quad \begin{cases} p(\frac{x}{m}|\alpha,n), & 0 \leq x \leq m \\ p(\frac{1-x}{1-m}|\alpha,n), & m < x < 1 \end{cases} \tag{B.5}$$

where

$$p(x|\alpha,n) = \alpha + n(1-\alpha)x^{n-1}$$

and, for $0 \leq x \leq 1$,

$$\begin{cases} 0 \leq \alpha \leq \frac{n}{n-1}, & n > 1 \\ 0 \leq \alpha \leq 1, & 0 < n \leq 1. \end{cases}$$

If x is on an interval $[a,b]$, then it should be scaled by transforming it to a variable y on the interval $[0,1]$:

$$y \quad = \quad \frac{x-a}{b-a} \tag{B.6}$$

Thus,

$$f(y|\alpha,m,n) = f(\frac{x-a}{b-a}|\alpha,m,n)$$

.

B.4 Generalized Trapezoidal Distribution

Suppose X is a random variable on the bounded support $[a,b]$. If X follows the Generalized Trapezoidal distribution [24], its probability distribution function is defined as follows:

$$f(x|a,b,c,d,n_1,n_3,\alpha) = \begin{cases} 0, & x < a \\ \frac{2\alpha n_1 n_3}{2\alpha(b-a)n_3+(\alpha+1)(c-b)n_1 n_3+2(d-c)n_1}(\frac{x-a}{b-a})^{n_1-1}, & a \leq x < b \\ \frac{2n_1 n_3}{2\alpha(b-a)n_3+(\alpha+1)(c-b)n_1 n_3+2(d-c)n_1}((\alpha-1)\frac{c-x}{c-b}+1), & b \leq x < c \\ \frac{2n_1 n_3}{2\alpha(b-a)n_3+(\alpha+1)(c-b)n_1 n_3+2(d-c)n_1}(\frac{d-x}{d-c})^{n_3-1}, & c \leq x < d \\ 0, & x \geq d \end{cases} \tag{B.7}$$

Provided that $n_1 > 0, n_3 > 0, \alpha > 0$ and $a < b < c < d$.

Appendix C

Tanker Data

Compartment location	Port	Center	Starboard
Bow	1865.4	3641.1	1865.4
	2640.8	0.0	2640.8
	2673.5	3646.1	2673.5
	0.0	3644.4	0.0
	2668.0	3643.6	2668.0
Stern	2529.1	3642.2	2529.1

Table C.1: Tanker compartment volumes (m^3), SH40, collisions

Compartment location	Port	Center	Starboard
Bow	13102.9	17779.5	13102.9
	0.0	21566.6	0.0
	15311.4	21563.4	15311.4
	0.0	18864.3	0.0
	8364.9	19658.5	8364.9
Stern	3820.4	19658.5	3820.4

Table C.2: Tanker compartment volumes (m^3), SH150, collisions

Compartment location	Port	Port Center	Starboard Center	Starboard
	0.0	2269.7	2267.7	0.0
	0.0	2825.3	2825.3	0.0
	0.0	2845.9	2845.9	0.0
	0.0	2845.9	2844.9	0.0
	0.0	0.0	0.0	0.0
	0.0	2276.5	2276.5	0.0
	0.0	2845.9	2844.9	0.0
	0.0	2845.9	2845.9	0.0
Stern	0.0	2669.5	2671.5	0.0

Table C.3: Tanker compartment volumes (m^3), DH40, collisions

Compartment location	Port	Port Center	Starboard Center	Starboard
Bow	0.0	11694.3	11694.3	0.0
	0.0	14674.2	14674.2	0.0
	0.0	14650.4	14650.4	0.0
	0.0	14651.2	14651.2	0.0
	0.0	14650.8	14650.8	0.0
	0.0	13861.9	13861.9	0.0
Stern	0.0	5514.7	5514.7	0.0

Table C.4: Tanker compartment volumes (m^3), DH150, collisions

Compartment location	Port	Center	Starboard
Bow	413,688	792,528	413,688
	585,552	0	585,552
	592,944	808,632	592,944
	0	808,104	0
	591,624	808,104	591,624
Stern	560,736	783,816	560,736

Table C.5: Tanker compartment volumes (gallons), SH40, groundings

Compartment location	Port	Center	Starboard
Bow	2,911,920	3,951,288	2,911,920
	0	4,793,184	0
	3,402,960	4,792,392	3,402,960
	0	4,192,584	0
	1,859,088	4,368,936	1,859,088
Stern	849,024	0	849,024

Table C.6: Tanker compartment volumes (gallons), SH150, groundings

Compartment location	Port	Port Center	Starboard Center	Starboard
Bow	0	505,560	505,560	0
	0	626,472	626,472	0
	0	629,376	629,376	0
	0	630,168	630,168	0
	0	503,712	503,712	0
	0	630,168	630,168	0
	0	628,320	628,320	0
Stern	0	590,832	590,832	0

Table C.7: Tanker compartment volumes (gallons), DH40, groundings

Compartment location	Port	Port Center	Starboard Center	Starboard
Bow	0	2,593,272	2,593,272	0
	0	3,254,064	3,254,064	0
	0	3,248,784	3,248,784	0
	0	3,249,048	3,249,048	0
	0	3,249,048	3,249,048	0
	0	3,074,016	3,074,016	0
Stern	0	1,083,192	1,083,192	0

Table C.8: Tanker compartment volumes (gallons), DH150, groundings

Transversal bulkheads (Location from FP (m))			
SH40	SH150	DH40	DH150
14.63	12.3	16.46	12.3
37.948	53.9	33.99	43.5
61.265	95.5	51.51	74.7
84.582	137.1	69.04	105.9
107.899	173.5	86.56	137.1
131.216	199.5	90.07	168.3
154.534	214.3	104.09	199.5
		121.62	214.3
		139.14	
		156.67	

Longitudinal bulkheads (Location from port bow (m))			
SH40	SH150	DH40	DH150
8.23	14.8	2.438	3.34
19.202	35.2	14.63	25
		26.822	46.66

Table C.9: Bulkhead locations

Appendix D

Collision Model Results

	SH40	SH150	SHCOM	DH40	DH150	DHCOM
number of data points	7467	7473	14940	7454	7466	14920
R^2-value	70.9%	68.1%	68.9%	71.5%	69.9%	70.6%
Mallows C_p-value	19.0	19.8	13.1	14.2	24.0	16.0
Coefficients						
β_0	-2.914	-2.661	-2.982	-2.931	-2.786	-2.632
$\beta_{1,1}$	3.078	-1.215	2.246	2.128	2.047	-0.117
$\beta_{2,1}$	5.550	5.303	5.231	6.180	4.692	4.670
$\beta_{3,1}$	0.031	-2.493	-3.369	0.708	-3.224	-1.973
$\beta_{4,1}$	0.546	1.613	1.188	0.655	1.429	1.155
$\beta_{5,1}$	-	-	0.223	-	-	0.052
$\beta_{1,2}$	-	10.181	0.687	0.598	-	5.792
$\beta_{2,2}$	-	-	-	-5.563	-	-
$\beta_{3,2}$	-	20.261	25.010	-	24.187	16.819
$\beta_{4,2}$	-	-0.931	-0.560	-	-0.784	-0.566
$\beta_{5,2}$	-	-	-	-	-	-
$\beta_{1,3}$	-	-8.145	-	-	-	-
$\beta_{2,3}$	-11.982	-6.405	-6.750	-	-5.410	-5.756
$\beta_{3,3}$	-	-68.750	-75.742	-13.309	-69.908	-53.668
$\beta_{4,3}$	-	-	-	-0.158	-	-
$\beta_{5,3}$	-	-	-	-	-	-
$\beta_{1,4}$	-2.924	-	-	-	-	-10.900
$\beta_{2,4}$	9.403	-	-	-	-	-
$\beta_{3,4}$	-	94.811	96.400	27.442	85.081	69.372
$\beta_{4,4}$	-	-	-	-	-	-
$\beta_{5,4}$	-	-	-	-	-	-
$\beta_{1,5}$	2.823	2.008	-	-	0.542	7.798
$\beta_{2,5}$	-	4.134	4.529	2.291	3.724	4.031
$\beta_{3,5}$	-0.480	-44.783	-43.224	-15.354	-36.872	-31.216
$\beta_{4,5}$	-	-	-	-	-	-
$\beta_{5,5}$	-	-	-	-	-	-

Table D.1: Polynomial linear regression coefficients for $\ln y_l$, collisions

	SH40	SH150	SHCOM	DH40	DH150	DHCOM
α	1	1	1	1	1	1
A	-17.266	-16.802	-17.261	-15.478	-15.402	-15.851
B	-0.153	-0.362	-0.278	-0.191	-0.312	-0.254
C	0.217	0.426	0.352	0.254	0.425	0.356
D	5.304	5.585	5.585	5.250	5.585	5.585
N1	35.833	26.036	30.196	31.101	26.547	29.222
N3	10.299	8.089	9.221	9.995	10.133	10.471

Table D.2: Parameters of GT distributions, R_l, collisions

	SH40	SH150	SHCOM	DH40	DH150	DHCOM
number of data points	7470	7478	14948	7455	7467	14922
R^2-value	73.8%	70.4%	71.4%	74.6%	72.6%	73.5%
Mallows Cp-value	14.0	18.2	15.0	12.8	20.1	20.6
Coefficients						
β_0	-3.730	-3.507	-3.977	-3.655	-3.629	-3.681
$\beta_{1,1}$	8.661	4.492	6.767	6.527	6.793	6.650
$\beta_{2,1}$	5.439	3.479	4.828	4.585	2.790	3.985
$\beta_{3,1}$	-4.126	1.357	-3.234	-0.321	0.308	0.427
$\beta_{4,1}$	0.010	0.378	1.267	0.030	0.289	0.051
$\beta_{5,1}$	-	-	0.227	-	-	0.044
$\beta_{1,2}$	-6.939	-	-3.339	-3.250	-4.298	-3.758
$\beta_{2,2}$	-7.083	-	-5.251	-5.971	-	-4.329
$\beta_{3,2}$	28.940	-6.123	23.896	5.613	-	-
$\beta_{4,2}$	-	-	-1.313	-	-	-
$\beta_{5,2}$	-	-	-	-	-	-
$\beta_{1,3}$	-	-	-	-	-	-
$\beta_{2,3}$	-	-5.602	-	-	-4.492	-
$\beta_{3,3}$	-80.644	-	-72.669	-25.920	-6.807	-9.296
$\beta_{4,3}$	-	-	-	-	-	-
$\beta_{5,3}$	-	-	-	-	-	-
$\beta_{1,4}$	3.268	-	-	-	-	-
$\beta_{2,4}$	3.229	-	-	2.848	-	-
$\beta_{3,4}$	96.373	19.916	93.704	40.495	16.125	20.693
$\beta_{4,4}$	-	-0.585	-	-0.345	-0.531	-
$\beta_{5,4}$	-	-	-	-	-	-
$\beta_{1,5}$	-	0.243	1.534	1.462	2.212	1.828
$\beta_{2,5}$	-	3.841	2.074	-	3.285	1.872
$\beta_{3,5}$	-41.499	-15.976	-42.700	-20.501	-10.209	-12.407
$\beta_{4,5}$	-0.263	-	-	-	-	-0.354
$\beta_{5,5}$	-	-	-	-	-	-

Table D.3: Polynomial linear regression coefficients for $\ln y_t$, collisions

	SH40	SH150	SHCOM	DH40	DH150	DHCOM
α	1	1	1	1	1	1
a	-15.282	-17.654	-17.346	-16.113	-14.270	-16.355
b	0.056	-0.207	-0.099	0.030	-0.256	-0.110
c	0.192	0.355	0.287	0.182	0.372	0.304
d	3.312	3.912	3.912	3.376	3.912	3.912
n_1	29.369	25.266	27.822	30.668	25.556	29.228
n_3	7.299	5.577	6.580	7.161	7.128	7.761

Table D.4: Parameters of GT distributions, R_t, collisions

	SH40	SH150	SHCOM	DH40	DH150	DHCOM
No. Cases	7440	7430	14811	7423	7436	14788
Coefficients						
β_0	-0.229	-0.864	-0.511	-7.026	-10.823	-7.142
β_t	0.162	0.164	0.158	5.943	7.330	5.443
β_l	0.536	0.514	0.498	0.257	0.283	0.143
MLR	-4534	-4367	-9065	-1114	-796	-2190
Pearson Test	0	0	0	0	0	0
Deviance Test	0	0	0	1	1	1
Hosmer-Lemeshow Test	0	0	0	0	0	0

Table D.5: Binary logistic regression coefficients, collisions

	SH40	SH150	SHCOM	DH40	DH150	DHCOM
No. Cases	7440	7430	14811	7423	7436	14788
r_{bp} (data)	0.40	0.43	0.41	0.85	0.86	0.82
p-value (data)	0	0	0	0	0	0
r_{bp} (random)	-0.01	-0.02	-0.00	0.00	0.01	0.01
p-value (random)	0.50	0.17	0.78	0.80	0.36	0.14

Table D.6: Binary logistic regression point-biserial correlation tests, collisions

	SH40	SH150	SHCOM	DH40	DH150	DHCOM
No. of cases	4045	3183	7228	1404	1026	2430
% correct predictions	97.11%	97.86%	97.40%	94.87%	96.78%	95.60%
m	0.112	0.098	0.112	0.061	0.091	0.091
n	5.90	6.20	5.91	4.59	5.60	5.62
avg. absolute error (m^3)	88	289	189	134	417	255
conditional average absolute error (m^3)	3045	13513	7248	2609	12950	5800

Table D.7: Damage location coefficients

Appendix E

Grounding Model Results

	SH40	SH150	SHCOM	DH40	DH150	DHCOM
number of data points	1806	5899	7705	609	2673	3282
R^2-value	93.3%	93.3%	93.2%	87.0%	90.8%	79.4%
Mallows Cp-value	21.8	23.4	30.8	18.2	15	21.7
Coefficients						
β_0	-2.866	-1.327	-1.403	-3.925	-2.403	-0.592
$\beta_{1,1}$	41.818	41.940	30.664	50.806	41.949	16.217
$\beta_{2,1}$	3.398	1.141	4.703	6.133	3.761	4.394
$\beta_{3,1}$	0.102	-0.044	0.085	-0.326	-0.150	-0.136
$\beta_{4,1}$	-4.750	-2.277	-3.194	-5.365	-3.027	-3.708
$\beta_{5,1}$	-0.406	-0.226	0.085	1.298	-0.610	1.175
$\beta_{6,1}$	-	-	-0.146	-	-	-0.320
$\beta_{1,2}$	-104.639	-116.403	-74.472	-139.873	-106.135	-25.308
$\beta_{2,2}$	-	-	-12.152	-20.431	-4.750	-8.377
$\beta_{3,2}$	-	-	-	-	-	-
$\beta_{4,2}$	11.369	4.509	7.174	8.726	4.519	6.078
$\beta_{5,2}$	-	-1.842	-2.851	-1.951	6.895	-
$\beta_{6,2}$	-	-	-	-	-	-
$\beta_{1,3}$	96.878	140.345	85.822	168.169	98.551	-
$\beta_{2,3}$	-5.096	0.286	14.138	20.867	-	4.459
$\beta_{3,3}$	-	-	-	-	-	-
$\beta_{4,3}$	-12.822	-4.769	-8.234	-5.621	-2.568	-3.568
$\beta_{5,3}$	1.362	4.033	5.109	-	-11.504	-3.524
$\beta_{6,3}$	-	-	-	-	-	-
$\beta_{1,4}$	-	-59.455	-35.523	-70.533	-	47.300
$\beta_{2,4}$	-	-	-	-	-	-
$\beta_{3,4}$	0.206	0.104	-	-	-	-
$\beta_{4,4}$	5.047	1.853	3.453	-	-	-
$\beta_{5,4}$	-	-	-	-	-	-
$\beta_{6,4}$	-	-	-	-	-	-
$\beta_{1,5}$	-26.548	-	-	-	-26.883	-32.250
$\beta_{2,5}$	-	-	-5.977	-	-	-
$\beta_{3,5}$	-	-	-	-	-	-
$\beta_{4,5}$	-	-	-	-	-	-
$\beta_{5,5}$	-2.361	-	5.330	-	5.330	2.444
$\beta_{6,5}$	-	-	-	-	-	-

Table E.1: Polynomial linear regression coefficients for $\ln y_l$, groundings

	SH40	SH150	SHCOM	DH40	DH150	DHCOM
number of data points	2720	5904	8624	644	2724	3368
R^2-value	90.0%	93.6%	91.6%	92.5%	93.7%	92.7%
Mallows Cp-value	21.7	23.1	21.2	18	25.2	33.7
Coefficients						
β_0	1.473	2.049	1.112	1.229	1.769	1.095
$\beta_{1,1}$	0.065	0.111	0.096	0.170	0.095	0.142
$\beta_{2,1}$	-5.088	-4.060	-4.251	-0.775	-3.258	-4.002
$\beta_{3,1}$	0.720	1.239	0.740	0.008	0.767	0.782
$\beta_{4,1}$	7.520	5.857	6.397	9.308	6.709	7.575
$\beta_{5,1}$	-0.148	-0.186	-0.002	-0.825	0.103	-0.488
$\beta_{6,1}$	-	-	1.004	-	-	0.692
$\beta_{1,2}$	-	-0.093	-	-	-	-
$\beta_{2,2}$	25.437	12.507	8.287	-14.912	6.663	7.987
$\beta_{3,2}$	-2.210	-2.624	-1.025	-	-1.153	-1.315
$\beta_{4,2}$	-19.182	-14.714	-16.229	-28.430	-17.836	-20.824
$\beta_{5,2}$	0.175	-	-	2.922	-	1.652
$\beta_{6,2}$	-	-	-	-	-	-
$\beta_{1,3}$	-	-	-	-	-	-
$\beta_{2,3}$	-104.542	-17.161	-	-	-	-
$\beta_{3,3}$	2.893	2.865	0.593	-	0.668	0.801
$\beta_{4,3}$	22.161	16.975	18.870	37.140	21.247	25.400
$\beta_{5,3}$	-	1.303	-	-	-	-
$\beta_{6,3}$	-	-	-	-	-	-
$\beta_{1,4}$	-	-	-	-	-	-
$\beta_{2,4}$	187.918	-	-23.858	72.857	-37.722	-37.565
$\beta_{3,4}$	-1.291	-1.078	-	-	-	-
$\beta_{4,4}$	-9.019	-6.974	-7.793	-16.758	-8.939	-10.917
$\beta_{5,4}$	-	-1.734	-	-11.801	-2.828	-6.571
$\beta_{6,4}$	-	-	-	-	-	-
$\beta_{1,5}$	-	-	-0.058	-	-	-
$\beta_{2,5}$	-106.772	7.761	19.393	-62.279	37.674	36.762
$\beta_{3,5}$	-	-	-	-	-	-
$\beta_{4,5}$	-	-	-	-	-	-
$\beta_{5,5}$	-0.753	-	-0.591	9.846	2.639	5.347
$\beta_{6,5}$	-	-	-	-	-	-

Table E.2: Polynomial linear regression coefficients for $\ln y_t$, groundings

	SH40	SH150	SHCOM	DH40	DH150	DHCOM
α	1	1	1	1	1	1
a	-10.994	-10.103	-13.431	-9.172	-13.119	-13.650
b	0.006	-0.090	-0.106	-0.037	0.033	0.105
c	0.006	0.049	0.105	0.157	0.033	0.296
d	5.304	5.585	5.585	5.250	5.585	5.585
n_1	64.487	61.720	71.475	33.447	67.252	34.301
n_3	30.138	27.469	27.964	20.649	30.055	23.793

Table E.3: Parameters of GT distributions, R_l, groundings

	SH40	SH150	SHCOM	DH40	DH150	DHCOM
α	1	1	1	1	1	1
a	-6.125	-5.983	-6.776	-5.504	-7.561	-7.433
b	0.012	-0.026	0.014	-0.047	-0.006	0.012
c	0.012	0.013	0.014	0.041	-0.006	0.012
d	3.312	3.912	3.912	3.376	3.912	3.912
n_1	61.834	85.192	65.877	69.486	126.004	88.989
n_3	36.823	49.919	43.771	37.596	57.874	52.855

Table E.4: Parameters of GT distributions, R_t, groundings

	SH40	SH150	SHCOM	DH40	DH150	DHCOM
No. Cases	2812	7035	9847	3116	7323	10439
Coefficients						
β_0	-1.274	-0.348	-0.694	-6.431	-9.818	-8.648
β_v	2.339	2.590	2.438	3.356	5.204	4.597
MLR	-1044	-1365	-2518	-984	-1981	-3003
Pearson Test	0	0	0	1	0	0
Deviance Test	1	1	1	0.831	1	1
Hosmer-Lemeshow Test	0	0	0	0.18	0	0

Table E.5: Binary logistic regression coefficients, groundings

	SH40	SH150	SHCOM	DH40	DH150	DHCOM
No. Cases						
r_{pb} (data)	0.71	0.78	0.76	0.58	0.80	0.76
p-value (data)	0	0	0	0	0	0
r_{pb} (random)	-0.02	0.00	-0.00	0.00	0.01	-0.01
p-value (random)	0.32	0.82	0.78	0.81	0.48	0.40

Table E.6: Binary logistic regression point-biserial correlation tests, groundings

TECHNICAL APPENDIX F: FUTURE SCENARIOS

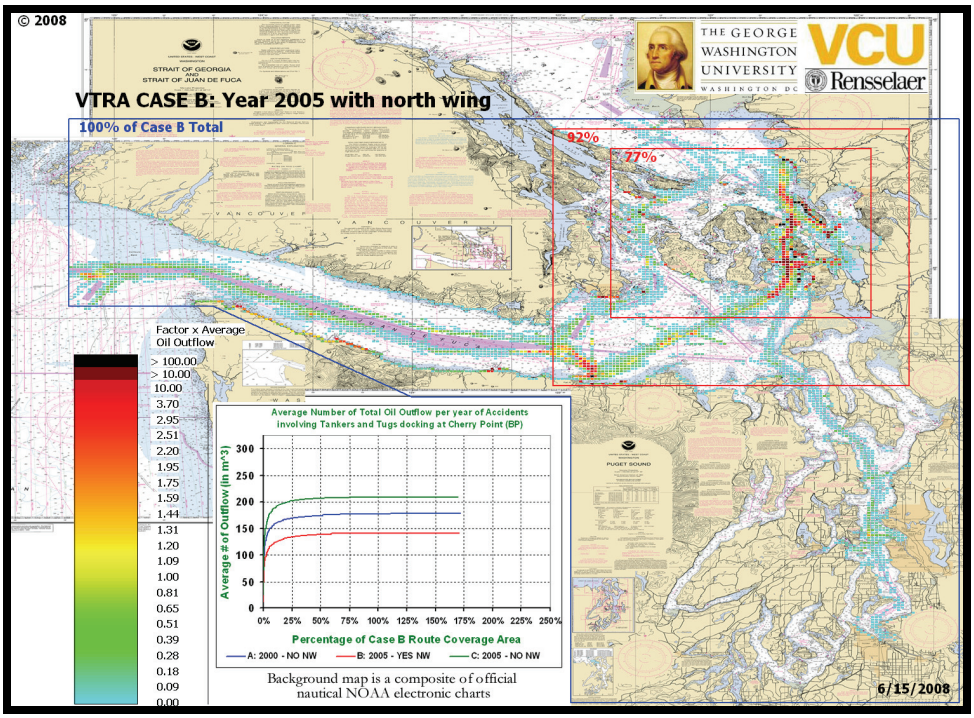

Assessment of Oil Spill Risk due to Potential Increased Vessel Traffic at Cherry Point, Washington

Submitted by VTRA TEAM:

Johan Rene van Dorp (GWU), John R. Harrald (GWU),

Jason R.. W. Merrick (VCU) and Martha Grabowski (RPI)

August 31, 2008

TABLE OF CONTENTS

F-1. Historical data on traffic levels 5
F-2. BP's projection of Cherry Point Traffic 6
F-3. Overview of the development of future scenarios 8
F-4. Time Series Forecasting of Traffic Levels 13
F-5. Traffic Levels Projected for 2025 18

TABLE OF FIGURES

Figure F-1. Puget Sound Marine Exchange Visit Data 5
Figure F-2. US Coast Guard Transit Data 6
Figure F-3. Historical visit data for container vessels. 8
Figure F-4. Historical visit data for bulk carriers. 9
Figure F-5. Historical visit data for cruise vessels. 9
Figure F-6. Historical visit data for roll on-roll off vessels. 10
Figure F-7. Historical visit data for vehicle carriers. 10
Figure F-8. Historical visit data for tank vessels. 11
Figure F-9. Historical data on the number of transits per visit for tank vessels. 11
Figure F-10. Historical transit data for public vessels. 12
Figure F-11. Historical transit data for ferries. 12
Figure F-12. Historical transit data for tugs with tows or barges. 13
Figure F-13. The statistical forecast for bulk carrier visits. 14
Figure F-14. The statistical forecast for container vessel visits. 15
Figure F-15. The statistical forecast for ro-ro vessel visits. 15
Figure F-16. The statistical forecast for vehicle carrier visits. 16
Figure F-17. The statistical forecast for tank vessel visits. 16
Figure F-18. The statistical forecast for tanker transits per visit. 17
Figure F-19. The statistical forecast for tug transits. 17
Figure F-20. The statistical forecast for ferry transits. 18

TABLE OF TABLES

Table F-1. BP's projections of future traffic levels at the BP Cherry Point docks. 6
Table F-2. Percentage Changes from 2005 Traffic Levels Used in 2000 and 2025. 8
Table F-3. Percentage Changes from 2005 Traffic Levels Used in 2000 and 2025. 18

F-1. Historical data on traffic levels

The Marine Exchange of Puget Sound collects data on commercial vessels that visit the Puget Sound. This data was provided from January 1992 to December 2006 as monthly counts of a variety of vessel types. Not all the vessels types included are used in the VTOSS database, so we used monthly visit counts from the Marine Exchange data where the vessel types matched those used in the simulation. Figure F-1. shows all the data provided by the Marine Exchange.

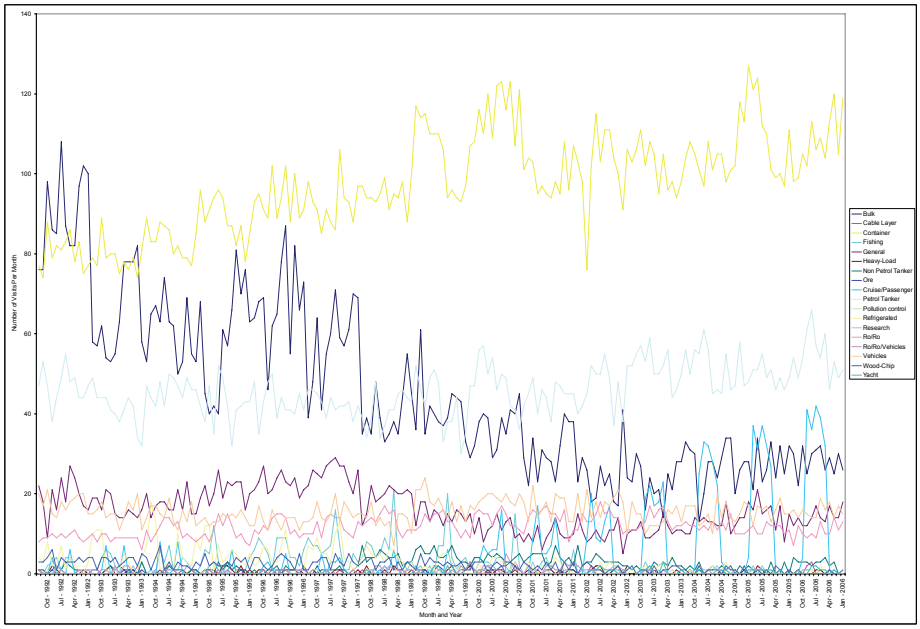

Figure F-1. Puget Sound Marine Exchange Visit Data

The USCG Seattle VTS collects data on the number of transits by VTS participating traffic within their area of responsibility. We should draw a distinction here between a visit and a transit. A visit occurs when a vessel enters the study area and then leaves again. In between, the vessel may make a number of shifts, or movements between ports within the area. A transit is counted every time the vessel moves (not including movements between docks in the same port. Thus each visit will lead to at least two transits (inbound and outbound) and, possibly, a number of shifts. Figure F-2 shows the Seattle VTS transit data, provided from January 1996 to December 2006.

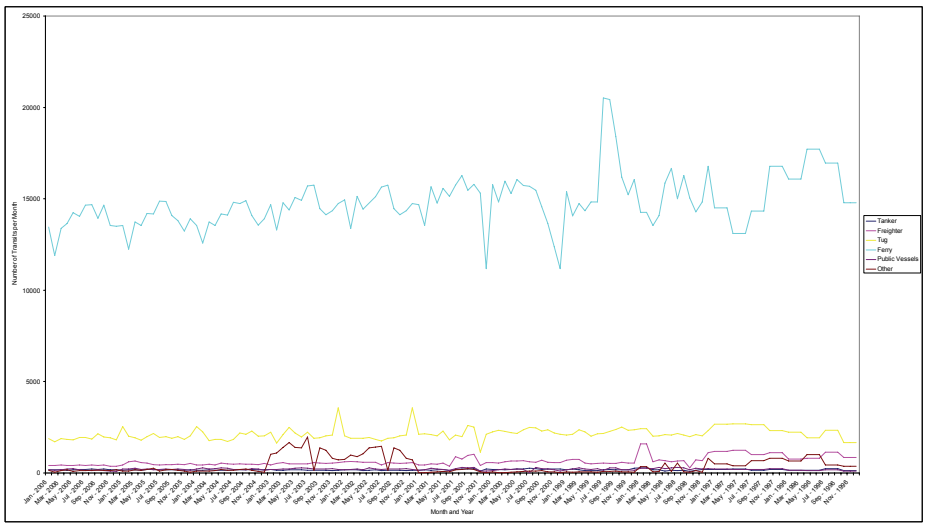

Figure F-2. US Coast Guard Transit Data

The Marine Exchange and Seattle VTS data was used to forecast traffic levels for non-BP vessels in 2025. This data was also used to find the change in traffic levels from 2000 to 2005. For BP vessels, projections were provided by BP.

F-2. BP's projection of Cherry Point Traffic

Table F-1 shows the projections provided by BP for both crude tankers and product vessels.

Table F-1. BP's projections of future traffic levels at the BP Cherry Point docks.

Vessel Traffic Scenario	Annual Total Vessel Range					Probability of Occurrence	
	crude vessels	product vessels		crude vessels	product vessels	within 10yrs	by 2025
Increased Crude Oil Delivery by Pipeline from Canada	170		to	220		very low	low
	15	155		20	200		
Current Range of Operations	320		to	400		low	medium
	150	170		180	220		
Growth Based On Historical Market Demand	340		to	370		medium	low
	170	170		185	185		
Growth Based On High Market Demand	350		to	450		very low	very low
	120	230		150	300		

From these projections, we need projections for the year 2025 at a low, medium, and high level. Our projections are somewhat limited by the scope of the Environmental Impact Study that the VTRA is an input to. We consider changes to BP traffic for the BP Cherry Point Refinery within currently permitted operating conditions. Thus the refinery handled 225,000 barrels of crude per day in 2005. The maximum permitted capacity under any previously authorized permits is 250,000 barrels per day. Thus they can at most handle an 11% increase in crude deliveries.

The projections provided by BP include a range from a 90% decrease in crude tankers arriving at the refinery (if most deliveries switch to a pipeline) up to a 17% increase in crude tanker visits (under the highest point in the range for the projections using historical market demand). We, therefore, use the 90% decrease assumed from the pipeline scenario for our low case (15 crude tanker visits) and the 17% increase assumed under historical market demand scenario for our high case (185 crude tanker visits). The 17% increase is higher than the 11% increase in barrels per day under historical permits, so we must assume that BP intended that these crude tankers to arrive at a lower capacity than currently seen. For the medium case, we use the middle of the range from the historical market demand scenario, or 177.5 crude tanker visits, which is a 13% increase.

The number of product tankers is not limited by the delivery capacity of the refinery, so the range is larger. The lowest number of product vessel visits included in the BP projections is 155, which is a 2% decrease from those in the 2005 simulation. The highest number of product vessel visits is 300, which is a 90% increase. These figures were used for the low and high cases. For the medium case, we again used the middle of the range for the historical market demand scenario, which is again 177.5 and a 13% increase from 2005 levels.

Table F-2 shows the changes in traffic levels used in the simulation for the low, medium, and high versions of the 2025 future scenario cases.

Table F-2. Percentage Changes from 2005 Traffic Levels Used in 2000 and 2025.

Traffic Type	2025		
	Low	Medium	High
BP Crude Tankers	-90%	+13%	+17%
BP Product Vessels	-2%	+13%	+90%

F-3. Overview of the development of future scenarios

The first step in determining forecasts for the non-BP traffic in 2025 is to examine the data. Separate forecasts are need for each vessel type where changes are forecasted. To maintain greater accuracy in traffic patterns, vessel types that are not forecasted to change will use 2005 transit data.

Figures F.3 through F.12 show the visit or transit data for each vessel type in the simulation for which historical data was available. Figures F.3, F.4, and F.5, for container vessels, bulk carriers, and cruise vessels show strong patterns. Container vessels visits have shown strong growth, while bulk carriers visits have been decreasing. Cruise vessels have shown seasonal growth, but the growth is slowing.

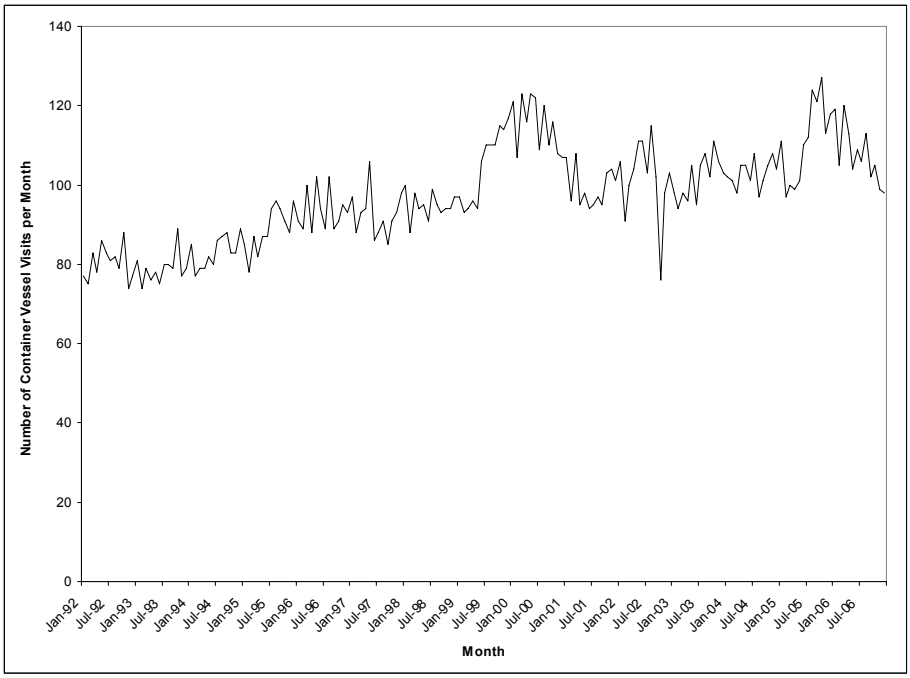

Figure F-3. Historical visit data for container vessels.

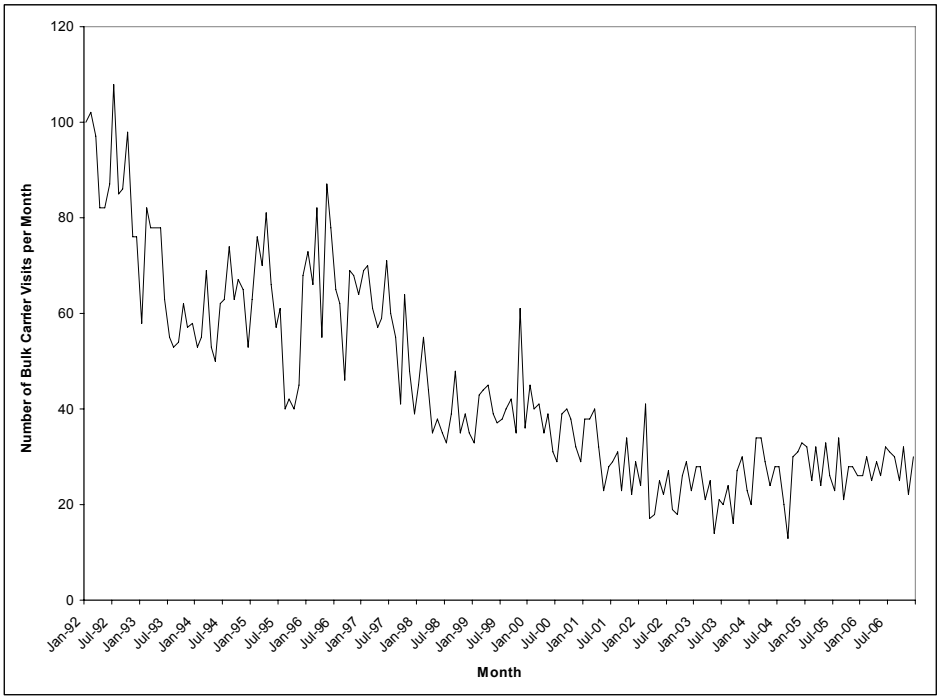

Figure F-4. Historical visit data for bulk carriers.

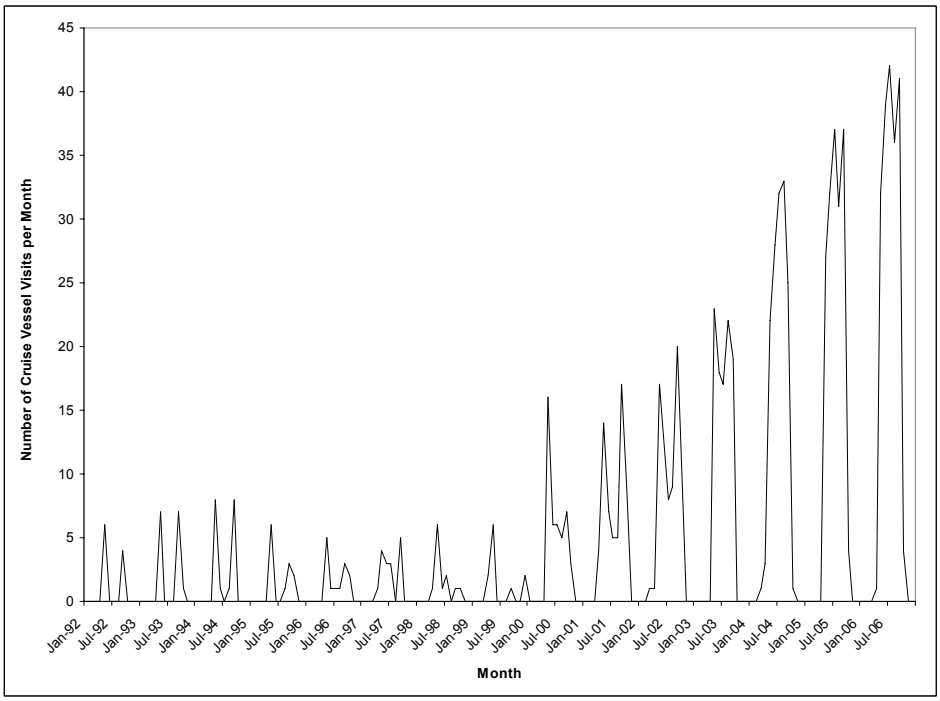

Figure F-5. Historical visit data for cruise vessels.

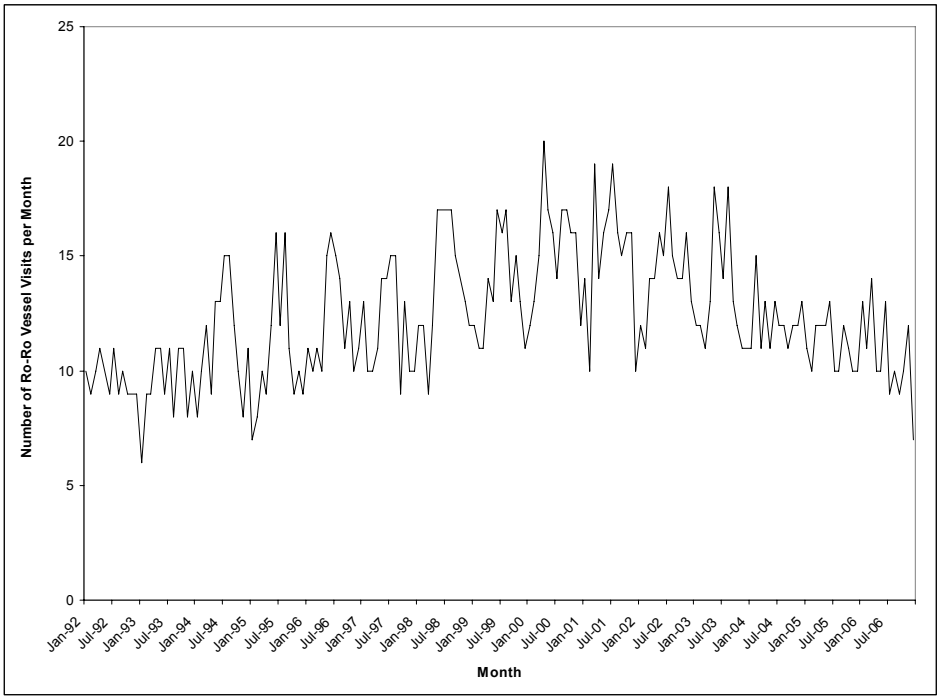

Figure F-6. Historical visit data for roll on-roll off vessels.

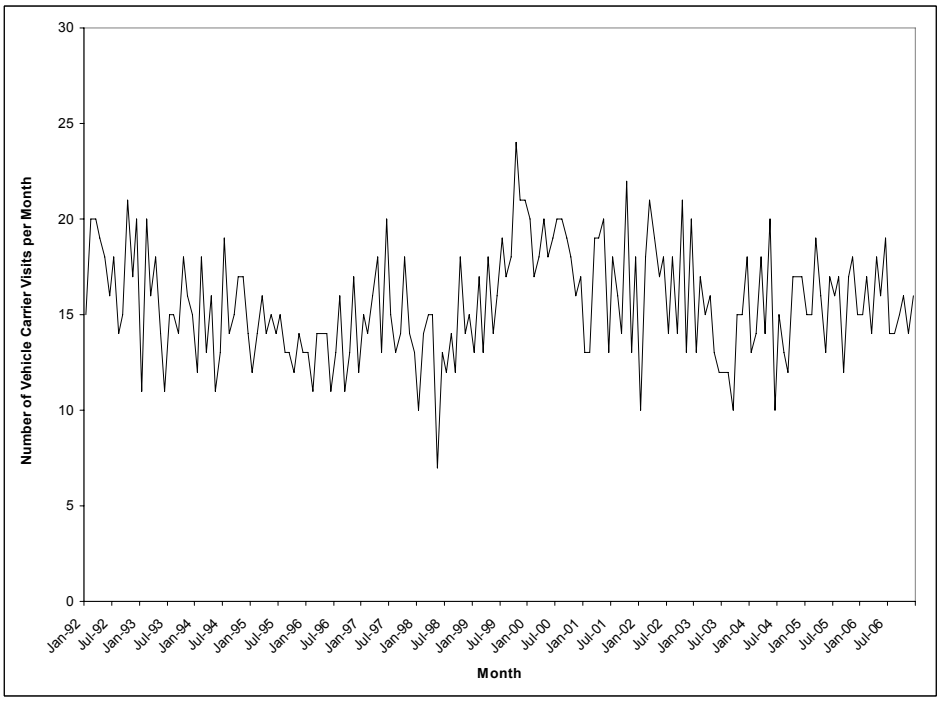

Figure F-7. Historical visit data for vehicle carriers.

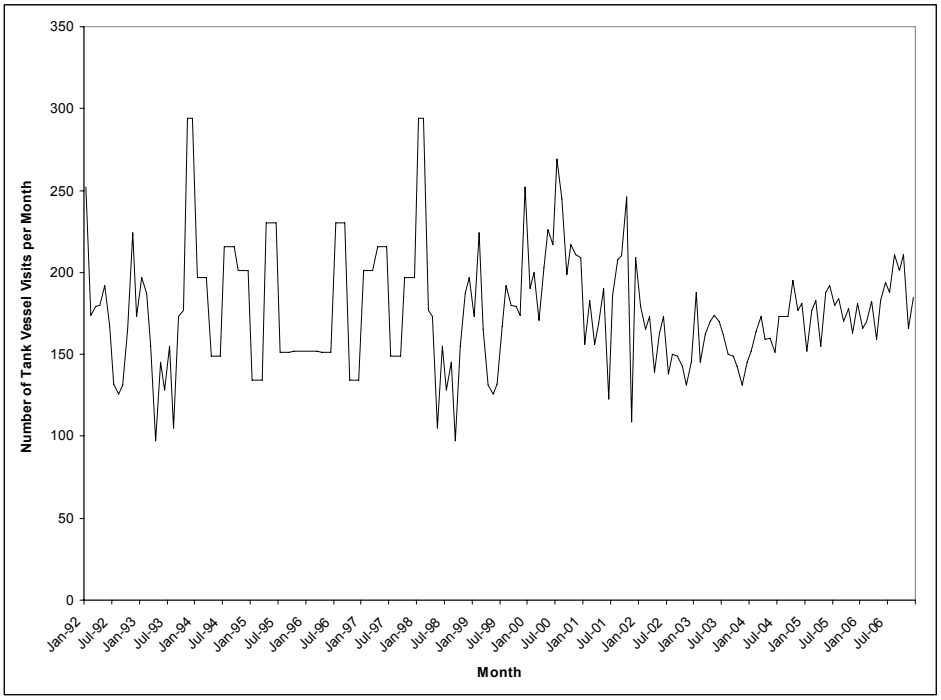

Figure F-8. Historical visit data for tank vessels.

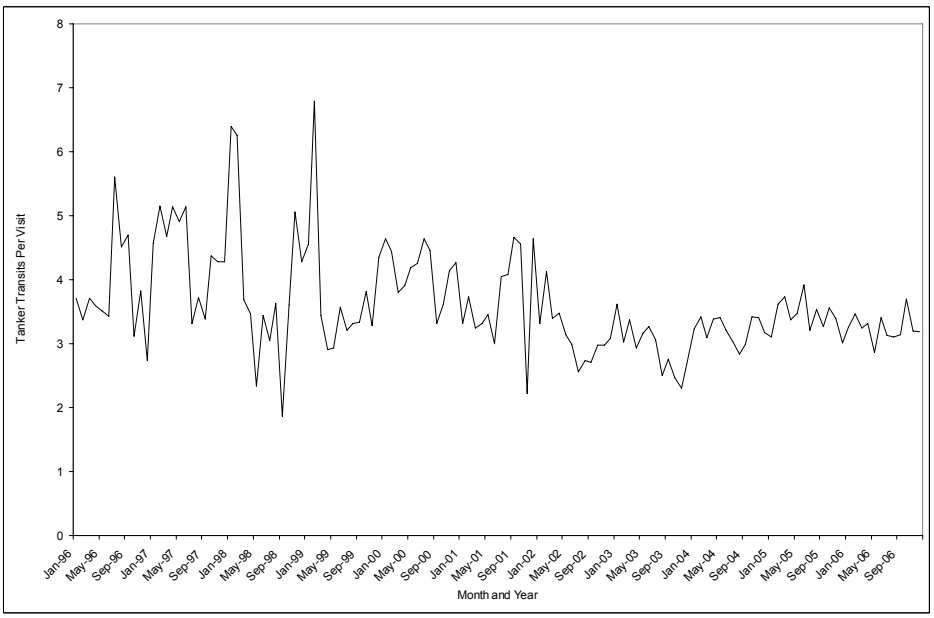

Figure F-9. Historical data on the number of transits per visit for tank vessels.

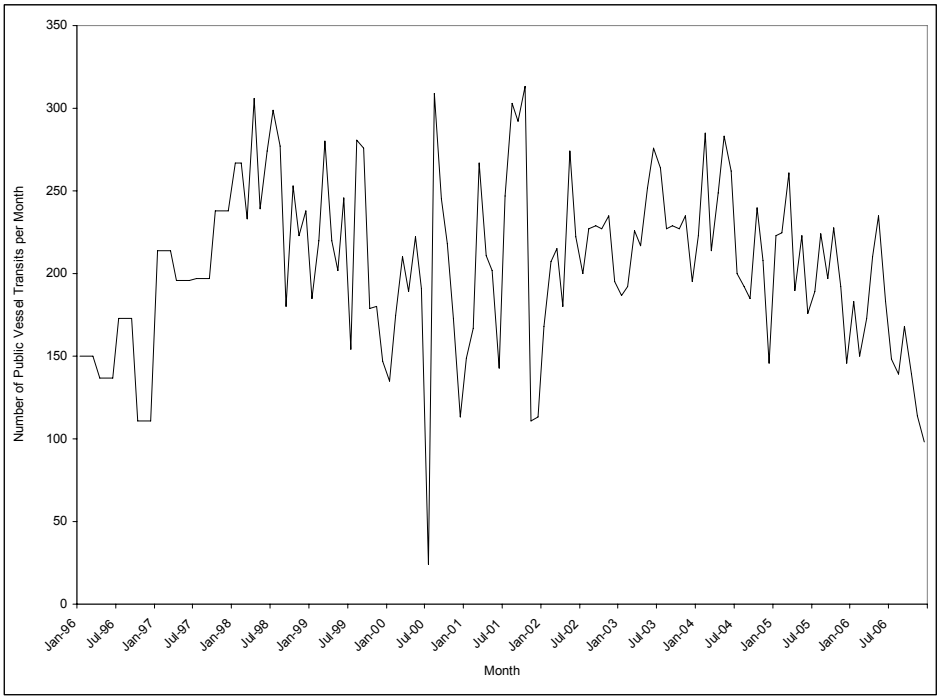

Figure F-10. Historical transit data for public vessels.

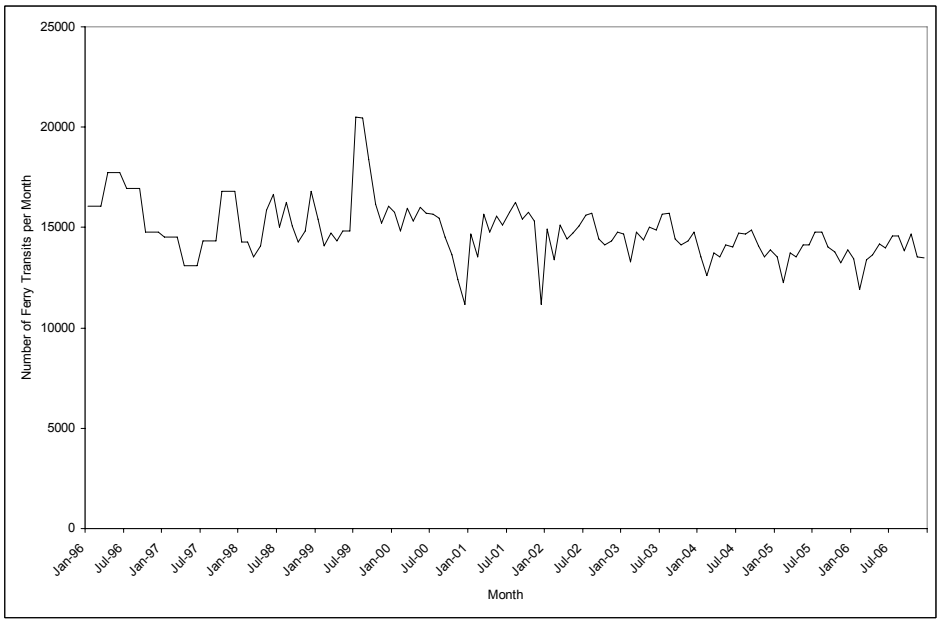

Figure F-11. Historical transit data for ferries.

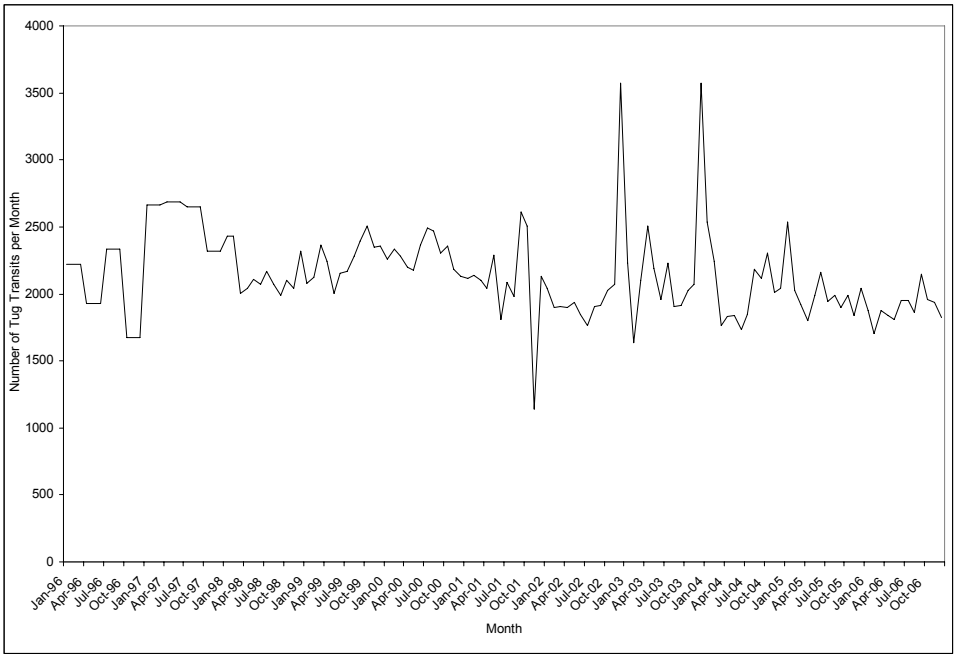

Figure F-12. Historical transit data for tugs with tows or barges.

Figure F-6, F.7, F.10, F.11, and F.12 show no obvious trends for ro-ro vessels, vehicle carriers, public vessels, ferries, or tugs. However, Figures F.8 and F.9 deserve more attention. Figure F-8 shows the historical number of visits by tankers there has been a lot of variability in these numbers, there is a pattern of steady growth since 2001. Figure F-9 shows the number of transits per visit. Recall that each visit must correspond to at least an inbound and an outbound transit. If the number of transits per visit is above two then the vessels must be performing shifts between ports in the study area. Thus we can see that tankers usually perform one or two shifts per visit and sometimes many more. From 1996 to 2001, there was a large variability in the number of shifts performed, but since then the average number of shifts per visit has settled down to about one. This is important as we can use forecasts for the number of visits for the number of non-BP tankers and the movement patterns between refineries is not shown to change from those in the 2005 data by Figure F-9.

F-4. Time Series Forecasting of Traffic Levels

With a visual understanding of the historical patterns in hand, we may now turn to statistical methods to achieve forecasts and an understanding of the range of forecasted traffic levels. The method used is called time series analysis, which allows us to model patterns of growth,

seasonal patterns, and historical dependencies in the data. The models used are called Seasonal, Auto-regressive, Integrative, Moving-Average models, SARIMA models for short. The range of possible models is large and various diagnostic tools can be used to find the best predictive model. We also obtain a confidence bound on the model, or a range within which the model predicts the traffic levels will fall. This allows us to use the models' predicted traffic levels for the medium case and the upper and lower bounds of the confidence interval for the high case and low case, respectively. It should be noted thought that we are attempting to forecast traffic levels based on 10-14 years of data with our forecast being for 19 years past the end of the data. Thus the range of uncertainty is obviously large.

Figures F. 13 to F.20 show the models fitted to the historical data. The model is shown as a solid line and the historical data is shown as individual points. The upper and lower confidence bounds are shown as dotted lines. A flat forecast, such as in Figure F-13 for bulk carriers, from the last historical data point shows that the traffic level is not forecasted to change and so the traffic levels for these vessel types are kept at the 2005 levels. We can see in Figure F-13 that bulk carriers have decreased over time, but then visit levels have flattened off and are forecasted to remain steady in the future.

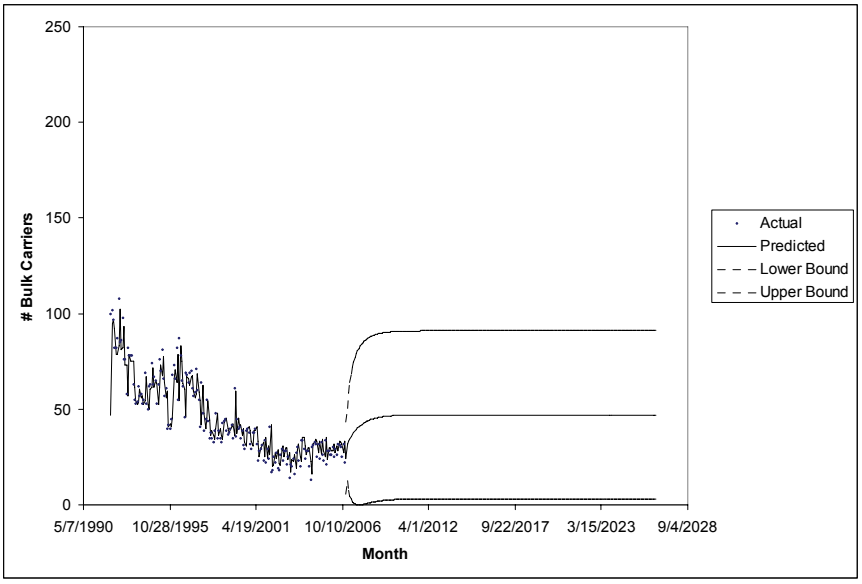

Figure F-13. The statistical forecast for bulk carrier visits.

Figure F-14 indicates a steady increase in container vessel visits. Taking this forecast, the low, medium, and high cases use a 54% decrease, a 20% increase and a 93% increase respectively. Figures F.15 and F. 16 show steady levels for ro-ro vessels and vehicle carriers. The increasing upper bound is a side-effect of the data transformations used for statistical fitting purposes.

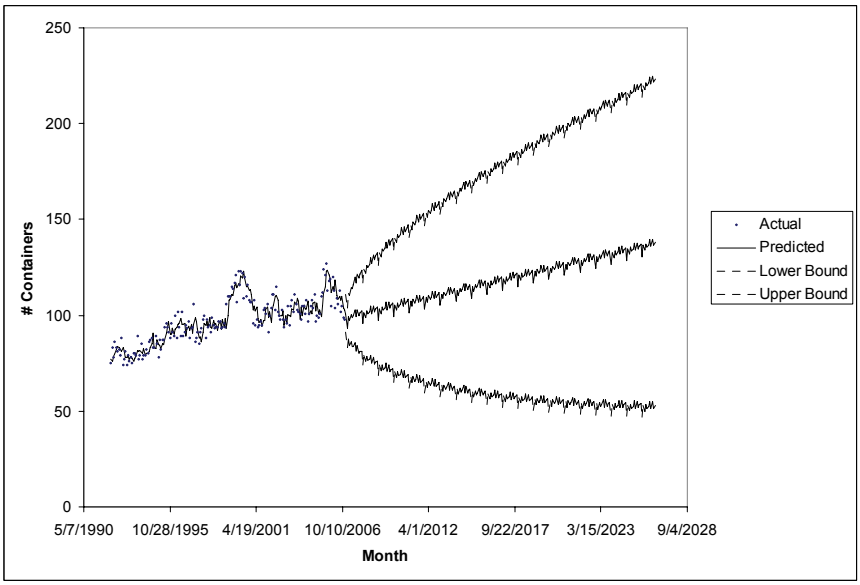

Figure F-14. The statistical forecast for container vessel visits.

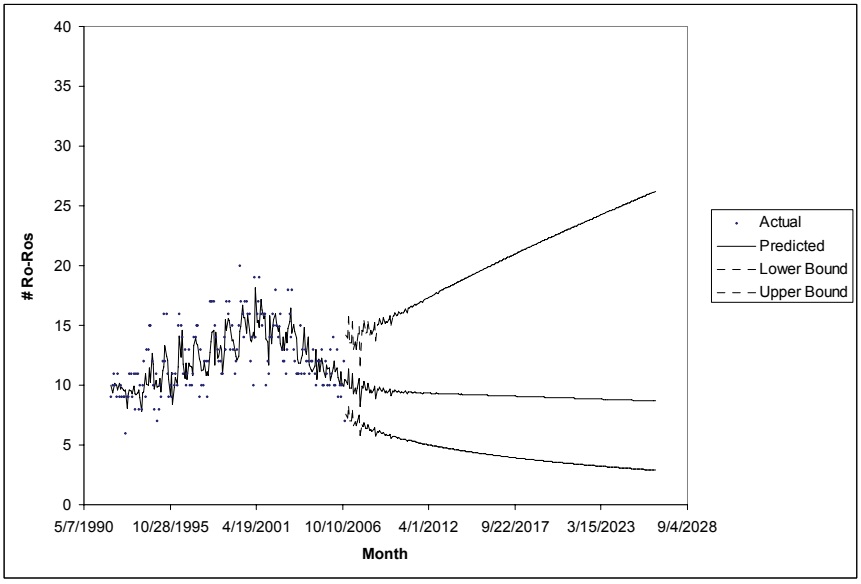

Figure F-15. The statistical forecast for ro-ro vessel visits.

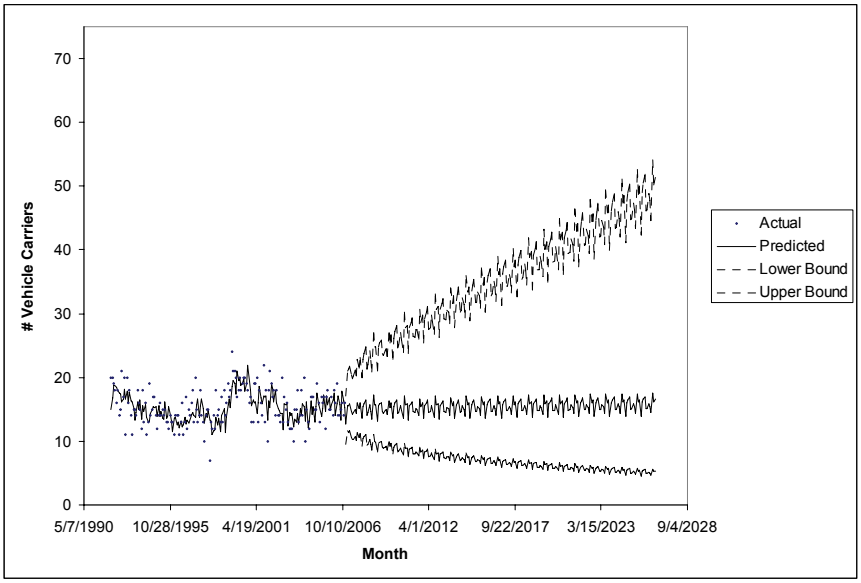

Figure F-16. The statistical forecast for vehicle carrier visits.

Figure F- 17 shows a steady increase in tanker visits to the area. Thus for non-BP tankers, the low, medium, and high cases use a 54% decrease, a 55% increase and a 162% increase respectively. The high range is a result of the volatility in the historical data.

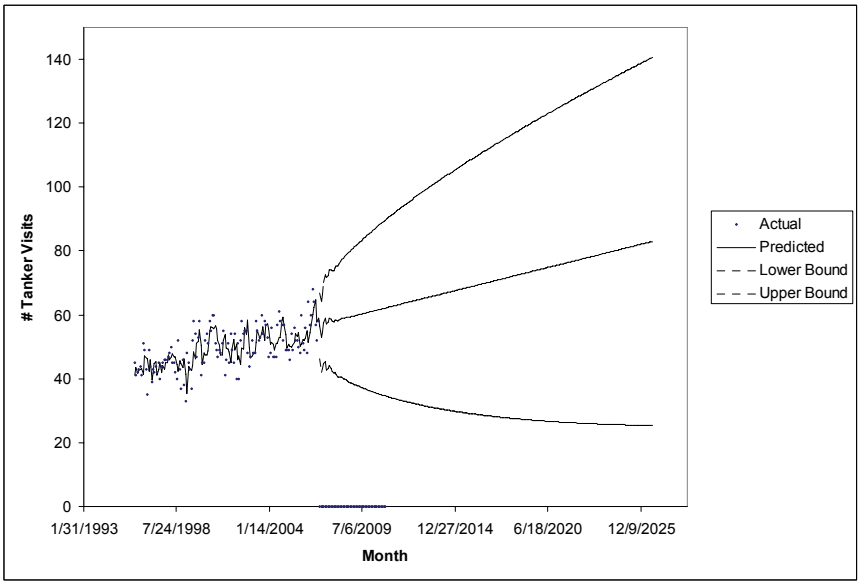

Figure F-17. The statistical forecast for tank vessel visits.

Figure F- 18 confirms our initial observation from the data about the number of shifts that tankers perform. There is no forecasted change in shifts evidenced by the historical data. Figures F.19 and F.20 show no change either for tug and ferry transits.

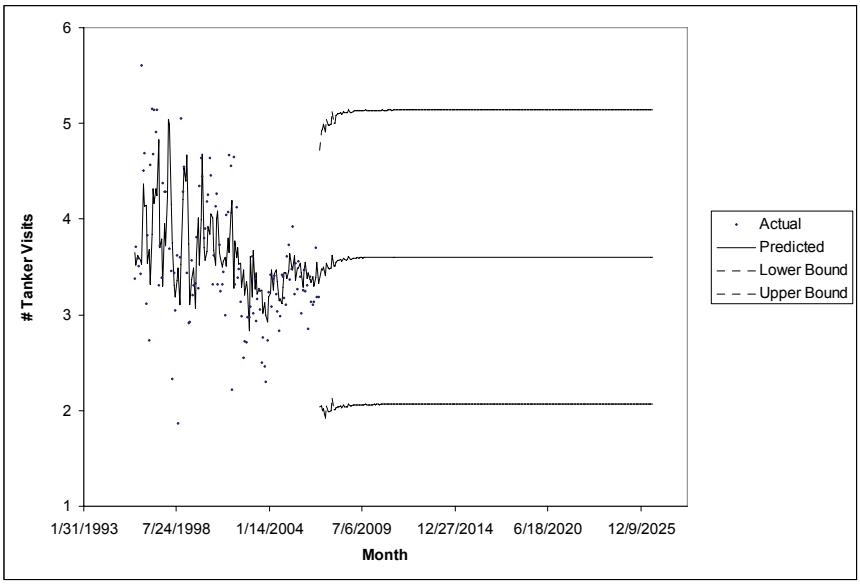

Figure F-18. The statistical forecast for tanker transits per visit.

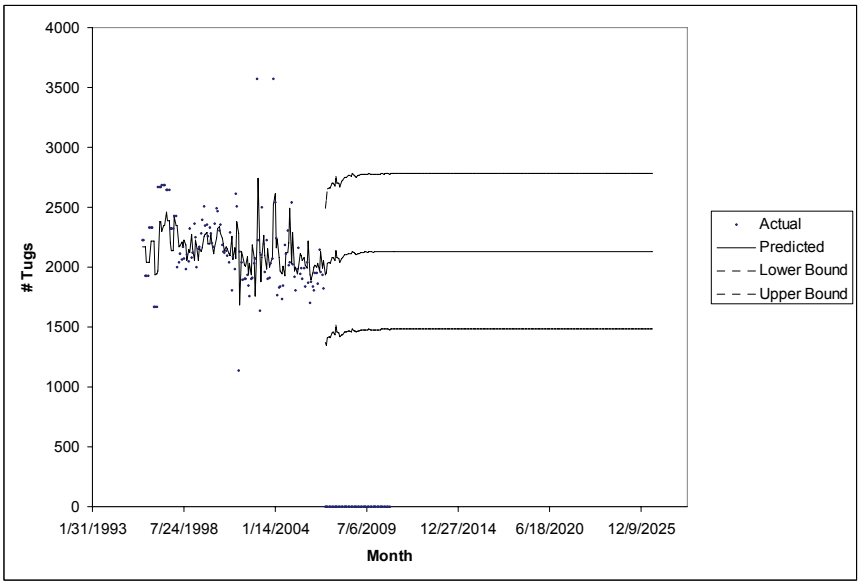

Figure F-19. The statistical forecast for tug transits.

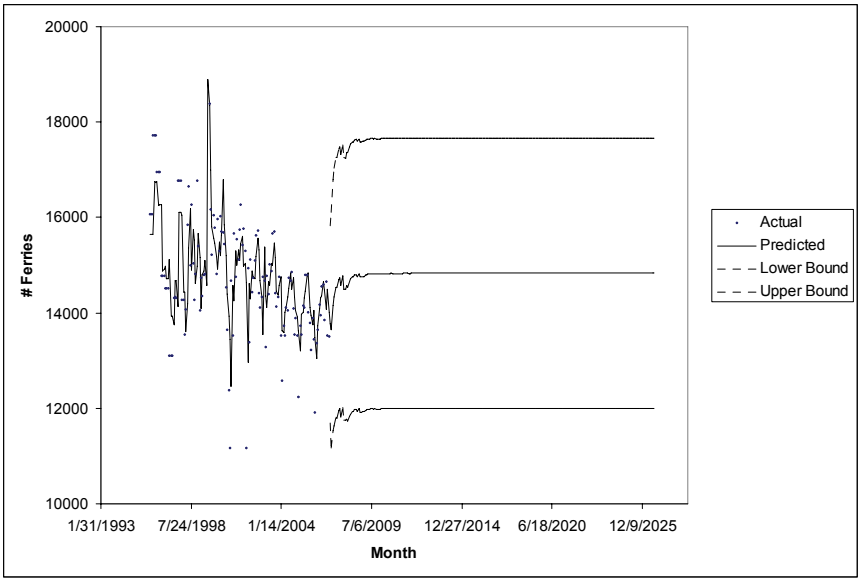

Figure F-20. The statistical forecast for ferry transits.

F-5. Traffic Levels Projected for 2025

Taking all forecasts together, along with the historical traffic levels in the year 2000, we can obtain the traffic levels for our year 2000 and year 2025 cases. The traffic levels for vessel types that do not have a forecasted change used the historical transit data for the year 2005. For the traffic types where changes had to be modeled, stochastic arrival models were fitted to the 2005 data and the parameters of these models were calibrated to achieve the forecasted levels. Table F-3 shows changes made for the year 2000 and the year 2025 low, medium, and high cases as developed throughout this Appendix.

Table F-3. Percentage Changes from 2005 Traffic Levels Used in 2000 and 2025.

Traffic Type	2000	2025		
		Low	Medium	High
BP Crude Tankers	-20%	-90%	+13%	+17%
BP Product Vessels	-	-2%	+13%	+90%
Other Tank Vessels	+23%	-54%	+55%	+162%
Bulk Carriers	+30%	-	-	-
Container Vessels	-	-54%	+20%	+93%

TECHNICAL APPENDIX G: GEOGRAPHIC EXPOSURE, ACCIDENT AND OIL OUTFLOW PROFILES

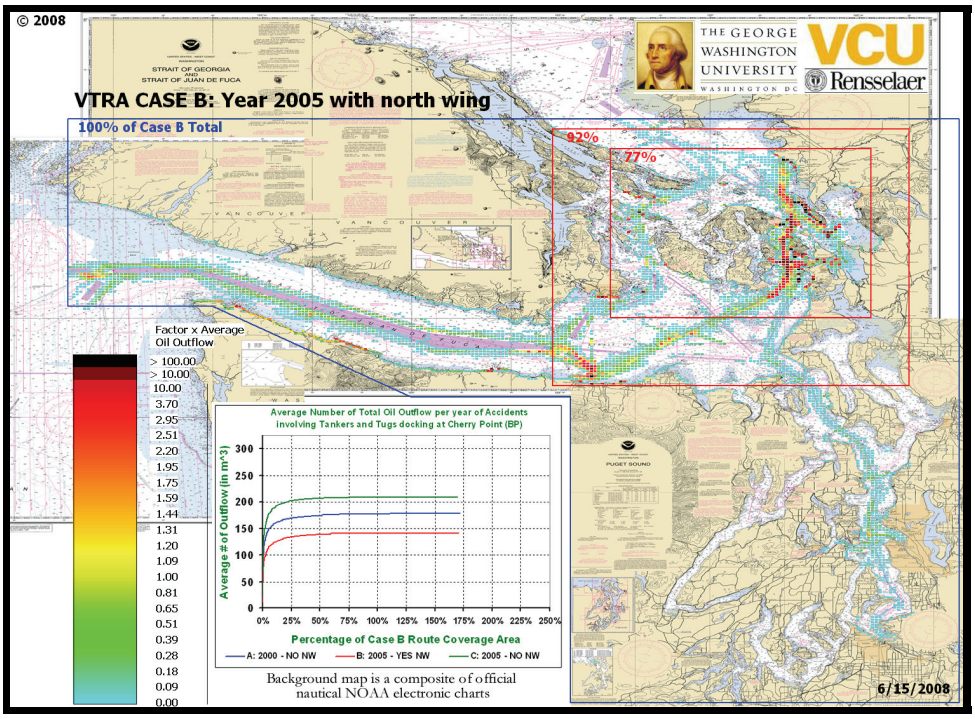

Assessment of Oil Spill Risk due to Potential Increased Vessel Traffic at Cherry Point, Washington

Submitted by VTRA TEAM:

Johan Rene van Dorp (GWU), John R. Harrald (GWU),

Jason R.. W. Merrick (VCU) and Martha Grabowski (RPI)

August 31, 2008

TABLE OF CONTENTS

G-1. Roadmap of Appendix G..... G-5

G-2. System Context Presentation..... G-8

G-3. Summary Aggregate Results Presentations.....G-20

G-4. Callibration VTRA CASE B Presentations

G-4.1. VTRA CASE B: Traffic Density..... G-45
G-4.2. VTRA CASE B: Aggregate Results..... G-47
G-4.3. VTRA CASE B: Collision..... G-55
G-4.4. VTRA CASE B: Powered Grounding.....G-63
G-4.5. VTRA CASE B: Drift Grounding..... G-69
G-4.6. VTRA CASE B: Allisions.....G-75
G-4.7. VTRA CASE B: Accident Probability Presentation.....G-81

G-5. VTRA Case Comparison: A-B-C Presentations

G-5.1. A-B-C: Exposure Presentation..... G-86
G-5.2. A-B-C: Accident Frequency Presentation.....G-90
G-5.3. A-B-C: Aggregate Oil Outflow Presentation.....G-94
G-5.4. A-B-C: BP Persistent Oil Outflow Presentation.....G-98
G-5.5. A-B-C: BP Non- Persistent Oil Outflow Presentation.....G-102
G-5.6. A-B-C: Interacting Vessel Persistent Oil Outflow Presentation..... G-106
G-5.7. A-B-C: Interacting Vessel Persistent Oil Outflow Presentation..... G-110

G-6. VTRA Case Comparison: B-D-E Presentations

G-6.1. B-D-E: Exposure Presentation..... G-114
G-6.2. B-D-E: Accident Frequency Presentation..... G-118
G-6.3. B-D-E: Aggregate Oil Outflow Presentation.....G-122
G-6.4. B-D-E: BP Persistent Oil Outflow Presentation.....G-126
G-6.5. B-D-E: BP Non- Persistent Oil Outflow Presentation..... G-130
G-6.6. B-D-E: Interacting Vessel Persistent Oil Outflow Presentation.....G-134
G-6.7. B-D-E: Interacting Vessel Persistent Oil Outflow Presentation.....G-138

TABLE OF CONTENTS (Continued)

G-7. VTRA Case Comparison: B-F-G Presentations

G-7.1. B-F-G: Exposure Presentation.....G-142
G-7.2. B-F-G: Accident Frequency Presentation.....G-146
G-7.3. B-F-G: Aggregate Oil Outflow Presentation..... G-150
G-7.4. B-F-G: BP Persistent Oil Outflow Presentation..... G-154
G-7.5. B-F-G: BP Non- Persistent Oil Outflow Presentation.....G-160
G-7.6. B-F-G: Interacting Vessel Persistent Oil Outflow Presentation..... G-162
G-7.7. B-F-G: Interacting Vessel Persistent Oil Outflow Presentation..... G-166

G-8. VTRA Case Comparison: B-H-I Presentations

G-8.1. B-H-I: Exposure Presentation.....G-170
G-8.2. B-H-I: Accident Frequency Presentation.....G-174
G-8.3. B-H-I: Aggregate Oil Outflow Presentation..... G-178
G-8.4. B-H-I: BP Persistent Oil Outflow Presentation.....G-182
G-8.5. B-H-I: BP Non- Persistent Oil Outflow Presentation.....G-186
G-8.6. B-H-I: Interacting Vessel Persistent Oil Outflow Presentation..... G-190
G-8.7. B-H-I: Interacting Vessel Persistent Oil Outflow Presentation..... G-194

G-9. VTRA Case Comparison: B-J-H-K Presentations

G-9.1. B-J-H-K: Exposure Presentation..... G-198
G-9.2. B-J-H-K: Accident Frequency Presentation.....G-203
G-9.3. B-J-H-K: Aggregate Oil Outflow Presentation.....G-208
G-9.4. B-J-H-K: BP Persistent Oil Outflow Presentation.....G-213
G-9.5. B-J-H-K: BP Non- Persistent Oil Outflow Presentation.....G-217
G-9.6. B-J-H-K: Interacting Vessel Persistent Oil Outflow Presentation..... G-223
G-9.7. B-J-H-K: Interacting Vessel Persistent Oil Outflow Presentation..... G-228

TABLE OF CONTENTS (Continued)

G-10. VTRA Case Comparison: B-L-H-M Presentations

G-10.1. B-L-H-M: Exposure Presentation..... G-233
G-10.2. B-L-H-M: Accident Frequency Presentation..... G-237
G-10.3. B-L-H-M: Aggregate Oil Outflow Presentation.....G-243
G-10.4. B-L-H-M: BP Persistent Oil Outflow Presentation.....G-248
G-10.5. B-L-H-M: BP Non- Persistent Oil Outflow Presentation..... G-253
G-10.6. B-L-H-M: Interacting Vessel Persistent Oil Outflow Presentation.....G-258
G-10.7. B-L-H-M: Interacting Vessel Persistent Oil Outflow Presentation.....G-263

G-11. VTRA Case Comparison: B-N-H-O Presentations

G-11.1. B-N-H-O: Exposure Presentation.....G-268
G-11.2. B-N-H-O: Accident Frequency Presentation.....G-273
G-11.3. B-N-H-O: Aggregate Oil Outflow Presentation..... G-278
G-11.4. B-N-H-O: BP Persistent Oil Outflow Presentation..... G-283
G-11.5. B-N-H-O: BP Non- Persistent Oil Outflow Presentation.....G-288
G-11.6. B-N-H-O: Interacting Vessel Persistent Oil Outflow Presentation..... G-293
G-11.7. B-N-H-O: Interacting Vessel Persistent Oil Outflow Presentation..... G-298

G-1. Roadmap of Appendix G

This Appendix is a compilation of the various analysis results that were generated over the course of the VTRA project. The VTRA project studies in various levels of detail the difference cases presented in Table 1 below. The calibration case for this project was the year 2005 (VTRA Case B). For this year we are effectively replaying the movement of vessels rather than having to make use of additional probabilistic traffic arrival generators. Hence, VTRA CASE B is a natural calibration scenario. Also please note that in VTRA CASE B the north wing of the Cherry Point dock is in operation. VTRA CASE C runs the same traffic but without this north wing in operation. A more detailed description of the various cases is provided in the main report. Within the main report we have distilled the various general trends within the analysis results across the different VTRA Cases. Appendix G and its presentations allow a reader of the report to study the analysis results and comparisons discussed in the main report in more detail.

Table G-1. The 15 VTRA Cases

	Case	CP Traffic	Other Traffic	North Wing?	Saddlebags?	Extend Escorting?	Neah Bay?	Gate Way?
1	A	2000	2000	No	Yes	No	Yes	No
2	B	2005	2005	Yes	Yes	No	Yes	No
3	C	2005	2005	No	Yes	No	Yes	No
4	D	2025 Low	2025 Low	Yes	Yes	No	Yes	Yes
5	E	2025 Low	2025 Low	No	Yes	No	Yes	Yes
6	F	2025 Medium	2025 Medium	Yes	Yes	No	Yes	Yes
7	G	2025 Medium	2025 Medium	No	Yes	No	Yes	Yes
8	H	2025 High	2025 High	Yes	Yes	No	Yes	Yes
9	I	2025 High	2025 High	No	Yes	No	Yes	Yes
10	J	2005	2005	Yes	No	No	Yes	No
11	K	2025 High	2025 High	Yes	No	No	Yes	Yes
12	L	2005	2005	Yes	Yes	Yes	Yes	No
13	M	2025 High	2025 High	Yes	Yes	Yes	Yes	Yes
14	N	2005	2005	Yes	Yes	No	No	No
15	O	2025 High	2025 High	Yes	Yes	No	No	Yes

Our study was limited to those vessels that dock at the BP Cherry Point dock. These vessels involve both tankers, articulated tug barges (ATB) and integrated tug barges (ITB) docking at BP Cherry Point. This class of vessels are here an in the various appendices and main report referred to as the BPCHPT vessels.

The summary aggregate results presentation provides a quick overview of aggregate results across all the cases in Table 1 in terms of interactions (i.e. exposure), accident frequency and oil outflow. If a one is intrigued by a particular comparison as a result of this aggregate result presentation, one can further study this comparison using one of the comparison

presentations. Each presentation is a power point file with in it various geographic profiles from an exposure, accident frequency and oil outflow perspective. Separate presentations are provided that compare oil outflow by:

- Persistent oil outflow from BPCHPT vessels (specifically crude oil and heavy fuel),
- Non-persistent oil outflow from BPCHPT vessels (specifically refined products and diesel fuel).
- Persistent oil outflow from interacting vessels (specifically crude oil and heavy fuel) involved in a potential collision with a BPCHPT vessel,
- Non-persistent oil outflow from interacting vessels (specifically refined products and diesel fuel) involved in a potential collision with a BPCHPT vessel.

For the VTRA CASE B we analyzed a total annual average oil outflow of about 141 cubic meters. Of this total, 122.1 cubic meters was average persistent oil outflow from BPCHPT Vessels and 15.3 cubic meters was non-persistent oil outflow from BPCHPT vessels. Summarizing, of the total annual average oil outflow analyzed only about 2.5% can be attributed to an oil outflow from interacting vessel involved in a potential collision with a BPCHPT vessel.

The first presentation in the table of contents of Appendix G provides a system context for the traffic that we were tasked to investigate. From the systems context presentation one observes immediately the following very interesting results for the calibration VTRA CASE B:

- Of the total simulated traffic, the CHPT vessel traffic only constitutes 1.1%.
- Of the total simulated traffic, all tankers, ATB's and ITB's only constitutes 3%.
- Of the total simulated deep draft traffic, the CHPT vessel traffic only constitutes 7%.
- Of the total simulated deep draft traffic, all tankers, ATB's and ITB's only constitutes 16%.

As a result a disclaimer is in order: One should tread extremely cautiously when deriving recommendations from any study that only evaluated 1.1% of the total traffic. One primary limitation of the VTRA study is that, due to scoping constraints, the results reflect only on a small percentage of the vessel traffic described in the maritime simulation. If risk interventions have an appreciable effect beyond the BPCHPT vessels analyzed in this study, they should also be tested against this larger class of vessels to determine their effects on

system wide accident frequencies and oil outflows. For example, a risk intervention that reduces accident frequency and or oil outflow of BP Cherry Point vessels, but results in a larger potential increase of accident frequency and/or oil outflows from the other traffic should not be implemented. Conversely, risk mitigation measures that have little or no impact on the BP Cherry Point vessels accident frequency or oil outflow may in fact significantly reduce risk to other vessels.

From our oil outflow analysis it followed that in VTRA CASE B 97.5% of the total annual average oil outflow originated from BP Cherry Point vessels and only 2.5% from interacting vessels involved in a potential collision with a BP Cherry Point vessels. This class of interacting vessels also included tank vessels that do not dock at Cherry Point. Hence, we may cautiously infer that of the total average oil outflow that we analyzed for VTRA CASE B only a small percentage can be attributed to diesel fuel of heavy fuel losses and the dominant part results from cargo losses. With the observations above, one could argue that any risk interventions to reduce oil outflow potential that are in place or being considered for implementation (now or in the future) should first be tested at a minimum for annual average oil outflow reduction effectiveness from all tank vessels. It should be noted that this study did not analyze the oil outflow of tank vessels of those accidents that do not involve BPCHPT vessels.

This page intentionally left blank.